NUREG/CR-4082
BMI-2120
Vol. 6

Degraded Piping Program - Phase II

Sixth Program Report
October 1986 - September 1987

Prepared by G. M. Wilkowski, J. Ahmad, C. R. Barnes, F. Brust, N. Ghadiali, D. Guerrieri, G. Kramer, M. Landow, C. W. Marschall, M. Nakagaki, R. Olson, V. Papaspyropoulos, M. Rosenfeld, P. Scott

Battelle Columbus Division

Prepared for
U.S. Nuclear Regulatory
Commission

NUREG/CR-4082
BMI-2120
Vol. 6
RF, R5

Degraded Piping Program - Phase II

Sixth Program Report
October 1986 - September 1987

Manuscript Completed: December 1987
Date Published: April 1988

Prepared by
G. M. Wilkowski, J. Ahmad, C. R. Barnes, F. Brust, N. Ghadiali,
D. Guerrieri, G. Kramer, M. Landow, C. W. Marschall, M. Nakagaki,
R. Olson, V. Papaspyropoulos, M. Rosenfeld, P. Scott

Battelle Columbus Division
505 King Avenue
Columbus, OH 43201

Prepared for
Division of Engineering
Office of Nuclear Regulatory Research
U.S. Nuclear Regulatory Commission
Washington, DC 20555
NRC FIN B8134

PREVIOUS DOCUMENTS IN SERIES

"Degraded Piping Program - Phase II", Semiannual Report, NUREG/CR-4082, Vol. 1, October 1984.

"Degraded Piping Program - Phase II", Semiannual Report, NUREG/CR-4082, Vol. 2, June 1985.

"Degraded Piping Program - Phase II", Semiannual Report, NUREG/CR-4082, Vol. 3, March 1986.

"Degraded Piping Program - Phase II", Semiannual Report, NUREG/CR-4082, Vol. 4, July 1986.

"Degraded Piping Program - Phase II", Semiannual Report, NUREG/CR-4082, Vol. 5, December 1986.

"NRC Leak-Before-Break (LBB.NRC) Analysis Method for Circumferentially Through-Wall Cracked Pipes Under Axial Plus Bending Loads", Topical Report, NUREG/CR-4572, March 1986.

"Elastic-Plastic Finite Element Analysis of Crack Growth in Large Compact Tension and Circumferentially Through-Wall-Cracked Pipe Specimen--Results of the First Battelle/NRC Analysis Round Robin", Topical Report, NUREG/CR-4573, September 1986.

"An Experimental and Analytical Assessment of Circumferential Through-Wall Cracked Pipes Under Pure Bending", Topical Report, NUREG/CR-4574, June 1986.

"Predictions of J-R Curves With Large Crack Growth From Small Specimen Data" Topical Report, NUREG/CR-4575, August 1986.

"An Assessment of Circumferentially Complex-Cracked Pipe Subjected to Bending. Topical Report, NUREG/CR-4687, September 1986.

"Analysis of Cracks in Stainless Steel TIG Welds", Topical Report, NUREG/CR-4806, November 1986.

"Approximate Methods for Fracture Analyses of Through-Wall Cracked Pipes", Topical Report, NUREG/CR-4853, January 1987.

"Assessment of Design Basis for Load-Carrying Capacity of Weld-Overlay Repair Topical Report, NUREG/CR-4877, February 1987.

"Analysis of Experiments on Stainless Steel Flux Welds", Topical Report, NUREG/CR-4878, February 1987.

"Experimental and Analytical Assessment of Circumferentially Surface-Cracked Pipes Under Bending", Topical Report, NUREG/CR-4872, April 1987.

ABSTRACT

Presented herein is an Annual Report of the U.S. NRC's Degraded Piping Program - Phase II. This is the sixth program report on this program. Prior reports were semiannual reports. The intent of this program is to experimentally validate and enhance available analytical methods for evaluating the mechanical behavior of nuclear power plant piping containing circumferentially oriented defects.

Fifty-seven pipe experiments have been conducted to date. These and approximately fifty additional pipe experiments from other programs have been analyzed.

In the analytical effort, a screening criterion has been developed to show when the net-section-collapse analysis is valid. This shows that even tough materials such as stainless steel can fail at less than net-section-collapse loads if the pipe diameter is sufficiently large. Numerous predictive J-estimation schemes have been evaluated and modified. A finite length surface-cracked pipe estimation scheme has also been developed and incorporated into a computer code called NRCPIPE. This code provides a convenient way of analyzing cracked pipe with a number of currently accepted analytical methods.

Supporting research efforts involve investigating geometry effects on J-R curves, as well as characterizing the material properties for each pipe tested. The significance of all of the efforts to date relative to pipe fracture analyses and flaw assessment criteria are discussed.

CONTENTS

LIST OF FIGURES

LIST OF TABLES

ACRONYMS AND ABBREVIATIONS

ACRS	Advisory Committee on Reactor Safeguards
AEC	U.S. Atomic Energy Commission
ASME	American Society of Mechanical Engineers
ASTM	American Society for Testing and Materials
BMI	Battelle Memorial Institute
BWR	boiling-water reactor
CFR	U.S. Code of Federal Regulations
CSNI	Committee on the Safety of Nuclear Installations
CTOA	crack tip opening area, angle
C(T)	compact (tension)
DSA	dynamic strain aging
DTRC	David Taylor Research Center, formerly David Taylor Naval Research and Development Center (DTNRDC)
DEGB	double-ended guillotine break
EDM	electric-discharge machine, machining
EPFM	elastic-plastic fracture mechanics
EPRI	Electric Power Research Institute
FWFN(T)	full-width-face-notch[ed] (tension)
GDC	General Design Criterion
GE	General Electric
GTAW	gas-tungsten arc weld, welding
GMAW	gas-metal arc weld, welding
HAZ	heat-affected zone
IGSCC	intergranular stress corrosion crack, cracking
J/T	J-integral/tearing modulus
KWU	Kraftwerk Union
LBB	leak-before-break
LWR	light-water reactor
MEA	Materials Engineering Associates
NRC	U.S. Nuclear Regulatory Commission
NRR	Office of Nuclear Reactor Regulation
ORNL	Oak Ridge National Laboratory
PVP	Pressure Vessel and Piping division of ASME

ACRONYMS AND ABBREVIATIONS
(CONTINUED)

PWR	pressurized-water reactor
PZSC	plastic-zone screening criterion
SAW	submerged arc weld, welding
SMAW	shielded-metal arc weld, welding
SSE	safe shutdown earthquake
TIG	tungsten-inert-gas
UT	ultrasonic testing
UTS	ultimate tensile strength
VCE	virtual crack extension
WOR	weld-overlay repair

ACKNOWLEDGMENTS

This work is supported by the U.S. Nuclear Regulatory Commission through the Materials Engineering Branch of the Office of Nuclear Regulatory Research under Contract No. NRC-04-84-103. M. Mayfield was the NRC program manager during this period. J. Strosnider, the initial program manager, oversaw the program from March 15, 1984 to September 1984. Subsequently, until October 1985, M. Vagins was the NRC program manager. We would like to express thanks to the David Taylor Naval Ship Research and Development Center (R. Hayes and J. Gudas), Materials Engineering Associates (B. Menke, A. Hiser, and Dr. F. Loss), Battelle Pacific Northwest Division (Dr. S. Doctor), Oak Ridge National Laboratories (Dr. R. Bass), and Argonne National Laboratories (Dr. W. Shack) for their cooperation during the course of this program. R. Hayes (DTNSRDC) and B. Menke and A. Hiser (MEA) have been especially cooperative. We would also like to thank Dr. D. Norris of the Electric Power Research Institute for the donation of stainless steel submerged-arc welds to this program. Finally, we would like to acknowledge M. Steve's effort in coordinating this report.

EXECUTIVE SUMMARY

This is the sixth program report on the Degraded Piping Program, Phase II. The objective of the Degraded Piping Program is to verify and improve fracture mechanics analysis methods for nuclear power plant piping. Results of this program, which is now in its fourth and final year, will contribute to the bases for evaluating pipe fracture analyses that are part of the NRC's leak-before-break (LBB) analyses and in-service flaw assessment criteria.

It is now possible to evaluate the benefits that this program, when completed, will provide to the NRC. Numerous tasks have been undertaken and completed to satisfy regulatory needs. This executive summary briefly describes the technical issues that will have been addressed before the end of this program, and the impact of these issues on current or future regulatory needs. Technical concerns that may require further evaluation are also reviewed.

Technical Issues Addressed

Key technical issues were addressed by the Degraded Piping Program. Among other efforts, the program

- Verified the ASME IWB-3640 (limit-load) analysis for cracks in austenitic piping
- Evaluated the complex crack geometry both experimentally and analytically
- Provided for the writing and evaluation of an IBM PC code for performing automated pipe fracture analyses
- Found that detailed finite element analyses consistently underpredict the experimental maximum load for through-wall cracked pipe
- Evaluated the ASME IWB-3640 flux weld analysis through seven full-scale pipe fracture experiments
- Tested cracked pipe with weld-overlay repairs, showing that at light-water reactor (LWR) conditions, large deformations developed in the unwelded pipe adjacent to the weld overlay prior to fracture.

The ASME IWB-3640 (limit-load) analysis for cracks in austenitic piping has been verified. Experimental results have shown that the analysis procedure provides a better than average value for the advertised safety factor rather than a minimum safety margin. The results have also shown that a correction factor may be needed for the pipe radius-to-thickness ratio for surface-cracked pipe. Surface-cracked pipe with a thinner wall fails at lower stresses, probably due to ovalization effects.

The definition of the "flow stress of the material" has been an issue in flaw assessment and pipe fracture analyses. The concept of flow stress provides an approximate means of accounting for the strain-hardening of the material. A

large pipe-fracture database was developed and used to statistically evaluate methods of defining flow stress for limit-load analyses, as applied to in-service flaw inspection and pipe fracture analyses. This statistical analysis showed that an average value of the flow stress was 1.15 (yield and ultimate)/2 for both stainless and carbon steel pipes. A 95 percent reliability level relation (that is, two standard deviations below the average of the failure stresses) was close to the average of the yield plus ultimate strength. A simple screening criterion was developed to show when limit-load analyses can be used in pipe fracture and in-service flaw assessments.

For low-toughness, large-diameter pipe with a through-wall crack, a large safety margin between the load at crack initiation and maximum load was experimentally demonstrated. Hence, current LBB analysis procedures, which are primarily concerned with the load at crack initiation, could incorporate crack growth considerations to take advantage of this margin.

The complex crack geometry was experimentally and analytically evaluated. This crack geometry involves a through-wall crack with a surface crack in the remaining cross section. The Duane Arnold plant safe end cracks (due to IGSCC) and the D.C. Cook plant feedwater thermal fatigue cracks are two examples of such cracks found in service. For a pipe with a complex crack geometry, the internal surface flaw was found to reduce the apparent fracture resistance significantly.

For performing automated circumferential crack stability analyses used for LBB assessments, an IBM PC code, NRCPIPE, has been written by Battelle and submitted to the NRC. This code takes into account existing and newly developed through-wall cracked pipe elastic-plastic fracture mechanics analyses used in LBB evaluations. These are approximate analyses typically called J-estimation schemes. These analyses were generally found to be conservative when a deformation theory material fracture resistance curve (J-R curve) was used. The modified J-R curve parameter could lead to an overprediction of the loads that would result in pipe failure, and is not recommended for use.

Detailed finite element analyses, which are more accurate than the approximate J-integral estimation schemes, were found to consistently underpredict the experimental maximum load for through-wall cracked pipe. This observation results from several of this program's analyses and from the findings of an international finite element round robin. Hence, licensing applications submitted with prudent finite element analyses of circumferential through-wall cracked pipe should provide conservative estimates of the load-carrying capacity of the pipe.

Conversely, recent evaluations of round-robin finite element analyses of a surface-cracked pipe showed that if the mesh were properly refined, and if the finite element analyses were used with an appropriate material J-R curve, then the predicted loads would be higher than the actual loads. The analysis on this one experiment indicates a trend of nonconservative predictions of failur loads for the finite element analysis of a circumferentially surface-cracked pipe.

The ASME IWB-3640 flux weld analysis was compared to the results of seven full-scale pipe fracture experiments with through-wall or surface cracks. This flux weld criterion was developed from a through-wall cracked pipe analysis. Experimental data generated as part of this program showed that the through-wall cracked pipe analysis is inherently conservative with respect to the surface-cracked pipe analysis. As such, the flux weld criterion was found to have inherent safety margins. However, in this program it was recently found that the material property data used in this criterion were higher than typical values for the flux welds. The experimental data indicate that the additional margins seem to compensate for the higher than actual toughness values used in developing the criterion. This result has been reported to the ASME Section XI Flaw Evaluation Task Group.

Fracture tests at LWR conditions showed that cracked pipe with weld-overlay repairs had large plastic deformations in the unwelded pipe adjacent to the weld overlay. These large plastic deformations occurred prior to the fracture of a crack in the overlay. In evaluating the design analysis procedures, it was found that well-defined guidelines do not exist. One could predict either very low loads relative to the experimental data, or loads slightly higher than the experimental data, depending on radius, thickness, or flaw depth used. In an analytical round robin for weld overlay design calculations, different assumptions were made by the different participants. The final predictions by the participants, however, were very close to each other.

A large database has been developed from the pipe fracture experiments. This has been used to develop a unified statistical criterion to predict maximum loads for carbon or stainless steel pipe, and can be applied to through-wall or surface-cracked pipe. This simplified procedure, which could easily be incorporated into a code procedure, can be used for in-service flaw evaluations or pipe fracture analyses. The simplified plastic-zone statistical method was presented to the ASME Section XI Pipe Flaw Evaluation Task Group as a suggested replacement to the existing criterion for evaluating flaws in stainless steel and carbon steel pipe. It is to be published in the refereed journal Nuclear Engineering and Design.

Correlations between Charpy data and fracture toughness have been verified for ferritic nuclear piping materials at LWR temperatures. This is useful for in-service flaw assessment criteria, and could be applied to mill quality control requirements for new plant construction. This was incorporated into the statistical pipe flaw analysis described above.

Procedures for calculating material crack growth resistance curves were found to be consistent among NRC contractors, adding support to the data used for analysis of the experiments, and to the data provided to the NRC pipe material property database.

Technical Issues Requiring Further Consideration

Certain technical issues will need further work to assess their impact on regulatory applications. Most of these evolved from investigations conducted during this program. The most significant issues are summarized below.

Included among the areas that may deserve further study are:

- Prototypical evaluations of cracks in carbon steel welds and thermally aged pipe
- Through-wall-cracked pipe behavior under combined pressure and bending at LWR temperatures
- Crack instabilities in many nuclear grade carbon steel piping materials at 550 F (288 C)
- Theoretical finite-length surface-cracked pipe analysis

More data are needed for prototypical evaluations of cracks in carbon steel welds and thermally aged pipe. These data are needed for verification of tentative ASME carbon steel pipe flaw evaluations and plant life extension evaluations. Several tests are being conducted as part of the extension to this program. Additional ferritic shielded metal arc weld (SMAW) data are also needed, but are not being evaluated in this program.

Through-wall-cracked pipe behavior under combined pressure and bending at LWR temperatures may need further evaluation. Analysis of this behavior is the central part of the pipe fracture analyses used in the NRC's LBB evaluation procedure. One experiment conducted on a stainless steel pipe had a much lower experimental maximum load than predicted by limit-load analysis. An additional experiment on a lower toughness carbon steel pipe is to be conducted in the near future in this program. These results, if also low, could affect the margin of safety in the LBB analysis.

For pipe fracture analyses, the presence of allowable shallow surface flaws (such as those allowed by ASME IWB-3514.3) could contribute to lowering the apparent toughness of the pipe. The current complex-cracked pipe results show that such a shallow flaw could lower the apparent fracture resistance by 25 to 50 percent. Further data are needed to assess this margin and evaluate its significance for pipe fracture analyses.

Crack instabilities have been observed in many nuclear grade carbon steel piping materials at 550 F (288 C) during the course of this program. These instabilities have occurred in both laboratory and full-scale pipe experiments. By contrast, only stable tearing was observed in 300 F (149 C) laboratory specimen tests. Although the cause of the instabilities is not well understood, it is believed to be related to dynamic strain aging that occurs in many carbon steels. The net result is a significant reduction in the crack propagation resistance. In addition, one particular carbon steel submerged arc weld that had been stress-relieved exhibited crack instability immediately after crack initiation in a laboratory specimen tested at 550 F (288 C). This specimen simulated surface-crack growth in a girth weld. This dynamic strain aging phenomenon needs further evaluation to:

(1) understand why some of the carbon steels are susceptible to unstable cracking while others are not,

(2) predict its effect on pipes using laboratory specimen data,

(3) assess its impact on fracture behavior at seismic as well as at normal operating condition strain rates (given that dynamic strain aging is a temperature and strain-rate sensitive phenomenon), and

(4) evaluate the possibility that dynamic strain aging may lower the initiation toughness for a surface-cracked pipe under a seismic loading.

The technical concepts involved in an energy balance approach used to predict the onset of crack instability and arrest have been validated. This approach could be used to predict a maximum crack opening area if a surface-cracked pipe were to fail. Also, it would contribute to a technical basis for replacing the double-end guillotine break (DEGB) criterion in the future.

The crack propagation toughness along a stainless steel SMAW fusion line was recently found to be approximately half of the fracture resistance in the SMAW. This is significant since the SMAW weld metal is currently believed to be one of the lower toughness austenitic materials. Moreover, stress corrosion cracks more frequently grow along the fusion line than into the weld metal. Further attention should be given to evaluation of crack initiation toughness and crack growth resistance along the fusion line of welds. This could impact both in-service flaw acceptance criteria, such as IWB-3640, and LBB acceptance criteria. Neither of these analyses addresses the question of fusion line toughness, since this observation is a recent finding. In addition, no data exist for bimetallic welds such as those between carbon steel pipe and stainless steel safe-ends.

A theoretical finite-length surface-cracked pipe analysis is needed to verify the approximate ASME Code criteria for conditions where there are no experimental data. Pioneering efforts to develop such an analysis have been completed in this program. Two slightly different analyses were developed and compared to experimental data in a recent topical report. The comparisons showed that the thin shell analysis overpredicted the experimental loads, while a thick shell version consistently underpredicted the failure stresses. This analysis would be useful in improving the ASME Section XI flaw assessment criterion, where the length of the surface crack is not considered in the current stress multiplier for low toughness effects. The analysis needs combined pressure and bending modifications before it can be used to evaluate the ASME Code procedure. In addition, experimental data are needed for shorter length surface-cracked pipe under combined pressure and bending to evaluate tentative in-service flaw acceptance criteria.

For determination of crack growth resistance curves from laboratory specimens, when using the Modified J-integral approach, it currently appears that two specimen sizes are needed to account for geometry effects. The results from several series of specimen size effect tests show that, when using the Modified J analysis, a small standard size specimen gives a lower bound J_{Ic}, where a larger specimen (of the same thickness) gave a lower tearing resistance. Results to date show that the larger specimen should have a planform size that is four times larger than the standard specimen used for that thickness.

The Modified J-integral fracture parameter was extensively investigated during the course of this program. One concern is that to apply it to piping predictions, similar crack growth modifications, as employed in the Modified J-integral parameter for specimen testing, should be incorporated into the piping analyses. Another more fundamental concern is that the Modified J-integral values continually increase with crack growth, whereas experimental measurements show that the crack tip opening angle (and hence the associated crack tip strain field) reaches a steady-state value. Incremental plasticity versions of the J-integral fracture parameter, like the CTOA, also predict a steady-state toughness. These analyses need to be developed into simple estimation schemes rather than time-consuming and expensive finite element analyses. Such a revision would improve pipe fracture analyses by simplifying the procedures to extrapolate a crack growth resistance curve. An approach based on incremental plasticity would also eliminate difficulties in evaluating crack growth into a bimetallic weld, as well as evaluating possible history dependence from cyclic loading during a seismic event.

Tests of submerged arc welds on stainless steel pipe of different thicknesses were conducted. In this procedure, the root pass and initial hot passes of the weld were made with a TIG weld material that was tougher than the rest of the weld made with a low toughness flux weld. For the thinner weld, the composite toughness was higher than that of the thicker weld. This result illustrates that to evaluate the fracture behavior of a thick pipe, test results from a thinner specimen should not be used.

It has been found that material anisotropy affects the fracture toughness and direction of crack propagation in full-scale pipe experiments and in some laboratory specimen tests. The anisotropy's potential for both beneficial and detrimental effects should be examined more closely. For instance, most circumferential cracks in seamless carbon steel pipe propagate in a helical direction, even under pure bending. What would happen if the pipe were subjected to combined pressure and bending stress or torsional stresses where the principal stress is in the low toughness direction?

A large database on nuclear material properties has been developed and will be incorporated in the NRC pipe material property database. This will help to determine generic lower bound properties, but is not a statistically significant sample size by itself. Further data are needed, particularly for carbon steel welds, heat affected zones, and fusion lines.

The technical accomplishments of this program, and the issues and implications raised, have provided a significant advance in the fundamental and practical understanding of piping fracture mechanics.

1. PROGRAM OBJECTIVES, RATIONALE, AND APPROACH

Accurate assessment of the mechanical behavior of degraded (that is, cracked) piping is of vital importance to the safety of nuclear power plants. The U.S. Nuclear Regulatory Commission (NRC) and their licensees, the nuclear power plant operators, must account for and provide back-up safety systems for the unlikely event of a leak or a rupture in the piping system of a nuclear power plant to avoid both damage to the reactor core and a major accident involving loss of coolant. Adequate provision must be made to ensure that the effects of potential piping breaks are controllable until a safe reactor shutdown can be effected. Limits must be established regarding the sizes of piping defects that can be safely tolerated without an unscheduled shutdown. The aim of Phase II of the Degraded Piping Program is to provide the NRC with state-of-the-art, proven analysis methods for predicting the behavior of degraded piping under light-water reactor (LWR) conditions.

The approach being taken by Battelle to provide state-of-the-art analysis methods consists of reviewing existing analytical methodology, enhancing it where feasible and appropriate, and validating it by means of full-scale pipe fracture experiments. The analytical methodology includes simple limit-load analyses, elastic-plastic fracture mechanics (EPFM) techniques, and finite element analyses. The behaviors of simple crack geometries and loading systems were considered first. The work has progressed to the consideration of more realistic crack geometries and loading systems. Because of the nature of the operational loads and stresses imposed on nuclear plant piping, axial crack propagation in such piping is generally thought to be of minor significance. The main concern in this program is with circumferentially oriented crack propagation: that is, whether a circumferentially oriented crack will merely grow through the pipe thickness and become a leak or whether it will become a double-ended rupture. As such, this work is confined to circumferentially oriented flaws and the effects of longitudinal loads and stresses.

Progress on this project during the period from October 1986 through September 1987 is presented herein. Additionally, we have summarized significant results from our five previous semiannual reports and appropriate topical reports in the beginning of each section. Some of these sections now represent work that is completed. Recently the program was extended for one year, until September 1988. The new work concentrates on more prototypical pipe fracture experiments or materials, including thermally aged, centrifugally cast stainless steel, carbon steel submerged-arc welds, and pipe under combined pressure and bending.

2. PIPE FRACTURE EVALUATIONS
(G. Wilkowski)

The research efforts on pipe fracture evaluations are divided into eleven work packages. These work packages and the corresponding sections of this report are listed below. Sections 2.1 through 2.10 are numbered consistently with sections from the previous semiannual report; Section 2.11 introduces a new work package. Since this is the last semiannual report prior to the final report, each section contains a subsection summarizing results to date.

Section 2.1 Circumferentially Through-Wall-Cracked Pipe in Pure Bending

Section 2.2 Finite-Length Internal Circumferentially Surface-Cracked Pipe in Pure Bending

Section 2.3 Circumferentially Complex-Cracked Pipe in Bending

Section 2.4 Circumferentially Cracked Pipe Under Axial Membrane Stress

Section 2.5 Fracture Behavior of Weld-Overlay Repaired Pipe

Section 2.6 Stainless Steel TIG Welds

Section 2.7 Stainless Steel Flux Welds

Section 2.8 Circumferentially Through-Wall-Cracked and Surface-Cracked Pipe Subjected to Combined Pressure and Bending

Section 2.9 Instability of Surface-Cracked Pipe in Compliant Bending

Section 2.10 Carbon Steel Flux Welds

Section 2.11 Centrifugally Cast Stainless Steel

Each work package consists of subtasks involving analytical efforts, material characterizations of laboratory specimens, and full-scale pipe fracture experiments. Tables 2.1, 2.2, 2.3, and 2.4 summarize the full-scale pipe fracture experiments that were generally conducted on surplus pipe purchased from cancelled nuclear power plants. Table 2.4 summarizes the new experiments planned during the last year of the program. Characterizations of these pipe materials include chemical analyses, Charpy V-notch impact tests, true stress-true strain tensile tests, standard laboratory specimen J-R curve tests, and nonstandard specimen J-R curve evaluations (when necessary). Tensile testing is conducted at room temperature, 300 F (149 C), and 550 F (288 C). These material characterizations are discussed in Section 3.1. Full-scale pipe fracture experiments are conducted at 550 F (288 C). Analytical efforts involve assessment of limit-load analyses, finite element analyses (in some cases), and the verification and improvement of engineering EPFM techniques (that is, J-estimation schemes).

In a carefully planned series of pipe fracture experiments, critical analytic assumptions were evaluated one at a time. Consequently, initial efforts involved developing the necessary simple cracked pipe analyses (see Sections 2.1 through 2.4). Studies on prototypically cracked pipe are continuing (see Sections 2.5 through 2.11). The significance of the results to date is discussed in Section 4. By conducting the program in the manner described, the sensitivity of analyses to different variables can be realistically assessed. Ultimately, this will result in analysis methodologies with a known and uniform degree of conservatism. Reduced margins of safety could then be tolerated without a loss of safety. Added confidence in the analysis methodologies would also facilitate licensing decisions.

Table 2.1 First-year pipe acture test matrix[a]

	Subtask and Experiment Number	Diameter, inches	Schedule[b]	Wall Thickness, inches	Material Type[c]	
Diameter Effects on Through Wall Cracks Under Bending	4111-0	4	80	0.337	SA 333 GR#6	No Fla
	-1	4	80	0.337	SA 333 GR#6	Circum
	-2	28	NA	0.875	A 155-CK70-CL1	Circum
	-3	42	NA	0.25	SA 358 304 SS	Circum
	-4	42	NA	0.625	API 5LX65	Circum
Thickness Effects on Surface Cracks Under Bending	4112-1	16	40S	0.375	SA 376 316 SS	Interna
	-2	6	40	0.280	SA 376 304 SS	Interna
	-3	6	120	0.562	SA 376 304 SS	Interna
	-4	6	XXS	0.864	SA 376 304 SS	Interna
	-5	6	40	0.280	A 106 B	Interna
	-6	6	120	0.562	A 106 B	Interna
	-7	6	XXS	0.864	A 106 B	Interna
Complex Cracks Under Bending	4113-1	6	120	0.562	SA 376 304 SS	Interna
	-2	6	120	0.562	SA 376 304 SS	Interna
	-3	6	80	0.432	Inconel 600	Interna
	-4	6	80	0.432	Inconel 600	Interna
	-5	6	120	0.562	A 106 B	Interna
	-6	6	120	0.562	A 106 B	Interna
Instability of Complex Cracks Under Bending	4114-1	6	120	0.562	A 106 B	Interna
	-2	6	120	0.562	SA 376 304 SS	Interna
	-3	16	100	1.031	SA 358 304 SS	Interna
	-4	16	100	1.031	SA 358 304 SS	Interna
Various Crack Geometries Under Axial Tension	4121-1	6	120	0.562	SA 376 304 SS	Circum
	-2	6	120	0.562	SA 376 304 SS	Externa
	-3	6	120	0.562	SA 376 304 SS	Externa
	-4	10	100	0.719	SA 333 GR#6	Circum
	-6	10	100	0.719	SA 333 GR#6	Externa
Prototypical Cracked Pipe Weld Overlay Repair	4142-1	6	120	0.562	SA 376 304 SS	Interna
	-2	6	120	0.562	SA 376 304 SS	Interna
	-3	6	120	0.562	SA 376 304 SS	Interna

(a) March 1, 1984, to February 28, 1985.
(b) "XXS" designates "extra extra strong" pipe. Typically greater than schedule 160.
(c) ASTM standards are designated "A". ASME standards are designated SA.
(d) TWC = Through-Wall crack.
SC = Surface crack.
(e) SMN = Sharp machine notch (approx. 0.003-inch radius); F = fatigue.

Crack Orientation	Crack[d] Geometry	Initial[e] Crack Condition	Test Temperature, F	Loading Method	Crack Length, % circumference	Crack Depth, % wall
	-	-	550	Bending	-	-
	TWC	SMN	550	Bending	37	100
	TWC	SMN	550	Bending	37	100
	TWC	SMN	AMB	Bending	37	100
	TWC	SMN	AMB	Bending	37	100
1 Circum	SC	SMN	550	Bending	50	66
1 Circum	SC	SMN	550	Bending	50	66
1 Circum	SC	SMN	550	Bending	50	66
1 Circum	SC	SMN	550	Bending	50	66
1 Circum	SC	SMN	550	Bending	50	66
1 Circum	SC	SMN	550	Bending	50	66
1 Circum	SC	SMN	550	Bending	50	66
1 Circum	TWC/SC	SMN	550	Bending	37	33
1 Circum	TWC/SC	SMN	550	Bending	37	66
1 Circum	TWC/SC	SMN	550	Bending	37	33
1 Circum	TWC/SC	SMN	550	Bending	37	66
1 Circum	TWC/SC	SMN	550	Bending	37	33
1 Circum	TWC/SC	SMN	550	Bending	37	66
1 Circum	TWC/SC	SMN	550	Compliant Bend	37	50
1 Circum	TWC/SC	SMN	550	Compliant Bend	37	66
1 Circum	TWC/SC	SMN	550	Compliant Bend	37	33
1 Circum	TWC/SC	SMN	550	Compliant Bend	37	33
	TWC	SMN	550	Pressure (oil)	37	100
1 Circum	TWC/SC	SMN	550	Pressure (oil)	37	100/66
1 Circum	SC	SMN	550	Pressure (oil)	50	66
	TWC	SMN	550	Pressure (oil)	37	100
1 Circum	SC	SMN	550	Pressure (oil)	50	66
1 Circum	SC	F	550	Bending & Press. (water)	50	66
1 Circum	SC	F	550		50	66
1 Circum	SC	F	550	Bending & Press. (water)	50	66

Table 2.2 Second-year pipe fracture test matrix[a]

	Subtask and Experiment Number	Diameter, inches	Schedule	Wall Thickness, inches	Material Type[b]	
Diameter Effects on Through-Wall Cracks Under Bending	4111-5	28	N/A	0.875	SA376 316SS SMAW	Circum
Thickness Effects on Surface Cracks Under Bending	4112-8	16	100	1.031	A106 Gr. B	Intern
	4112-9	16	40	0.500	A106 Gr. B	Intern
Instability of Surface Cracks Under Bending	4115-1	10	100	0.719	SA333 Gr. 6	Intern
	4115-2	10	100	0.719	SA333 Gr. 6	Intern
	4115-4	6	120	0.562	SA376 304SS	Intern
	4115-5	6	120	0.562	SA376 304SS	Intern
	4115-7	6	120	0.562	SA376 304SS	Intern
	4115-8	6	120	0.562	SA376 304SS	Intern
	4115-9	6	120	0.562	SA376 304SS	Intern
Combined Pressure and Bending	4131-1	6	120	0.562	SA376 304SS	Circum
	4131-2	6	120	0.562	SA376 304SS	Intern
	4131-3	10	100	0.719	SA333 Gr. 6	Circum
	4131-4	10	100	0.719	SA333 Gr. 6	Intern
Supplementary to Combined Pressure and Bend	4131-5	6	120	0.562	SA376 304SS	Circum
	4131-6	6	120	0.562	SA376 304SS	Intern
	4131-7	10	100	0.719	SA333 GR. 6	Circum
	4131-8	10	100	0.719	SA333 Gr. 6	Intern
Prototypical Cracks in Weld Metal	4141-1	6	120	0.562	SA376 304SS/SAW	Circum
	4141-2	6	120	0.562	SA376 304SS/SAW	Intern
	4141-3	16	100	1.031	SA358 304SS/SAW	Circum
	4141-4	16	100	1.031	SA358 304SS/SAW	Intern
Prototypical Cracked Pipe Weld Overlay Repair	4142-4	16	100	1.031	SA358 304SS	Intern

(a) March 1, 1985, to February 28, 1986.
(b) SS = Stainless Steel.
(c) SC = Surface Crack
TWC = Through-Wall Crack
TWC/SC = Complex Crack.
(d) SMN = Sharp Machine Notch (Radius of 0.005 inch or less)
FC = Fatigue Crack.

Crack Orientation	Crack[c] Geometry	Initial[d] Crack Condition	Test Temperature, F	Loading Method	Crack Length, % circumference	Crack Depth, % wall
erential	TWC	SMN	550	Bending	37	100
l Circumferential	SC	SMN	550	Bending	50	66
l Circumferential	SC	SMN	550	Bending	50	66
l Circumferential	SC	SMN	550	Compliant Bending	37	66
l Circumferential	SC	SMN	550	Compliant Bending	37	66
l Circumferential	SC	SMN	550	Compliant Bending	37	66
l Circumferential	SC	SMN	550	Compliant Bending	37	66
l Circumferential	SC	SMN	550	Compliant Bending	100	66
l Circumferential	SC	SMN	550	Compliant Bending	100	66
l Circumferential	SC	SMN	550	Compliant Bending	100	66
erential	TWC	SMN	550	Pressure and Bending	37	100
l Circumferential	SC	SMN	550	Pressure and Bending	50	72
erential	TWC	SMN	550	Pressure and Bending	37	100
l Circumferential	SC	SMN	550	Pressure and Bending	50	72
erential	TWC	SMN	550	Bending	37	100
l Circumferential	SC	SMN	550	Bending	50	72
erential	TWC	SMN	550	Bending	37	100
l Circumferential	SC	SMN	550	Bending	50	72
erential	TWC	SMN	550	Bending	37	100
l Circumferential	SC	SMN	550	Pressure and Bending	50	66
erential	TWC	SMN	550	Bending	37	100
l Circumferential	SC	SMN	550	Pressure and Bending	50	66
l Circumferential	SC	FC	550	Pressure and Bending	50	66

Table 2.3 Third-year pipe fracture test matrix[a]

	Subtask and Experiment Number	Diameter, inches	Schedule	Wall Thickness, inches	Material Type[b]	Cr
Diameter Effects on Through Wall Cracks Under Bending	4111-6	37	-	2.75	A516 Gr. 70 with TP304L SS Cladding	Circ
Prototypical Cracks in Weld Metal	4141-5	6	120	0.562	SA376 304SS/SAW	Circ
	4141-6	16	100	1.031	SA358 304SS/SAW	Inte
	4141-7	37	-	3.25	A516 Gr. 70 with TP304L SS Cladding	Circ
Prototypical Cracks in Thermally Aged Centrifugally Cast Stainless Steel	4143-1	15.73	-	1.968	316SS CF8M	Inte
	4143-2	12	160	1.312	SA351 CF8M	Circ

(a) March 1, 1986, to February 28, 1987.
(b) SS = Stainless Steel.
(c) SC = Surface Crack
TWC = Through-Wall Crack
TWC/SC = Complex Crack.
(d) SMN = Sharp Machine Notch (Radius of 0.005 inch or less)
FC = Fatigue Crack.

ack Orientation	Crack(c) Geometry	Initial(d) Crack Condition	Test Temperature, F	Loading Method	Crack Length, % Circumference	Crack Depth, % wall
mferential	TWC	SMN	550	Be: 'ing	37	100
mferential	TWC	SMN	550	Bending	37	100
nal Circumferential	SC	SMN	550	Pressure and Bending	50	72
mferential	TWC	SMN	550	Bending	37	100
nal Circumferential	SC	FC	550	Compliant Bending and Pressure	50	50
mferential	TWC	SMN	550	Bending	37	100

Table 2.4 Fourth-year pipe fracture test matrix[a]

	Subtask and Experiment Number	Diameter, inches	Schedule	Wall Thickness, inches	Material Type[b]	Crack Orientation	Crack[c] Geometry	Crack Length, % Circumference	Crack Depth, % Wall
Prototypical Cracks in Weld Metal	4141-8	16	100	1.031	A106 Gr. B	Internal Circumferential	SC	50	67
	4141-9	16	100	1.031	A106 Gr. B	Circumferential	TWC	37	100
Combined Pressure and Bending	4131-9	6	120	0.562	SA376 304SS	Circumferential	TWC	27	100
Prototypical Cracks in Thermally Aged Centrifugally Cast Stainless Steel	4143-1	15.73	--	1.968	316SS CF8M	Internal Circumferential	SC	(d)	(d)
	4143-2	12	160	1.312	SA351 CF8M	Internal Circumferential	SC	50	67
	4143-3	12	160	1.312	SA351 CF8M	Internal Circumferential	SC	50	67
	4143-4	12	160	1.312	SA351 CF8M	Internal Circumferential	SC	50	67

(a) Tests conducted March 1, 1987 to September 30, 1988. Initial crack condition = sharp machine notch (radius of 0.005 inch or less); test temperature = 550 F; loading method = pressure and bending.

(b) SS = Stainless Steel.

(c) SC = Surface Crack; TWC = Through-Wall Crack.

(d) To be determined.

2.1 Circumferentially Through-Wall-Cracked Pipe in Pure Bending

(F. Brust, M. Nakagaki, P. Scott, R. Olson and G. Wilkowski)

The objective of this effort is to develop experimental data and evaluate available limit-load analyses and J-estimation schemes for the simplest of the circumferentially cracked pipe geometries, a through-wall crack. One such limit-load analysis method is the net-section-collapse method. This approach is of particular interest since it is currently used in several internationally accepted criteria as a means of evaluating postulated cracks in nuclear piping systems. A screening criterion validated by Degraded Piping Program experiments has been presented. It allows assessment of those pipe geometry and material toughness conditions for which the net-section-collapse method underpredicts actual failure loads, as opposed to those for which it overpredicts failure loads.

Since the last semiannual report, a new topical report has been written concerning this work:

> "Approximate Methods for Fracture Analyses of Through-Wall-Cracked Pipes", F. W. Brust, NUREG/CR-4853, February 1987.

The key aspects of this report are included in the summary below. Other topical reports resulting from efforts reported in this section are

> "NRC Leak-Before-Break (LBB.NRC) Analysis Method for Circumferentially Through-Wall Cracked Pipes Under Axial Plus Bending Loads", R. Klecker, F. W. Brust, and G. M. Wilkowski, NUREG/CR-4572, May 1986.
>
> "An Experimental and Analytical Assessment of Circumferential Through-Wall-Cracked Pipes Under Pure Bending", P. M. Scott and F. W. Brust, NUREG/CR-4574, September 1986.

2.1.1 Summary of Results

The analysis of circumferentially through-wall-cracked pipe is an essential part of the overall understanding of the behavior of circumferential cracks in general. Whether or not such a crack is stable or propagates to a double-ended rupture under a given loading system is essential to predicting whether a defect will leak before it breaks. Two analysis methods have been found useful for analyzing through-wall cracks: limit-load analyses and EPFM methods based on the J-integral. The progress in validating these methods for through-wall-cracked pipe is summarized in this section of the report.

One objective of this effort is to evaluate available limit-load analyses for circumferentially through-wall-cracked pipes subjected to pure bending. One useful limit-load analysis technique is the net-section-collapse analysis. The net-section-collapse analysis was originally developed as part of Electric Power Research Institute (EPRI) project RP-585 (Ref. 2.1.1). It is a simple,

straightforward analysis procedu frequently used to assess the load-carrying capacity of cracked nuclear piping. The net-section-collapse analysis is of particular interest as a means of evaluating postulated cracks in nuclear piping systems. For example, NUREG-0313 Revision 2 (Ref. 2.1.2) and IWB-3640 of the ASME Code (Ref. 2.1.3) use this analysis procedure to assess circumferential cracks in stainless steel base metals and nonflux stainless steel weld metals. The use of this method is predicated on the assumption that nuclear piping materials are tough enough to assure that gross yielding of the net section occurs prior to failure, regardless of pipe size, pipe strength, or crack size.

Pipe Fracture Experiments and Limit-Load Analyses

Experimental data generated as part of this program indicate that gross yielding of the net section may not always occur prior to the attainment of maximum load. For example, for one large-diameter (42-inch [1,067-mm]) stainless steel through-wall-cracked pipe experiment, the maximum stress was only 58.4 percent of the predicted net-section-collapse stress. The reason for overpredicting the failure stress appears to be that the maximum load occurred before the pipe section containing the crack became fully plastic.

To separate the cases in which net-section-collapse conditions are met (fully plastic) from those in which they are not (contained plasticity), a relatively simple screening criterion has been developed and applied (Refs. 2.1.4, 2.1.5, 2.1.6). In this criterion, a simple Irwin-type model was used to estimate the size of the plastic zone ahead of the crack tip. When the plastic zone becomes equal to the tensile ligament (that is, the distance from the crack tip to the neutral axis), it is assumed that fully plastic conditions have been reached.

Experimental data from this program, as well as programs conducted at David Taylor Research Center (DTRC) (Ref. 2.1.7), the Naval Academy (Ref. 2.1.8), and Battelle for EPRI (Ref. 2.1.9), were used to assess this plastic-zone screening criterion (PZSC). Table 2.1.1 presents a comparison of the experimental load at crack initiation and the maximum experimental load with the predicted net-section-collapse failure load. Figure 2.1.1 shows the experimental load at crack initiation relative to the predicted net-section-collapse load as a function of a dimensionless plastic-zone parameter for circumferentially through-wall-cracked pipe in bending. These data show a well-defined experimental trend curve. Figure 2.1.1 also shows a trend curve representing the ratio of the maximum experimental load to the predicted net-section-collapse load as a function of the same dimensionless plastic-zone parameter. If the dimensionless plastic-zone parameter is greater than 1.0, fully plastic conditions exist and both the load at crack initiation and the maximum load are close to the predicted net-section-collapse load. However, if the dimensionless plastic-zone parameter is less than 1.0, Figure 2.1.1 indicates that contained plasticity exists and that the net-section-collapse load overpredicts both the experimental load at crack initiation and the maximum load.

Table 2.1.1 Comparison of crack initiation loads and maximum loads from experimental results for through-wall-crack pipe experiments with maximum loads predicted by net-section-collapse analysis.

Reference Number	Program	Experiment Number	Pipe Diameter		Wall Thickness		Load at Crack Initiation (P_i)		Maximum Experimental Load (P_{max})		Predicted Limit Load (P_L) [a]		Predicted Limit Load (P_L) [b]		P_i/P_L [a]	P_i/P_L [b]	P_{max}/P_L [a]	P_{max}/P_L [b]
			inch	[mm]	inch	[mm]	pounds	[kN]	pounds	[kN]	pounds	[kN]	pounds	[kN]				
1	Degraded Piping	4111-1	4	(107)	0.35	(8.9)	16,300	(72.5)	19,850	(88.3)	17,630	(78.5)	18,720	(83.3)	0.925	0.871	1.126	1.060
2	"	4111-2	28	(711)	0.93	(23.6)	89,000	(396)	131,600	(586)	186,570	(830)	204,880	(912)	0.477	0.426	0.705	0.642
3	"	4111-3	42	(1,067)	0.28	(7.1)	67,200	(299)	99,600	(443)	136,100	(606)	170,600	(759)	0.494	0.394	0.732	0.584
4	"	4111-4	42	(1,067)	0.625	(15.9)	161,300	(718)	291,500	(1300)	--	--	416,310	(1850)	--	0.387	--	0.700
5	BCL/EPRI (Ref. 2.1.9)	1T	2	(51)	0.237	(6.0)	3,950	(17.6)	3,995	(17.8)	3,215	(14.3)	3,970	(17.7)	1.229	0.995	1.243	1.006
6	"	1T	4	(102)	0.354	(9.0)	13,900	(61.7)	13,900	(62.1)	12,450	(55.4)	15,370	(68.4)	1.114	0.902	1.120	0.908
7	"	8T	16	(406)	1.03	(26.2)	50,900	(227)	53,800	(240)	44,340	(197)	58,900	(262)	1.149	0.864	1.214	0.914
8	OTMSROC (Ref. 2.1.7)	7	8	(203)	0.54	(13.7)	89,500	(398)	92,500	(412)	104,270	(464)	112,700	(502)	0.859	0.794	0.888	0.821
9	"	14	8	(203)	0.573	(14.6)	157,500	(701)	175,600	(781)	198,500	(883)	215,100	(957)	0.793	0.732	0.884	0.816
10	Degraded Piping	4131-5	6	(152)	0.549	(13.9)	13,200	(58.8)	16,700	(74.3)	15,830	(70.4)	15,460	(68.8)	0.834	0.854	1.055	1.080
11	"	4131-7	10	(254)	0.719	(18.3)	23,300	(104)	31,700	(141)	38,240	(170)	45,000	(200)	0.609	0.518	0.829	0.704
12	"	4141-1	6	(152)	0.562	(14.3)	13,800	(61.3)	16,600	(73.3)	19,680(c)	(87.6)(c)	25,500(d)	(113)(d)	0.701(c)	0.540(d)	0.842(c)	0.649(d)
13	"	4141-3	16	(406)	1.03	(26.2)	21,300	(94.9)	41,500	(185)	54,630(c)	(243)(c)	70,820(d)	(315)(d)	0.390(c)	0.301(d)	0.760(c)	0.586(d)
14	USNA (Ref. 2.1.8)	P3	4	(102)	0.237	(6.0)	9,700	(43.2)	12,050	(53.6)	--	--	18,680(e)	(83.1)(e)	--	0.519(e)	--	0.645(e)
15	"	P9	4	(102)	0.237	(6.0)	8,600	(38.3)	10,720	(47.7)	--	--	15,870(e)	(70.6)(e)	--	0.542(e)	--	0.675(e)
16	"	P11	4	(102)	0.237	(6.0)	10,000	(44.5)	11,270	(50.2)	--	--	15,370(e)	(68.4)(e)	--	0.651(e)	--	0.733(e)
17	Degraded Piping	4111-5	28	(711)	1.189	(30.2)	105,740	(471)	139,330	(620)	214,000(c)	(952)(c)	260,470(f)	(1159)(f)	0.494(c)	0.406(f)	0.651(c)	0.535(f)
18	"	4111-6	36	(914)	2.868	(72.8)	510,000	(2270)	787,000	(3500)	852,700	(3790)	860,500	(3830)	0.598	0.593	0.923	0.915
19	"	4141-5	6	(152)	0.555	(14.1)	10,400	(46.3)	13,600	(60.5)	18,260(c)	(81.3)(c)	19,780(d)	(88.0)(d)	0.570(c)	0.526(d)	0.745(c)	0.688(d)

(a) Flow Stress = $3S_m$.

(b) Flow Stress = $1.15(\sigma_y + \sigma_u)/2$.

(c) Using $3S_m$ for base metal.

(d) Using weld metal properties.

(e) Author did not report a yield or ultimate strength. Only the flow stress was reported.

(f) Using weld metal properties reported in Reference 2.1.10.

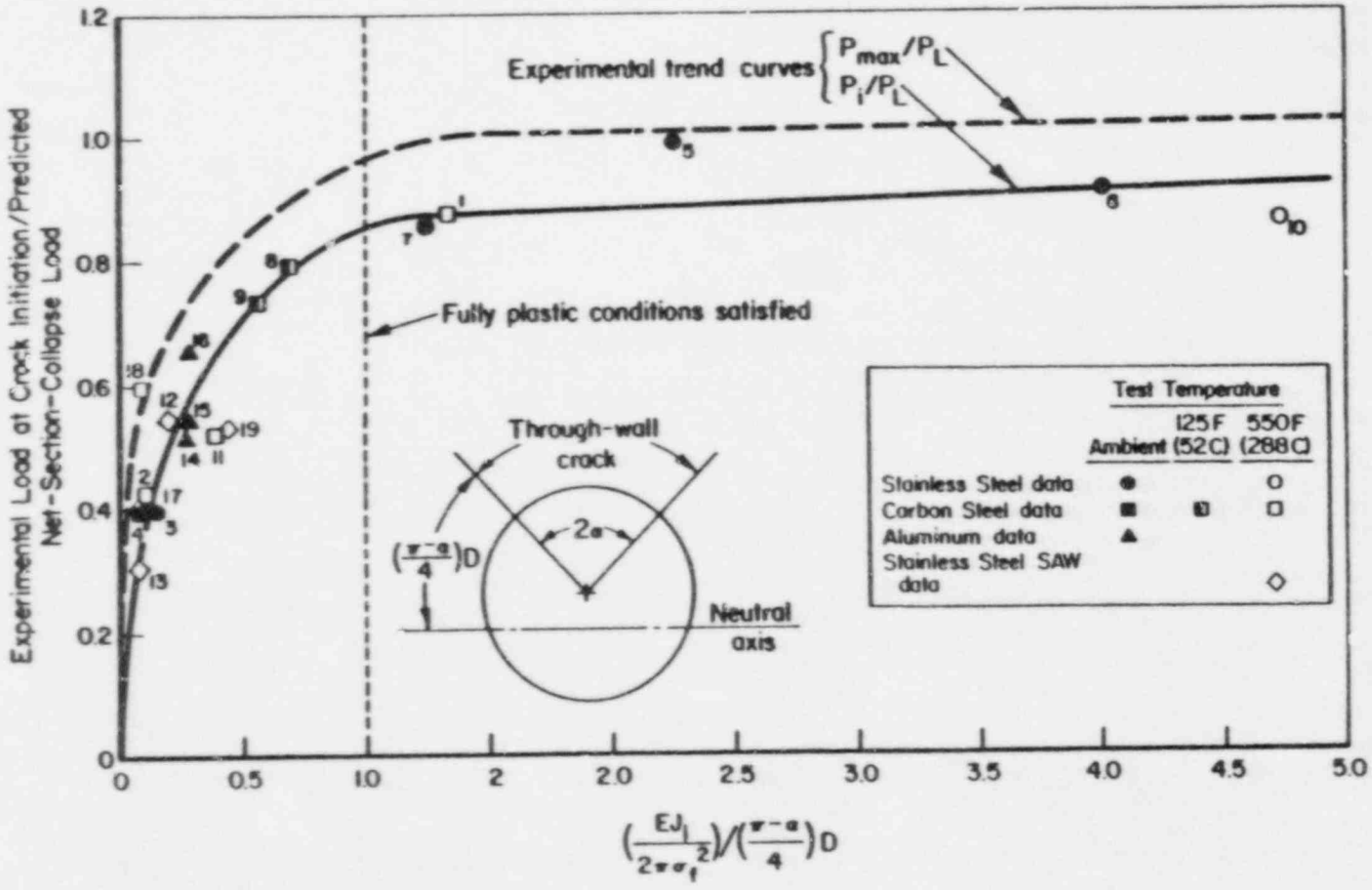

Figure 2.1.1 Ratio of load at crack initiation to predicted net-section-collapse load as a function of a dimensionless plastic-zone size parameter. [Flow stress = $1.15(\sigma_y + \sigma_u)/2$.]

SA-12/87-F2.1.1

When simple limit-load techniques are not adequate (for example, when contained plasticity exists), one must rely on other methods of analysis, such as EPFM. Such techniques focus on the J-integral. The J-integral can be used in an appropriate analytical expression to predict both the load at crack initiation and the maximum load (that is, the failure load).

J-Estimation Scheme Analyses

Evaluating the fracture behavior of through-wall-cracked pipes subjected to bending loads is a formidable task. When a cracked pipe is subjected to bending loads, plastic deformation occurs at the crack tips. Because of this nonlinear material behavior, precise theoretical closed-form solutions to the problem are not available. Such numerical techniques as the finite element method are required to predict accurately the fracture behavior of piping system components. However, because of the cost and time requirements necessary for finite element analyses, simple engineering estimation schemes are often employed.

For through-wall-cracked pipes subjected to bending loads, five predictive J-estimation schemes are available:

1. EPRI/GE (Ref. 2.1.10)
2. NUREG/CR-3464 (Ref. 2.1.11)
3. LBB.NRC (Ref. 2.1.12)
4. LBB.BCL1 (Ref. 2.1.13)
5. LBB.BCL2 (Ref. 2.1.14).

Detailed descriptions of each method may be found in the cited references. In addition, detailed discussions of the accuracy of all of these methods may be found in References 2.1.4, 2.1.5, 2.1.6, and 2.1.14.

In summary, when deformation J is used, all of the methods tend to underpredict crack initiation and maximum loads when compared with experimental data. This is the case for stainless and carbon steel pipes at room temperature and at 550 F (288 C) and for pipes ranging in diameter from 2 to 42 inches (50.8 to 1067 mm). The results cited in References 2.1.4, 2.1.5, 2.1.6, and 2.1.13 suggest that, when using the J_D-R curve, the EPRI/GE method tends to give the lowest predicted loads and displacements, whereas the LBB.NRC, LBB.BCL1, and LBB.BCL2 methods seem to be more accurate.

Additional work has been carried out on the use of J-estimation schemes for predicting load versus load-line displacement for through-wall-cracked pipes under bending. Two basic problems are associated with the use of these J-estimation schemes.

1. All estimation schemes relate a far-field moment to a far-field rotation. Certain assumptions are necessary to predict the load-line displacement from the rotations so that it can be compared with the experimental data from the four-point bend pipe experiment. The

experimental data from the four-point bend test is usually in the form of load versus load-point displacement.

2. Fracture analyses based on the J-integral become inherently invalid after a small amount of crack growth.

In addition to these two problems, many assumptions are involved in developing the J-estimation schemes. Some of the major assumptions are (1) modeling of the material stress-strain curve, (2) choice of J_D-R or J_M-R curves, and (3) extrapolation of J-R curves to larger amounts of crack growth. Also, cracked pipe experiments have shown that crack behavior is not always consistent with theory. For example, cracked pipes may ovalize under bending loads, wall thinning may occur in the vicinity of the crack, material property discontinuities (such as at weld locations) may be present, crack propagation may be affected by crack instabilities caused by dynamic strain aging (DSA), and/or the crack may grow out of the circumferential plane.

Because these factors cannot be precisely accounted for, a somewhat empirical but conservative estimation procedure was adopted. For licensing purposes, margins that include postulated cracks to compensate for the various uncertainties must be incorporated in an overall evaluation of a pipe or piping system. The results suggest that J-estimation techniques can be used to give conservative but reasonably accurate predictions of the load versus displacement relationship of a through-wall-cracked pipe subjected to bending. When using the deformation J-R curve (J_D-R), the most accurate analyses that still underpredicts the experimental results are the LBB.BCL1 and LBB.BCL2 methods. The EPRI/GE method tends to give the least accurate but the most underpredictive results when the J-deformation resistance curve is used in the analysis.

The use of a modified J-R curve (J_M-R) tends to give more accurate predictions of the load-displacement relationship than does the deformation J-R curve. However, underpredictive results cannot always be assured for the NUREG/CR-3464, LBB.NRC, LBB.BCL1, and LBB.BCL2 analyses. The J_M-R curve, when used in conjunction with the EPRI/GE estimation scheme, appears to give more accurate predictions of load versus displacement in through-wall-cracked pipes subjected to four-point bending.

Finite Element Analyses

In the absence of precise theoretical closed-form solutions, the most accurate analytical technique for determining the failure loads of elastic-plastic materials containing cracks is generally believed to be the finite element analysis. However, this technique is prohibitively expensive for routine analyses because of the need for extensive numerical computations requiring much computer capacity and time. Hence, finite element analysis is reserved for solving certain classes of problems and for establishing and validating J-estimation schemes.

To provide a benchmark for the accuracy of finite element analyses as applied by various research groups, a finite element round-robin was conducted by Battelle and the NRC. The purpose of this round-robin was to assess the differences in results between various participants throughout the world. Two problems were analyzed, the compact (tension) [C(T)] specimen and a through-wall-cracked pipe. In general, the solutions by the different participants examining C(T) specimens were very close for computed loads and the J-integral. For the problem of through-wall-cracked pipe, the predictions via the finite element method were reasonably consistent among the various participants, although each tended to underpredict the loads past crack initiation. Hence, finite element analyses of through-wall-cracked pipes appear to be in need of some improvement. A complete discussion of the round-robin results is found in Reference 2.1.15, and is reviewed in Section 3.5.

2.1.2 Discussion of Circumferential Through-Wall-Cracked Pipe Bending Efforts

Prior to the start of this program, the net-section-collapse analysis was believed to be generally applicable to nuclear piping. In many cases this is true. The efforts in this program involved development of experimental data to determine the accuracy of this application. From this, the PZSC evolved. This method shows in a simple manner when net-section collapse conditions are satisfied and when they are not, and hence when EPFM analyses are needed. A statistically based simplified plastic-zone criterion was subsequently developed, as described in Section 4 of the last semiannual report (Ref. 2.1.16). This is an easy method for estimating the maximum load under confined plasticity conditions. It showed that the size of the pipe is as important as the toughness of the material. The R6 analysis, another method for predicting loads, can be applied to both crack initiation and maximum load. In principle these two methods are similar.

J-estimation schemes for circumferentially through-wall-cracked pipe also have evolved considerably since the start of this program. The NUREG/CR-3464 approach evolved into the LBB.NRC analysis method by including the strain hardening of the material. The LBB.BCL methods were subsequently developed in this program to eliminate the mixing of an approach based on plastic-zone correction with one using power-law hardening assumptions of deformation plasticity. The LBB.BCL1 method does this by using the EPRI/GE h_3 deformation function to calculate the pipe rotation.

The LBB.BCL2 method eliminates the theoretical concerns by using an engineering approach to account for the rotation of the pipe. These methods are more complicated than the simple EPRI/GE method, but give more accurate predictions. All of these methods are included in the NRCPIPE Code (see Section 3.4 of this report).

Some important aspects worthy of further evaluation are the verification of the current data trends, specifically the PZSC and J-estimation schemes, with additional larger-diameter prototypical pipe experiments.

A second important aspect is that most of the pipe experiments used in the analyses efforts involved through-wall cracks that were 37 percent of the pipe

circumference. Since this crack length was sufficient so that the pipe did not experience general yielding, the η-factor analysis could be readily used to calculate J-R curves from pipe test data. In addition, these data could also be used to assess the J-estimation schemes that are used to predict loads and displacements. Additional data for different crack sizes would be of value to check the analyses and pipe ovalization effects.

Finally, additional data are needed to assess an ovalization correction factor for through-wall-cracked pipe. Such a correction factor was developed in a past EPRI program at Battelle (Ref. 2.1.9). This program tested 4-inch-(102-mm-) diameter pipe with cracks of different lengths. From this, an empirical ovalization correction factor was developed as a function of through-wall-crack length. What remains is to assess the effect, if any, of the pipe R/t ratio on this correction.

References for Section 2.1

2.1.1 Kanninen, M. F., and others, "Mechanical Fracture Predictions for Sensitized Stainless Steel Piping with Circumferential Cracks", EPRI NP-192, September 1976.

2.1.2 Hazelton, W. S., "Technical Report on Material Selection and Processing Guidelines for BWR Coolant Pressure Boundary Piping", Draft Report, NUREG-0313 Rev. 2, June 1986.

2.1.3 "Evaluation of Flaws in Austenitic Steel Piping" (Technical basis document for ASME IWB-3640 analysis procedure), prepared by Section XI Task Group for Piping Flaw Evaluation, EPRI Report NP-4690-SR, April 1986.

2.1.4 Wilkowski, G. M., and others, "Degraded Piping Program - Phase II", Semiannual Report, October 1984-March 1985, NUREG/CR-4082, Vol. 2, July 1985.

2.1.5 Wilkowski, G. M., and others, "Degraded Piping Program - Phase II", Semiannual Report, April 1985-September 1985, NUREG/CR-4082, Vol. 3, March 1986.

2.1.6 Wilkowski, G. M., and others, "Degraded Piping Program - Phase II", Semiannual Report, October 1985-March 1986, NUREG/CR-4082, Vol. 4, September 1986.

2.1.7 Vassilaros, M. G., and others, "J-Integral Testing Instability Analysis for 8-Inch-Diameter ASTM A106 Steel Pipe", U.S. David W. Taylor Naval Ship Research and Development Laboratory, NUREG/CR-3740, April 1984.

2.1.8 Joyce, J. A., "Instability Testing of Compact and Pipe Specimens Utilizing a Test System Made Compliant by Computer Control", ASTM STP 803, 1983, pp. II-348 to II-463.

2.1.9 Kanninen, M. F., and others, "Instability Predictions for Circumferentially Cracked Type 304 Stainless Steel Pipes Under Dynamic Loading", Final Report on EPRI Project T118-2, EPRI Report Number NP-2347, April 1982.

2.1.10 Kumar, V., and others, "Advances in Elastic-Plastic Fracture Analysis", EPRI NP-3607, August 1984.

2.1.11 Paris, P. C., and Tada, H., "The Application of Fracture-Proof Design Methods Using Tearing Instability Theory to Nuclear Piping Postulating Circumferential Through-Wall Cracks", NUREG/CR-3464, September 1983.

2.1.12 Klecker, R., and others, "NRC Leak-Before-Break (LBB.NRC) Analysis Method for Circumferentially Through-Wall-Cracked Pipes Under Axial Plus Bending Loads", NUREG/CR-4572, May 1986.

2.1.13 Brust, F. W., "Approximate Methods for Fracture Analysis of Through-Wall-Cracked Pipe", NUREG/CR-4853, February 1987.

2.1.14 Scott, P. M., and Brust, F. W., "An Experimental and Analytical Assessment of Circumferential Through-Wall-Cracked Pipes Under Pure Bending", NUREG/CR-4574, September 1986.

2.1.15 Ahmad, J., and others, "Elastic-Plastic Finite Element Analysis of Crack Growth in Large Compact (Tension) and Circumferentially Through-Wall-Cracked Pipe Specimens - Results of the First Battelle/NRC Analysis Round-Robin", NUREG/CR-4573, October 1986.

2.1.16 Wilkowski, G. M., and others, "Degraded Piping Program - Phase II", Semiannual Report, April 1986-September 1986, NUREG/CR-4082, Vol. 5, April 1987.

2.2 Finite-Length, Internal Circumferentially Surface-Cracked Pipe in Pure Bending

(J. Ahmad, M. Nakagaki, V. Papaspyropoulos, P. Scott, G. Wilkowski, and F. Brust)

The objectives of this effort are to develop experimental data, determine when limit-load analyses are valid, and develop and verify an elastic-plastic analysis to predict the fracture behavior of finite-length, surface-cracked pipe when limit-load analyses are not valid. From the standpoint of an elastic-plastic analysis, two specific technical hurdles had to be overcome.

The first hurdle was the lack of an elastic-plastic J-estimation analysis to predict loads and displacements at crack initiation and maximum load. To overcome this problem, J-estimation methods for both thin-walled and thick-walled pipes were developed and presented in a topical report published since the last semiannual report:

> "Experimental and Analytical Assessment of Circumferentially Surface-Cracked Pipes Under Bending", P. M. Scott and J. Ahmad, NUREG/CR-4872, September 1986.

The results from this topical report are summarized in the following section.

The second technical hurdle was to evaluate the potential effects of geometry and crack orientation on the fracture resistance (J-R curve) of the material. To solve this, full-width-face-notched (tension) [FWFN(T)] specimens were fabricated from the pipes (see Section 3.1). This specimen type allows a crack to grow through the pipe thickness, and the specimen ligament is essentially in tension, just as the ligament of the surface crack in the pipe would be. The η-factor J-estimation scheme for this specimen is currently undergoing additional verification. The final results will be included in a future topical report.

2.2.1 Summary of Surface-Cracked Pipe Evaluations

This effort involved considerable interaction among pipe fracture experiments, laboratory specimen testing, and analytical fracture mechanics. All of these efforts have been completed; they are reported in detail in Ref. 2.2.1 and summarized below.

Material Characterization Efforts

The material characterization efforts involved standard testing, as noted in Section 3.1 of this report, as well as testing of FWFN(T) specimens. The FWFN(T) specimen was used to determine the crack growth resistance in the L-R direction that corresponds to the direction of crack growth for a circumferential surface crack. Section 3.2.1 of this report discusses the development of this specimen. Section 3.2.5 of this report discusses the analytical verification efforts of the J-estimation scheme for this specimen.

Pipe Fracture Experiments

The 19 pipe fracture experiments conducted in this effort are summarized in Table 2.2.1. The experiments involved carbon and stainless steel pipes with internal circumferential surface cracks. The bulk of the test matrix was designed to evaluate specifically the effect of the pipe radius-to-thickness ratio. Stainless steel and ferritic steel pipes were used, each in 6- and 16-inch (152- and 406-mm) nominal pipe diameter and each with three different R/t ratios. To evaluate the effect of the pipe R/t ratio, the dimensionless crack size was held constant at d/t = 0.66 and 2c/πD = 0.5. This reference crack size was chosen because it had been evaluated in some experiments from a previous EPRI program conducted at Battelle (Ref. 2.2.2). The test results are also reported in Table 2.2.1.

Assessment of Net-Section-Collapse Analysis, Plastic-Zone Screening Criterion, and the ASME IWB-3640 Analysis

Net-Section-Collapse Analysis

For the assessment of the net-section-collapse analysis, actual material property data were used. The ratio of the maximum experimental stress to the stress predicted by net-section-collapse analysis is compared with the pipe R/t ratio in Figure 2.2.1. As the pipe R/t ratio increases, the ratio of the maximum experimental stress to the stress predicted by net-section-collapse analysis decreases. This may result from the pipe's toughness, its ovalization, or both. To determine whether lower failure stresses resulted from toughness or ovalization, the PZSC, developed for through-wall-cracked pipe (Ref. 2.2.3), was modified slightly and used to separate ovalization effects from toughness effects. The data points for which the dimensionless plastic-zone parameter was greater than 1.0, and hence fully plastic conditions were developed, were used to define statistically an ovalization correction factor for pipe as a function of the pipe R/t ratio. This correction for the prediction of maximum load using the net-section-collapse analysis is given in Eq. 2.2.1a when $\sigma_f = 1.15(\sigma_y + \sigma_u)/2$

$$M_v = 1.222 - 0.0294(R_m/t), \qquad (2.2.1a)$$

and in Eq. 2.2.1b when $\sigma_f = (\sigma_y + \sigma_u)/2$

$$M_v = 1.403 - 0.0338(R_m/t). \qquad (2.2.1b)$$

For the case of combined pressure and bending, the following expression was postulated:

$$M_{pb} = 1 + [\sigma_b/(\sigma_a + \sigma_b)](M_v - 1) \qquad (2.2.2)$$

Table 2.2.1 Summary of test parameters and key experimental results for surface-cracked pipe experiments

(Page 1 of 2)

Reference Number	Experiment Number	Pipe Material	Outside Pipe Diameter, in (mm)	Thickness, in (mm)	Flaw Dimensions 2c/πD	Flaw Dimensions a/t	Pipe Pressure, psi (MPa)	Test Temperature, F (C)	Axial Membrane Stress (a), ksi (MPa)	Bending Stress at Crack Initiation (b), ksi (MPa)	Maximum Bending Stress (b), ksi (MPa)
1	4112-1	Stainless Steel	15.95 (405)	0.386 (9.8)	0.511	0.658	--	550 (288)	--	24.85 (171)	28.42 (196)
2	4112-2	Stainless Steel	6.59 (167)	0.276 (7.0)	0.502	0.634	--	550 (288)	--	27.61 (191)	32.65 (225)
3	4112-3	Stainless Steel	6.64 (169)	0.536 (13.6)	0.518	0.659	--	550 (288)	--	35.90 (248)	38.41 (265)
4	4112-4	Stainless Steel	6.63 (168)	0.885 (22.5)	0.442	0.653	--	550 (288)	--	47.27 (326)	48.84 (337)
5	4112-5	Carbon Steel	6.67 (169)	0.293 (7.4)	0.508	0.631	--	550 (288)	--	24.02 (166)	38.38 (265)
6	4112-6	Carbon Steel	6.59 (167)	0.582 (14.8)	0.503	0.680	--	550 (288)	--	40.12 (277)	47.52 (328)
7	4112-7	Carbon Steel	6.62 (168)	0.845 (21.5)	0.526	0.663	--	550 (288)	--	44.97 (310)	54.45 (376)
8	3S	Stainless Steel	4.50 (114)	0.355 (9.0)	0.500	0.594	--	72 (22)	--	63.86 (441)	65.29 (451)
9	10S	Stainless Steel	4.50 (114)	0.365 (9.3)	0.500	0.575	--	72 (22)	--	60.59 (418)	62.99 (435)
10	13S	Stainless Steel	16.28 (414)	1.040 (26.4)	0.588	0.660	--	72 (22)	--	48.12 (332)	62.51 (431)

Table 2.2.1 (Page 2 of 2)

Reference Number	Experiment Number	Pipe Material	Outside Pipe Diameter, in (mm)	Thickness, in (mm)	Flaw Dimensions 2c/πD	Flaw Dimensions a/t	Pipe Pressure, psi (MPa)	Test Temperature, F (C)	Axial Membrane Stress (a), ksi (MPa)	Bending Stress at Crack Initiation (b), ksi (MPa)	Maximum Bending Stress (b), ksi (MPa)
11	4141-2	Stainless Steel SAW(c)	6.58 (167)	0.584 (14.8)	0.500	0.642	2,200 (15.2)	550 (288)	6.20 (42.8)	23.24 (160)	23.99 (166)
12	4112-8	Carbon Steel	15.85 (403)	1.040 (26.4)	0.532	0.662	--	550 (288)	--	36.27 (250)	39.36 (272)
13	4131-2	Stainless Steel	6.63 (168)	0.529 (13.4)	0.521	0.709	3,550 (24.5)	550 (288)	11.12 (76.7)	19.84 (137)	21.08 (145)
14	4131-4	Carbon Steel	10.74 (273)	0.654 (16.6)	0.525	0.659	2,650 (18.3)	550 (288)	10.88 (75.1)	25.54 (176)	28.71 (198)
15	4131-6	Stainless Steel	6.25 (159)	0.563 (14.3)	0.535	0.690	--	550 (288)	--	36.56 (252)	37.19 (257)
16	4131-8	Carbon Steel	10.65 (271)	0.593 (15.1)	0.480	0.678	--	550 (288)	--	35.92 (248)	38.63 (267)
17	4141-4	Stainless Steel SAW(c)	16.28 (413)	1.031 (26.2)	0.500	0.670	1,600 (11.0)	550 (288)	6.32 (43.6)	24.86 (172)	25.05 (173)
18	4141-6	Stainless Steel SAW(d)	16.39 (416)	1.040 (26.4)	0.500	0.686	1,600 (11.0)	550 (288)	6.30 (43.5)	21.65 (149)	21.78 (150)
19	4112-9	Carbon Steel	15.94 (405)	0.500 (12.7)	0.535	0.662	--	550 (288)	--	29.30 (202)	35.63 (246)

(a) Based on thin-wall Barlow expressions using the outside radius, that is, $pr_o/2t$.
(b) Bending stress calculated using expression $(M)(D_o)/2I$ where $I = 0.0491\ (D_o^4 - D_i^4)$ as suggested in Articles NC3652 and NB3683 of the ASME Code for Class 1 piping systems.
(c) As welded stainless steel submerged-arc weld.
(d) Solution annealed stainless steel submerged-arc weld.

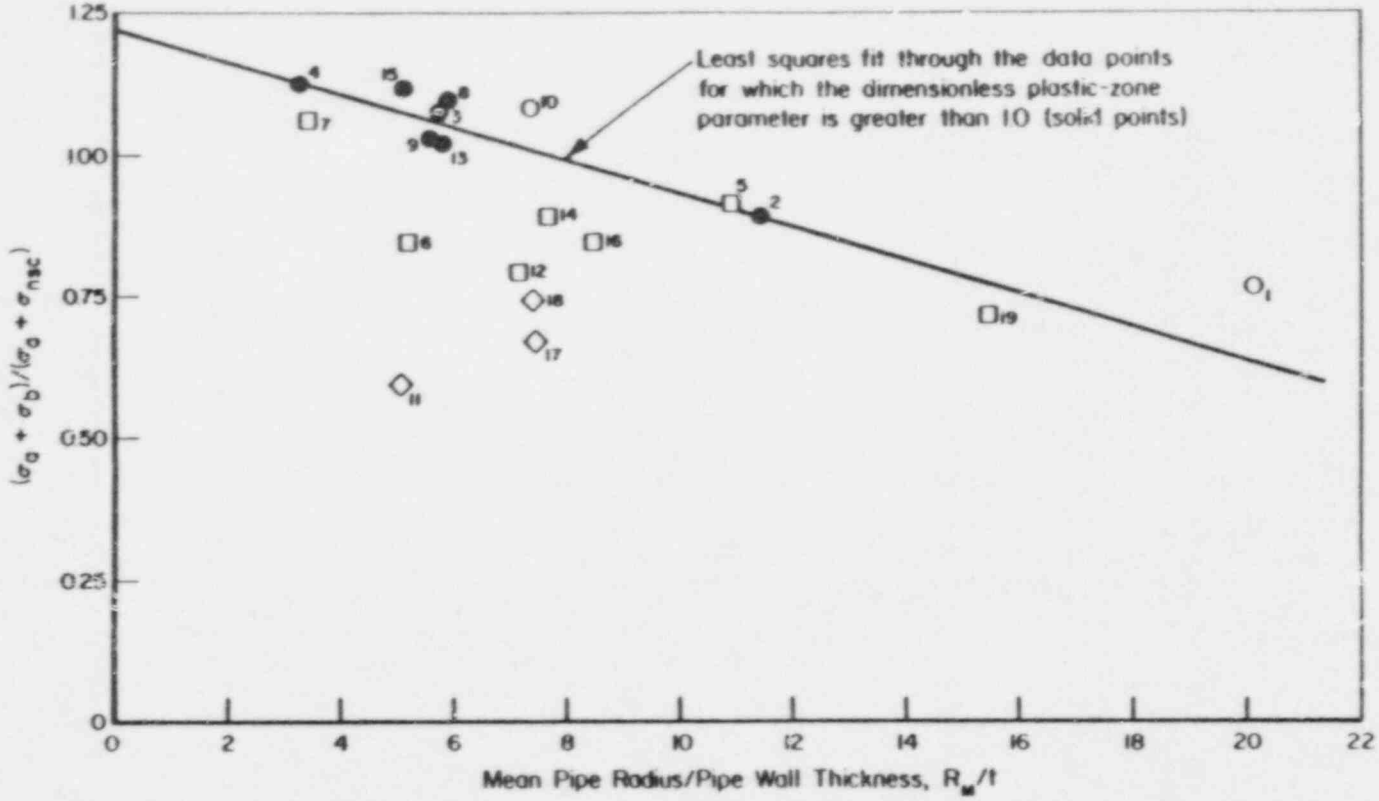

Figure 2.2.1 Ratio of the maximum experimental stress to the net-section-collapse stress as a function of the ratio of the mean pipe radius to the pipe wall thickness. [Flow stress = $1.15(\sigma_y + \sigma_u)/2.$]

T48-72-F2.2

Note that this hypothesized correction assumes that the ovalization effect decreases linearly as axial stress increases.

An important point about surface crack ovalization corrections is that they are based on data for crack sizes where $2c/\pi D = 0.5$ and $d/t = 0.66$. The ovalization correction may be different for other crack sizes. Some additional work would be required to determine a generally applicable ovalization correction factor.

Plastic-Zone Screening Criterion

The above ovalization correction factor was then used with the limit-load analysis to assess the surface-cracked-pipe PZSC. The results are shown in Figures 2.2.2 and 2.2.3. Figure 2.2.2 demonstrates that, in general, the load at crack initiation for the surface-cracked pipe was very close to the maximum load. Figure 2.2.3 compares the surface-cracked-pipe data with the through-wall-cracked pipe data trend curve. From Figure 2.2.3 it can be seen that a surface-cracked pipe can have a lower toughness than a corresponding through-wall-cracked pipe and still reach limit-load conditions. This is an important point since the ASME IWB-3640 surface crack analysis procedure actually uses a toughness correction for flux welds based on a through-wall-cracked pipe analysis. Hence the IWB-3640 flux weld approach has an inherent safety factor for surface-cracked pipe.

A simplified plastic-zone fracture criterion has also been developed. This criterion is discussed in detail in Section 4.1 of Reference 2.2.5. The dimensionless plastic-zone parameter for this simplified criterion is much easier to use and define than the parameter shown in Figures 2.2.2 and 2.2.3. The physical crack dimensions are not needed for this simplified parameter. Figure 2.2.4 shows the ratio of the maximum experimental stress to the net-section-collapse stress as a function of this simplified dimensionless parameter.

Assessment of the ASME IWB-3640 Analysis

Stainless steel pipe data were used to assess the ASME IWB-3640 flaw evaluation criteria for stainless steel pipe (Ref. 2.2.4). Table 2.2.2 gives the comparisons of the experimental data with the IWB-3640 analysis procedure predictions. The safety factors in the ASME code procedure were not included in these comparisons. This comparison used the precise ASME stress analysis equations, and the flow stress was defined as $3S_m$. Note that, for the stainless steel submerged-arc weld (SAW) experiments, base metal S_m values were used in the definition of the flow stress. In addition, the predicted failure stresses were reduced by the Z-factor to account for the low-toughness flux weld. Both the IWB-3640 Source Equations and the simplified tables were evaluated. For the Source Equations, the average ratio of the experimental stress to the predicted stress was 1.272 with a standard deviation of 0.207; for the IWB-3640 tables, the average ratio of the experimental stress to the predicted stress was 1.65 with a standard deviation of 0.243. This shows that the ASME approach has an inherent safety factor for a case of cracks in

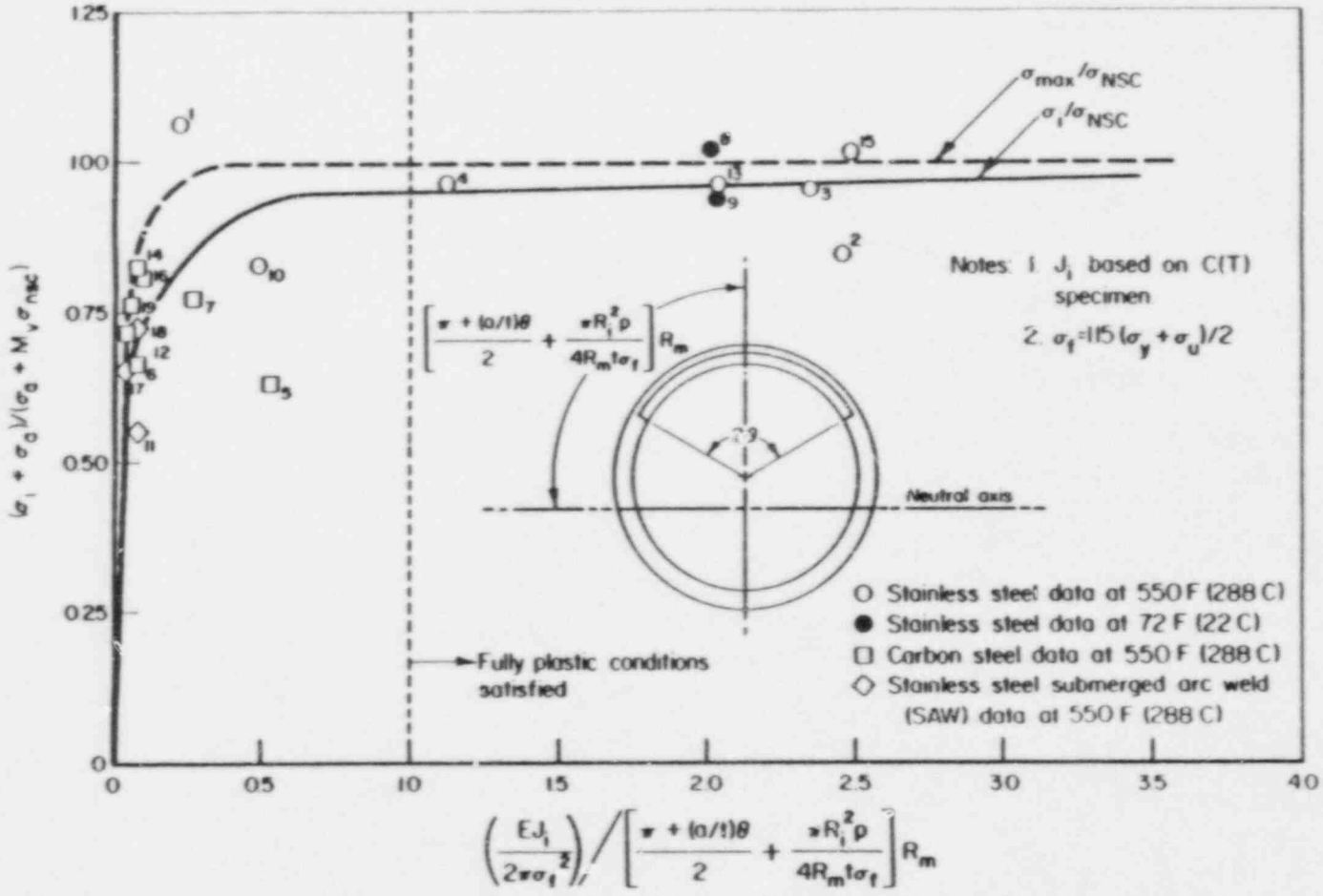

Figure 2.2.2 Ratio of crack initiation stress to net-section-collapse stress for surface-cracked pipe experiments as a function of the dimensionless plastic-zone size. [Flow stress = $1.15(\sigma_y + \sigma_u)/2$.]

T-4872-F2.4

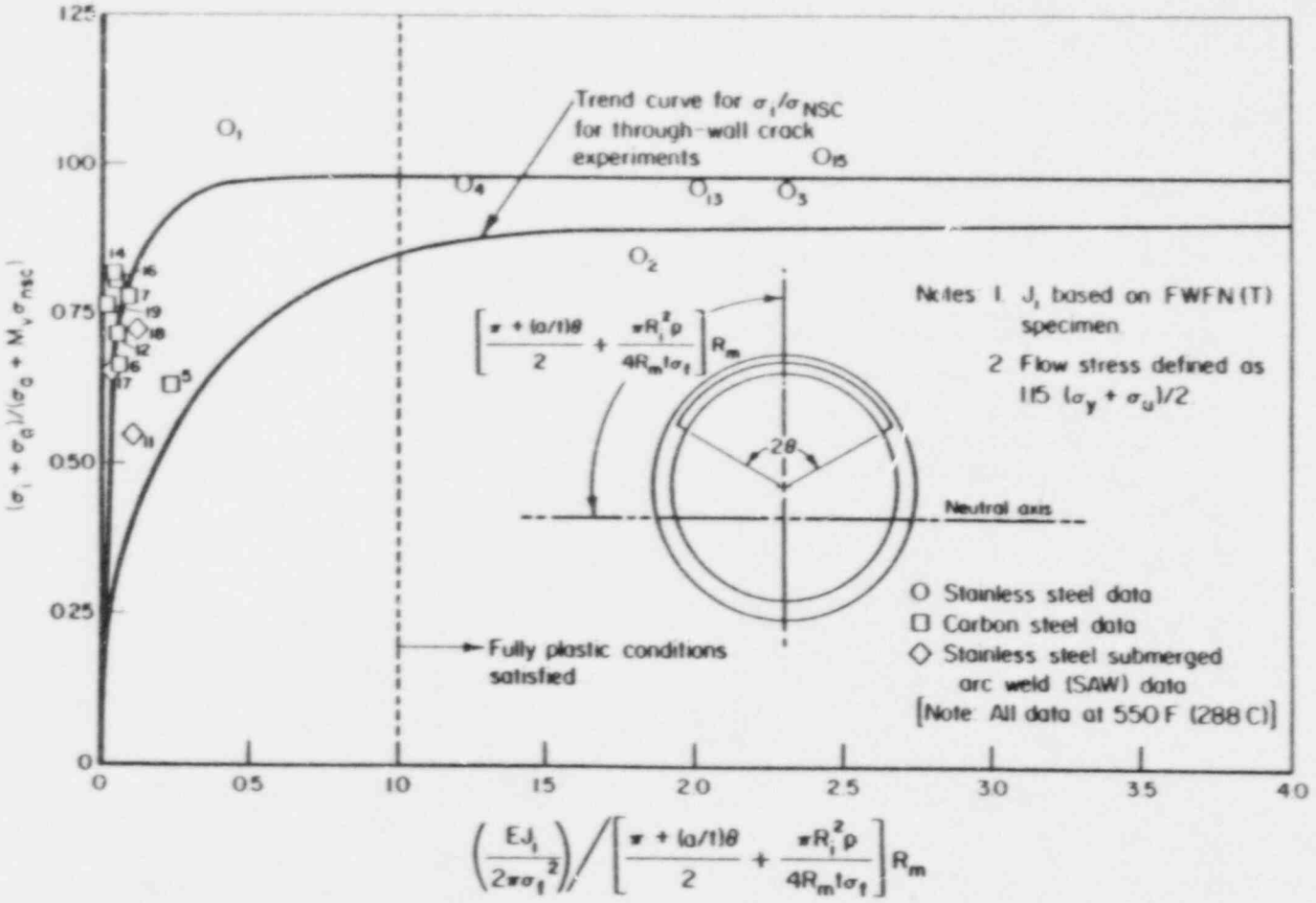

Figure 2.2.3 Ratio of crack initiation stress to net-section-collapse stress for surface-cracked pipe experiments as a function of the dimensionless plastic-zone parameter. [Note that the value of J_i used to calculate the dimensionless plastic-zone parameter is based on FWFN(T) specimen data. Flow stress = $1.15(\sigma_y + \sigma_u)/2$.]

SA-12/87-F2.2.3

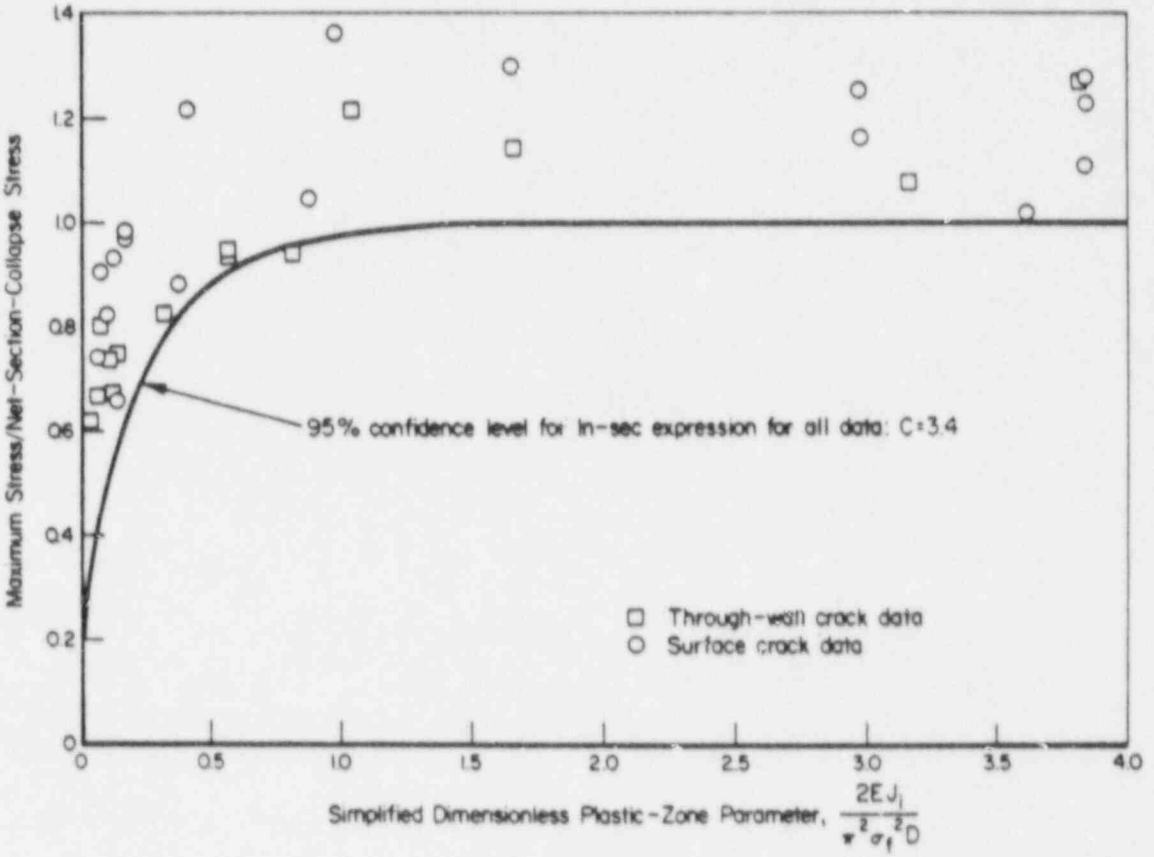

Figure 2.2.4 Compiled data using simplified dimensionless plastic-zone parameter and flow stress = $(\sigma_y + \sigma_u)/2$. Note: C is a curve-fitting parameter in the equation, $\sigma_m/\sigma_{nsc} = (2/\pi) \arccos [e^{-C(DPZP)}]$.

SA-12/86-F4.1.2

Table 2.2.2 Comparison of experimental results with IWB-3640 predictions for stainless steel surface-cracked pipe experiments (flow stress defined as $3S_m$ for base metal)

Experimental Reference Number	Outside Pipe Diameter, inch (mm)	Thickness, inch (mm)	Axial Membrane Stress (P_m)[a] ksi (MPa)	Maximum Bending Stress (P_b)[b] ksi (MPa)	IWB-3640 Predicted Failure Stress (σ_{IWB}) Using Source Equations	IWB-3640 Predicted Failure Stress (σ_{IWB}) Using Tables	$(P_m+P_b)/(P_m+\sigma_{IWB})$ Source Equations	$(P_m+P_b)/(P_m+\sigma_{IWB})$ Tables
1	15.95 (405)	0.386 (9.8)	--	28.42 (196)	28.50 (197)	20.48 (141)	1.00	1.39
2	6.59 (167)	0.276 (7.0)	--	32.65 (225)	36.30 (250)	27.70 (191)	0.90	1.18
3	6.64 (169)	0.536 (13.6)	--	38.41 (265)	34.36 (237)	24.88 (172)	1.12	1.54
4	6.63 (168)	0.885 (22.5)	--	48.84 (337)	37.41 (258)	32.87 (227)	1.31	1.49
8	4.50 (114)	0.355 (9.0)	--	65.69 (453)	45.54 (314)	37.67 (260)	1.44	1.74
9	4.50 (114)	0.365 (9.3)	--	62.99 (435)	46.77 (323)	39.33 (271)	1.35	1.60
10	16.28 (413)	1.040 (26.4)	--	62.51 (431)	38.38 (265)	29.36 (203)	1.63	2.13
11[c]	6.58 (167)	0.584 (14.8)	6.20 (42.8)	23.99 (166)	16.31 (113)	11.84 (82)	1.34	1.67
13	6.63 (168)	0.529 (13.4)	11.12 (76.7)	21.08 (145)	16.13 (111)	8.13 (56)	1.18	1.67
15	6.25 (159)	0.563 (14.3)	--	37.19 (257)	31.96 (221)	21.13 (146)	1.16	1.76
17[c]	16.28 (413)	1.031 (26.2)	6.32 (43.6)	25.05 (173)	14.99 (103)	10.25 (75)	1.47	1.89
18[c]	16.39 (416)	1.040 (26.4)	6.30 (43.5)	21.78 (150)	14.33 (99)	9.57 (66)	1.36	1.77

(a) $P_m = pD_o/4t$.
(b) $P_b = MD_o/2I$ where $I = 0.0491\ (D_o^4 - D_i^4)$ as suggested in Articles NC3652 and NB3683 of the ASME Code for Class I piping systems.
(c) Stainless steel submerged arc weld experiment. Base metal S_m value used in definition of flow stress. IWB-3640 predicted failure stresses reduced by the Z-factor to account for the low toughness flux weld.

stainless steel base metals and welds, and the safety factor is higher if the tables are used rather than the Source Equations. Of the pipe experiments evaluated, only one experiment - using a pipe whose yield strength approached the minimum value in the ASME code - had a maximum load below that predicted by IWB-3640 analysis. The higher values for the ratio of experimental to predicted stress were for pipe tests conducted at room temperature instead of 550 F (288 C). If only the high-temperature data are considered, then the average values are 1.20 and 1.60 for the IWB-3640 Source Equations and the tables, respectively.

Development of Finite-Length Surface Crack J-Estimation Schemes

J-estimation scheme solutions for a finite-length, internal circumferentially surface-cracked pipe did not exist prior to this effort. The existing approaches were either for a 360-degree circumferentially surface-cracked pipe (Ref. 2.2.6) or used a toughness correction based on a through-wall-cracked pipe correction on the net-section collapse analysis (Ref. 2.2.4). Perhaps the best available approach at that time for a finite-length surface-cracked pipe was the R6 method that interpolates between a linear elastic solution and a limit-load solution.

The J-estimation methods developed in this effort can be best described with the aid of Figure 2.2.5. As shown in Figure 2.2.5(a), a circumferential surface crack of depth "d" is assumed to exist in the pipe wall of thickness "t". The crack is located sufficiently far from the pipe ends. The pipe is subjected to an applied moment, M, and the rotation of one pipe end relative to the other is denoted by ϕ. The pipe section containing the crack is shown in Figure 2.2.5(b). The crack extends over an angle of 2θ at the pipe center. Although the present work assumes that the crack has a constant depth, this assumption is not necessary; other crack shapes can be accommodated in the development of the J-estimation scheme formulae. The angles ρ_n and ρ_{on} in Figure 2.2.4(b) define the location of the neutral axis. R_i and R_o are the inner and outer pipe radii, respectively, and b is the uncracked ligament length in the domain of $0 \leq \gamma \leq \theta$.

The pipe material's uniaxial stress-strain behavior is assumed to be elastic-plastic. The stress-strain behavior in the plastic range is assumed to be power-law hardening, as given in Eq. 2.2.3

$$\epsilon/\epsilon_o = \alpha(\sigma/\sigma_o)^n \qquad (2.2.3)$$

where σ_o is a reference stress (that is, the yield strength), n is the hardening exponent, and $\epsilon_o = \sigma_o/E$ (E is Young's modulus). In the analytic development, it is further assumed that the pipe deformations remain small compared with all the dimensions. Therefore, ovalization of the pipe section, often observed in the pipe experiments, is not included in the analysis modeling.

With the above assumptions, we now consider a plane normal to the circumferential plane at $\gamma < \theta$, with dimensions t by 2L as shown in Figure 2.2.5(c). The

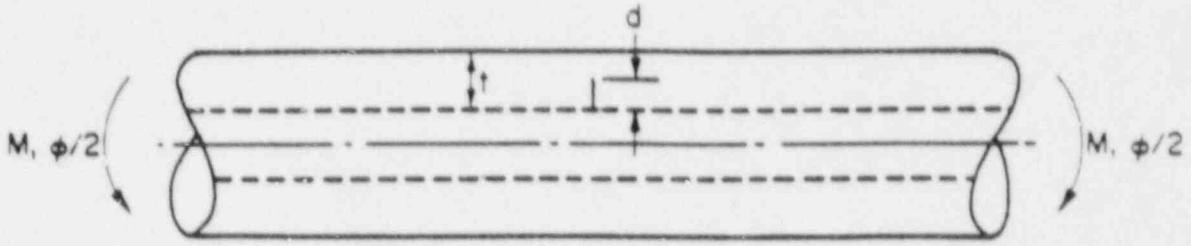

(a) Surface-cracked pipe under pure bending

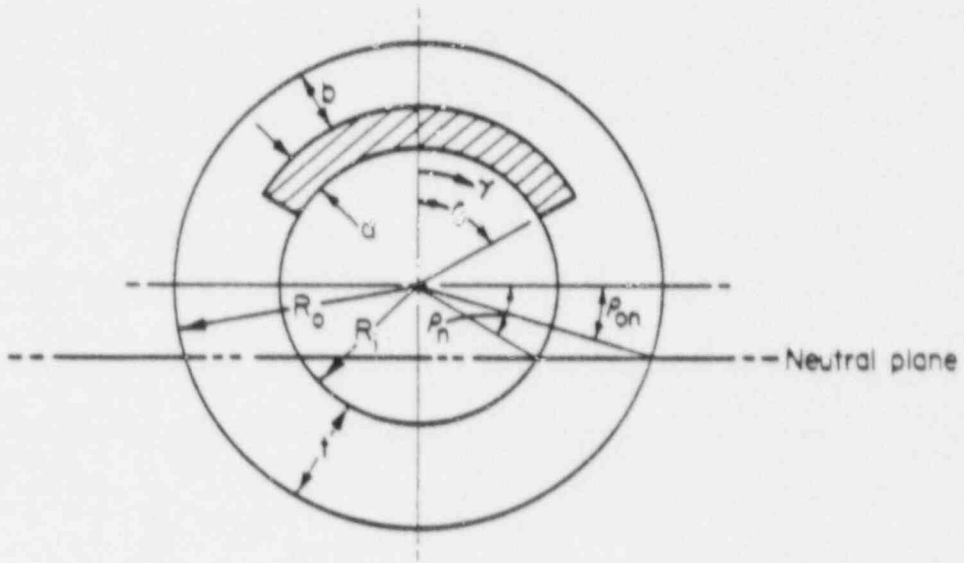

(b) Cross-section containing internal surface crack

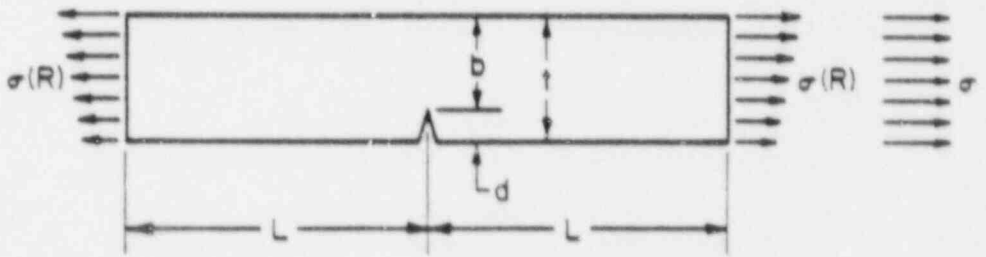

(c) Plane at $\gamma < \theta$, $L = Ct$

Figure 2.2.5 Geometry and loading of a pipe with an internal circumferential surface crack.

T-4872-F-3.1

length, L, is large enough so that the stress acting at the ends is the remote stress in the pipe wall caused by the applied global bending moment. Because the stress variation through the thickness is small, we can consider the plane as subjected to a uniform average stress of σ as shown.

At first glance, Figure 2.2.5(c) resembles an edge-notched panel subjected to uniform remote tension (for which a J-estimation formula can be found in Ref. 2.2.6). If such were the case, one could utilize the edge-cracked panel formula in developing an expression of J for the surface-cracked pipe. However, the stress distribution in the uncracked ligament of an edge-cracked panel is different from that in the surface-cracked pipe: in the edge-cracked panel, a significant bending component of stress contributes to J, but in the surface-cracked pipe, the bending component is restrained.

As an alternative, one can consider the section shown in Figure 2.2.5(c) as representing a plane from an axisymmetrically surface-cracked pipe subjected to remote uniform tensile stress (σ). For this geometry, that is, a 360-degree flaw in a pipe under tension, Reference 2.2.6 also provides a formula for J. In the present work, this J formula from Reference 2.2.6 was used to develop an expression of J for the surface-cracked pipe geometry of Figure 2.2.5 (see Appendix B of Ref. 2.2.1 for details). Depending on whether the pipe can be considered as a thin (large R_o/t) or a relatively thick (small R_o/t) shell, two expressions for J are derived. In the analysis method for thin-walled pipe, SC.TNP in the NRCPIPE Code, the thin-shell formula for J is used. The formula corresponding to relatively small R_o/t ratios is used in the analysis method for thick-walled pipe, SC.TKP. In the following, the J-estimation methods corresponding to SC.TNP and SC.TKP are outlined.

J-Estimation in SC.TNP

Step 1.1: For the given material, find the Ramberg-Osgood constants α, n, σ_o, and ϵ_o of Eq. 2.2.3.

Step 1.2: For the given n and the t/R_i and a/t ratios, find h_1 and h_3 values from the EPRI/GE handbook (Ref. 2.2.5) solution for axisymmetrically surface-cracked pipe under remote tension. Also, using the above values and the crack angle θ, find H_n and ρ_n from Tables B-1 to B-60 in Appendix B of Reference 2.2.1.

Step 1.3: Depending upon whether applied moment (M) or applied rotation (ϕ) is prescribed, use one of the following equations to find σ:

$$\sigma = \frac{M}{4 R_m^2 t H_n} \left(\frac{\sin \rho_n + \cos \gamma}{1 + \frac{dh_3}{2t} \left(\frac{\sqrt{3}}{2} \frac{t}{b}\right)} n \right)^{1/n} \qquad (2.2.4)$$

$$\sigma = \sigma_o \left[\left(\frac{\phi \, R_m}{2a \, \varepsilon_o \, t} \right) \right]^{1/n} \left[\frac{\sin \rho_n + \cos \gamma}{1 + \frac{dh_3}{2t} \left(\frac{\sqrt{3}}{2} \frac{t}{b} \right)^n} \right]^{1/n} \qquad (2.2.5)$$

where γ defines the location along the crack-front.

Also, using Eqs. 2.2.4 and 2.2.5, find M or ϕ, as

$$\phi = \frac{2a \, \varepsilon_o \, t}{R_m \, (4t \, \sigma_o \, H_n \, R_m^2)^n} \cdot M^n \qquad (2.2.6)$$

Step 1.4: Assuming J ≈ Jp, find J using the following equation:

$$J_p = a \, \varepsilon_o \, \sigma_o \, (1 - \frac{d}{t}) \, d \, h_i \, (\frac{\sqrt{3}}{2} \cdot \frac{t}{b} \cdot \frac{\sigma}{\sigma_o})^{n+1} \qquad (2.2.7)$$

J-Estimation in SC.TKP

Step 2.1: Same as Step 1.1.

Step 2.2: Same as Step 1.2, but instead of Tables B.1 to B.60 in Appendix B of Reference 2.2.1, use Tables B.61 to B.120 to find ρn and G_n. Then, find

$$G_n = \bar{G}_n \, (t)^{(\frac{3n+1}{n})} \qquad (2.2.8)$$

Step 2.3: Depending upon whether applied moment or applied rotation is prescribed, use one of the following equations to find σ:

$$\sigma = \frac{M}{4G_n} \left(\frac{R_i \sin \rho_n + R_c \cos \gamma}{1 + \frac{dh_3}{2t} \left(\frac{\sigma_o k}{P_o} \right)^n} \right)^{1/n} \qquad (2.2.9)$$

$$\sigma = \sigma_o \left(\frac{\phi}{2\alpha\,\varepsilon_o\,t}\right)^{1/n} \left[\frac{R_i \sin\sigma_n + R_c \cos\gamma}{1 + \frac{dh_3}{2t}\left(\frac{\sigma_o k}{P_o}\right)^n}\right]^{1/n} \tag{2.2.10}$$

where, $k = \pi (R_o^2 - R_i^2)$ (2.2.11)

$$R_c = R_i + d \tag{2.2.12}$$

$$P_o = \frac{2}{\sqrt{3}} \pi (R_o^2 - R_c^2)\,\sigma_o \tag{2.2.13}$$

Also, M or ϕ can be found using the following equation:

$$\phi = \frac{2\alpha\,\varepsilon_o\,t}{(4\,G_n\,\sigma_o)^n} \cdot M^n \tag{2.2.14}$$

Step 2.4: Assuming $J = J_p$, find J using the following equation:

$$J_p = \alpha\,\varepsilon_o\,\sigma_o\,(1 - \tfrac{d}{t})\,d\,h_1\,\left(\frac{k\sigma}{P_o}\right)^{n+1} \tag{2.2.15}$$

Pipe Fracture Analyses Using the J-estimation Schemes

The J-estimation methods described above were used in calculating the load at crack initiation and the maximum load in pipe fracture Experiments 4112-1 4112-2, 4112-3, 4112-5, 4112-6, 4112-8, 4112-9, 4115-1, 4115-7, 4131-6, and 4131-8. The pipe material, geometry, flaw geometry, and test conditions for each of these experiments are summarized in Table 2.2.1. All these experiments were performed at 550 F (288 C), and the pipe specimens were loaded in four-point bending.

The two pieces of information that were required to perform the analyses but are not contained in Table 2.2.1 are the materials' uniaxial stress-strain curves and the J-resistance (J-R) curves at 550 F (288 C). Both the choice of stress-strain curve-fitting constants and the choice of an appropriate J-R curve can significantly affect the accuracy of the analysis results (for example, see Ref. 2.2.7). Eqs. 2.2.7 and 2.2.15 show that a relatively small change in the strain-hardening exponent, n, can significantly affect the calculated value of J. Therefore, accurate determination of n for a prescribed α of the material is crucial. On the other hand, the value of J is linearly dependent on α. Therefore, accurate determination of α, while important, is not as critical. The problem is that for many materials, including those in

the present study, n is not a constant but rather varies with plastic strain. Therefore, no single combination of α and n can be selected such that Eq. 2.2.3 accurately represents the material's stress-strain behavior over the entire range of plastic strain. Consequently, one must choose the range of plastic strain over which one should attempt to represent accurately the stress-strain behavior.

Since the pipe containing the crack experiences a wide range of strain, no specific choice of strain range is better than any other. A pragmatic approach is to choose different strain ranges to find α and n values. Then, for predicting failure of nuclear power plant piping, choose the α and n that result in the largest applied J. Table 2.2.3 gives the corresponding values of the curve-fitting constants for this and all other materials used in the fracture mechanics analyses and shows that, depending upon the strain-range chosen to fit the data, the α and n values vary considerably.

J-Resistance Curves Used in the Analyses

The material's J-resistance curve is one of the principle inputs to any J/T analysis. The appropriateness of a J-R curve is properly questioned primarily because of its geometric dependence. To circumvent this difficulty, the common practical approach is to use J-R curves from C(T) or three-point-bend specimens because, of all the commonly used laboratory specimen types, the C(T) and bend specimens provide the lowest J-R curves. Thus, in predictive analyses, the use of C(T) or bend specimen J-R curves is expected to result in an underprediction of the pipe's load-carrying capacity. Accordingly, in the present work J-R curves drawn from C(T) specimen data were initially used. The details of how these curves were obtained are given in Reference 2.2.1.

Since J-R curves offer no clear evidence of direction independence, additional J/T analyses were performed using J-R curves obtained from FWFN(T) specimen data. This specimen type and the corresponding J-R curve development are given in Appendix D of Reference 2.2.1 and are discussed in Sections 3.2.1 and 3.2.5 of this report. The FWFN(T) specimen offers two notable features: (1) that crack growth occurs in the L-R plane, and (2) that stress distribution in the specimen's uncracked ligament is similar to that in the uncracked ligament of a circumferentially surface-cracked pipe in bending.

The verification of the FWFN(T) specimen J-R curve analysis procedure is currently underway, and a preliminary analysis was used to calculate the J-R curves from this specimen. The J-R curves for the C(T) and FWFN(T) specimens are significantly different. The difference may be attributable both to the (crack growth) direction dependence and to the stress distribution in the uncracked ligament of the two specimen types. The uncracked ligament of a C(T) specimen experiences combined bending and tension. In a FWFN(T) specimen, the uncracked ligament is in (nonuniform) tension.

Table 2.2.3 Ramberg-Osgood constants for the pipe materials

Pipe Experiment Numbers	α			n			σ_0, ksi (MN)			ε_0		
	Regression	High	Low	Regression	High	Low	Regression	High	Low	Regression	High	Low
4112-1	32.144	36.856	50.173	4.396	3.459	5.358	46.2 (0.21)	46.2 (0.21)	46.2 (0.21)	0.00179	0.00179	0.00179
4112-2	45.742	43.564	59.209	3.265	3.364	4.053	43.2 (0.19)	43.2 (0.19)	43.2 (0.19)	0.00167	0.00167	0.00167
4112-3, 4115-7, 4131-6	47.504	55.052	326.0	4.142	2.981	6.937	42.65 (0.18)	42.65 (0.18)	42.65 (0.18)	0.00165	0.00165	0.00165
4112-4	34.49	38.37	30.4	4.149	3.675	4.04	45.55 (0.20)	45.55 (0.20)	45.55 (0.20)	0.00176	0.00176	0.00176
4112-5	12.084	5.149	11.456	5.315	8.589	5.069	49.3 (0.22)	49.3 (0.22)	49.3 (0.22)	0.00179	0.00179	0.00179
4112-6	7.469	6.143	9.516	5.997	6.675	6.762	68.2 (0.30)	68.2 (0.30)	68.2 (0.30)	0.00248	0.00248	0.00248
4112-7	8.315	6.429	12.981	5.2	5.967	6.342	60.1 (0.26)	60.1 (0.26)	60.1 (0.26)	0.00218	0.00218	0.00218
4112-8	10.328	10.595	40.457	4.962	4.135	7.235	61.45 (0.27)	61.45 (0.27)	61.45 (0.27)	0.00223	0.00223	0.00223
4112-9	2.277	13.479	278.0	5.367	4.083	11.478	63.3 (0.28)	63.3 (0.28)	63.3 (0.28)	0.0023	0.0023	0.0023
4115-1, 4131-8	15.65	4.368	20.769	4.74	5.967	5.272	55.6 (0.25)	55.6 (0.25)	55.6 (0.25)	0.00202	0.00202	0.00202

Analysis Results

The J-T analyses were performed using the methods SC.TNP and SC.TKP of the NRCPIPE computer code. For both methods, both C(T) and FWFN(T) specimen J-R curves and the appropriate stress-strain curve parameters (Table 2.2.3) were used. This amounted to a total of 132 cases. In all the analyses it was assumed that crack growth occurred equally at all points along the crack-front and only in the radial direction since only the experimental data at the center of the surface crack were reduced. In both SC.TNP and SC.TKP methods, the applied J and dJ/da were calculated at the midpoint of the crack front and compared with the appropriate J-R curves.

Table 2.2.4 presents the results obtained by the SC.TNP method in terms of the ratio of the predicted initiation and maximum loads to the corresponding experimental loads. In most cases the ratio is larger than 1.0; that is, the predicted loads are higher than the corresponding measured loads. Also, whether the stress-strain curve or J-R curve results in more accurate predictions is not apparent from Table 2.2.4.

The results corresponding to the SC.TKP method are given in Table 2.2.5. Except for the prediction of initiation load in pipe fracture Experiment 4112-5, all other predicted initiation and maximum loads are lower than the corresponding measured values. This means that the SC.TKP method generally provides an underprediction of the initiation and maximum loads. Again, whether the different stress-strain curve fits or different J-R curves result in more accurate predictions is not apparent.

Effect of Finite Crack Length

One point requiring further consideration is the effect of the length of a surface crack on failure load. Crack length effects must be considered for pure bending, pure pressure, and combined pressure and bending stresses. The tests conducted in this program concentrated on a crack depth of 66 percent of the pipe thickness and a crack length of 50 percent of the pipe circumference with pipes under pure bending. The pipe diameters, materials, and R_m/t ratios were systematically varied.

The effect of surface-crack length on the failure stress relative to the stress predicted by net-section collapse was found to be very significant from the past experiments conducted by Eiber (Ref. 2.2.8). As shown in Figure 2.2.6 for Eiber's pressure test results on 24-inch (610-mm) diameter A106 Grade B pipe at 550 F (288 C), the ratio of the experimental stress to that predicted by net-section collapse actually decreased for surface-crack lengths of 25- to 87-percent of the pipe circumference.

On the other hand, the discrepancy between the experimental failure stress levels of Figure 2.2.6 and the net-section-collapse stress predictions is of concern to the current ASME Code IWB-3640 stainless steel approach. In this approach, the low-toughness correction (Z-factor) on the failure loads is a function of the pipe diameter and weld toughness, but not of the length of the surface crack.

Table 2.2.4 Summary of fracture mechanics analysis results using the SC.TNP method

(Page 1 of 2)

Pipe Fracture Experiment No.	Curve Fit Type	$\frac{P_1 \text{ (Predicted)}}{P_1 \text{ (Measured)}}$		$\frac{P_{max} \text{ (Predicted)}}{P_{max} \text{ (Measured)}}$	
		Using C(T) J-R Curve	Using FWFN(T) J-R Curve	Using C(T) J-R Curve	Using FWFN(T) J-R Curve
4112-1	Linear Regression	1.3	1.5	1.2	1.4
	High Strain Range	1.3	1.4	1.2	1.3
	Low Strain Range	1.3	1.4	1.2	1.3
4112-2	Linear Regression	1.5	1.6	1.2	1.3
	High Strain Range	1.5	1.6	1.3	1.3
	Low Strain Range	1.4	1.5	1.2	1.2
4112-3	Linear Regression	1.1	1.1	1.0	1.0
	High Strain Range	1.1	1.1	1.0	1.0
	Low Strain Range	0.8	0.8	0.8	0.8
4112-5	Linear Regression	1.8	1.8	1.2	1.3
	High Strain Range	2.0	1.9	1.2	1.3
	Low Strain Range	1.8	1.8	1.2	1.3
4112-6	Linear Regression	1.2	1.1	1.0	1.0
	High Strain Range	1.2	1.2	1.0	1.1
	Low Strain Range	1.1	1.1	1.0	1.0

Table 2.2.4 (Page 2 of 2)

Pipe Fracture Experiment No.	Curve Fit Type	$\frac{P_i \text{ (Predicted)}}{P_i \text{ (Measured)}}$		$\frac{P_{max} \text{ (Predicted)}}{P_{max} \text{ (Measured)}}$	
		Using C(T) J-R Curve	Using FWFM(T) J-R Curve	Using C(T) J-R Curve	Using FWFM(T) J-R Curve
4112-8	Linear Regression	1.1	1.0	1.0	1.2
	High Strain Range	1.0	1.0	1.0	1.2
	Low Strain Range	1.0	1.0	0.9	1.0
4112-9	Linear Regression	1.4	1.2	1.2	1.4
	High Strain Range	1.3	1.1	1.1	1.3
	Low Strain Range	1.2	1.1	1.0	1.0
4131-6	Linear Regression	1.0	1.0	1.0	1.0
	High Strain Range	1.0	1.0	1.0	1.0
	Low Strain Range	0.8	0.8	0.8	0.8
4131-8	Linear Regression	1.1	0.9	1.0	1.0
	High Strain Range	1.3	1.1	1.3	1.2
	Low Strain Range	1.0	0.9	1.0	1.0
4115-1	Linear Regression	1.0	0.8	1.0	0.9
	High Strain Range	1.3	1.1	1.2	1.1
	Low Strain Range	1.0	0.8	1.0	0.8
4115-7	Linear Regression	1.1	1.1	1.0	1.0
	High Strain Range	1.1	1.1	1.0	1.0
	Low Strain Range	0.8	0.8	0.8	0.8

Table 2.2.5 Summary of fracture mechanics analysis results using the SC.TKP method

(Page 1 of 2)

Pipe Fracture Experiment No.	Curve Fit Type	$\frac{P_i \text{ (Predicted)}}{P_i \text{ (Measured)}}$		$\frac{P_{max} \text{ (Predicted)}}{P_{max} \text{ (Measured)}}$	
		Using C(T) J-R Curve	Using FWEN(T) J-R Curve	Using C(T) J-R Curve	Using FWEN(T) J-R Curve
4112-1	Linear Regression	0.8	0.9	0.8	0.8
	Best Fit in High Strain Range	0.7	0.8	0.6	0.7
	Best Fit in Low Strain Range	0.8	0.8	0.7	0.7
4112-2	Linear Regression	1.0	1.0	0.8	0.9
	Best Fit in High Strain Range	1.0	1.0	0.8	0.9
	Best Fit in Low Strain Range	1.0	1.0	0.8	0.8
4112-3	Linear Regression	0.7	0.7	0.6	0.6
	Best Fit in High Strain Range	0.6	0.6	0.6	0.6
	Best Fit in Low Strain Range	0.5	0.5	0.5	0.5
4112-5	Linear Regression	1.2	1.1	0.7	0.8
	Best Fit in High Strain Range	1.3	1.3	0.8	0.8
	Best Fit in Low Strain Range	1.2	1.1	0.7	0.8
4112-6	Linear Regression	0.8	0.8	0.7	0.7
	Best Fit in High Strain Range	0.8	0.8	0.7	0.7
	Best Fit in Low Strain Range	0.8	0.8	0.8	0.7

Table 2.2.5 (Page 2 of 2)

Pipe Fracture Experiment No.	Curve Fit Type	$\frac{P_i \text{ (Predicted)}}{P_i \text{ (Measured)}}$		$\frac{P_{max} \text{ (Predicted)}}{P_{max} \text{ (Measured)}}$	
		Using C(T) J-R Curve	Using fWFM(T) J-R Curve	Using C(T) J-R Curve	Using fWFM(T) J-R Curve
4112-8	Linear Regression	0.7	0.7	0.7	0.7
	High Strain Range	0.7	0.7	0.6	0.7
	Low Strain Range	0.7	0.7	0.6	0.7
4112-9	Linear Regression	0.9	0.8	0.7	0.8
	High Strain Range	0.8	0.7	0.7	0.8
	Low Strain Range	0.8	0.7	0.7	0.7
4131-6	Linear Regression	0.7	0.7	0.7	0.7
	High Strain Range	0.7	0.7	0.6	0.7
	Low Strain Range	0.5	0.5	0.5	0.5
4131-8	Linear Regression	0.7	0.6	0.7	0.7
	High Strain Range	0.9	0.8	0.9	0.8
	Low Strain Range	0.7	0.6	0.7	0.6
4115-1	Linear Regression	0.8	0.6	0.7	0.6
	High Strain Range	1.0	0.8	0.9	0.8
	Low Strain Range	0.7	0.6	0.7	0.6
4115-7	Linear Regression	0.7	0.6	0.6	0.6
	High Strain Range	0.6	0.6	0.6	0.6
	Low Strain Range	0.5	0.5	0.5	0.5

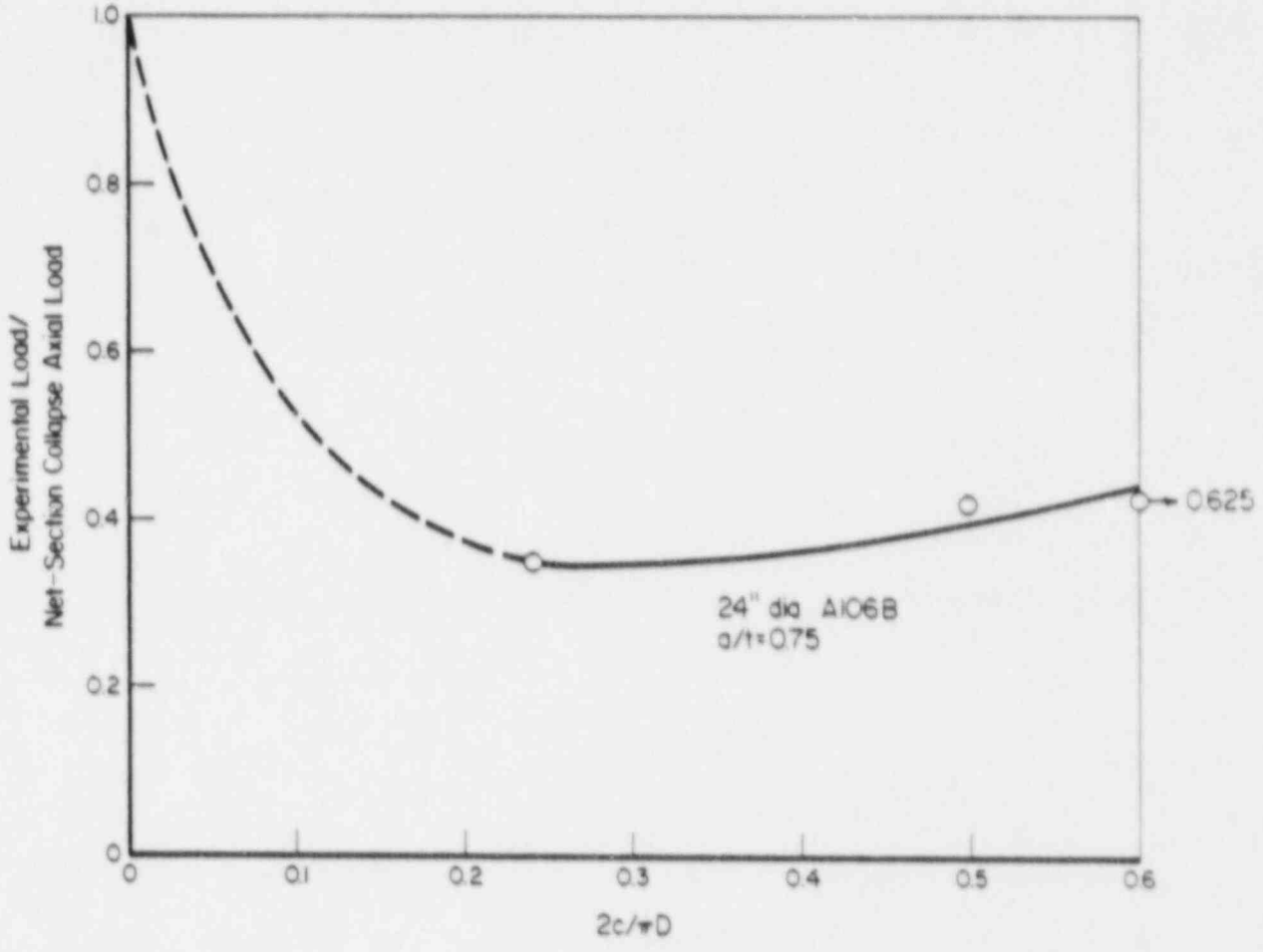

Figure 2.2.6 Comparison of experimental failure stresses with net-section-collapse predictions for pipe pressurized to failure (Ref. 2.2.8).

To further assess the effect of surface-crack length, calculations were made under pure bending using SC.TKP, and the maximum bending loads were compared with those predicted by net-section collapse. Crack depth was held constant at 66 percent of the pipe thickness, and the surface-crack length was varied. The material and pipe geometry corresponded to Experiment 4212-8, which involved 16-inch- (406-mm-) diameter, 1-inch- (25.4-mm-) thick A106 Grade B pipe at 550 F (288 C). For the loads calculated by net-section collapse, the flow stress was defined in two ways, one as 1.15 $(\sigma_y + \sigma_u)/2$ and the other as $(\sigma_y + \sigma_u)/2$. The comparisons are shown in Figure 2.2.7. These calculations predict that as the crack length becomes shorter, the loads will approach the net-section-collapse load in approximately a linear manner. This trend for pure bending over crack lengths of 25 to 50 percent of the pipe circumference is markedly different from the trend for pressure loading (axial membrane stresses) shown in Figure 2.2.6.

To clarify this effect of crack length and loading (bending, pressure, and combined loading), additional sensitivity study calculations should be conducted to define what experimental data would be the most useful in verifying the current EPFM analyses and the margins of safety in the ASME Code analysis.

2.2.2 Discussion of Finite Surface-Cracked Pipe Efforts

The efforts in this area involved the development of considerable pipe fracture experimental data. A correction for the effect of pipe ovalization as a function of the pipe R/t ratio was first developed as a result of this program. The PZSC showed that the toughness required to obtain limit-load conditions was lower for a surface-cracked pipe than for a through-wall-cracked pipe. Finally, the development of finite-length, surface-cracked pipe J-estimation schemes was a major accomplishment since no other solutions were available.

From these results arise several concerns. The first is how to account for crack length in the ovalization correction factor; additional experiments may be needed. Secondly, the ovalization correction must be included in the finite-length J-estimation scheme, and the J-estimation scheme should be expanded to include the elastic contribution of J. The general concept of including axial tension with bending loads has been developed, but has yet to be incorporated into the NRCPIPE code and verified. Finally, further application of the finite-length, surface-cracked pipe estimation scheme should be made to assess the ASME surface-cracked pipe criterion. Currently, the ASME criterion correction for toughness is independent of the size of the surface crack. These are some aspects yet to be addressed, even though the efforts in this area are now completed.

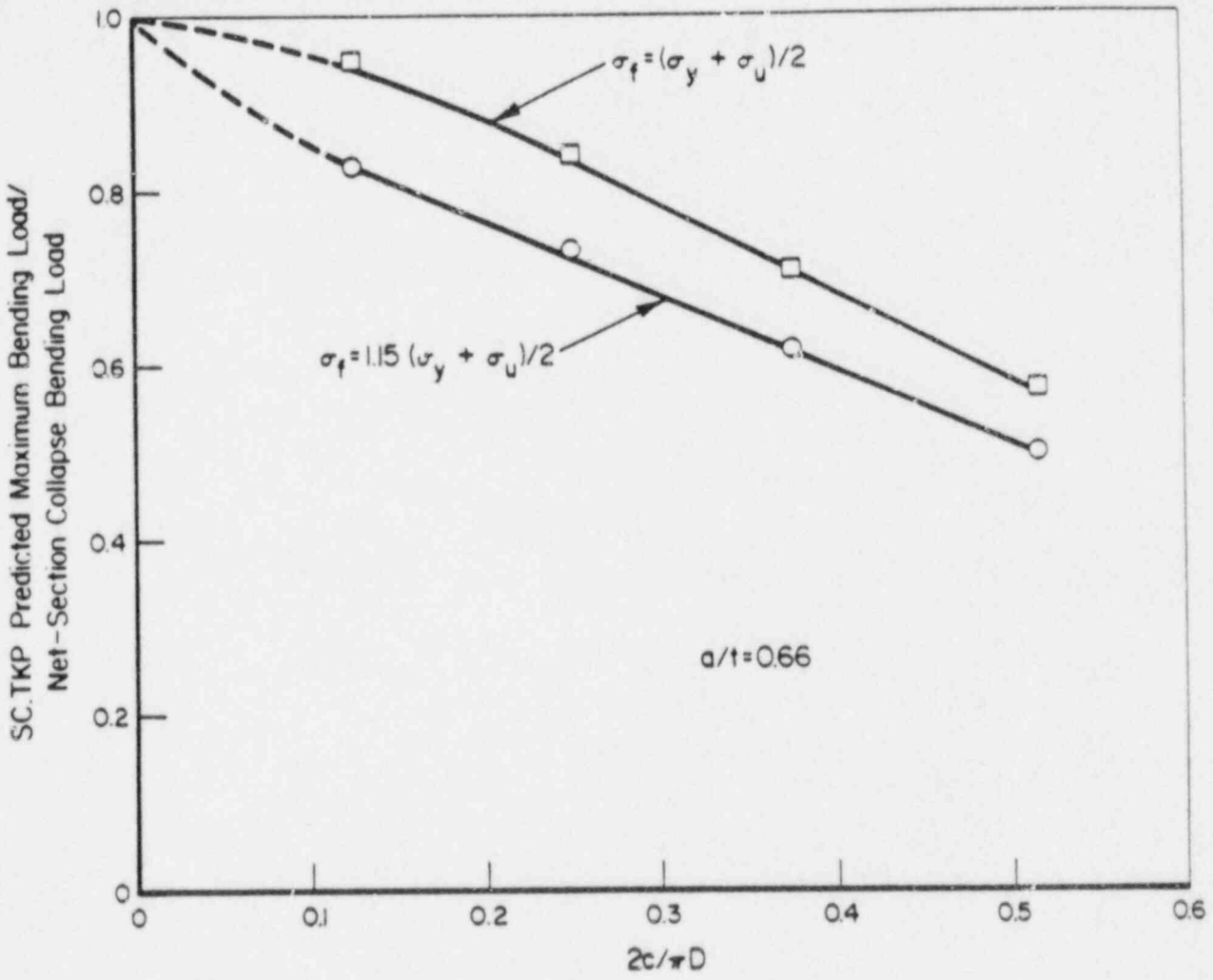

Figure 2.2.7 Comparison of SC.TKP predictions with net-section-collapse predictions for 16-inch- (406-mm-) diameter, 1-inch- (25.4-mm-) thick A106 Grade B pipe in pure bending.

T-4872-F-4.2

References for Section 2.2

2.2.1 Scott, P. M., and Ahmad, J. A., "Experimental and Analytical Assessment of Circumferentially Surface-Cracked Pipes Under Bending", NUREG/CR-4872, April 1987.

2.2.2 Kanninen, M. F., and others, "Instability Predictions for Circumferentially Cracked Type 304 Stainless Steel Pipes Under Dynamic Loading", Final Report on EPRI Project T118-2, EPRI Report NP-2347, April 1982.

2.2.3 Scott, P. M., and Brust, F. W., "An Experimental and Analytical Assessment of Circumferential Through-Wall-Cracked Pipes Under Pure Bending", NUREG/CR-4574, September 1986.

2.2.4 "Evaluation of Flaws in Austenitic Steel Piping" (Technical basis document for ASME IWB-3540 analysis procedure), prepared by Section XI Task Group for Piping Flaw Evaluation, EPRI Report NP-4690-SR, April 1986.

2.2.5 Wilkowski, G. M., and others, "Degraded Piping Program - Phase II" Semiannual Report, April 1986-September 1986, NUREG/CR-4082, Vol. 5, April 1987.

2.2.6 Kumar, V., and others, "An Engineering Approach for Elastic-Plastic Fracture Analysis", EPRI NP-1931, July 1981.

2.2.7 Brust, F. W., "Approximate Methods for Fracture Analyses of Through-Wall-Cracked Pipe", NUREG/CR-4853, January 1987.

2.2.8 Eiber, R. J., Maxey, W. A., and Duff, A., "Investigation of the Initiation and Extent of Ductile Pipe Rupture", BMI Report 1908 to the AEC, June 1971.

2.2.9 Kumar, V., and others, "Advances in Elastic-Plastic Fracture Analyses," EPRI NP-3607, August 1984.

2.3 Circumferentially Complex-Cracked Pipe in Bending
(G. Kramer and V. Papaspyropoulos)

The objectives of this effort are to verify current limit-load and EPFM analyses to predict loads and to improve fracture instability evaluations of complex-cracked pipes under compliant loading.

A complex crack is a very long surface crack that may have penetrated the pipe thickness for some of its length. Such a crack geometry has been found in nuclear plant piping (Ref. 2.3.1) and is relevant to understanding the stability of a long circumferentially surface-cracked pipe. Once the surface crack becomes a complex crack, the stability of the resulting crack will be governed by the stability of the complex crack.

Previous work at Battelle has shown that the calculated J-R curve from a complex-cracked pipe experiment was significantly lower than that from an experiment on the same pipe with a circumferential through-wall crack (Ref. 2.3.2). This can have a great effect on compliant instability predictions.

Results from low-compliance, complex-cracked pipe tests were reported in a prior topical report:

> "An Assessment of Circumferentially Complex-Cracked Pipe Subjected to Bending", G. Kramer and V. Papaspyropoulos, NUREG/CR-4687, October 1986.

These results are briefly reviewed in the following section. Current results and plans for compliant instability tests are then presented.

2.3.1 Summary of Results to Date

In order to verify the accuracy of load-displacement predictions from EPFM analyses, experimental data were required on complex-cracked pipes. The results of six low-compliance pipe fracture experiments conducted at 550 F (288 C) were used to assess the validity of these predictions. Two 6-inch (152-mm) nominal diameter pipe fracture experiments were conducted on SA-376 TP304 stainless steel pipe, two on Inconel 600 pipe, and two on A106 Grade B carbon steel pipe. Based on the results of these complex-cracked pipe investigations, the following observations were made.

Small unstable crack jumps were observed in the two complex-cracked pipe experiments on low-toughness A106 Grade B pipe. These instabilities occurred even though the lengths of pipe were relatively short (with a length-to-diameter ratio of less than 10) and the pipes were loaded under displacement control. Dynamic crack jumps have been observed in C(T) specimen tests on similar carbon steel pipe materials. It is currently hypothesized that the crack jumps may result from dynamic strain aging (DSA). The magnitude of these crack jumps will increase with additional system compliance.

A screening criterion developed for through-wall-cracked pipe under bending was shown to be applicable for complex-cracked pipe under bending. Results of the application of this criterion indicated that the net-section-collapse analysis could be used to predict limit loads fairly accurately in the stainless steel and Inconel pipe experiments, but not in the A106 Grade B pipe experiments. Net-section-collapse analyses also revealed that the actual net-section-collapse stress (accounting for crack growth) of the Type 304 stainless steel pipe sections became much larger than the flow stress of the material for large amounts of crack growth.

The η-factor analysis of the pipe experiments, using both the deformation-J and modified-J parameters, indicated that J-resistance curves for the pipes were lower than the curves generated for 20-percent side-grooved C(T) specimens. Furthermore, the pipe J-resistance curves were found to decrease as the ratio of surface-crack depth to pipe thickness increased.

Predictive J-estimation schemes [based on 20 percent side-grooved C(T) specimens] compared well with experimental pipe load and load-line displacement data up to maximum load. Once past maximum load, all J-estimation schemes overpredicted the experimentally measured loads.

Comparison of J-R curves from through-wall-cracked pipes and complex-cracked pipes suggested that an empirical constraint factor could be established to predict complex-cracked pipe J-R curves from through-wall-cracked pipe data. The experimental trend curve, see Figure 2.3.1, implies that a surface crack even 10 percent deep increases the triaxial stresses at the crack tip to reduce the J-R curve by 25 to 50 percent. Further details and discussions are contained in the topical report described at the beginning of this Section.

2.3.2 Status of Instability Experiments

Based on the data generated from previous complex-cracked pipe experiments with low compliance, a series of experiments were defined to examine the fracture instability behavior of complex-cracked pipe. This series of experiments was designed to assess current analytical methods of predicting the point of instability, as well as to develop experimental methods for performing such types of experiments. Energy balance approaches will also be evaluated for predicting whether or not crack arrest will occur in these experiments. See References 2.3.3 and 2.3.4 for further discussions about designing these experiments based on an energy balance approach.

The four instability experiments scheduled in this subtask are listed in Table 2.3.1. To date, the first three experiments have been completed and were discussed in Reference 2.3.5. A summary of the test parameters and initiation and maximum load data are presented in Table 2.3.2. The fourth (Experiment 4114-4) is being conducted at the time of this writing; its design is described below.

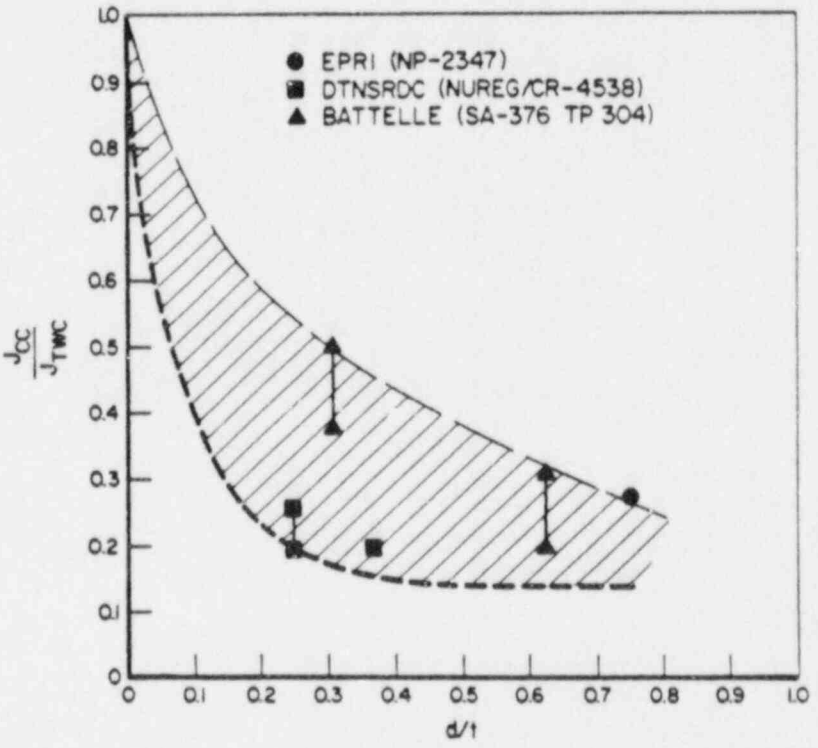

Figure 2.3.1 Ratio of J of the complex crack to J of the simple through-wall crack as a function of d/t for various experiments.

T-4687-F5.19

Table 2.3.1. Test matrix of complex-cracked pipe experiments under compliant bending.

Experiment Number	Pipe Material	Nominal Pipe Diameter, inches (mm)	Nominal Wall Thickness, inch (mm)	$2c/\pi D$(a)	$2a/\pi D$(b)	d/t(c)
4114-1	A106 Grade B	6 (152)	0.562 (14.3)	0.37	1.0	0.465
4114-2	SA-376 TP304 SS	6 (152)	0.562 (14.3)	0.37	1.0	0.32
4114-3	SA-358 TP304 SS	16 (406)	1.031 (26.2)	0.37	1.0	0.33
4114-4	SA-358 TP304 SS	16 (406)	1.031 (26.2)	0.37	1.0	0.33

All tests conducted at 550 F (288 C).

(a) 2c is through-wall crack length, D is the pipe diameter.
(b) 2a is internal surface crack length.
(c) d is internal surface crack depth, t is the pipe thickness.

Table 2.3.2. Summary of data from compliant bend experiments on complex-cracked pipe.

	Experiment Number			
	4114-1	4114-2	4114-3	4114-4[a]
Pipe Material	A106 Gr. B	SA-376 TP304	SA-358 TP304	SA-358 TP304
Pipe Material I.D.	DP2-F31A	DP2-A23G	DP2-A8	DP2-A8
Outside Diameter, inches (mm)	6.50 (165)	6.560 '167)	16.3 (414)	16.3 (414)
Wall Thickness, inches (mm)	0.501 (12.7)	0.530 (13.5)	1.03 (26.2)	1.03 (26.2)
Through-Wall Crack Length/Circumference	0.370	0.370	0.373	0.37
Surface Crack Length/Circumference	1.00	1.00	1.00	1.00
Surface Crack Depth/Wall Thickness	0.465	0.321	0.33	0.33
4 Pt. Bend - Outer Span, inches (m)	92.0 (2.34)	164.0 (4.17)	456.0 (11.58)	456.0 (11.58)
4 Pt. Bend - Inner Span, inches (m)	48.0 (1.22)	48.0 (1.22)	132.0 (3.35)	132.0 (3.35)
Test Temperature, F (C)	550 (288)	550 (288)	550 (288)	550 (288)
Tensile Yield Strength, ksi (MPa)	46.4 (320)	20.1 (139)	26.1 (179)	26.1 (179)
Ultimate Tensile Strength, ksi (MPa)	90.0 (621)	65.2 (450)	66.5 (466)	66.5 (466)
CVN Upper Shelf Energy, ft-lb (J)	110.0 (149)	N/A	N/A	N/A
Initiation Load, lb (kN)	14,000 (62.3)	5,850 (26)	32,850 (146)[b]	
Maximum Load, lb (kN)	18,650 (83)	6,540 (29.1)	35,475 (157.8)[b]	

(a) Experiment to be completed in next reporting period.
(b) Corrected for dead-weight loads.

Design of Experiment 4114-4

A simplified instability analysis can be developed for Experiment 4114-4 using the load versus load-line displacement data from Experiment 4114-3. In this analysis, the compliance of the uncracked pipe and the compliance of the machine are not considered since the pipe geometry and basic load frame configuration are the same in each experiment.

A schematic of the load frame configuration for Experiment 4114-4 is shown in Figure 2.3.2. In this arrangement, two additional springs have been incorporated into the load train, each with a compliance of C_s. Figure 2.3.3 illustrates the determination of the instability point for this arrangement. Suppose that the load-displacement response of the low-compliance experiment is shown by Curve A in this figure and that the load-displacement response of the combined spring assemblies is given by Curve C. The response of the entire structure is given by adding Curves A and C. The resulting load versus total displacement will appear as Curve B in Figure 2.3.3.

Instability occurs when the slope of Curve B becomes infinite, or when

$$\frac{\partial \delta_T}{\partial_P} = 0 \qquad (2.3.1)$$

But from Figure 2.3.2, $\delta_T = \delta_L + PC_s/2$. Eq. 2.3.1 is satisfied when

$$\frac{\partial \delta_L}{\partial_P} = \frac{-C_s}{2} \qquad (2.3.2)$$

Thus, a value of C_s can be determined quite easily from the measured load-displacement data without any transformations or conversions. However, this approach can only be used when identical experiments are being performed.

In order to provide the spring compliance required for Experiment 4114-4, two adjustable Belleville disc spring assemblies were installed into the load train. Figure 2.3.4 is a photograph of the spring assemblies mounted on the hydraulic actuator at one load point. Each assembly has been arranged into four stacks with 122 disc springs per stack. This initial configuration was designed based on the manufacturer's compliance data from a single disc spring.

In order to determine the actual compliance of the entire spring assembly, measurements were made of spring assembly load and deflection when loads were applied to an uncracked pipe specimen. The resulting load-displacement data, averaged for both spring assemblies, is shown in Figure 2.3.5 for three cycles of loading. Although the hysteresis was larger than anticipated, the three loading cycles showed excellent repeatability.

Finally, in the manner shown in Figure 2.3.2, the load-displacement data from Experiment 4114-3 (shown in Figure 2.3.6) was added to the total load-displacement data of the combined spring assemblies. A correction was made to

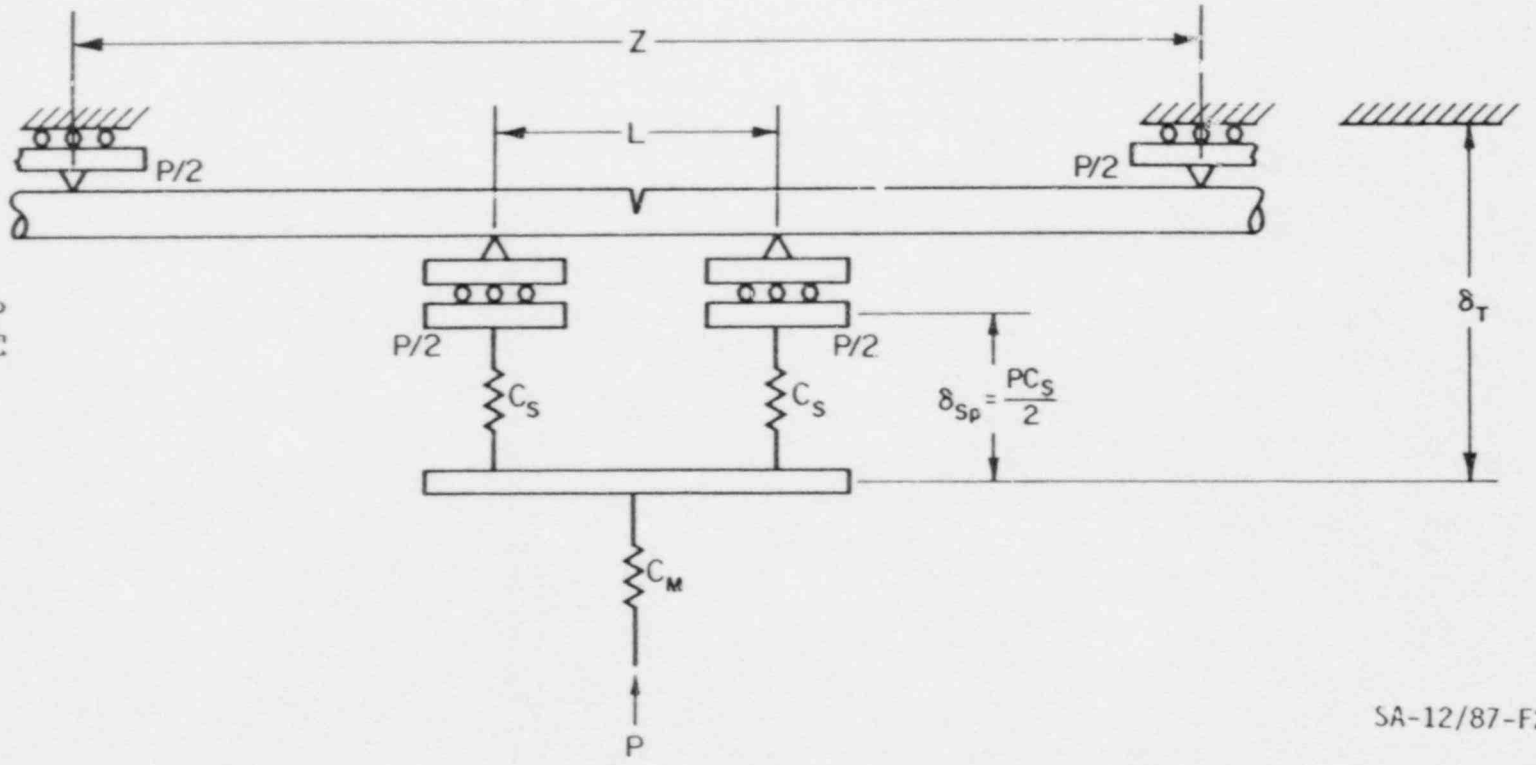

Figure 2.3.2 Schematic of high-compliance loading frame for Experiment 4114-4.

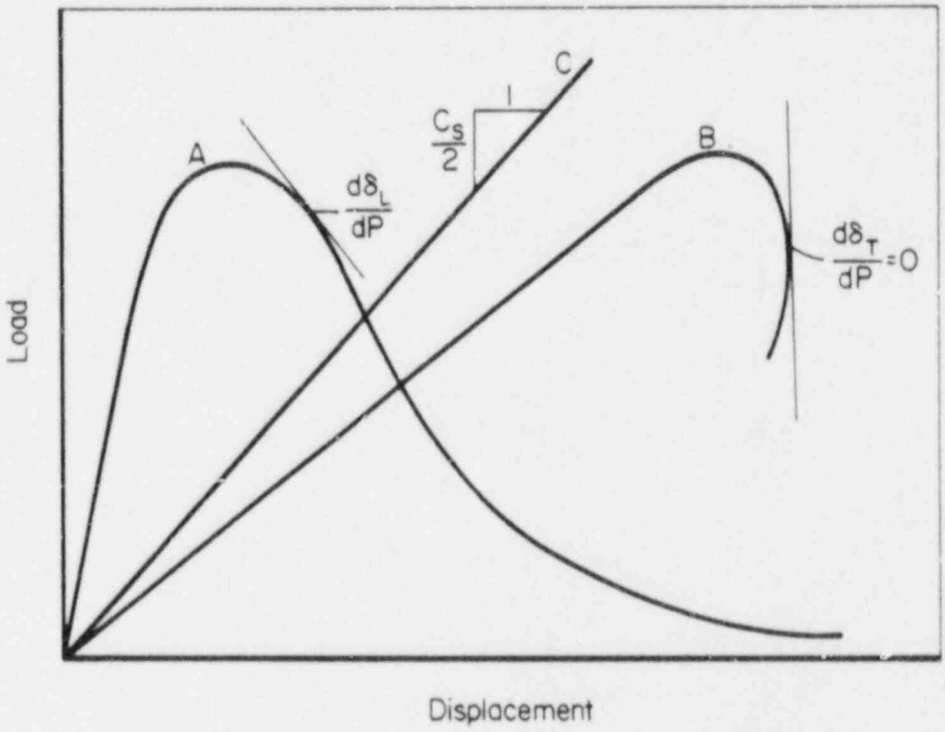

Figure 2.3.3 Illustration for determining the instability point based on load-displacement data.

SA-12/87-F2.3.3

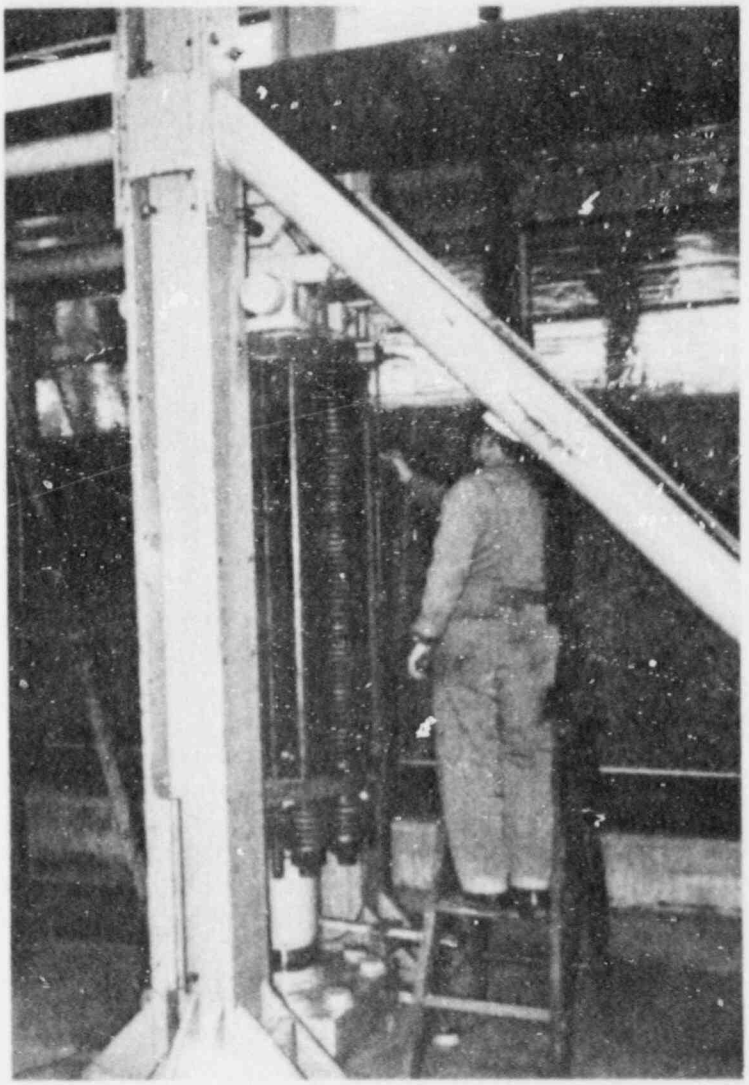

SA-12/87-F2.3.4

Figure 2.3.4 View of Belleville disc spring assembly incorporated into the load frame for complex-cracked pipe Experiment 4114-4.

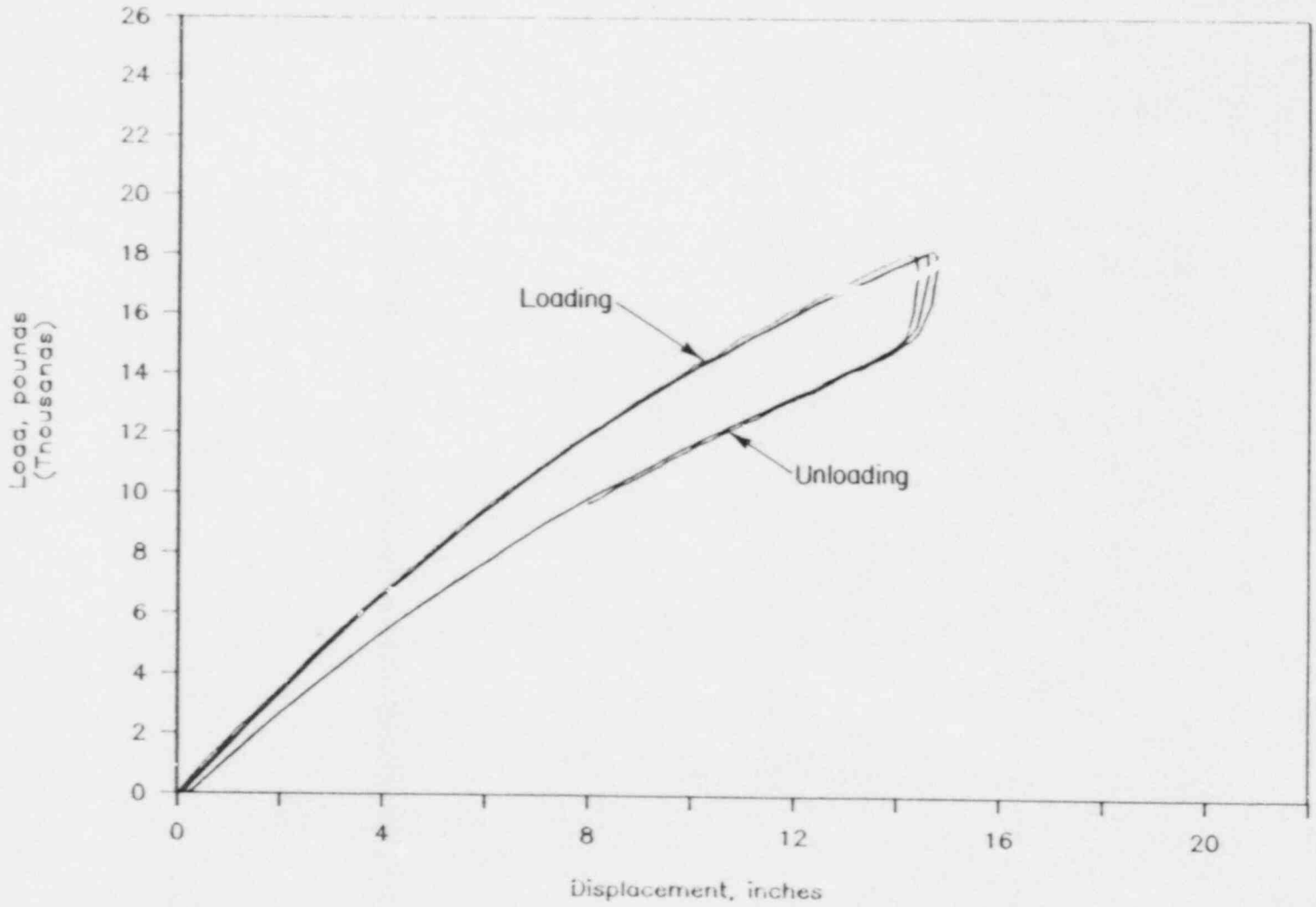

Figure 2.3.5 Average load versus displacement response for Belleville disc spring assemblies to be used in complex-cracked pipe Experiment 4114-4. (Data for three cycles of loading are shown.)

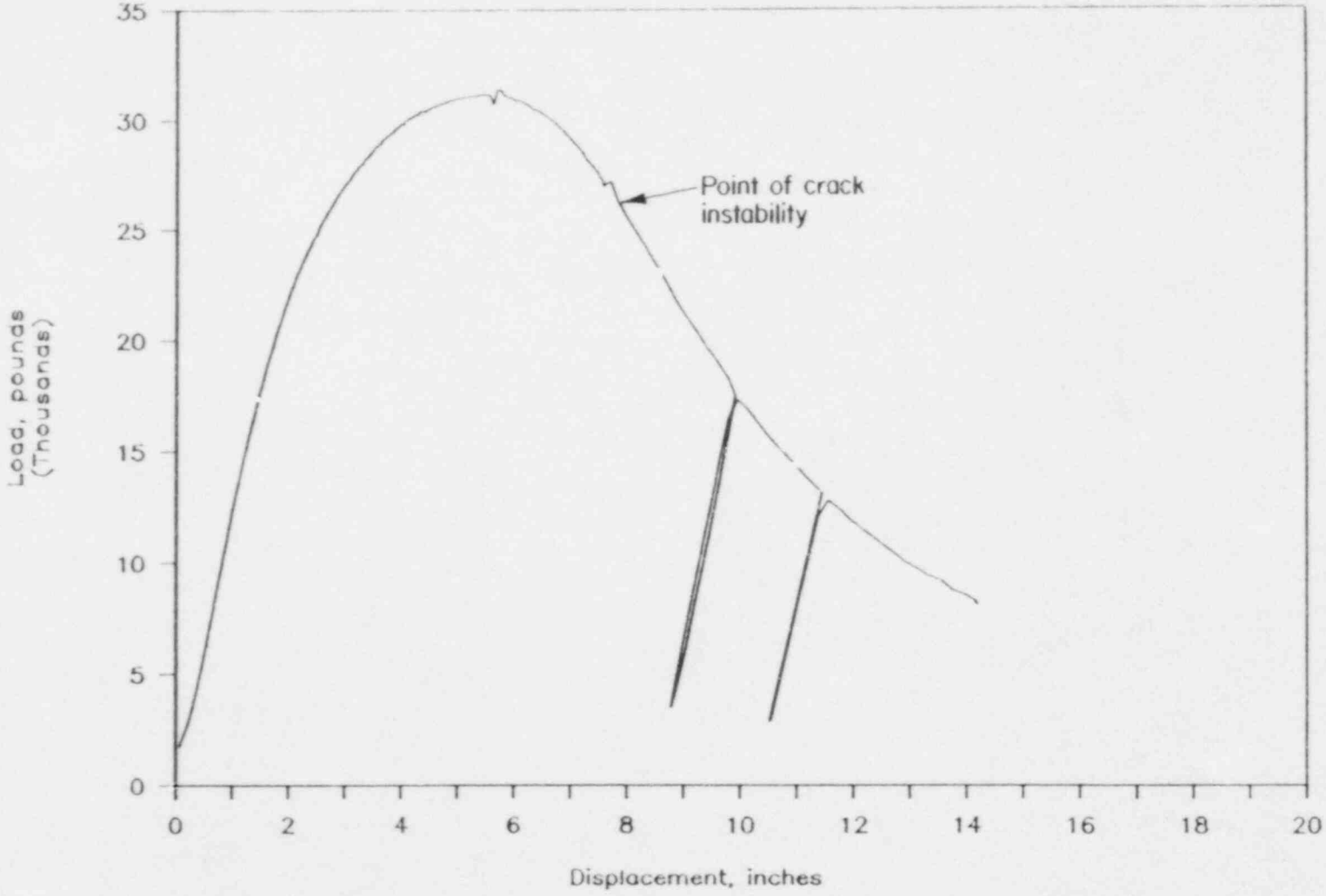

Figure 2.3.6 Measured load versus load-line displacement data from 16-inch-(406-mm-) diameter stainless steel complex-cracked pipe (Experiment 4114-3).

SA-12/87-F2.3.6

the spring assembly data to account for differences in dead-weight load between the uncracked pipe used and the actual test specimen. These results, shown in Figure 2.3.7, predict that a crack will become unstable at an applied load of approximately 26,000 pounds (116 kN).

2.3.3 Discussion and Future Plans

The method used for designing the instability experiments of Section 2.3.2 was based on results of previous low-compliance pipe fracture experiments. This should provide the most accurate method of determining the instability compliance for these experiments. Although the predictive J-estimation schemes offer a more universal method of calculating the compliance needed for instability, their accuracy must be improved before they can be used with confidence.

Critical factors in the design of these instability experiments on complex-cracked pipe was found to be the compliance of the test frame and the actual compliance of the spring devices used. It is very crucial to the success of these experiments that each of these compliances be well-documented both before the experiment for design purposes and during the instability experiment for interpretive purposes.

As discussed in previous semiannual reports, the accuracy of the critical compliance needed to produce an instability is dependent on the material used in the experiment. It was found that the A106 Grade B carbon steel (Experiment 4114-1) was much more sensitive to changes in critical compliance than the higher-toughness Type 304 stainless steel (Experiment 4114-2). Because the critical compliance value was so small for the A106 Grade B carbon steel, even a small change in system compliance would have significantly affected the extent of crack propagation.

Future plans call for the completion of Experiment 4114-4 and an analysis of the static and dynamic data. The actual point of instability in the experiment will be compared to pretest predictions and other current instability analyses. In addition, energy balance predictions will be evaluated with respect to the measured load-displacement data.

References for Section 2.3

2.3.1 U.S. Nuclear Regulatory Commission, "Investigation and Evaluation of Stress Corrosion Cracking in Piping of Light Water Reactor Plants", NUREG-0531, Chapter 7, February 1979.

2.3.2 Kanninen, M. F., and others, "Instability Predictions for Circumferentially Cracked Type 304 Stainless Steel Pipes Under Dynamic Loading", Final Report on EPRI Project T118-2, EPRI Report Number NP-2347, April 1982.

2.3.3 Wilkowski, G. M., and others, "Degraded Piping Program - Phase II", Semiannual Report, April 1985-September 1985, NUREG/CR-4082, Vol. 3, March 1986.

2.3.4 Wilkowski, G. M., and others, "Degraded Piping Program - Phase II", Semiannual Report, October 1985-March 1986, NUREG/CR-4082, Vol. 4, September 1986.

2.3.5 Wilkowski, G. M., and others, "Degraded Piping Program - Phase II", Semiannual Report, April 1986-September 1986, NUREG/CR-4082, Vol. 5, April 1987.

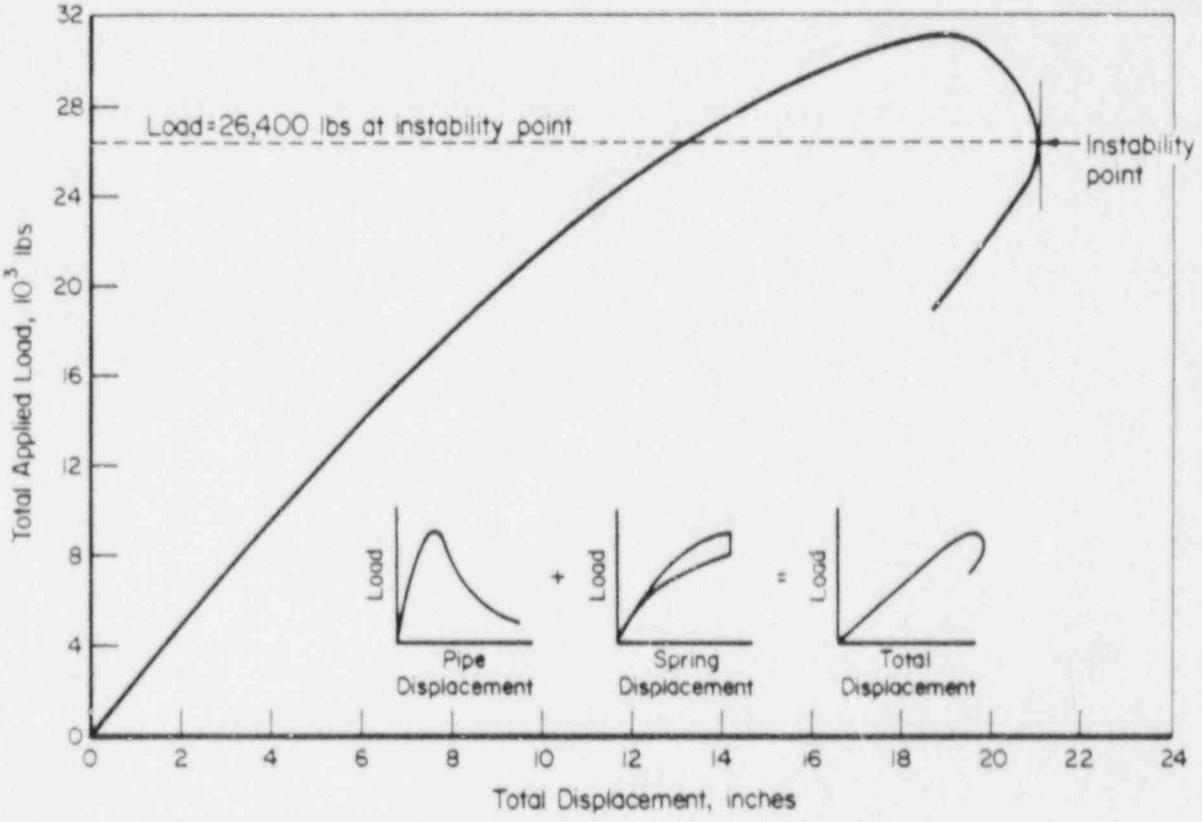

Figure 2.3.7 Determination of crack instability point for 16-inch-(406-mm-) diameter stainless steel complex-cracked pipe Experiment 4114-4.

SA-1[illegible]/87-F2.3.7

2.4 Circumferentially Cracked Pipe Under Axial Membrane Stress (D. Guerrieri and G. Kramer)

The objective of this effort is to develop an understanding of the fracture behavior of circumferential defects in pipes subjected to axial membrane stress. This effort will contribute to the case of pressure-induced axial membrane stresses combined with bending stresses. Before the interactions of pressure-induced axial tension stresses and bending can be understood, however, the effects of each loading condition must be studied separately.

This effort could have involved experiments under pure axial tension or under pressure. Axial tension testing involves considerably more complicated testing equipment than pressure testing. Axial tension testing must allow for the rotation of the pipe so that it is not subjected to bending stresses by unknown factors. Since the major application of this work is toward the understanding of pressure plus bending loads, the tests in this effort have involved pressurizing cracked pipe sections to failure. This requires the flaw lengths to be sufficiently long to prevent yielding in the hoop direction. More importantly, conducting the experiments in this way incorporates biaxial stresses.

Conducting pressurized, high-temperature, through-wall-cracked pipe tests presents the experimental difficulty of sealing through-wall-cracked pipe. At temperatures below 400 F (204 C) this is relatively easy; at 550 F (288 C), however, it is much more difficult. Efforts in this area have involved the development of a high-temperature rubber bladder sealing technique.

Past results and future plans are summarized in the following sections.

2.4.1 Summary of Results to Date

Results to date have concentrated on three specific areas: (1) development of an experimental method for conducting axial membrane experiments on through-wall-cracked pipe, (2) completion of three pipe fracture experiments, and (3) comparison of the pipe fracture results with net-section-collapse predictions using the PZSC. The results obtained in these three areas are summarized below.

Since axial membrane stresses are produced by internal pressurization of the pipe specimen in this subtask, a new experimental test method for sealing through-wall-cracked pipe was needed. Initial sealing methods that used metal patches and high-temperature silicone epoxies were not successful above 400 F (204 C). To solve the sealing problem, a new high-temperature internal bladder method was developed and successfully tested in one experiment.

However, problems were encountered when this bladder technique was applied to pipe experiments in other subtasks. It was found that the bladder material became brittle when overheated and could be punctured by metal chips left in

the pipe from the fabrication process. Also, the bladder had to be undersized in relation to the internal diameter of the pipe to prevent the bladder from folding over upon itself during pressurization. If a fold occurred, the bladder would tear under pressure and leak.

These complications have led to an advanced bladder design that replaces the bag shape with a simpler sleeve. The sleeve design will facilitate fluid flow and leak rate measurements in future pipe fracture experiments. Bladder thickness has been increased and diameter further decreased in relation to the internal pipe diameter. Simplified end closures have been developed to hold the sleeve against the internal pipe wall. This new bladder design should solve many of the problems encountered in the original design.

Six experiments were originally scheduled in this subtask to characterize the behavior of pipes with various crack geometries under axial membrane stresses. These six experiments are detailed in Table 2.4.1. To date, three of the experiments have been completed and analyzed. The two complex-cracked pipe experiments were determined to be of lesser importance to the overall objectives of the Degraded Piping Program and have been replaced by other more important activities. Hence, only Experiment 4121-4 remains to be conducted.

Results of the first two experiments (4121-3 and 4121-6) on surface-cracked pipe were presented in both the Second and Third Semiannual Reports of this program (Refs. 2.4.1 and 2.4.2). Results of the third experiment conducted (4121-1) were presented in the Fourth Semiannual Report (Ref. 2.4.3). Results of these three experiments are summarized in Table 2.4.2. Crack initiation occurred within 1 percent of maximum load for the two surface-cracked pipe experiments and within 11 percent of maximum load for the through-wall-cracked pipe experiment.

Comparison of experimental data with net-section-collapse failure loads is discussed in detail in Reference 2.4.2 and is shown in Figure 2.4.1. The trend observed in Figure 2.4.1 is similar to that observed for both through-wall-cracked pipe and surface-cracked pipe under bending. This trend illustrates that when the plastic-zone size is significantly less than 1.0, the applied stress at maximum load is significantly less than the net-section-collapse stress. Thus, Figure 2.4.1 assisted in explaining why past data from Eiber and others (Ref. 2.4.4) failed at such low stress levels. In these cases, the pipe size and toughness combined to produce constrained plasticity at the crack plane.

2.4.2 Discussion and Future Plans

A significant amount of induced bending was measured in each of the three experiments conducted. These observations indicate that the pressure loading method used, and the lack of end constraint associated with that method, do affect the failure characteristics of cracked pipe, as was our concern when we chose the loading method for these experiments. The pressurized loading condition used in these experiments is a worst-case condition. In an actual piping system, the end constraints may prohibit some induced bending and

Table 2.4.1 Test matrix for axial membrane stress pipe experiments.

Experiment No.	Pipe Material	Nominal Pipe Diameter, inch (mm)	Nominal Wall Thickness, inch (mm)	Flaw[a] Type	$2c/\pi D$[b]	$2a/\pi D$[c]	d/t[d]	Test Temperature, F (C)
4121-1	SA-376 TP304 SS	6 (152)	0.562 (14.3)	TWC	0.37	N/A	N/A	550 (288)
4121-2	SA-376 TP304 SS	6 (152)	0.562 (14.3)	CC	0.37	1.00	0.72	550 (288)
4121-3	SA-376 TP304 SS	6 (152)	0.562 (14.3)	SC	N/A	0.50	0.70	550 (288)
4121-4	SA-333 Grade 6	10 (254)	0.712 (18.1)	TWC	0.37	N/A	N/A	550 (288)
4121-5	SA-333 Grade 6	10 (254)	0.712 (18.1)	CC	0.37	1.00	0.72	550 (288)
4121-6	SA-333 Grade 6	10 (254)	0.712 (18.1)	SC	N/A	0.50	0.68	550 (288)

(a) TWC = Through-Wall Crack
SC = Surface Crack
CC = Complex Crack.

(b) 2c is the total through-wall circumferential crack length, D is the pipe diameter.

(c) 2a is internal surface crack length.

(d) d is internal surface crack depth, t is the pipe thickness.

Table 2.4.2 Comparison of pipe fracture data under axial membrane stress.

Experiment	4121-1	4121-3	4121-6
Diameter, inches (mm)	6.625 (168)	6.625 (168)	10.75 (273)
Actual wall thickness, inches (mm)	0.507 (12.9)	0.500 (12.7)	0.615 (16.4)
Material type	SA-376 TP304	SA-376 TP 304	SA-333 Grade 6
Pipe I.D.	DP2-A23	DP2-A24B	DP2-F9
Surface crack depth/thickness	N/A	0.68 to 0.75	0.67 to 0.69
Crack length, degrees	139	180	180
Yield stress at 550 F (288 C), psi (MPa)	20,100 (139)	20,100 (139)	34,700 (239)
Ultimate stress at 550 F (288 C), psi (MPa)	65,200 (449)	65,200 (449)	76,500 (527)
Internal pressure at initiation, psi (MPa)	3,900 (26.9)	6,050 (41.7)	6,100 (42.1)
Internal pressure at max. load, psi (MPa)	4,365 (30.2)	6,075 (41.9)	6,300 (43.4)
Initiation load/max. load	0.893	0.996	0.968
Nominal longitudinal stress at max. load, psi (MPa)	11,065 (76.3)	18,605 (139)	25,955 (181)
Final crack opening angle, degrees		6-7[a]	20-22[b]
Final crack opening area, in^2 (mm^2)		5.97 (3,852)[a]	59.8 (38,580)[b]
Final kink angle of pipe, degrees		2.2-2.5	10

(a) Crack extended along initial surface crack region.
(b) Crack grew 4 inches (102 mm) past the end of the surface crack.

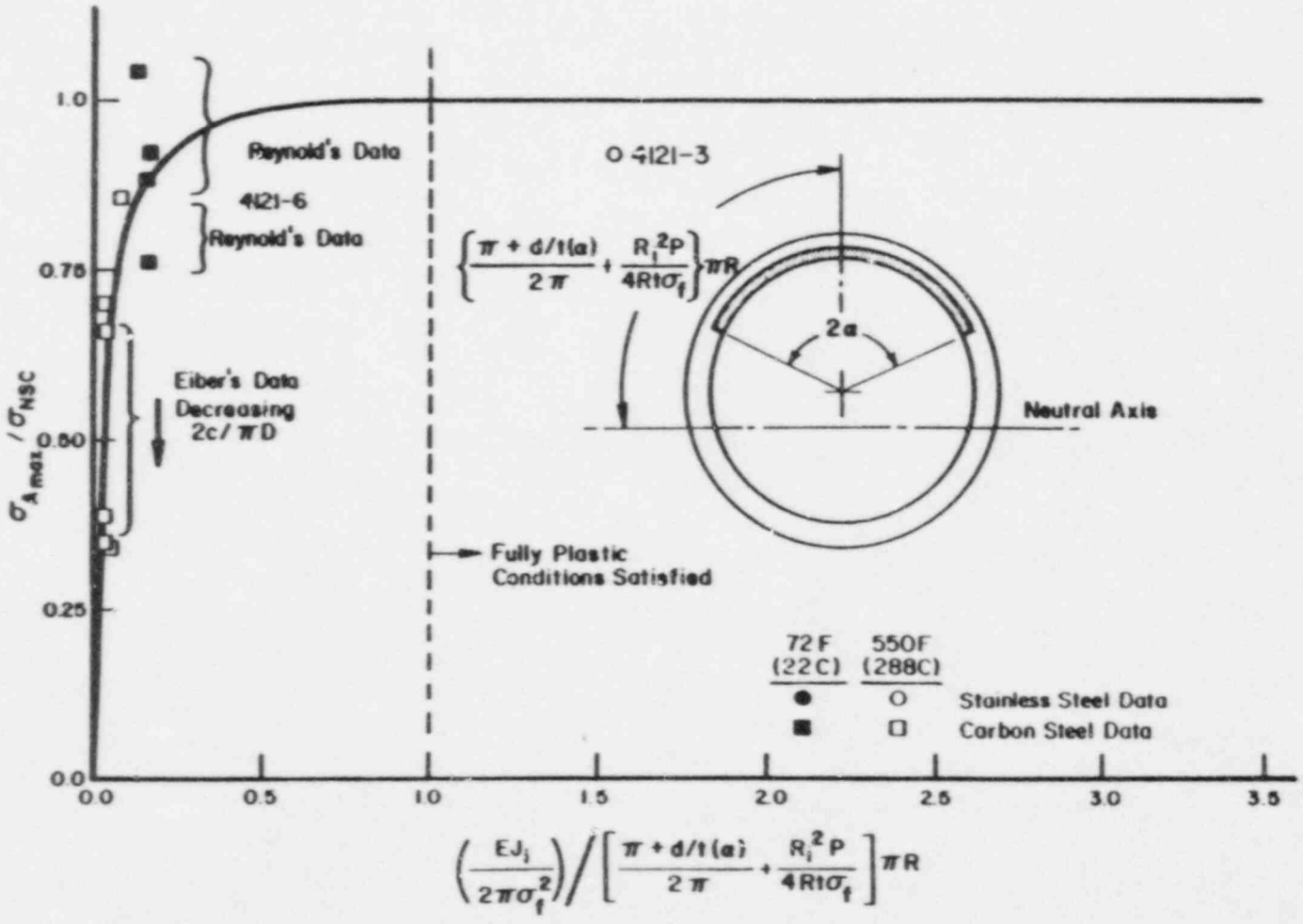

Figure 2.4.1 Ratio of maximum experimental stress for surface cracks subjected to axial membrane loading to net-section-collapse stress as a function of a dimensionless parameter relating to the plastic zone size. ($\sigma_f = 1.15(\sigma_y + \sigma_u)/2$)

SA-12/86-F2.4.1

increase the failure stress in the pipe. This behavior is discussed in Reference 2.4.1.

Future work involves fabrication and testing of the final experiment on a 10-inch (254-mm) nominal diameter carbon steel pipe with a through-wall crack. A bladder for this pipe fracture experiment has been ordered. This bladder should be received in early January 1988, and the experiment will be conducted by April of 1988.

References for Section 2.4

2.4.1 Wilkowski, G. M., and others, "Degraded Piping Program - Phase II", Semiannual Report, October 1984-March 1985, NUREG/CR-4082, Vol. 2, July 1985.

2.4.2 Wilkowski, G. M., and others, "Degraded Piping Program - Phase II", Semiannual Report, April 1985-September 1985, NUREG/CR-4082, Vol. 3, March 1986.

2.4.3 Wilkowski, G. M., and others, "Degraded Piping Program - Phase II", Semiannual Report, October 1985-March 1986, NUREG/CR-4082, Vol. 4, September 1986.

2.4.4 Eiber, R. J., Maxey, W. A., and Duffy, A., "Investigation of the Initiation and Extent of Ductile Pipe Rupture", BMI Report 1908 to the AEC, June 1971.

2.5 Fracture Behavior of Weld-Overlay Repaired Pipe (P. Scott and G. Wilkowski)

Weld-overlay repairs (WOR) are a common and acceptable means of repairing stress-corrosion-cracked stainless steel pipes in boiling-water reactor (BWR) plants in the U.S. and some foreign countries. In the U.S., the current design procedure for weld overlays follows the ASME Section XI IWB-3640 analysis procedure (Ref. 2.5.1), which is based on a modification of the net-section-collapse analysis. It is generally assumed that since WORs are fabricated using a gas-tungsten-arc welding (GTAW) process, which produces a relatively high-toughness weld metal, their failure stresses should be adequately predicted by the relatively simple net-section-collapse or IWB-3640 analyses.

The objective of this task is to develop experimental data to assess the limit-load analysis procedures embodied in ASME Section XI IWB-3640. To satisfy this objective, four full-scale pipe fracture experiments have been conducted. In each experiment, a pipe section with a fatigue-sharpened, circumferential through-wall crack was repaired by NUTECH Engineering in San Jose, California using the weld-overlay process. In each case, NUTECH used their current in-plant procedures. The repaired pipe sections were then appropriately instrumented and tested under combined internal pressure and four-point bending. Since the last semiannual report, the results and analysis of these experiments were published in the topical report listed below.

> "Assessment of Design Basis for Load-Carrying Capacity of Weld-Overlay Repairs", Paul M. Scott, NUREG/CR-4877, April 1987.

The topical report completed efforts in this area. The results are summarized in the following section.

2.5.1 Review of Topical Report on Weld-Overlay Repairs

The WOR technique involves applying multiple layers of weld metal that is resistant to intergranular stress corrosion cracking (IGSCC) over the cracked pipe section. The design thickness of the weld overlay is based on the spirit of the flaw acceptance evaluation procedures incorporated in the ASME Boiler and Pressure Vessel Code, Section XI, Article IWB-3640 (Ref. 2.5.1). NUREG-0313 Revision 2 (Ref. 2.5.2) guides the implementation of the procedures outlined in IWB-3640 in the case of weld-overlay design.

Prior to this research, no experimental pipe fracture data existed to evaluate the design procedures and guidelines outlined in IWB-3640 and NUREG-0313 Revision 2. The objective of this research is to develop experimental data for cracked pipe sections repaired by the weld-overlay technique so that the design procedures and guidelines embodied in these two documents may be assessed. As a result, the Office of Nuclear Reactor Regulation (NRR) will be in a better position to evaluate proposed overlay designs submitted for their consideration.

Four full-scale pipe fracture experiments were conducted as part of this program. In each case, a circumferential through-wall fatigue crack was repaired with a weld overlay by NUTECH Engineers using their current in-plant procedures. The repaired pipe sections were tested under combined pressure and four-point bending. The pressurizing medium was subcooled water, and the test temperature was 550 F (288 C).

The stresses at failure for each of these experiments were compared with the predicted failure stresses from the IWB-3640 analysis. As part of this analysis, two different flaw sizes were considered. The first was a flaw completely through the original pipe wall for the entire circumference of the pipe. According to NUREG-0313 Revision 2, this is the flaw size to be used in the design analysis for a Standard overlay. An overlay designed according to the design guidelines provided in NUREG-0313 Revision 2 for a Standard overlay is suitable for long-term plant operation provided that the overlay is inspected periodically in accordance with NRC guidance and subject to NRC approval. The Standard overlay is the design basis most commonly used today in weld-overlay design in the United States.

The second flaw size considered was that of the actual flaw in each of the test specimens evaluated. An overlay designed assuming the actual crack length in the analysis, instead of a full 360-degree circumferential flaw, would be considered a Limited Service overlay according to NUREG-0313 Revision 2. A Limited Service overlay is suitable only for short-term plant operation, not to exceed one fuel cycle.

As a result of the four WOR pipe experiments conducted as part of this effort, several comments can be made. Each of the four test specimens failed, or were on the verge of failure, at a stress level significantly higher than that predicted by the IWB-3640 analysis for a Standard overlay design. Thus, for the crack geometries evaluated herein, the margins of safety associated with the Standard overlay design are somewhat greater those used in the Code. Similarly, each of the four test specimens failed, or were on the verge of failure, at a stress level higher than that predicted by the IWB-3641 tables for the Limited Service design. However, when the IWB-3640 Source Equations were used in the Limited Service overlay design analysis, two of the four test specimens failed at a stress level lower than the predicted value. This fact poses an interesting question: if the crack to be repaired is a long (that is, 360-degree), deep crack, such as that found in service at the Duane Arnold Plant (Ref. 2.5.3), would the Standard overlay design analysis, which is generally used in service, always underpredict the failure stresses? For such a crack, the differences between the IWB-3640 Source Equations and the IWB-3641 tables are insignificant. Furthermore, for such a crack the extra conservatism embodied in the Standard overlay design analysis, from assuming that the crack is completely through the original pipe wall for the entire pipe circumference, is reduced. Therefore, the differences in predicted failure stresses from the Standard overlay design analysis and the Limited Service design analysis, where actual flaw dimensions are used, could be minimal.

An additional point to be addressed at this time is the ramifications of attempting to take credit for the higher strength of the weld-overlay material

in the limit-load analysis. It could be argued that, since one assumes in this analysis that the crack is completely through the original pipe wall, one should be able to take credit for the higher-strength weld metal. For the experiments conducted as part of this effort, if the flow stress were defined as 1.15 times the average of the yield and ultimate strengths of the overlay material (as suggested in Ref. 2.5.4), then the actual failure stresses would have been only 80 to 88 percent of the predicted limit-load stresses when actual flaw dimensions are used in the analysis (that is, a Limited Service overlay). Hence the weld metal strength should not be considered in a WOR analysis.

A very positive aspect that became apparent as a result of this research was the extremely large plastic deformations that occurred in the pipe sections adjacent to the weld overlays prior to fracture. These deformations resulted from both the low yield strengths of the pipe materials relative to the weld metal and the combined thickness of the overlay repair region. Such large deformations, as experienced in both the 6-inch (152-mm) and 16-inch (406-mm) diameter pipe experiments, could not physically occur in service without inducing more significant problems at other locations. Consequently, an analysis based on deformations or strains might result in a much higher safety factor than the load-based analysis.

WORs offer several additional advantages besides structural reinforcement. The radial shrinkage induced by the welding process produces a favorable compressive residual stress state on the inner surface of the weldment (Ref. 2.5.5). Also, the low-carbon, high-ferrite Type 308L weld metal used for the overlays is more resistant to IGSCC than sensitized Type 304 stainless steel (Ref. 2.5.5). Both of these factors tend to mitigate the further propagation of an IGSCC, unless the IGSCC propagated along the heat-affected zone (HAZ) at the pipe/WOR interface.

Another advantage associated with the use of weld overlays is the economic benefit. Weld overlays are economical from both cost and exposure standpoints. Repairing a cracked pipe section with a weld overlay is less expensive than replacing the pipe section with a new pipe fabricated from an IGSCC-resistant material. From an exposure standpoint, since the WOR process is highly automated, the extent of man-rem exposure is less than if the cracked pipe section were replaced.

Unfortunately, the use of weld overlays is not without some disadvantages. Weld shrinkage creates high-tensile residual stresses at other welds in the piping runs; these stresses could cause the initiation or further propagation of IGSCCs at these welds. Furthermore, the weld overlay makes it difficult to inspect the repaired weld by ultrasonic techniques (UT).

Although the research described herein has significantly increased knowledge of the fracture behavior of cracked pipe sections repaired by weld overlays, a few lingering questions remain. For each of the test specimens evaluated as part of this effort, a circumferential through-wall crack in the base metal was repaired using the weld-overlay technique because it was the simplest case to analyze. Recent results from the Degraded Piping Program (see Section 2.7.2 in Ref. 2.5.6) indicate that the fracture resistance along the fusion line of

a shielded-metal arc weld (SMAW) was lower than along a crack in the center of the SMAW. Since IGSCC cracks may grow along the fusion line, a question arises of how a surface crack would behave in this low-toughness location. Would the higher-toughness, weld-overlay material arrest such a crack, or would it continue to propagate through the thickness in much the same manner as observed in each of the experiments conducted to date?

Another question is how a long internal surface crack, as found in service at the Duane Arnold Plant, would behave. Past Degraded Piping Program experiments have shown this type of flaw geometry to offer very poor tearing resistance (Ref. 2.5.7). Once the internal surface crack broke through the wall, would it in some situations continue to propagate around the pipe circumference? In past experiments conducted as part of this effort, the amount of elastic energy stored in the piping system has been low enough that, once the crack broke through the wall, it propagated only to the ends of the internal surface crack. If the initial crack had been a long internal IGSCC, could it have propagated long enough to result in a complete pipe break at BWR conditions and at compliance levels representative of BWR piping systems? Further research is required to answer such questions.

Finally, neither IWB-3640 nor NUREG-0313 Revision 2 specifies what values are to be used for diameter or thickness in the design analysis. Are the original pipe diameter and thickness, the diameter and thickness of the repaired cross section (pipe plus overlay), or some combination of the two to be used in the design analysis? A computational round-robin conducted as part of this effort showed no general consensus of which terms are to be used among individuals with experience in the design of weld overlays. Additionally, not all designers used the ASME Code Class I piping stress equations; some used the Class II piping stress equations.

References for Section 2.5

2.5.1 ASME Boiler and Pressure Vessel Code, Section XI, "Rules for In-Service Inspection of Nuclear Power Plant Components", Article IWB-3640, Evaluation Procedures and Acceptance Criteria for Austenitic Piping, Winter 1985 Addendum.

2.5.2 Hazelton, W.S., "Technical Report on Material Selection and Processing Guidelines for BWR Coolant Pressure Boundary Piping", Draft Report, NUREG-0313 Rev. 2, June 1986.

2.5.3 U.S. Nuclear Regulatory Commission, "Investigation and Evaluation of Stress Corrosion Cracking in Piping of Light Water Reactor Plants", NUREG-0531, Chapter 7, February 1979.

2.5.4 Kanninen, M. F., and others, "Instability Predictions for Circumferentially Cracked Type 304 Stainless Steel Pipes Under Dynamic Loading", Final Report on EPRI Project T118-2, EPRI Project Number NP-2347, April 1982.

2.5.5 "Investigation and Evaluation of Stress Corrosion Cracking in Piping of Boiling Water Reactor Plants", prepared by the Pipe Crack Task Group, NUREG-1061, Vol. 1, August 1984.

2.5.6 Wilkowski, G. M., and others, "Degraded Piping Program - Phase II", Semiannual Report, April 1986-September 1986, NUREG/CR-4082, Vol. 5, April 1987.

2.5.7 Kramer, G., and Papaspyropoulos, V., "An Assessment of Circumferentially Complex-Cracked Pipe Subjected to Bending", NUREG/CR-4687, October 1986.

2.6 Stainless Steel TIG Welds
(M. Nakagaki, and F. Brust)

One of the major concerns regarding integrity of nuclear power plant piping is the behavior of cracks in girth welds. The objective of this effort is to assess the accuracy of J-estimation methods when applied to the analysis of specimens containing high-strength welds. Because of the higher strength of the weldment, the base metal adjacent to the weld metal can experience considerably larger plastic strain than the weld metal. When the size of the weldment is a small portion of the specimen (or structure), the base metal can undergo extensive plastic deformation compared with the contained deformation in the weld metal.

The experimental and analytical efforts have been completed, and a topical report on those results has been written:

> "Analysis of Cracks in Stainless Steel TIG Welds", M. Nakagaki, C. Marschall, and F. Brust, NUREG/CR-4806, December 1986.

A summary of results from this report is given in the following section. It includes a comparison of failure loads predicted by several J-estimation scheme methods for a circumferentially through-wall-cracked, tungsten-inert-gas (TIG) welded pipe specimen tested by the David Taylor Research Center (DTRC).

2.6.1 Summary of Results Reported in Past Semiannuals

The objective of this effort was to evaluate the significance of a through-wall crack in the center of a stainless steel TIG weld. Of particular interest is the fact that the weld makes the structure materially nonhomogeneous. All of the J-estimation schemes used for specimen or piping analyses are based on a homogeneous structure or specimen. Therefore, before making this evaluation, the theoretical basis for evaluating a crack in a weld was evaluated. This involved conducting finite element analyses of TIG-welded C(T) specimens and a circumferential through-wall crack in a pipe. The C(T) specimen tests were conducted at Battelle. Both welded specimens were tested, and all base metal specimens were tested to provide a reference. The pipe test was conducted at the DTRC (Ref. 2.6.1). The C(T) specimens were made from plate with approximately the same thickness as the pipe. Both C(T) and pipe specimens were tested at 550 F (288 C).

C(T) Specimen Evaluations

During the initial stages of this work, the validity of the J-integral for a crack near a bimaterial interface, such as a weldment, was theoretically examined. This examination, and a finite element verification, showed that the J-integral is path independent even if its contour path traverses the material interface. This path independence exists as long as the loading is monotonic and the crack is parallel to the weld (Figure 2.6.1). However, it

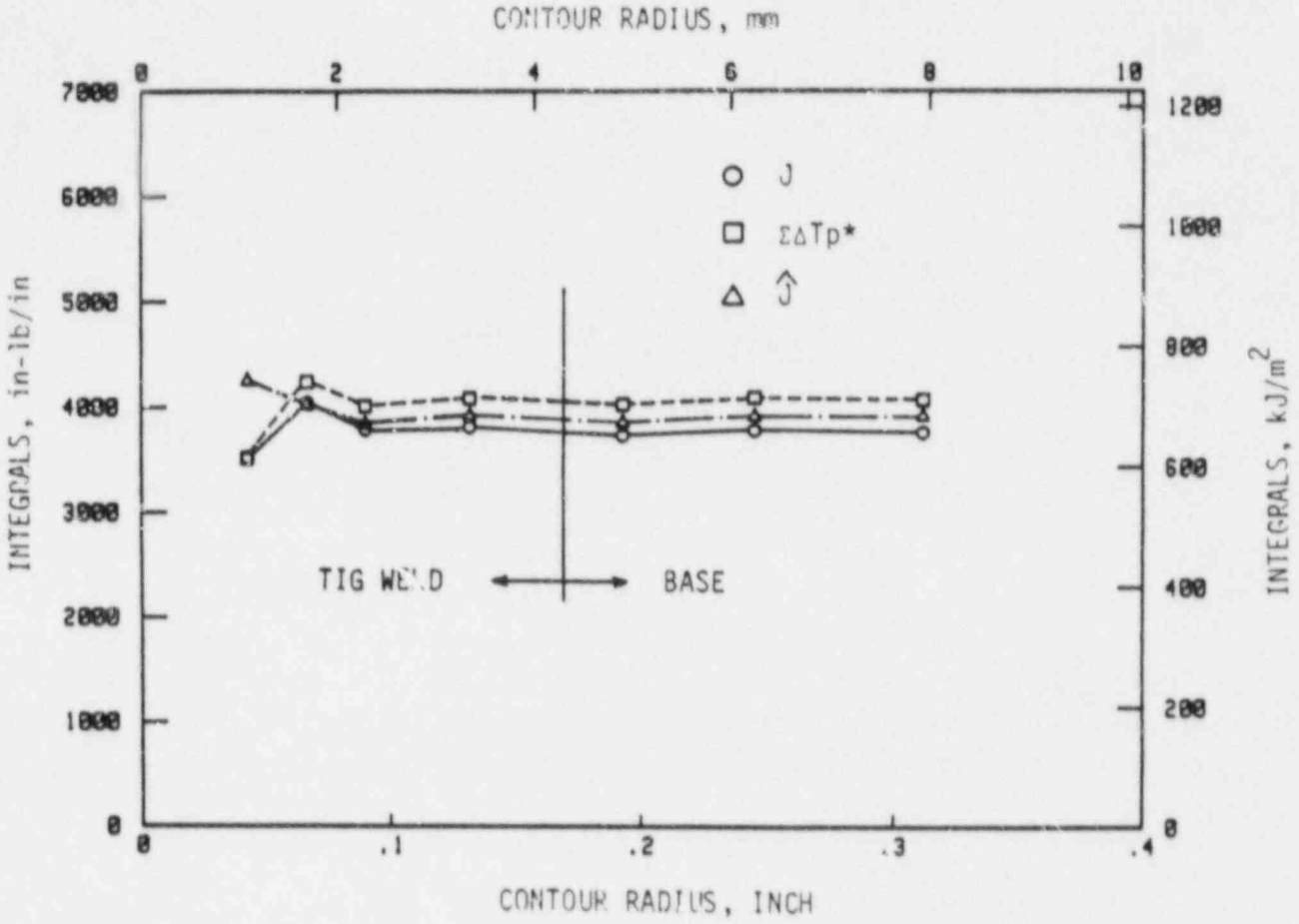

Figure 2.6.1 Path independence for the integral parameters at incipient crack growth in the TIG-welded C(T) specimen.

T-4806-F13

is well known that under a local unloading caused by ductile crack growth, J can become significantly path dependent. For this reason, the near-crack-tip integral parameters T* and $\hat{J}$, as well as the crack tip opening angle (CTOA) parameter were also evaluated in the finite element analyses. These integrals are path independent even under a loading that follows incremental plasticity theory, such as in global or local stress unloading situations, as well as deformation theory.

To evaluate the effect of the difference between the fracture parameters based on incremental plasticity and the conventional J (or the degree of nonproportional loading occurring in the cracked body), the parameter ΔI_p^* was suggested. (Actually I, a cumulative value of ΔI_p^* over load increments, was used.) The parameter I has the same units as J. It was theoretically proven and numerically verified that I reduces to zero under proportional loading (that is, when deformation plasticity is not violated) even in the presence of large plasticity. It was also shown that I monotonically increases during crack growth. A qualitative consistency between I and the ω parameter (Ref. 2.6.2), which is a measure of proportionality of loading, was also recognized.

For the 0.5T TIG-welded C(T) specimen, the 3T TIG-welded C(T) specimen, and the 3T base-metal stainless C(T) specimen, the behavior of near-crack-tip parameters during crack growth was investigated and compared with the behavior of J. T*, $(\Sigma\Delta T_p^*)$, and $\hat{J}$ remained relatively constant, creating a large discrepancy between these two parameters and the far-field J, which monotonically increased (see Figure 2.6.2 as an example). The CTOA behaved in a manner similar to T* and $\hat{J}$ (see Figure 2.6.3).

Pipe Finite Element Method Analysis

A TIG-welded 4.5-inch- (114-mm-) diameter Type 304 stainless steel pipe with a circumferential through-wall crack, tested at the DTRC, was analyzed by a 3-D finite element procedure. The calculated values of load versus load-line displacement are compared with the experimental results in Figure 2.6.4. The agreement is good until initiation, but the loads are underpredicted after crack initiation. This is typical for finite element analysis of through-wall-cracked pipe. For computing J, the virtual crack extension (VCE) method and the η-factor J-estimation method were employed. The calculated VCE J- and η-factor J results are shown for the circumferential crack growth in Figure 2.6.5; the J_D-R curve calculated from the TIG-welded 3T C(T) specimen is also shown in Figure 2.6.5 for comparison. Reasonable correlation between J values during the crack growth in the pipe and C(T) specimens was found.

Pipe J-Estimation Scheme Analysis

The use of simple J-estimation methods to predict the load versus load-line displacement response of the TIG-welded 4.5-inch (114-mm) outside diameter pipe was made. Since a welded structure is a bimetal composite, using the base metal Ramberg-Osgood constants and the weld metal J-resistance curve gave

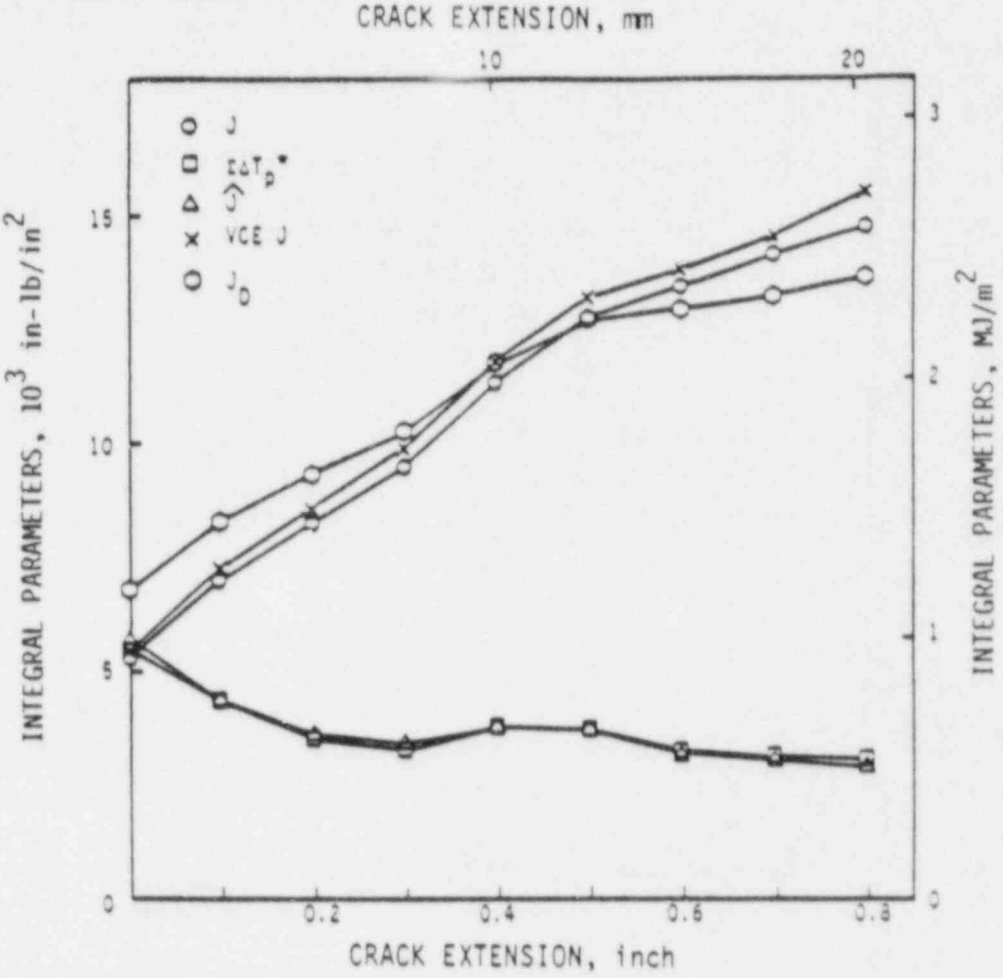

Figure 2.6.2 Integral parameter crack growth resistance curves for a 3T C(T) TIG-welded (A46-1) specimen tested at 550 F (288 C).

T-4806-F16

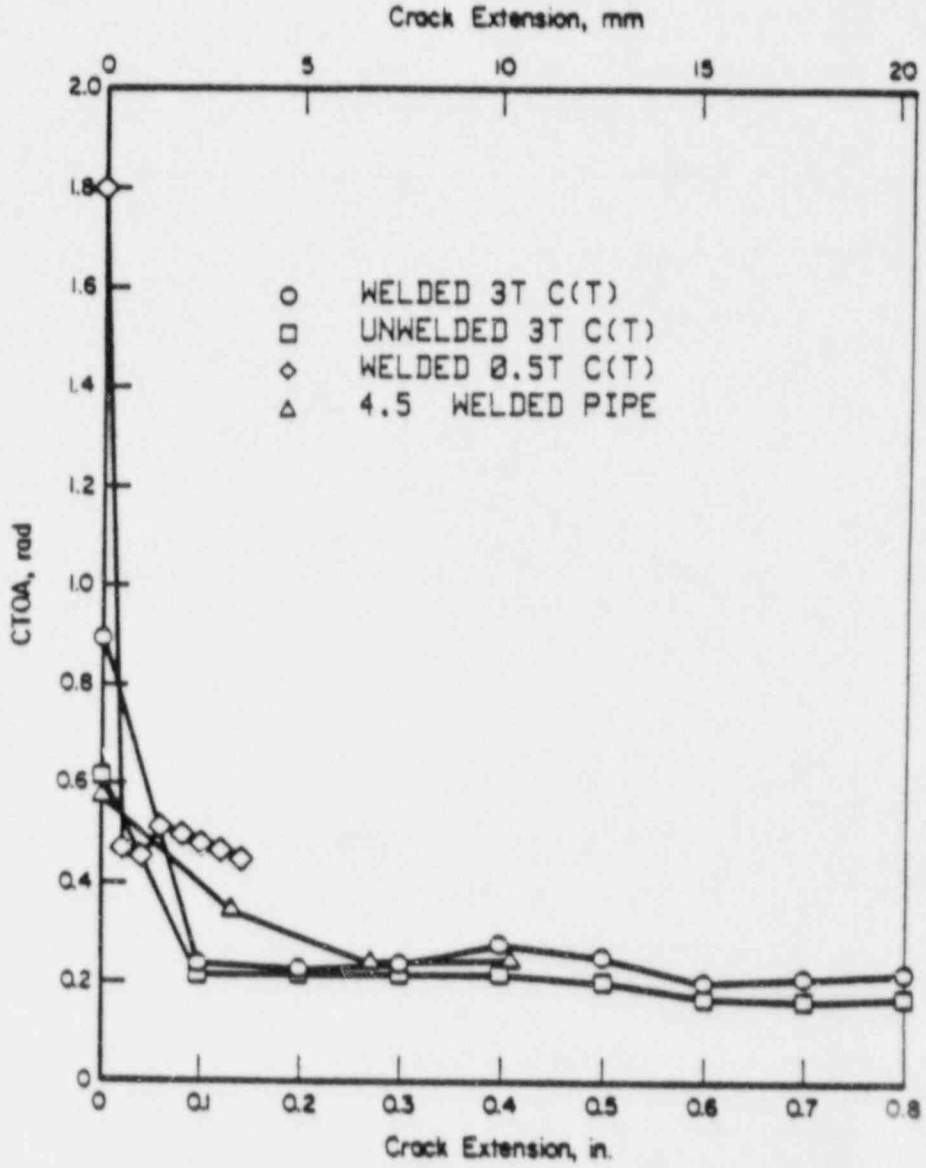

Figure 2.6.3 Comparison of CTOA resistance curves for TIG-welded and unwelded C(T) specimens and a TIG-welded DTRC pipe specimen at 550 F (288 C).

T-4806-F18

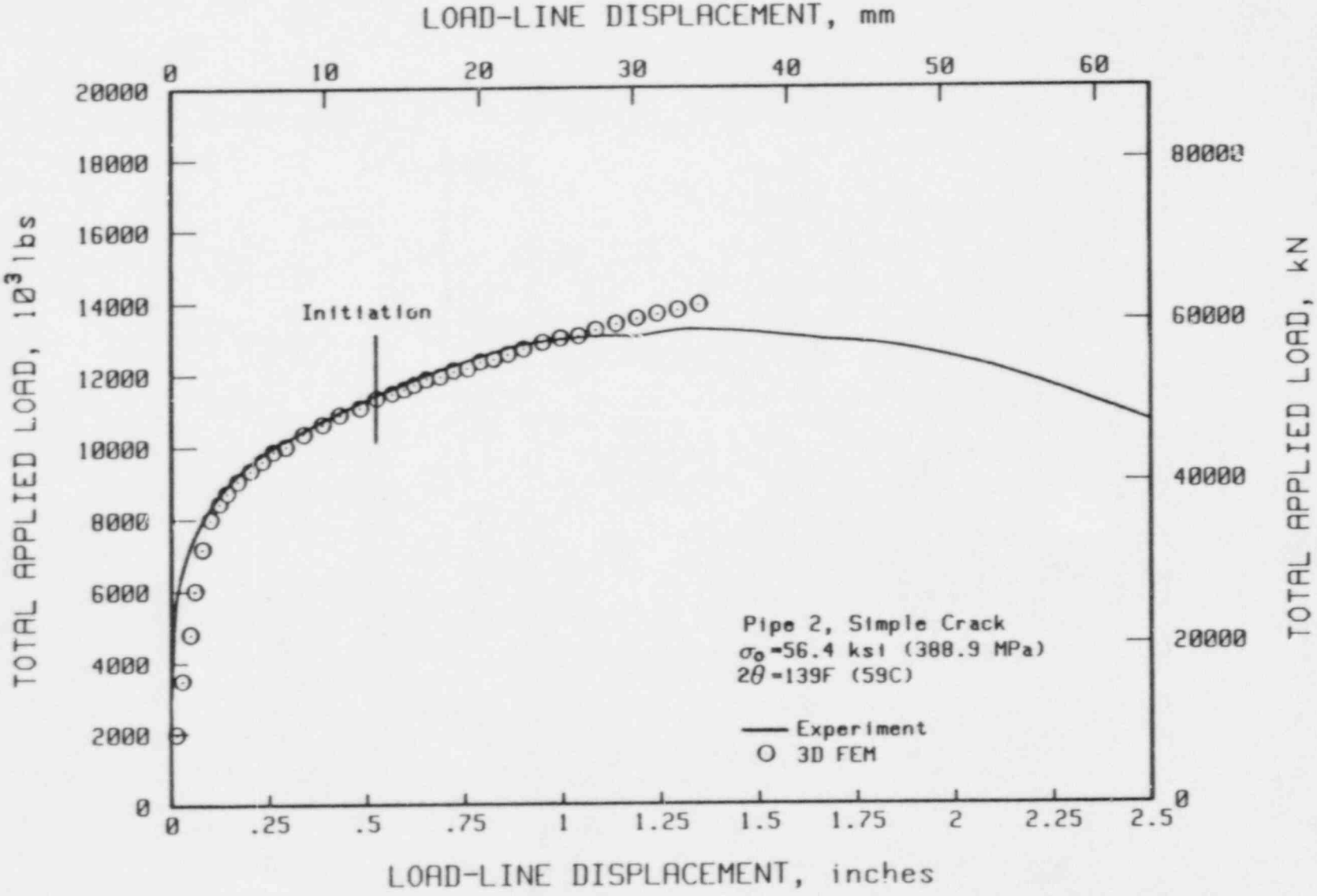

Figure 2.6.4 Load versus load-line displacement for DIRC-welded Type 304 stainless steel pipe Experiment No. 2 with a circumferential through-wall crack in the center of the 308L TIG weld. Tested at 550 F (288 C).

SA-6/85-F3.5.14

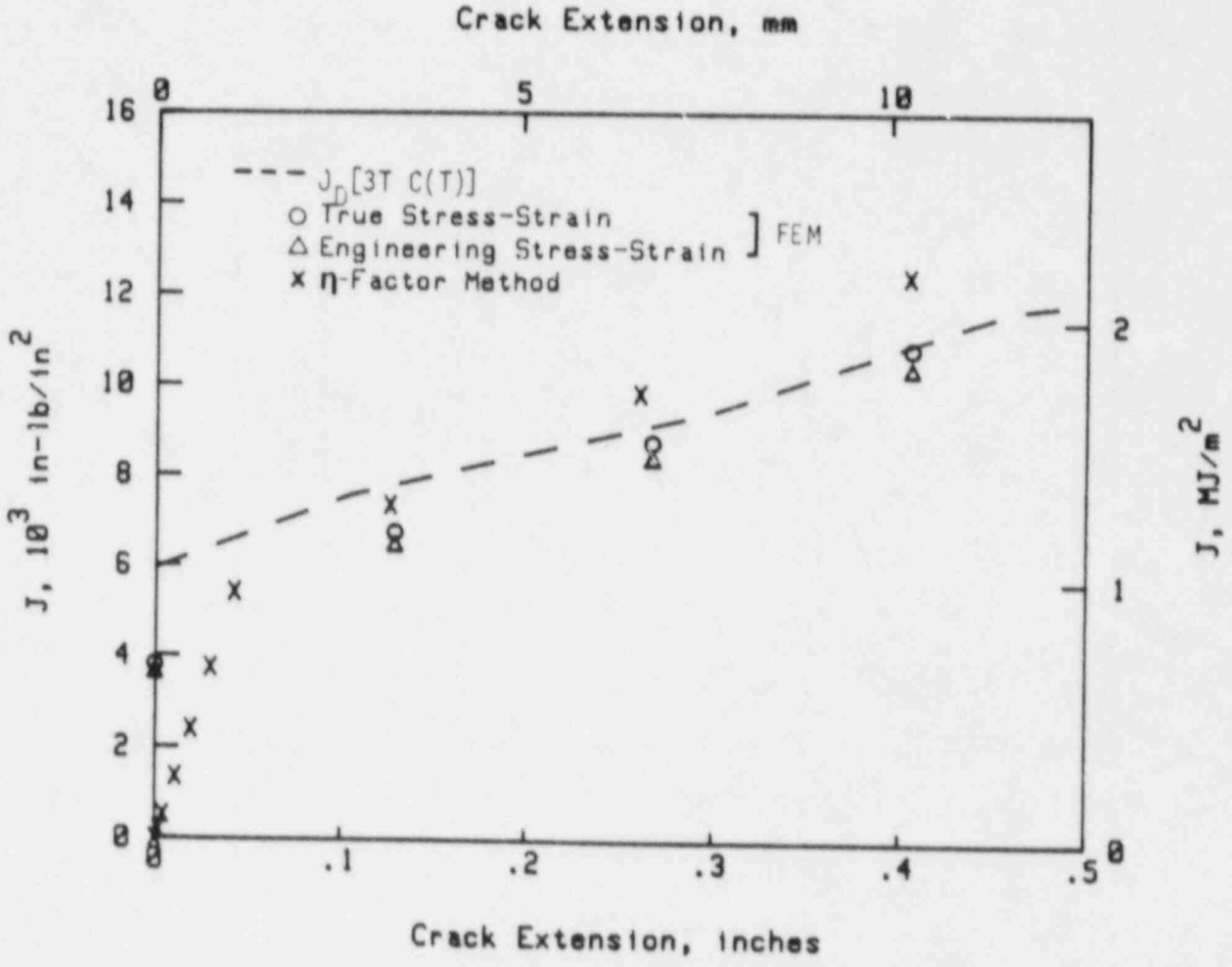

Figure 2.6.5 J-R curves for cracks in the TIG weld of stainless steel DTRC pipe Experiment No. 2. Tested at 550 F (288 C).

T-4806-F21

better prediction for this experiment than using the weld metal stress-strain curve. Figure 2.6.6 shows the predicted load versus load-line displacements for the pipe using five J-estimation schemes: the EPRI/GE, NUREG/CR-3464, LBB.NRC, LBB.BCL1, and LBB.BCL2 methods. The details of the recently developed LBB.BCL1 and LBB.BCL2 methods are fully described elsewhere (Ref. 2.6.3). In these predictions, the computed J_D-R curve from the TIG-welded 1.5T C(T) specimen was used. The results show that the EPRI/GE method gave the most conservative estimation (that is, underprediction of the load-displacement relationship), and the LBB.BCL predictions most nearly agreed with the experimental results. This trend is consistent with comparisons with pipe experiments on cracks in the base metal. The predictions of displacement past maximum load of the TIG-welded pipe test for all methods were not accurate as displacement predictions made for base metal pipe tests (see Ref. 2.6.3).

This study also revealed a significant variation of J-initiation (J_i) with the ratio of the weld size, D, to the specimen size, H. Because plane strain conditions are not satisfied, J_i also depends on specimen thickness. Therefore, to compare results from different specimens, the previously reported J_i values for the TIG-welded C(T) specimens (Ref. 2.6.4) were normalized by a representative J_i value of 3,100 in-lb/in^2 (0.543 MJ/m^2) for the base metal stainless steel plate of the same thickness. Figure 2.6.7 shows the results of the TIG-welded specimens for the various D/H ratios. It is evident that $J_{i(weld)}/J_{i(base)}$ varies with D/H, but a correlation between the C(T) specimens and the pipe can be seen. Also shown in Figure 2.6.7 are the results of 1-inch- (25.4-mm-) thick SAW C(T) specimens, for which the J_i values are normalized by a representative value of 14,000 in-lb/in^2 (2.45 MJ/m^2). The value of 14,000 in-lb/in^2 (2.45 MJ/m^2) is the J_i value for the base metal plate of the same thickness. Thus, initiation toughnesses of the two weldments and their trend over the ratio of weld to specimen size can be compared with the toughness of the base metal stainless steel. The apparent higher toughness of the TIG weldments and the considerably lower toughness of the SAW are apparent in this figure.

References for Section 2.6

2.6.1 Hays, R., Vassilaros, M. G., and Gudas, J. P., "Fracture Analysis of Welded Type 304 Stainless Steel Pipe", NUREG/CR-4538, Vol. 1, May, 1986.

2.6.2 Hutchinson, J. W., and Paris, P. C., "Stability Analysis of J-Controlled Crack Growth", Elastic-Plastic Fracture, ASTM STP 668, 1979, pp. 37-64.

2.6.3 Brust, F., "Approximate Methods for Fracture Analyses of Through-Wall-Cracked Pipes", NUREG/CR-4853, February 1987.

2.6.4 Nakagaki, M., Marschall, C., and Brust, F., "Analysis of Cracks in Stainless Steel TIG Welds", NUREG/CR-4806, December 1986.

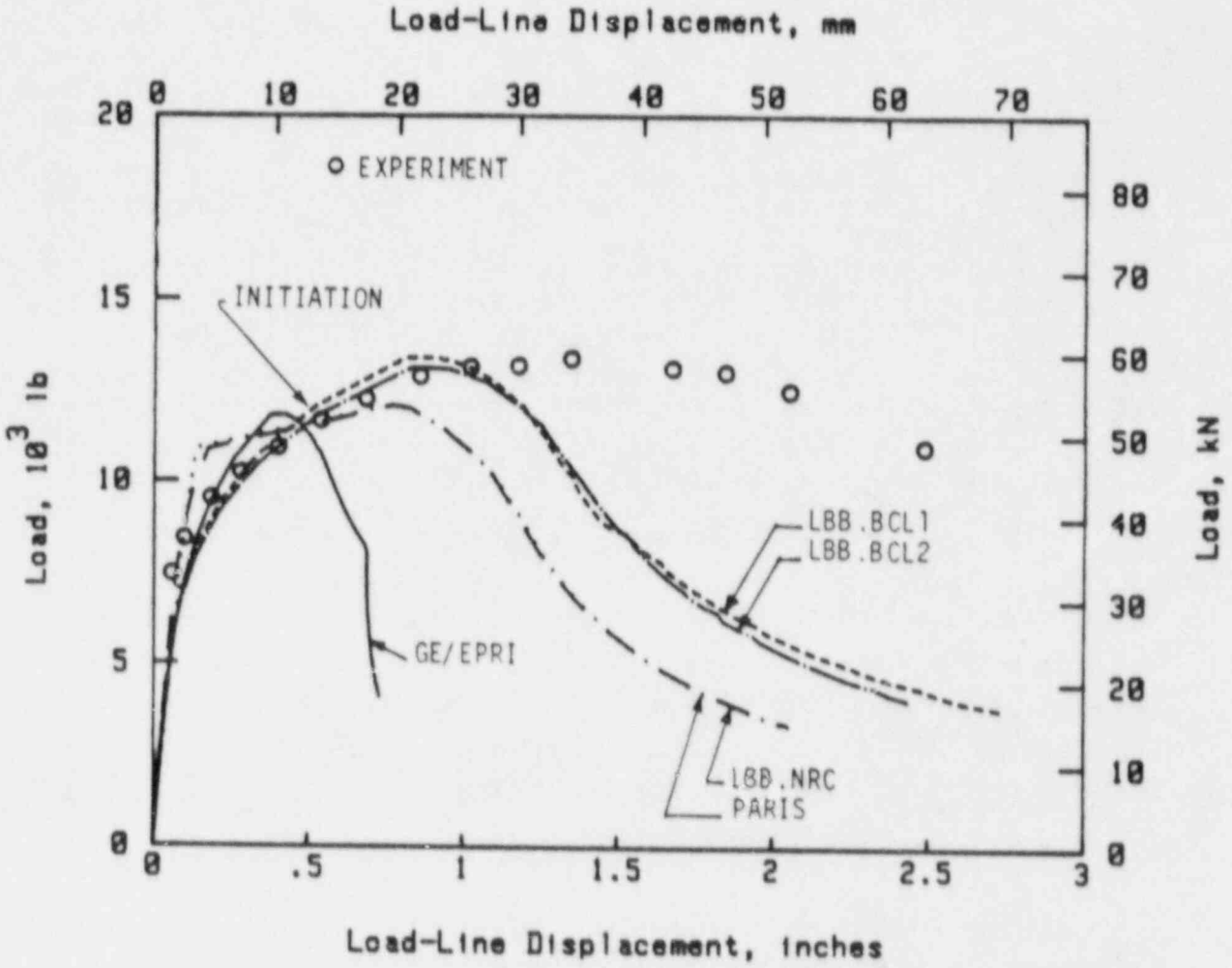

Figure 2.6.6 Predicted load versus load-line displacement for TIG-welded pipe by J-estimation schemes using TIG-welded 1.5T C(T) J-R curve.

T-4806-F22

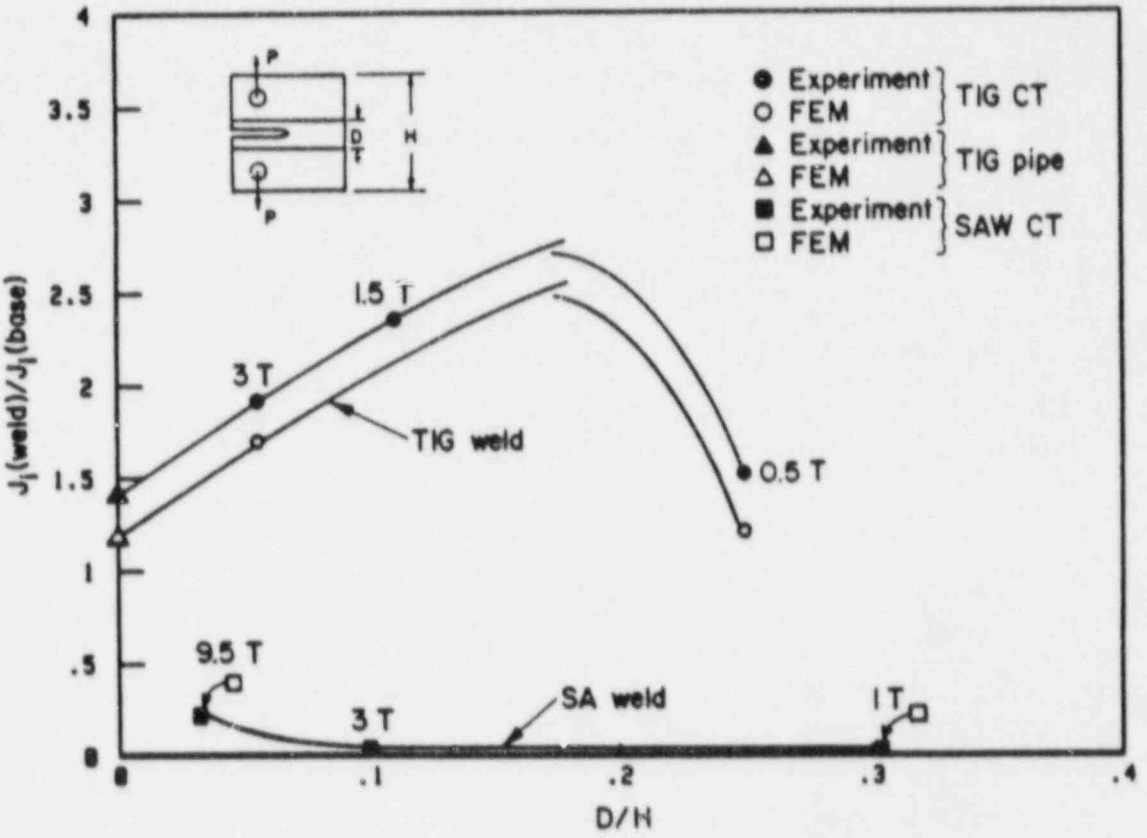

Figure 2.6.7 Effect of the ratio of weld size to specimen size on initiation toughness. (Note that D/H = 0.01 for pipe experiments.)

T-4806-F23

2.7 Stainless Steel Flux Welds

(F. Brust, D. Guerrieri, G. Kramer, M. Landow, C. Marschall, M. Nakagaki, P. Scott, and G. Wilkowski)

The objective of this evaluation is to verify the fracture behavior of cracks in stainless steel flux welds. For BWR piping, cracks generally occur in the HAZ. In a few cases (Ref. 2.7.1) cracks have occurred in the weld metal or have grown up the HAZ and followed the fusion line. Since stainless steel flux weld metals exhibit significantly less toughness than the parent stainless steel pipe material, this is a concern for flaw acceptance and pipe fracture analyses. The ASME Section XI IWB-3640 flaw evaluation procedure has been revised to account for the reduced weld metal toughness.

To better understand the fracture behavior of stainless steel flux welds and to provide validating data for the ASME flaw evaluation procedure, laboratory specimen tests and full-scale pipe fracture experiments were conducted. Analyses were carried out to evaluate laboratory and pipe fracture specimens with cracks in stainless steel flux welds. Since the last semiannual report, a topical report on this work has been published:

> "Analysis of Experiments on Stainless Steel Flux Welds", G. Wilkowski and others, NUREG/CR-4878, April 1987.

This topical report completed the efforts in this area; it is summarized in the following section. Similar work on carbon steel flux welds is presented in Section 2.10 of this report.

2.7.1 Summary of Results

The efforts in this section involved the following activities:

- Material characterization of an SAW in both as-welded and the solution-annealed conditions
- Testing of 1-inch- (25.4-mm-) thick planform-sized C(T) specimens (also see Section 3.3)
- Surface-cracked and through-wall-cracked pipe fracture experiments on the as-welded and the solution-annealed welds
- J-estimation scheme analyses of the pipe experiments
- Evaluation of net-section-collapse analysis, PZSC, and the ASME IWB-3640 analysis procedure for circumferentially surface-cracked pipe
- Finite element analysis of one through-wall-cracked pipe experiment.

Results From Material Characterization Efforts

Material characterization established that stainless steel SAW metal possesses much lower toughness than the parent material. Figure 2.7.1 compares the J_M-R curves from 1-inch- (25.4-mm-) thick, 1T C(T) SAW and Type 304 stainless steel base metal. A possible reason for the inherently low toughness of the SAW metal is that it possesses a higher oxygen content than does TIG weld metal. TIG-weld metal exhibits much better toughness, comparable to that of the parent plate, than SAW metal. This may also reflect the presence of more nonmetallic inclusions from the flux welding process.

The effect of solution-annealing on SAW metal behavior was also examined. The yield strength of the solution-annealed material was only slightly more than one-half that of the as-welded material. The ultimate tensile strength (UTS) was about the same for both (Figure 2.7.2). The J-R curve was only slightly higher for the solution-annealed weld than the as-welded metal (Figure 2.7.3).

A few FWFN(T) specimen tests were conducted in which the crack initiated in the HAZ of an SMAW. When the crack grew into the fusion line, the crack growth resistance in terms of the CTOA was about half the CTOA of a crack in the center of the SMAW metal. This implies that the fusion line toughness is lower than the flux weld metals. If further data are developed to substantiate this, then flaw assessment criteria and pipe fracture analyses should be based on the fusion line toughness rather than the weld metal toughness. This could affect the IWB-3640 criterion.

Results from Full-Scale Pipe Tests

Seven full-scale pipe fracture experiments were conducted to determine the effects of the lower toughness of the as-welded and solution-annealed weld procedures on the fracture behavior of six SAW cracked pipes and one SMAW cracked pipe (Table 2.7.1). Two experiments involved identical circumferentially through-wall-cracked pipes, one with the crack in an as-welded SAW and the other with the crack in a solution-annealed SAW (Figure 2.7.4). Two others involved identical circumferentially surface-cracked pipes, one with the crack in an as-welded SAW material and the other with the crack in a solution-annealed material (Figure 2.7.5). In each case, the solution-annealed specimen failed at a lower load than its as-welded counterpart. The amounts of the reductions in failure loads were consistent with the lower flow stress levels associated with the solution-annealed weld metal. In other words, the ratios of the failure loads approximately equalled the ratios of the flow stress levels of the weld metals. From this, it was found that solution-annealing does not enhance the SAW pipe's load-carrying capacity, a finding which is consistent with the weld metal tensile test results, but not the C(T) specimen results. This poses a potential problem with J-estimation scheme analyses, in which the base metal strength is used. These results indicate that the weld metal strength can be an important parameter. Perhaps an effective stress-strain curve combining weld metal and base metal properties should be used.

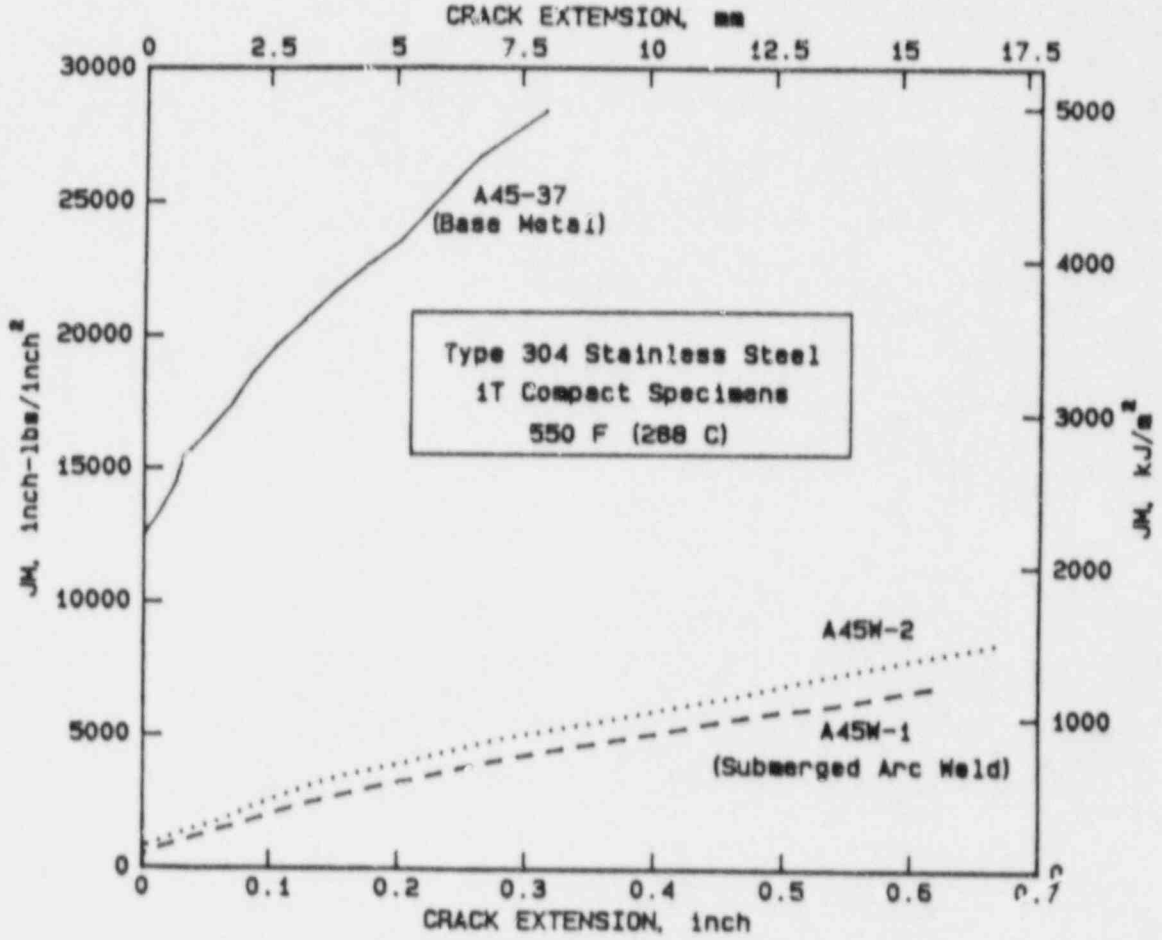

Figure 2.7.1 J_M-resistance curves for Type 304 stainless steel at 550 F (288 C) comparing base metal with SAW metal.

SA-12/85-F2.7.5

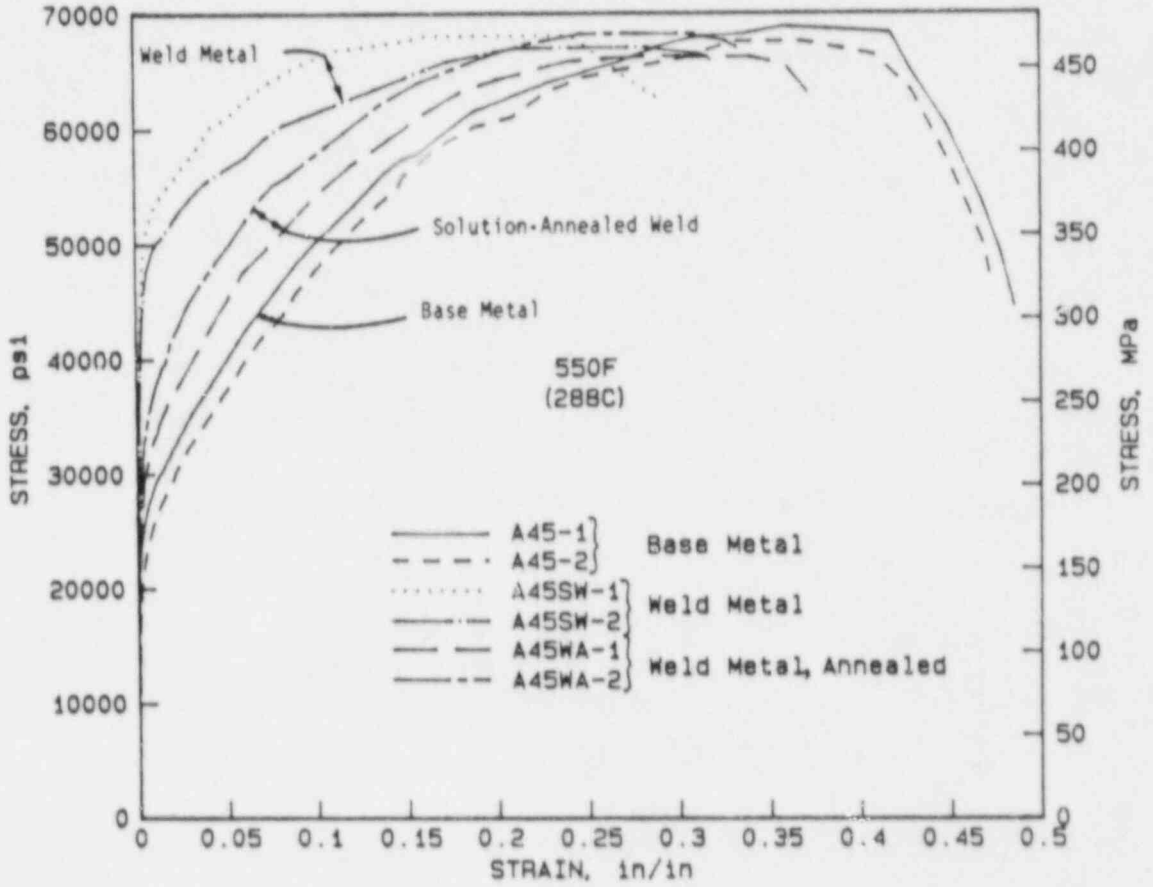

Figure 2.7.2 Comparison of engineering stress-strain curves for Type 304 stainless steel base metal, as-welded SAW, and solution-annealed SAW.

SA-6/86-F2.7.3

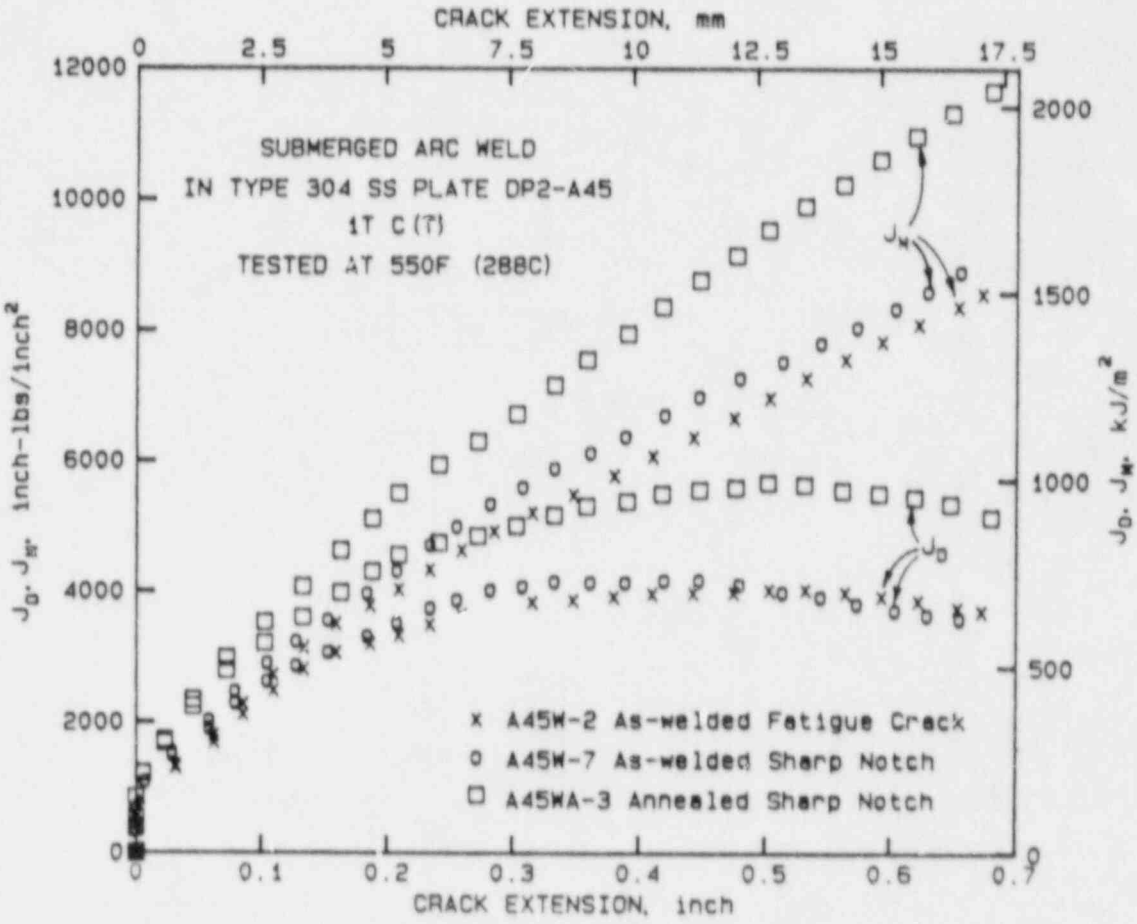

Figure 2.7.3 Effect of solution-annealing on J_D-R and J_M-R curves from stainless steel SAW C(T) specimens.

SA-6/86-F2.7.4

Table 2.7.1 Summary of stainless steel, flux weld, and pipe bend tests at 550 F (288 C)

Test No.	Diameter in. (mm)	Thickness in. (mm)	Weld[1] Type	Crack[2] Type	2c/πD	d/t	Pressure
4141-1	6 (152)	0.56 (14.3)	SAW	TWC	0.37	1.00	No
4141-2	6 (152)	0.58 (14.8)	SAW	SC	0.50	0.642	Yes
4141-3	16 (406)	1.03 (26.2)	SAW	TWC	0.37	1.00	No
4141-4	16 (406)	1.03 (26.2)	SAW	SC	0.5	0.666	Yes
4141-5	6 (152)	0.55 (14.3)	SAW-SA	TWC	0.37	1.00	No
4141-6	16 (406)	1.04 (26.4)	SAW-SA	SC	0.50	0.686	Yes
4111-5	28 (711)	1.19 (30.2)	SMAW	TWC	0.37	1.00	No

1 SAW-SA = SAW in solution-annealed condition.

2 TWC = through-wall crack; SC = surface crack.

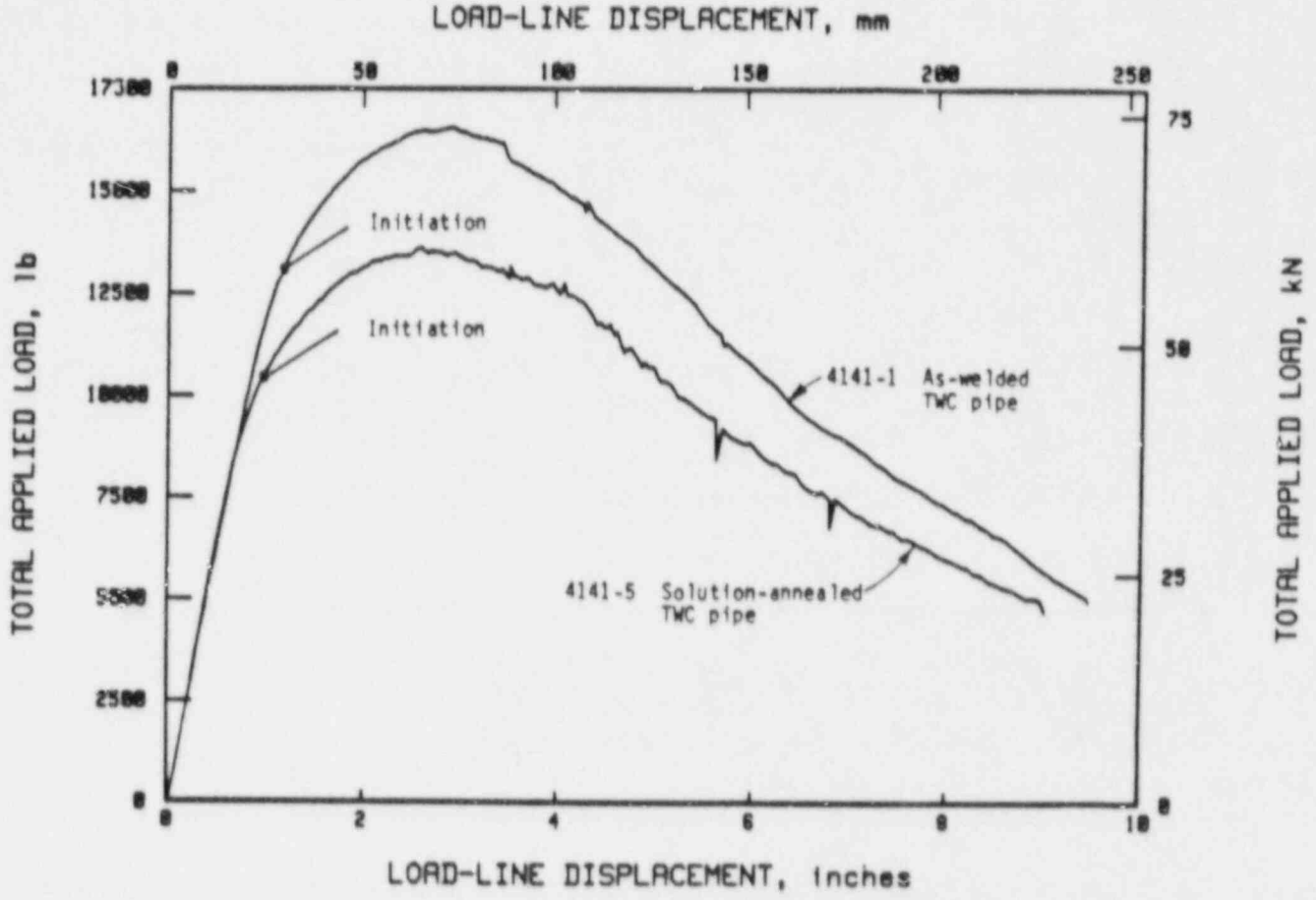

Figure 2.7.4 Comparison of total applied load as a function of load-line displacement for the 6-inch (152-mm) nominal diameter Type 304 stainless steel SAW through-wall-cracked pipe experiments with as-welded and solution-annealed stainless steel SAWs.

SA-6/86-F2.7.11

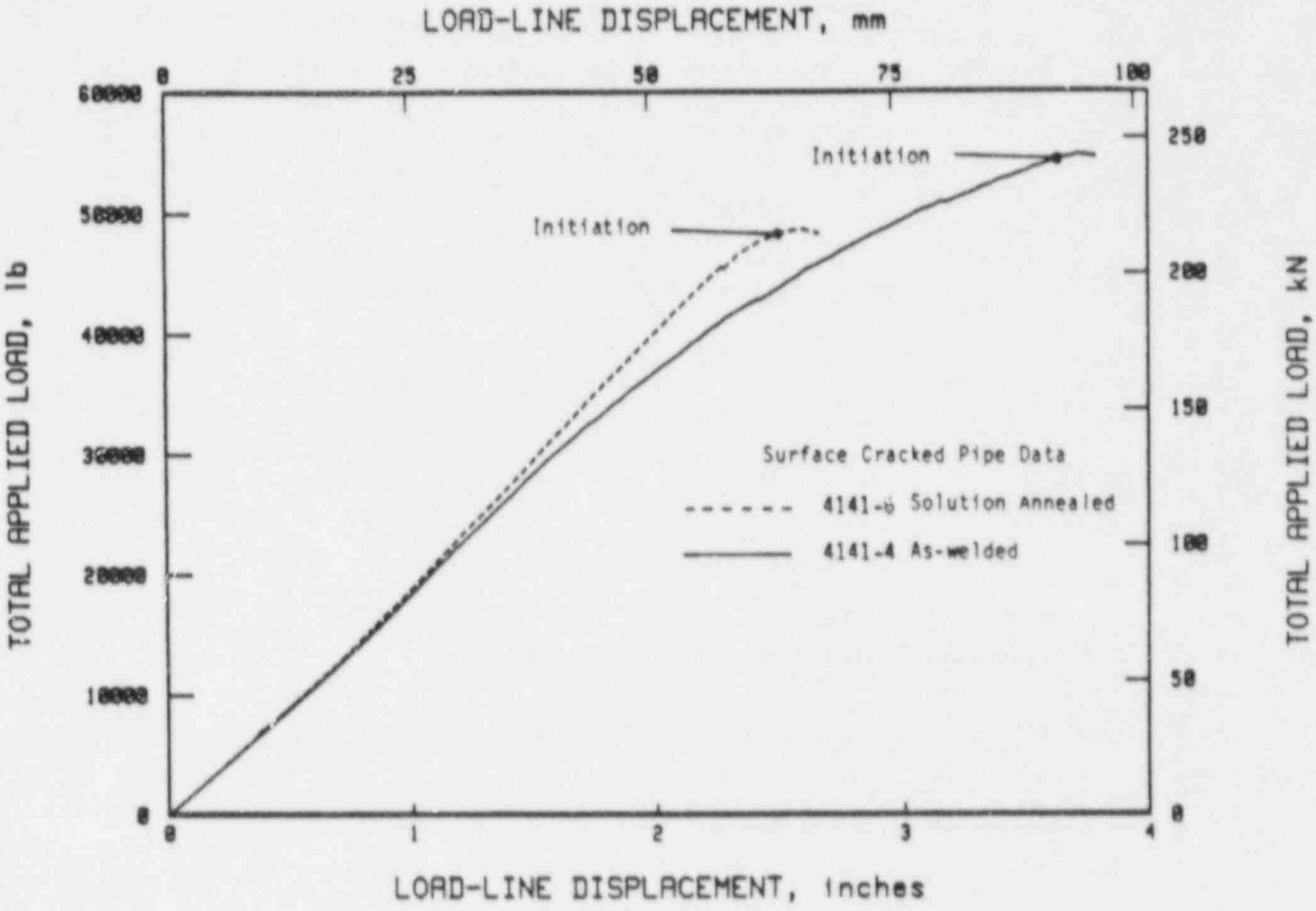

Figure 2.7.5 Comparison of total applied load as a function of load-line displacement for the 16-inch (406-mm) nominal diameter Type 304 stainless steel SAW surface-cracked pipe experiments with as-welded and solution-annealed stainless steel SAWs.

SA-6/86-F2.7.12

Evaluation of Net-Section-Collapse, Plastic-Zone, and the IWB-3640 Analyses

The results of the seven flux weld experiments were used to further evaluate the net-section-collapse analysis, the dimensionless plastic-zone analysis, and the IWB-3640 analysis procedure as modified for flux welds. The net-section collapse analysis overpredicted the failure loads in all the experiments. This result is not surprising, given the relatively low toughness of the weld metals. When weld metal tensile properties and J_i values are used to calculate the plastic-zone parameter, the dimensionless plastic-zone trend curve reveals the factor by which the net-section-collapse analysis must be derated to correctly predict the failure load. Figure 2.7.6 shows the through-wall-cracked pipe results, and Figure 2.7.7 shows the surface-cracked pipe data comparisons based on the dimensionless plastic-zone parameter. As is evident, the results from the seven plastic-zone experiments agreed well with the empirical trend curves for the dimensionless plastic-zone analysis. A simplified, statistically based plastic-zone parameter design curve, shown in Figure 2.7.8, was subsequently developed on all the data in the Degraded Piping Program (Ref. 2.7.2).

The SAW experimental results showed that the IWB-3640 source equations, as modified for SAW metal, underpredicted the failure loads by 20 to 47 percent. Thus, the use of the IWB-3640 tables, which contain additional factors of safety, would give an even higher margin of safety than initially advertised for the failure loads. For the SMAW pipe test, the factor of safety was less than 1 percent. This difference between the SAW and SMAW results is partially because the SAW pipe tests were smaller-diameter pipe experiments, and the flux weld stress multiplier in the Code for small diameter pipe defaults to a value for 24-inch- (610-mm-) diameter pipe. Thus, the flux weld stress multipliers used for the SAW experiments were artificially high.

An interesting finding was made when reviewing the J-R curve data from a 28-inch- (711-mm-) diameter pipe that was removed from the main recirculation line of the Nine Mile Point BWR nuclear power plant. While documenting the pedigree of the weld procedure, it was found that all the welds at that plant were SMAWs. This was an interesting discovery, in that the ASME Section XI IWB-3640 flux weld criteria used a J-R curve from a weld removed from the same recirculation line, believing that it was an SAW. The criteria, given in Reference 2.7.3, claims a higher toughness for SMAW than SAWs, but the results from this investigation showed that the SAW and the SMAW metals were close to each other in toughness. Consequently, only one stainless steel flux weld correction should be needed in the ASME IWB-3640 criteria.

J-Estimation Scheme Analyses

Various J-estimation schemes (EPRI/GE, NUREG/CR-3464, LBB.NRC, LBB.BCL1, LBB.BCL2) were used to predict crack initiation loads and maximum loads for several of the full-scale, SAW through-wall-cracked pipe experiments. The various schemes gave reasonable, if not always conservative, estimates of the crack initiation and maximum loads. With respect to predicting maximum loads, predictions using the J_M-R curve were usually less conservative than those

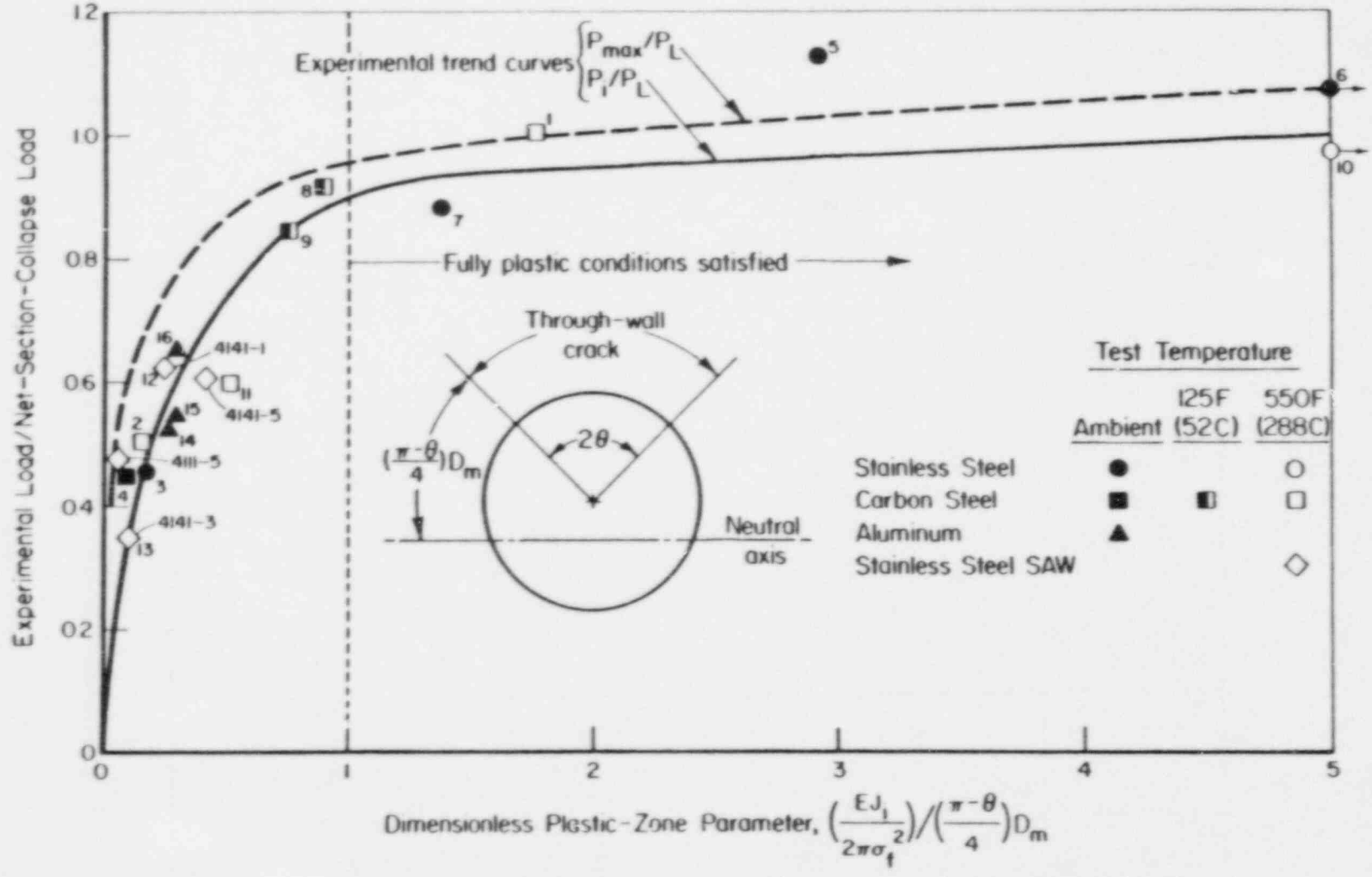

Figure 2.7.6 Ratio of experimental to predicted net-section-collapse load as a function of the dimensionless plastic-zone parameter. [Flow stress = $(\sigma_y + \sigma_u)/2$. Data points are given for crack initiation only.]

T-4878-F5.1

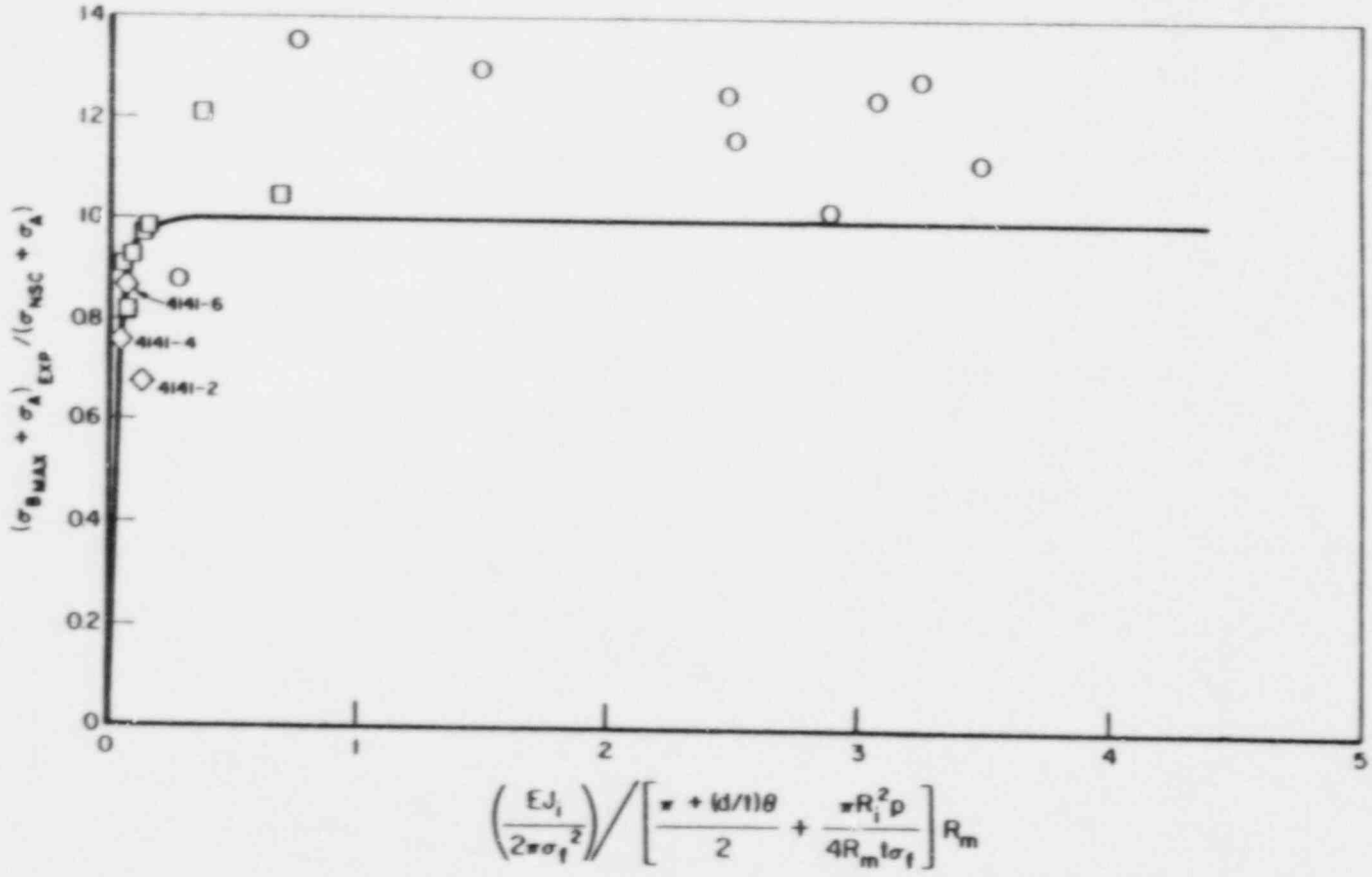

Figure 2.7.7 Ratio of experimental to predicted net-section-collapse load as a function of the dimensionless plastic-zone parameter for surface-cracked pipe.

SA-12/87-F2.7.7

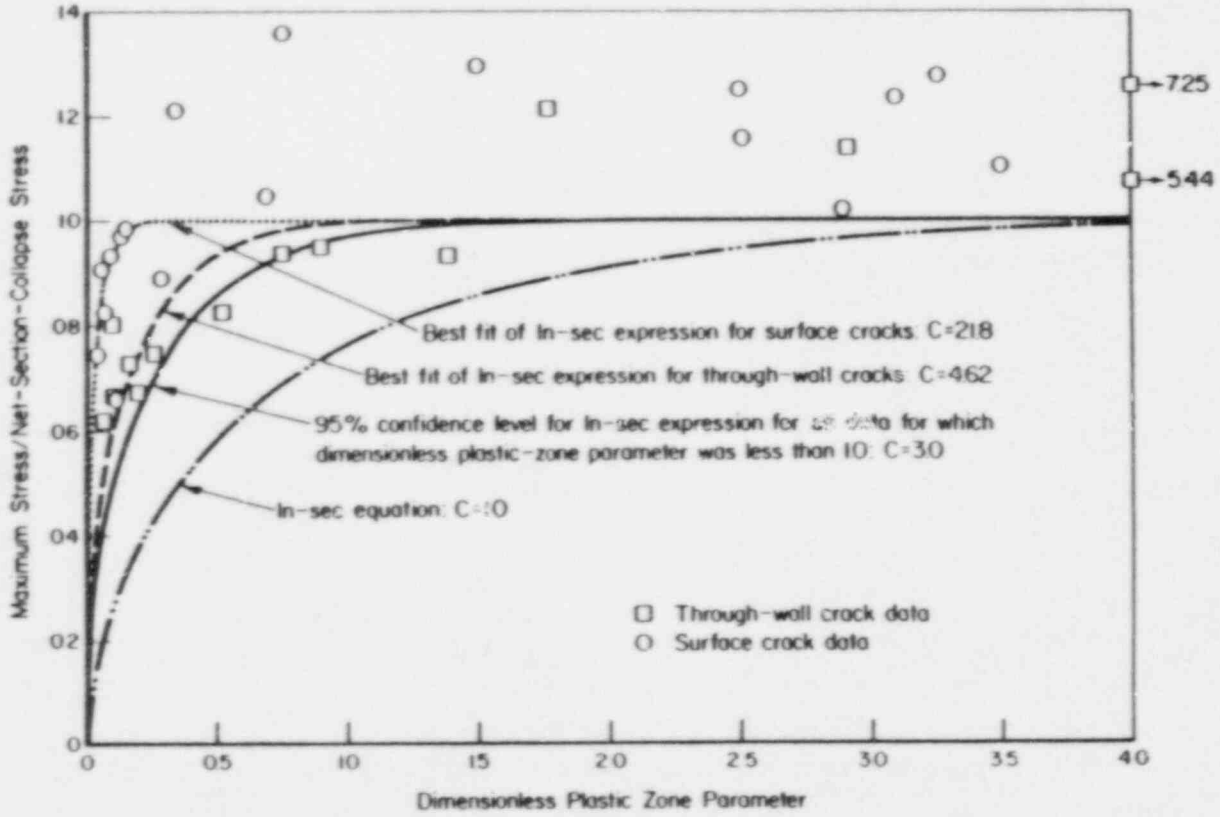

Figure 2.7.8 Compiled data using exact dimensionless plastic-zone parameter and flow stress = $(\sigma_y + \sigma_u)/2$. Note: C is a curve-fitting parameter in the equation, $\sigma_m/\sigma_{nsc} = (2/\pi)$ arc cos $[e^{-C(DPZP)}]$.

SA-12/86-F4.1.1

using the J_D-R curve. However, predictions of the load versus load-line displacements using the J_M-R curves were more accurate than those using the J_D-R curve (Figure 2.7.9). The best results were obtained by using the base metal stress-strain curve and the J_M-R curve of the weld metal with the LBB.BCL1 or LBB.BCL2 methods; an average or lower bound fit to the base metal stress-strain curve gave similar results. The EPRI/GE method gave the most conservative but least accurate predictions. Using the J_M-R curve with the NUREG/CR-3464 and LBB.NRC methods occasionally overpredicted the experimental loads.

The analyses of the through-wall-cracked pipe experiments showed that the 6-inch- (152-mm-) diameter pipe had a higher toughness than the 16-inch- (406-mm-) diameter pipe. Furthermore, J-R curves calculated from the 16-inch- (406-mm-) diameter pipe agreed well with all the planform C(T) specimen J-R curves, (Figure 2.7.10). The hypothesis that was developed to explain the above observations was based on the fact that the 16-inch- (406-mm-) diameter pipe and the C(T) specimens had the same thickness, 1 inch (25.4 mm), but the 6-inch- (152-mm-) diameter pipe was much thinner. Since the first two weld passes in the SAW procedure are made by the TIG process, which produces a higher-toughness weld metal, the thinner weld should have a higher relative toughness because of the composite nature of the weldment. A practical application of this knowledge is that the J-R curve from a thin weldment using a TIG root and hot passes should not be used to predict the fracture behavior of thicker weldments.

Finite Element Analyses

A finite element analysis was conducted for one 16-inch- (406-mm-) diameter through-wall-cracked pipe experiment. The analysis used the experimental crack growth versus load-line displacement data to calculate the J-R curve and the loads. Figure 2.7.11 compares the finite element and J-estimation scheme results with the experimental results, showing that the finite element results agree well until crack initiation, but underpredict the experimental results past crack initiation. This is consistent with other finite element results on a stainless steel base metal experiment (Ref. 2.7.4) and a stainless steel TIG-welded pipe experiment (Ref. 2.7.5). Figure 2.7.12 compares the J-R curves of the finite element analysis and the η-factor analysis from the pipe experiment with the C(T) specimen J-R curves. The finite element J-R curve is higher than the C(T) specimens, which is consistent with the base metal finite element analysis of the same size pipe (Ref. 2.7.4).

The significance of this investigation is that the finite element analysis generally gives a conservative estimate of the actual fracture behavior of the pipe. Several J-estimation schemes exist that can give as good or better predictions than the more costly finite element analysis. Why the finite element analysis consistantly underpredicts the experimental results is not known. This trend, however, may be why the GE-EPRI J-estimation scheme, which is based on finite element calculations, is consistantly conservative.

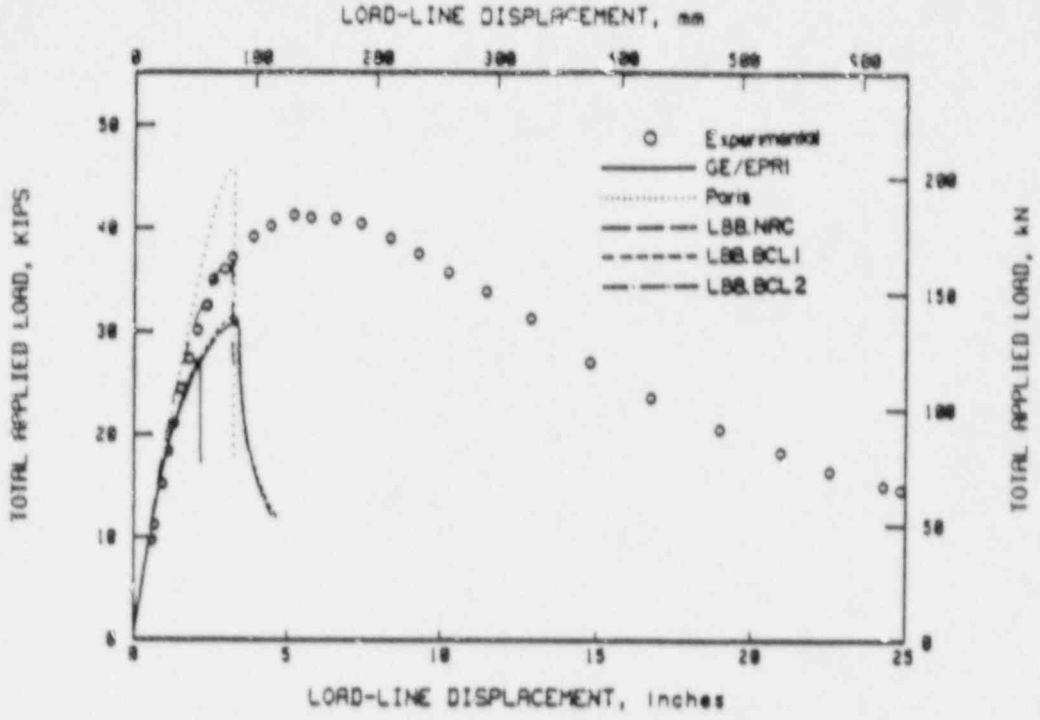

(a) Base metal stress-strain curve and J_D-R curve

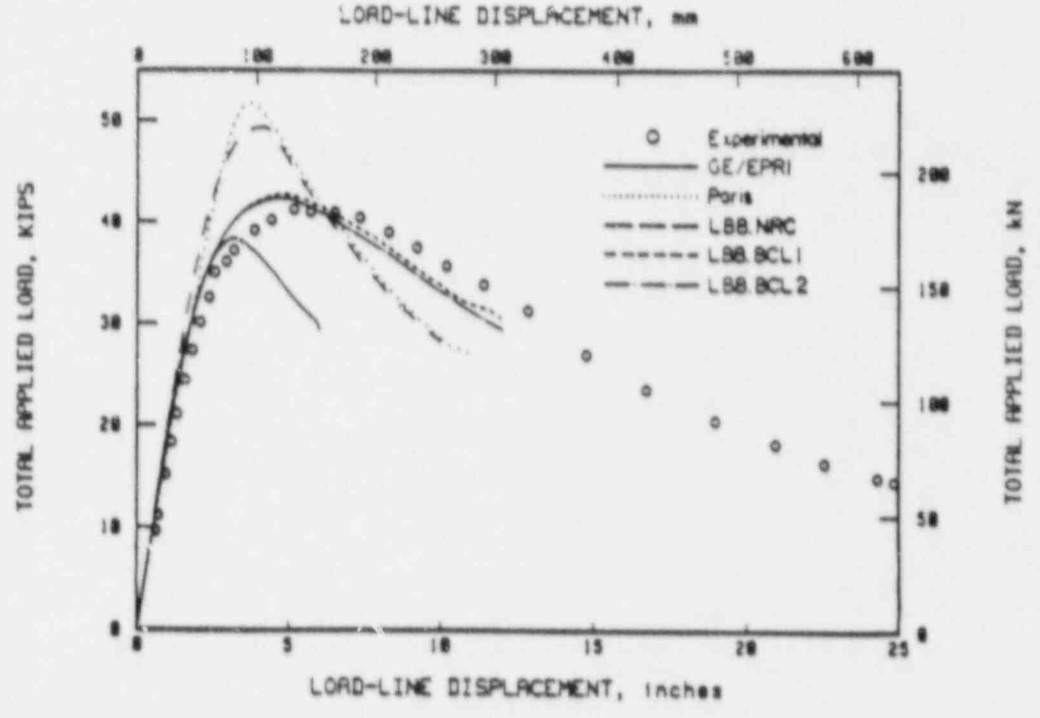

(b) Base metal stress-strain curve and J_M-R curve

Figure 2.7.9 Predicted load versus load-line displacements compared with results from Experiment 4141-3 on 16-inch- (406-mm-) diameter Type 304 stainless steel as-welded SAW pipe.

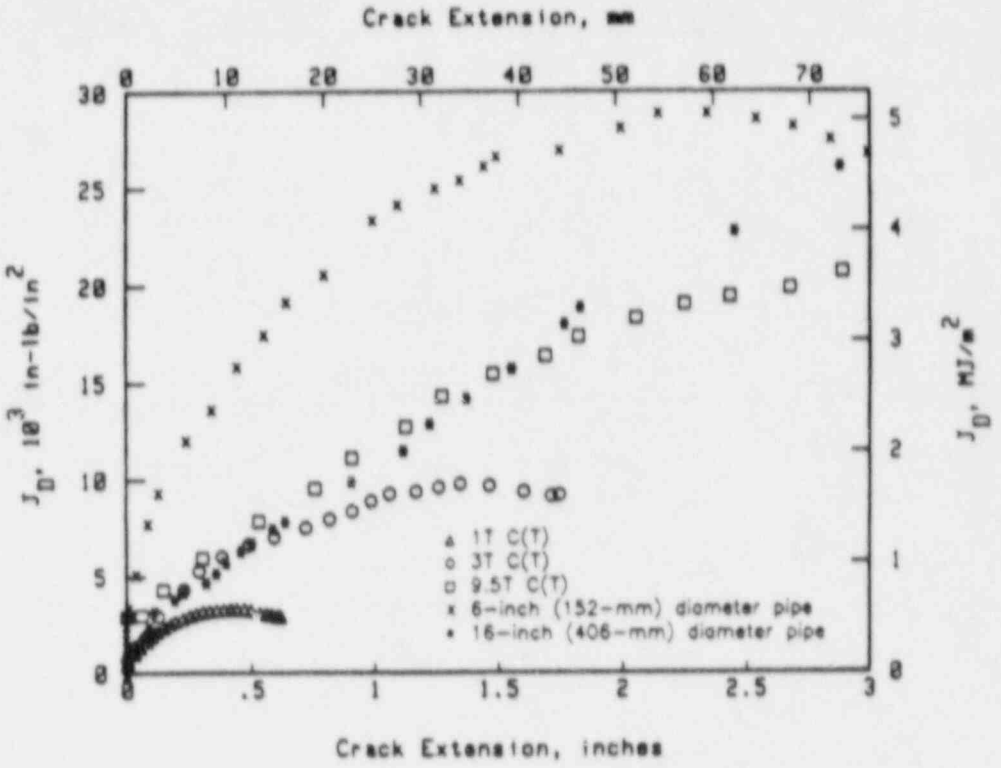

(a) J_D-R curves at 550 F (288 C)

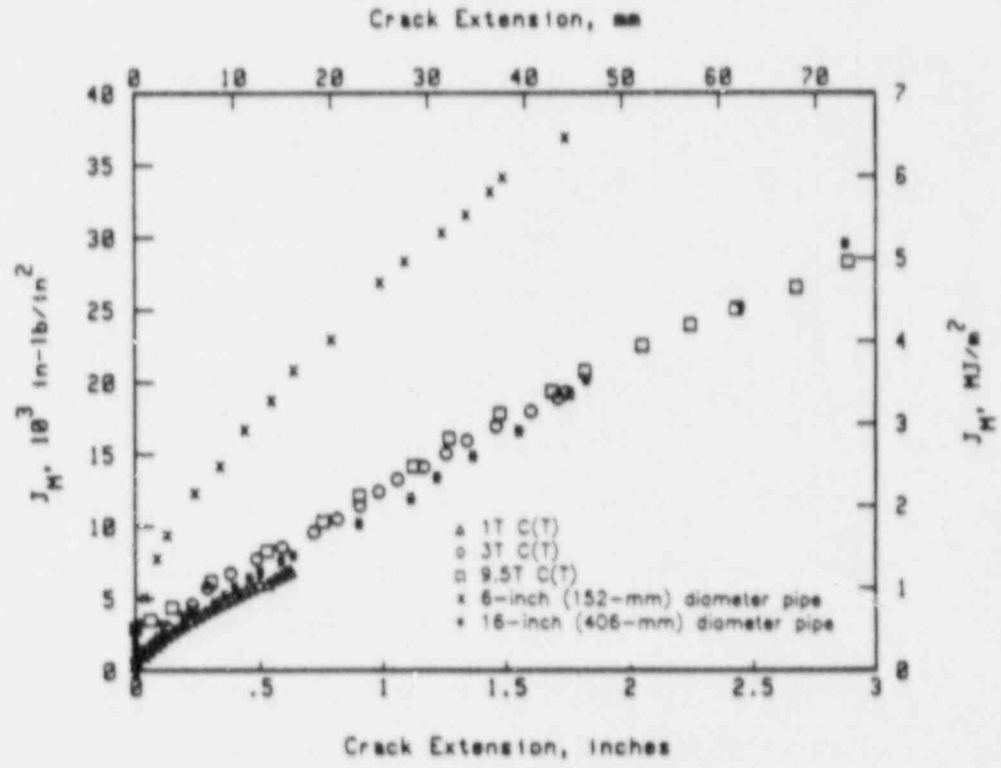

(b) J_M-R curves at 550 F (288 C)

Figure 2.7.10 Comparison of as-welded SAW J-R curves from various sized C(T) specimens and pipe experiments.

T-4878-F6.9

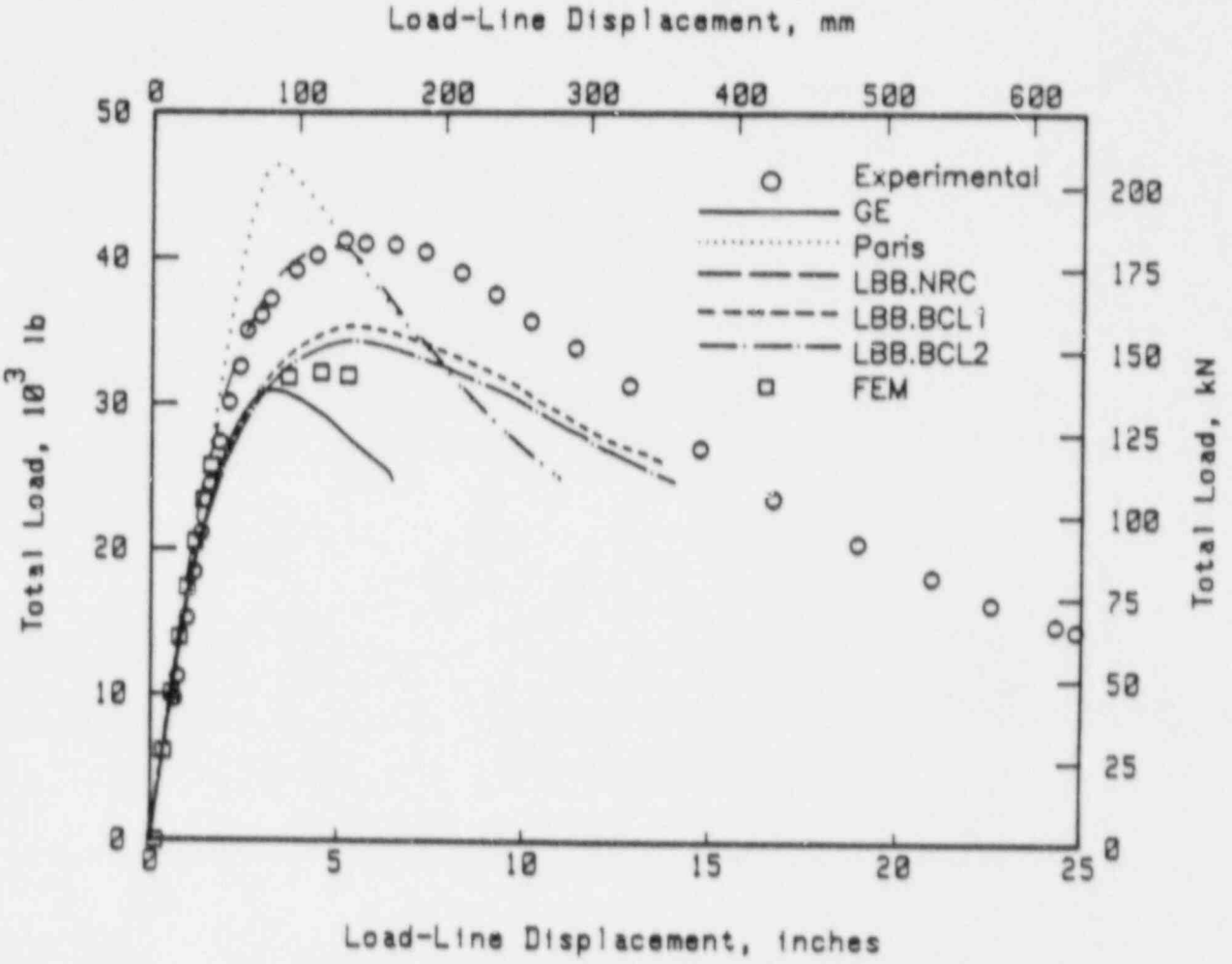

Figure 2.7.11 Predicted load versus load-line displacement record (using base metal properties and J_M-R curve) for estimation schemes compared with finite element analysis results and Experiment 4141-3 data.

SA-12/86-F2.7.8

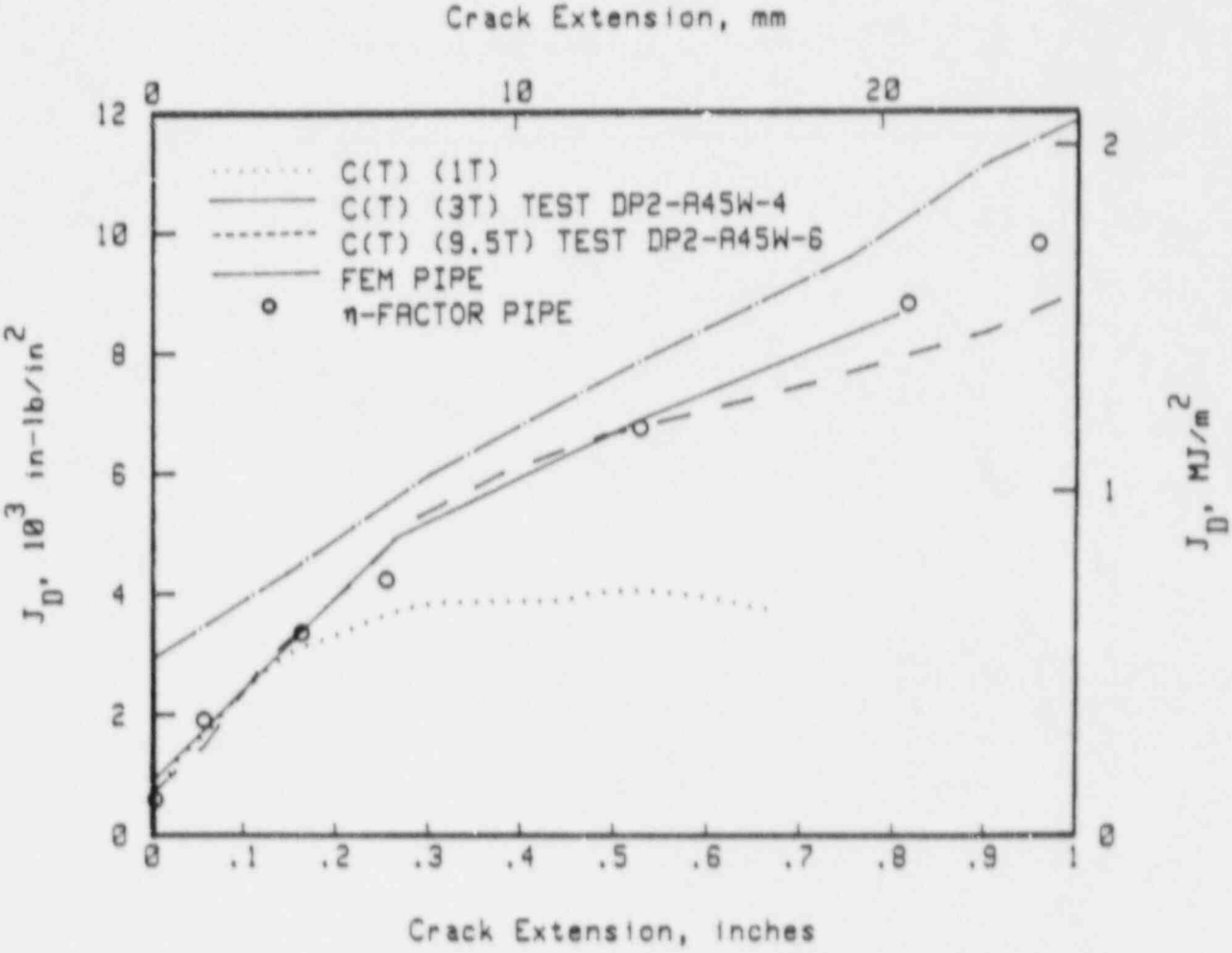

Figure 2.7.12 Comparison of three J_D-R curves from different C(T) sample sizes with the J-R curves derived from a finite element prediction using the virtual crack extension method and a J_D-R curve η-factor pipe analysis on Experiment 4141-3.

SA-12/86-F2.7.9

References for Section 2.7

2.7.1 Delwiche, D. E., and Gordon, G. M. (chair), G. E. San Jose CA (compilers), "Nine Mile Point 1 Pipe Crack Task Force Report", sponsored by Niagara Mohawk Power Corporation, Syracuse NY, June 20, 1983, pp. 5-4 and 5-5.

2.7.2 Wilkowski, G. M., and others, "Degraded Piping Program -Phase II", Semiannual Report, April 1986-September 1986, NUREG/CR-4082, Vol. 5, 1987.

2.7.3 "Evaluation of Flaws in Austenitic Steel Piping" (Technical Basis Document for ASME IWB-3640 analysis procedure), prepared by Section XI Task Group for Piping Flaw Evaluation, EPRI Report NP-4690-SR, April 1986.

2.7.4 Ahmad, J., and others, "Elastic-Plastic Finite Element Analysis of Crack Growth in Large Compact (Tension) and Circumferentially Through-Wall-Cracked Pipe Specimens - Results of the First Battelle/NRC Analysis Round-Robin", NUREG/CR-4573, October 1986.

2.7.5 Nakagaki, M., Marschall, C., and Brust, F., "Analysis of Cracks in Stainless Steel TIG Welds", NUREG/CR-4806, December 1986.

2.8 Circumferentially Through-Wall-Cracked and Surface-Cracked Pipe Subjected to Combined Pressure and Bending
(D. Guerrieri and P. Scott)

Much of the work on the Degraded Piping Program thus far has been directed at resolving the fracture behavior of pipe under relatively simple loading conditions, such as pure bending or pure axial membrane stress. This was necessary to build an adequate theoretical and empirical basis for understanding fracture behavior under various combinations of bending and axial load. However, piping systems in operating reactors are subjected to complex combinations of bending, membrane, and in some cases torsional stresses. In this section, we present the results of on-going studies of through-wall-cracked and surface-cracked pipes subjected to combined internal pressure and external bending loads. The results are used to evaluate the applicability the net-section-collapse analysis method and J-estimation schemes to combined loading situations. The following section summarizes results from past semiannual reports.

2.8.1 Summary of Results from Past Semiannual Reports

To evaluate the fracture behavior of circumferentially through-wall-cracked and surface-cracked pipe subjected to combined pressure and bending, the experimental test matrix outlined in Table 2.8.1 was developed. The test matrix includes twelve experiments: four pure pressure experiments[3], four pure bending experiments, and four combined pressure and bending experiments. For each set of four experiments, two different pipe materials are evaluated: one is a 6-inch- (152-mm-) nominal diameter, high-toughness stainless steel; the other is a 10-inch- (254-mm-) nominal diameter, lower-toughness carbon steel. Additionally, for each set of four experiments and for both materials, two different initial flaw geometries are evaluated: one is a through-wall crack whose length is nominally 37 percent of the pipe circumference; the other is a surface crack, nominally 50 percent of the pipe circumference in length and 67 or 70 percent of the pipe wall thickness in depth. As shown in Table 2.8.1, ten of twelve experiments have been completed to date.

Table 2.8.2 is a summary table of the test conditions and results for the ten experiments conducted to date. Note that the axial membrane stresses shown in Table 2.8.2 are based on the thin-wall Barlow expression ($PD_o/4t$) where D_o is the outside diameter of the pipe. This is the expression used in the ASME Code for Class 1 piping. Tables 2.8.3 and 2.8.4 compare the resulting maximum experimental stresses from Table 2.8.2 with the predicted net-section-collapse stresses. Table 2.8.3 applies to the six surface-cracked pipe experiments, and Table 2.8.4 applies to the four through-wall-cracked pipe experiments.

---

3 Note that the pure pressure experiments were conducted as part of another subtask of the Degraded Piping Program (see Section 2.4 of this report).

Table 2.8.1 Test matrix for evaluating the fracture behavior of circumferentially through-wall-cracked and surface-cracked pipes subjected to pressure and bending

Experiment Number	Loading Condition	Material	Nominal Diameter, inch (mm)	Flaw Type(a)	Nominal Flaw Dimensions 2c/πD	Nominal Flaw Dimensions d/t	Status
4121-1	Pressure	SA-376 TP304	6 (152)	TWC	0.37	1.00	Complete
4121-3	Pressure	SA-376 TP304	6 (152)	SC	0.50	0.70	Complete
4121-4	Pressure	SA 333 Gr6	10 (254)	TWC	0.37	1.00	To be done
4121-6	Pressure	SA 333 Gr6	10 (254)	SC	0.50	0.67	Complete
4131-5	Bending	SA-376 TP304	6 (152)	TWC	0.37	1.00	Complete
4131-6	Bending	SA-376 TP304	6 (152)	SC	0.50	0.70	Complete
4131-7	Bending	SA 333 Gr6	10 (254)	TWC	0.37	1.00	Complete
4131-8	Bending	SA 333 Gr6	10 (254)	SC	0.50	0.67	Complete
4131-1	Pressure + Bend	SA-376 TP304	6 (152)	TWC	0.37	1.00	Completed
4131-2	Pressure + Bend	SA-376 TP304	6 (152)	SC	0.50	0.70	Complete
4131-3	Pressure + Bend	SA 333 Gr6	10 (254)	TWC	0.37	1.00	To be done
4131-4	Pressure + Bend	SA 333 Gr6	10 (254)	SC	0.50	0.67	Complete

(a) TWC=through-wall crack; SC=surface crack.

Table 2.8.2. Summary of test conditions and results of pipe fracture experiments associated with the combined pressure and bending evaluation.

Experiment Number	Flaw Geometry	Material	Loading Condition	Internal Pressure, psi (MPa)	Actual Outside Diameter, inch (mm)	Actual Wall Thickness, inch (mm)	Dimensionless Circumferential Flaw Length, $2c/\pi$	Flaw Depth to Thickness Ratio, d/t	Bending Stress at Crack Initiation, ksi (MPa)	Maximum Bending Stress (σ_b), ksi (MPa)	Axial Membrane Stress at Crack Initiation(b), ksi (MPa)	Maximum Axial Membrane Stress (σ_a)(b), ksi (MPa)
4121-3	SC	SA-376 TP304	Pressure	Increasing(a)	6.625 (168)	0.500 (12.7)	0.50	0.708	--	--	20.04 (138)	20.12 (139)
4131-6	SC	SA-376 TP304	Bending	--	6.254 (159)	0.563 (14.3)	0.54	0.690	33.62 (232)	34.19 (236)	--	--
4131-2	SC	SA-376 TP304	Pressure & Bend	3,550 (24.5)	6.627 (168)	0.529 (13.4)	0.52	0.709	18.19 (126)	19.54 (135)	11.12 (76.7)	11.12 (76.7)
4121-6	SC	SA-333 Gr6	Pressure	Increasing(a)	10.750 (273)	0.615 (16.4)	0.50	0.670	--	--	25.42 (175)	26.25 (181)
4131-8	SC	SA-333 Gr6	Bending	--	10.655 (271)	0.593 (15.1)	0.48	0.678	34.05 (235)	36.62 (253)	--	--
4131-4	SC	SA-333 Gr6	Pressure & Bend	2,650 (18.28)	10.741 (273)	0.654 (16.6)	0.52	0.659	24.10 (166)	27.09 (137)	10.88 (75.07)	10.88 (75.07)
4121-1	TWC	SA-376 TP304	Pressure	Increasing(a)	6.620 (168)	0.507 (12.9)	0.386	1.0	--	--	12.73 (87.8)	14.25 (98.3)
4131-5	TWC	SA-376 TP304	Bending	--	6.254 (159)	0.549 (13.9)	0.388	1.0	18.24 (126)	23.80 (164)	--	--
4131-1	TWC	SA-376 TP304	Pressure & Bend	2,500 (17.2)	6.553 (106)	0.528 (13.4)	0.370	1.0	0.94 (61.7)	11.62 (80.2)	7.76 (53.5)	7.76 (53.5)
4131-7	TWC	SA-333 Gr6	Bending	--	10.75 (273)	0.719 (18.3)	0.346	1.0	17.47 (121)	24.12 (166)	--	--

(a) Pressure monotonically increasing throughout the course of the experiment.
(b) Axial membrane stress based on thin-wall Barlow expression ($PD_O/4t$) where D_O is the outside pipe diameter.

Table 2.8.3. Comparison of maximum experimental stresses to predict net-section-collapse stress for the six surface cracked pipe experiments.

Experiment Number	Material	Loading Condition	Maximum Bending Stress (σ_b), ksi (MPa)	Maximum Axial Membrane Stress (σ_a), ksi (MPa)	Net-Section-Collapse Stress(b) $(\sigma 1)_{NSC}$ ksi (MPa)	Net-Section-Collapse Stress(c) $(\sigma 2)_{NSC}$ ksi (MPa)	$\frac{(\sigma_b + \sigma_a)}{(\sigma_a + \sigma 1)_{NSC}}$	$\frac{(\sigma_b + \sigma_a)}{(\sigma_a + \sigma 2)_{NSC}}$
4121-3	SA-376 TP304	Pressure(a)	--	20.12 (139)	20.51 (142)	21.15 (146)	0.981	0.951
4131-6	SA-376 TP304	Bending	34.19 (236)	--	30.83 (213)	31.80 (219)	1.109	1.075
4131-2	SA-376 TP304	Pressure & Bend	19.54 (135)	11.12 (76.7)	18.96 (131)	20.13 (139)	1.019	0.981
4121-6	SA-333 Gr6	Pressure(a)	--	26.25 (181)	28.63 (198)	24.33 (168)	0.917	1.079
4131-8	SA-333 Gr6	Bending	36.62 (253)	--	43.43 (300)	36.91 (255)	0.843	0.992
4131-4	SA-333 Gr6	Pressure & Bend	27.09 (187)	10.88 (75.07)	32.10 (221)	25.36 (175)	0.883	1.047

(a) Pressure monotonically increasing throughout the course of the experiment.
(b) Based on a flow stress definition of 1.15 $(\sigma_y + \sigma_u)/2$.
(c) Based on a flow stress definition of 35 m.

Table 2.8.4. Comparison of maximum experimental stresses to predict net-section-collapse stress for the four through-wall crack pipe experiments conducted to date.

Experiment Number	Material	Loading Condition	Maximum Bending Stress (σ_b), ksi (MPa)	Maximum Axial Membrane Stress (σ_a), ksi (MPa)	Net-Section-Collapse Stress(b) $(\sigma 1)_{NSC}$ ksi (MPa)	Net-Section-Collapse Stress(c) $(\sigma 2)_{NSC}$ ksi (MPa)	$\frac{(\sigma_b + \sigma_a)}{(\sigma_a + \sigma 1)_{NSC}}$	$\frac{(\sigma_B + \sigma_A)}{(\sigma_a + \sigma 2)_{NSC}}$
4121-1	SA-376 TP304	Pressure(a)	--	14.25 (98.3)	14.89 (103)	15.45 (107)	0.957	0.922
4131-5	SA-376 TP304	Bending	23.80 (164)	--	21.87 (151)	22.70 (157)	1.088	1.048
4131-1	SA-376 TP304	Pressure & Bend	11.62 (80.2)	7.76 (53.5)	16.10 (111)	17.00 (117)	0.812	0.783
4131-7	SA-333 Gr6	Bending	24.12 (166)	--	33.65 (191)	28.47 (191)	0.717	0.847

(a) Pressure monotonically increasing throughout the course of the experiment.
(b) Based on a flow stress definition of 1.15 $(\sigma_y + \sigma_u)/2$.
(c) Based on a flow stress definition of 35 m.

Two definitions of flow stress are used to predict the net-section-collapse stresses in Tables 2.8.3 and 2.8.4. One is 1.15 times the average of the measured yield and ultimate tensile strengths of the pipe materials, and the other is a value of $3S_m$ as suggested in the ASME Code (Ref. 2.8.1).

Table 2.8.3 shows that for the stainless steel surface-cracked pipe experiments, the maximum experimental bending and/or membrane stress approached or exceeded the appropriate net-section-collapse stress in all cases. The flow stress, which was based on actual material properties (1.15 times the average of the yield and ultimate tensile strengths), is about the same as the $3S_m$ value of flow stress; thus, the above statement is true no matter which value of flow stress is used.

For the carbon steel surface-cracked pipe experiments, Table 2.8.3 shows that when actual material properties were used in defining the flow stress, the appropriate net-section-collapse analysis overpredicted the maximum stress by 10 to 15 percent. This occurs because not all of the assumptions embodied within the net-section-collapse analysis are being satisfied in the carbon steel experiments, whereas they are in the stainless steel experiments. Because the dimensionless plastic-zone parameter for the stainless steel experiments is always significantly greater than 1.0, fully plastic conditions were satisfied and net-section-collapse analysis is appropriate. In contrast, the dimensionless parameter of the PZSC for the carbon steel experiments is approximately 0.1. Thus, contained plasticity conditions existed, and consequently, the net-section-collapse analysis is not appropriate.

Table 2.8.4 shows that the maximum experimental bending and membrane stress approached or exceeded the appropriate net-section-collapse stress under both pure pressure and pure bending in the stainless steel, through-wall-cracked pipe experiments. However, for the combined pressure and bending experiment (Experiment 4131-1), the maximum experimental stress was only about 80 percent of the predicted net-section-collapse stress (Figure 2.8.1). This result was highly unexpected since this small-diameter pipe (6-inch [152-mm]) was fabricated from a high-toughness stainless steel. Fully plastic conditions should have been satisfied in this case, and net-section-collapse conditions should have been reached.

This was a significant experiment because it is the first experiment of its kind to be conducted. To the best of our knowledge, no pressure and bending experiment on circumferentially through-wall-cracked pipe has ever been successfully conducted at 550 F (288 C) because of the difficulties in sealing the through-wall crack at elevated temperatures. The test specimen used in this experiment was equipped with a special high-temperature bladder to contain the internal pressure.

Even though the experiment was the first of its kind, we have no basis for questioning its data. Figure 2.8.2 is the total applied load versus load-line displacement record for this experiment. A significant amount of displacement and associated crack growth was obtained in this experiment after maximum load was reached. The amount of crack growth experienced during the course of this

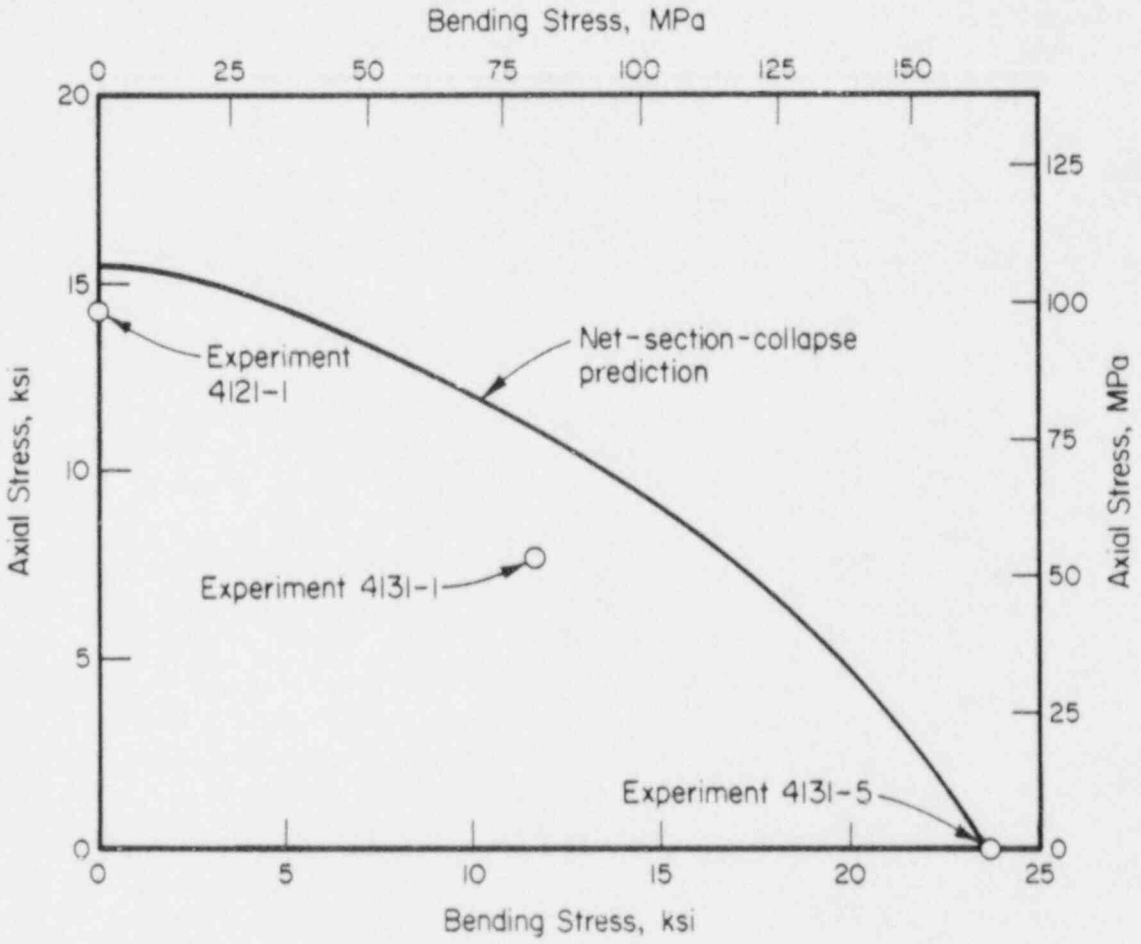

Figure 2.8.1 Comparison of stainless steel through-wall-cracked pipe data with maximum load predictions by net-section-collapse analysis. (Flow stress = $3S_m$.)

SA-12/87-F2.8.1

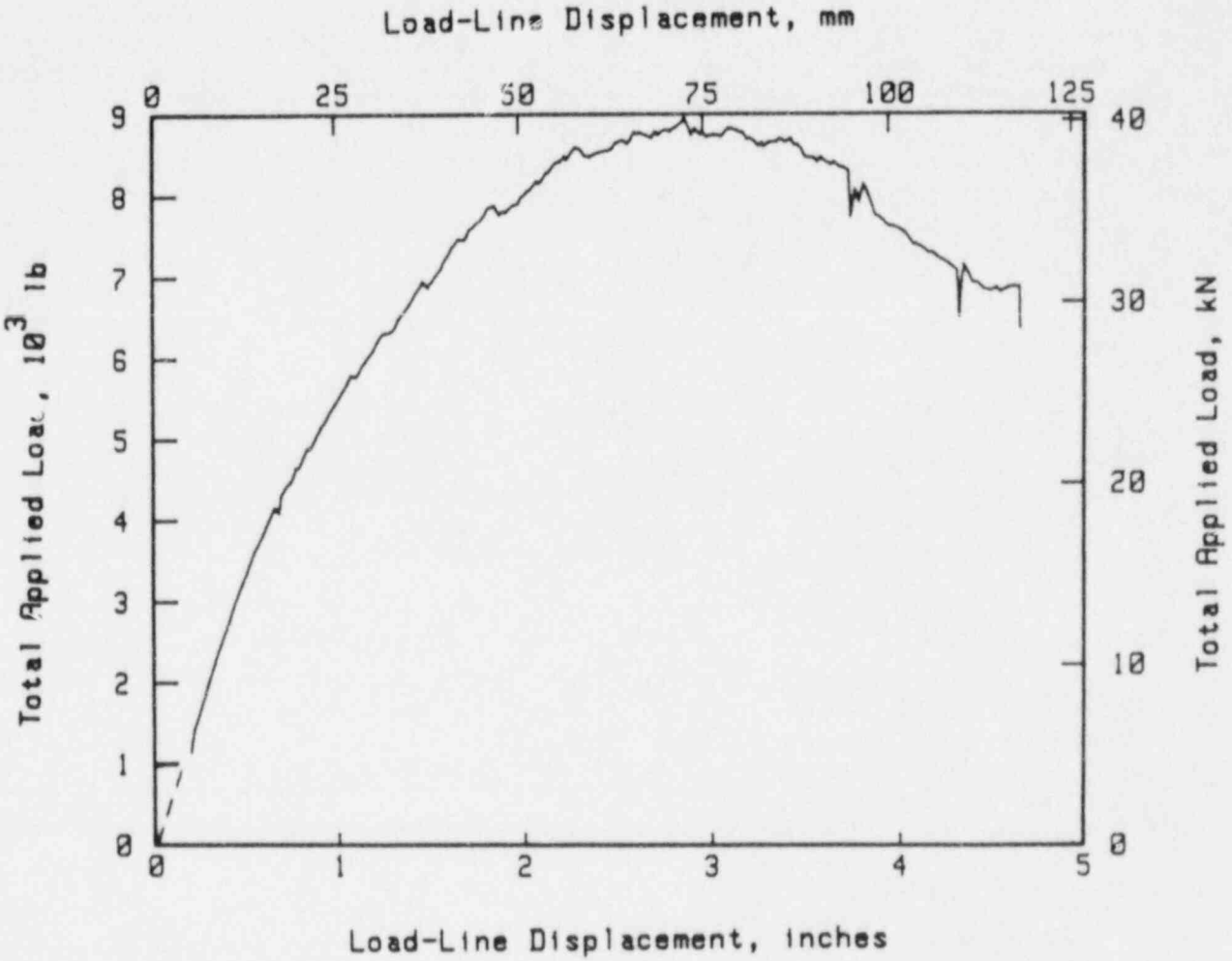

Figure 2.8.2 Total applied load versus load-line displacement for the 6-inch (152-mm) nominal diameter, stainless steel, combined pressure and bending, through-wall-cracked pipe experiment.

SA-12/86-F2.8.4

experiment was 0.9 inch (22.9 mm) at Crack Tip A and 1.0 inch (25.4 mm) at Crack Tip B.

The results from Experiment 4131-1 may be significant as far as the LBB philosophy embodied in General Design Criterion 4 (GDC-4) is concerned (Ref. 2.8.2). The procedures outlined in the recent modification to GDC-4 assume that a through-wall flaw exists at the location(s) identified as having the highest stresses and the poorest material properties. The size of the flaw should be large enough to ensure that the leak will be detected when the pipes are subjected to normal operating loads. Next, the flaw size margin is determined by comparing the selected leakage flaw size with the critical crack size. Using normal plus safe shutdown earthquake (SSE) loads, a margin of at least 2.0 between the leakage size flaw and the critical crack size is demonstrated. Next, the margin is determined by a crack stability analysis in terms of applied loads. Finally, it must be demonstrated that the leakage-sized cracks will not experience unstable crack growth even if larger loads (at least 1.4 times the normal plus SSE loads) are applied.

The results from this one experiment cast suspicion on the analysis method generally used to establish the critical crack size for through-wall flaws subjected to combined pressure and bending loads. Since this is an important point, this experiment is being repeated to confirm the results. If the current results are duplicated, then the calculated margins following the approach outlined in GDC-4 may be less than desired.

2.8.2 Future Plans

Due to the unexpected results of Experiment 4131-1 and the implications of the results on the recent modification to GDC-4, it has been decided to conduct an additional experiment as part of this subtask to replicate the conditions of Experiment 4131-1 and thereby ascertain whether the results of Experiment 4131-1 are valid. If so, the analysis embodied in GDC-4 may be problematic. On the other hand, if the problem rests with the experimental data, then any concerns about the GDC-4 analysis may be alleviated.

In addition, we will be conducting the final two 10-inch- (254-mm-) diameter carbon steel through-wall-cracked pipe experiments associated with this subtask (see Table 2.8.1). One is a pure pressure experiment, and the other is a combined pressure and bending experiment. Both involve the use of the special high-temperature bladder technique developed as part of this program.

References for Section 2.8

2.8.1 "Evaluation of Flaws in Austenitic Steel Piping" (Technical basis document for ASME IWB-3640 analysis procedure), prepared by Section XI Task Group for Piping Flaw Evaluation, EPRI Report NP-4690-SR, April 1986.

2.8.2 Federal Register, Volume 52, Number 207, October 27, 1987, 10 CFR Part 50, pp. 41288-41295.

2.9 Instability of Surface-Cracked Pipe in Compliant Bending

(D. Barnes, G. Kramer, M. Nakagaki, R. Olson, and G. Wilkowski)

In most LBB analyses, the stability of a through-wall-cracked pipe is evaluated under normal and faulted conditions. Current LBB analyses involve demonstrating that a postulated through-wall crack can be detected by leakage under normal operating conditions. This leakage must be detected before the crack reaches a critical size at anticipated faulted loads. The possibility that a surface crack will reach a critical size at faulted loads and result in a break is generally not considered.

However, the potential for the failure of a surface-cracked pipe is an important consideration. Such a failure could result in a double-ended guillotine break (DEGB) under faulted conditions where there would be no leakage at normal operating conditions. An important factor controlling the potential consequences of such a failure is the effect of the piping system compliance or stored elastic energy in the piping system. If the stored energy in the system is sufficient at the onset of unstable crack propagation, a double-ended pipe break may occur. On the other hand, if the stored energy is not sufficient, only a leak, or at worst, a partial rupture (that is, the crack will progress only part of the way around the pipe) will occur. This results in much less damage than a double-ended break.

This section of the report describes initial attempts to evaluate circumferential surface-crack instability and arrest, and quantify the final leakage area from the failure of a surface-cracked pipe. These results are of interest for a more general LBB approach, as well as for equipment qualification requirements from flooding and for pipe support design criteria (where the break thrust loads are assessed more realistically). The following sections summarize efforts in this area.

2.9.1 Initial Development of Instability Analysis Using an Energy Balance Method

The initial efforts in developing an engineering solution to predict the instability and extent of ductile crack growth during the instability were first given in Appendix B of our third semiannual report (Ref. 2.9.1). The following section describes initial development efforts for a general analysis method that can be used to predict the start of circumferential crack instability and to estimate the length of the crack jump, that is, whether it will be a small jump or a complete DEGB. Although this method is applicable to any laboratory specimen and many structures, it is particularly applicable to the problem of assessing the stability or instability of a circumferentially surface-cracked pipe. This approach incorporates the following:

1. Predicting load versus displacement caused by a crack under noncompliant conditions. In this step, the J-resistance curve of the material is used in the EPFM J-estimation scheme.

2. Predicting the amount of crack growth after an instability event by using an energy balance approach.

3. Predicting final crack opening area after the crack arrest. This may be of particular interest in predicting the maximum credible leakage to evaluate equipment qualification or subcompartment flooding rules.

The utility of this approach is that it can be applied to through-wall-, surface-, and complex-cracked pipe; it provides a means of predicting the extent of crack propagation in any system for which the compliance can be calculated, and it provides a means of estimating the final crack opening area.

Predicting the Start of Fracture Instability in Compliant Piping Systems

Elastic-plastic fracture instability predictions are frequently made using J-integral/tearing modulus theory (J/T). A common method used to predict instability is a J versus T plot (Ref. 2.9.2). This plot has a material J/T curve and an applied crack-driving force J/T curve. When the material curve intersects the driving force curve in J/T space, the start of an instability is predicted. Figure 2.9.1 shows a sample J/T plot. Such plots can become confusing since the accuracy of the compliance predictions is not obvious. In this section, we will discuss an alternative method of instability prediction using load versus load-point displacement caused by the crack, or moment versus rotation caused by the crack. Use of these physically significant parameters not only can predict the start of instability, but also can estimate the length of the crack jump (and, thereby, the size of the leak).

Most fracture mechanics specimens and flawed piping specimens exhibit load-displacement relationships that are similar in shape. These relationships can be normalized so that the displacement results only from the crack. Predicting this load-displacement behavior requires EPFM estimation schemes, such as those developed and verified in this program (see Section 3.4 of this report). These predictions incorporate the material's resistance to ductile crack initiation and crack growth. J-estimation schemes are the most popular analytical method, but alternative methods using such fracture mechanics parameters as CTOA, $\hat{J}$, and T_p* estimation schemes could be developed. The prediction of the start of a compliant instability in such a specimen is simple once the relationship between the load and the displacement resulting from the crack (P-δ_c) is known. Compliant instability can occur only when the displacement is increased beyond the displacement at maximum load. If system compliance during unloading is greater than that caused by the specimen's

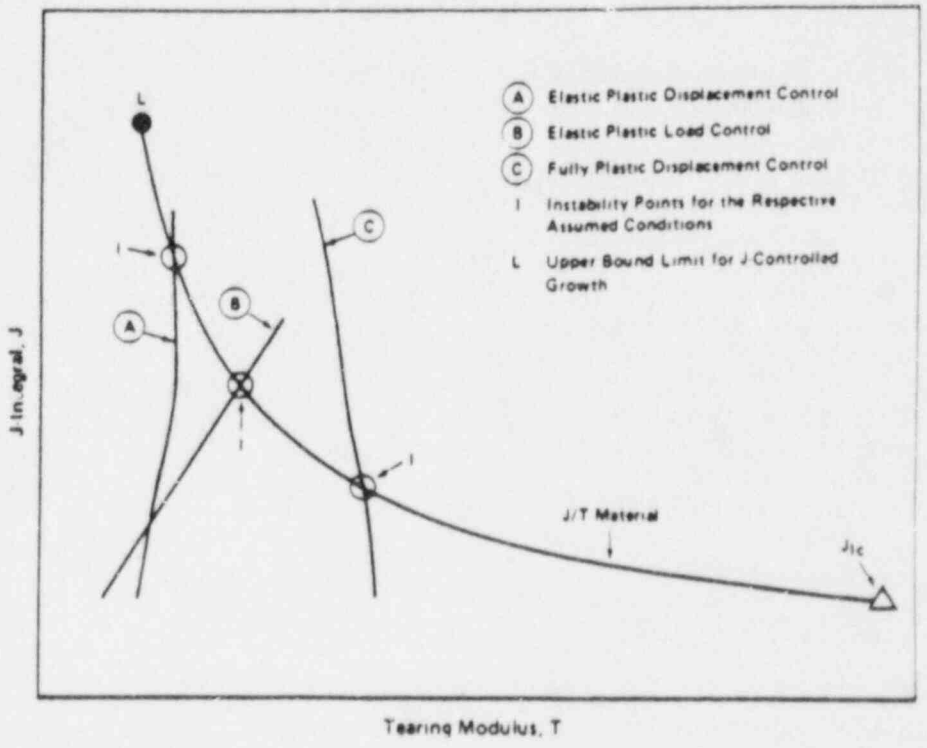

Figure 2.9.1 J/T plot frequently used in making EPFM instability predictions.

SA-12/85-FB.1

tearing, an instability will occur. The criterion for predicting the start of the compliant instability past maximum load is, therefore:

- If $(d\delta_c/dP)$ specimen $<$ system compliance, then instability starts.
- If $(d\delta_c/dP)$ specimen $>$ system compliance, then the system is stable.
- If $(d\delta_c/dP)$ specimen = system compliance, then the system is metastable.

Figure 2.9.2 schematically shows the effects of system compliance on a typical pipe or specimen P-δ_c record. For any specimen a variety of (δ_c/P) values can start an instability. For convenience we will denote the term "δ_c/P" as the specimen's tearing compliance. Note that Figure 2.9.2 includes a minimum specimen tearing compliance; this is typical. A system whose compliance equals this minimum compliance may experience only a small crack jump (Δa_1 in Figure 2.9.2) before stability is regained. A system with larger compliance might require a big crack jump (Δa_2 in Figure 2.9.2) before stability is regained. A load-controlled condition represents infinite system compliance. This would always result in a complete instability starting at the maximum load (Figure 2.9.2).

The above discussion on compliant system instability is generally true for a ductile fracture in any test specimen or structure and does not depend on the type of EPFM analysis used. It only depends on the accuracy to which the P-δ_c relationship for the structure can be predicted.

Predicting the Start of Instability for Through-Wall- and Complex-Cracked Pipe

Given the δ_c-P relationship for a circumferential through-wall crack in a pipe, the necessary compliance for the start of an instability is easily predicted. Joyce (Ref. 2.9.3) demonstrated limited instability by utilizing a test system made compliant by computer control (Figure 2.9.3).

The efforts on complex-cracked pipe (see Section 2.3 of this report) revealed that limited instabilities occur in a low-toughness A106 Grade B carbon steel complex-cracked pipe experiment. In that effort the biggest instability occurred when the tearing compliance (that is, δ_c/P of the test record) of the pipe was at its minimum (Figure 2.9.4). Similar behavior was observed in a simple circumferential through-wall-cracked carbon steel pipe test (Ref. 2.9.4). Hence, application of this tearing compliance approach to predict the start of instability is relatively straightforward for through-wall-cracked or complex-cracked pipe, once the load-displacement relation can be predicted.

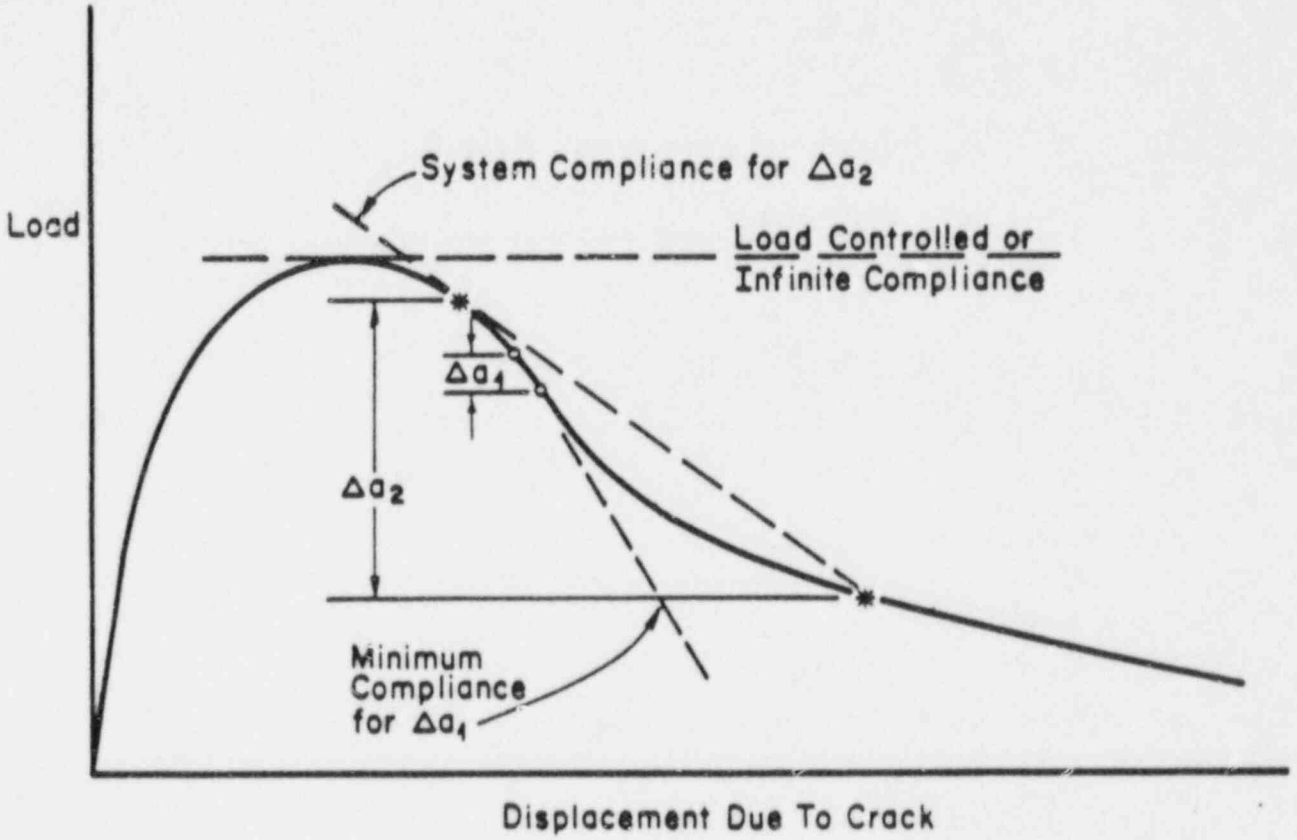

Figure 2.9.2 Schematic load versus displacement relationship for a typical specimen during ductile fracture.

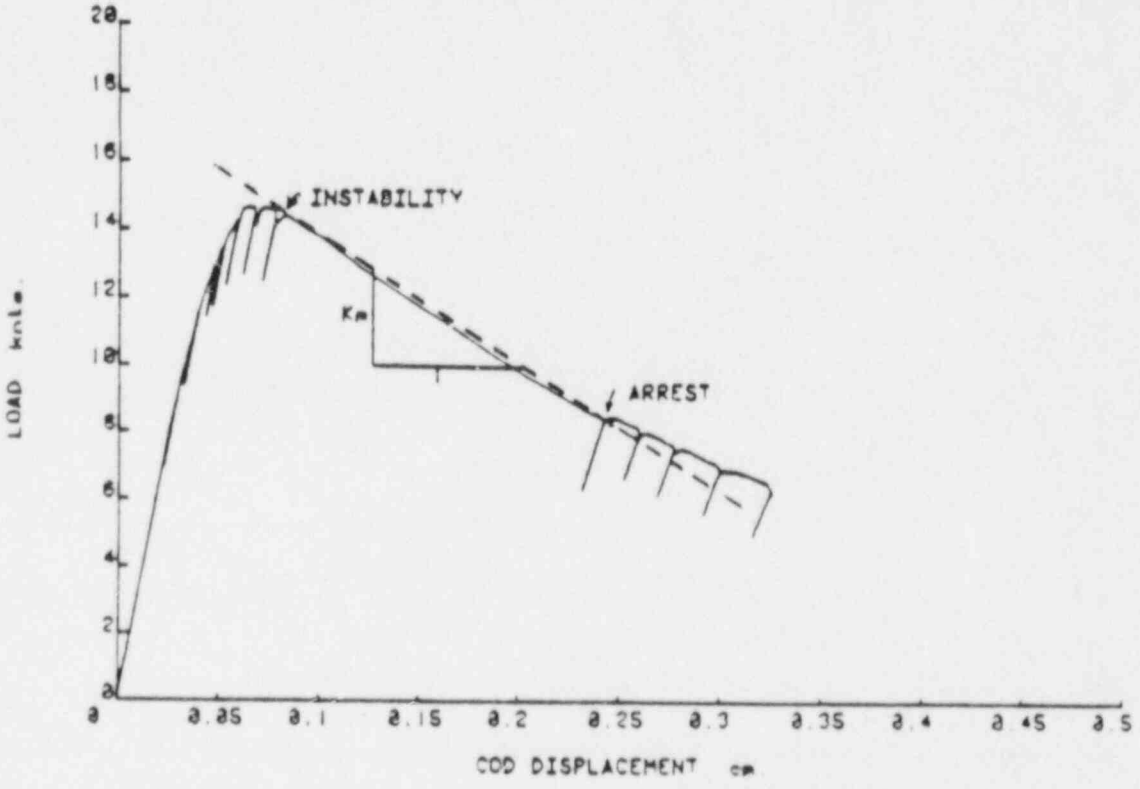

Figure 2.9.3 Load displacement record of a compact specimen from the computer compliance test system showing the instability and arrest points in comparison with a line of slope, $-K_M$. (Note: $K_M < C$.)

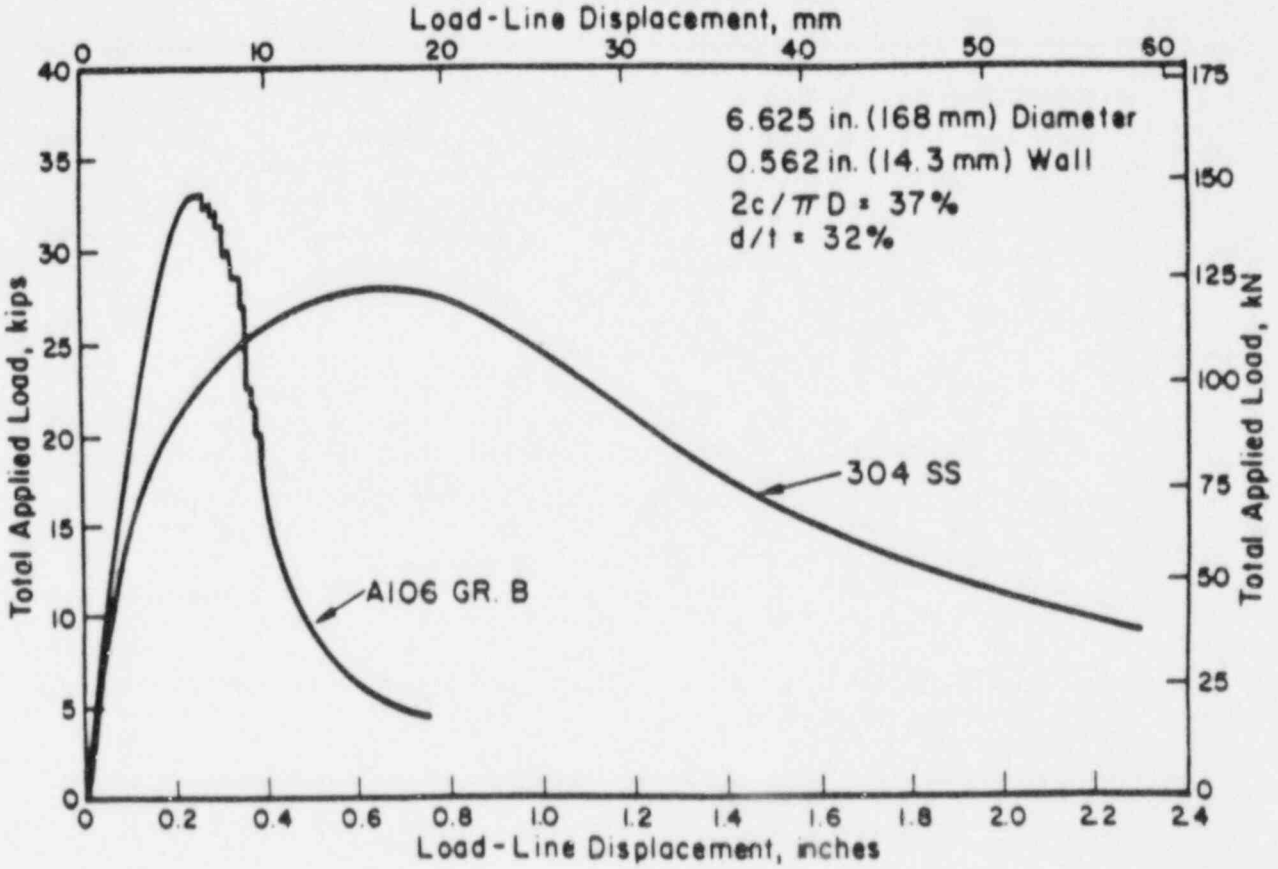

Figure 2.9.4 Load versus load-line displacement records from low-compliance complex-cracked pipe bending experiments at 550 F (288 C).

Predicting the Start of Instability for Surface-Cracked Pipe

Predicting instability behavior of surface-cracked pipe is simplified by using the tearing compliance approach. One of three specific surface-crack geometries is generally involved, and each requires slightly different consideration. These cases are discussed below.

Instability Analysis of Pipes with Short Surface Cracks

The P-δ relation for a surface-cracked pipe is affected by the strain-hardening and toughness of the pipe material. For instance, Figure 2.9.5 shows typical P-δ records from surface-cracked pipe bending experiments in this program. The A106 Grade B carbon steel pipe at 550 F (288 C) showed very little deformation up to maximum load, and the crack popped through the thickness in the low-compliance pipe test. The identical pipe size and flaw in a stainless steel pipe with the same pipe length showed greater ductility, and the crack grew through the thickness only under increasing displacement. Most important is the fact that, once the crack penetrates the thickness, the pipe follows the P-δ relationship of a through-wall-cracked pipe. Hence, if both the surface-cracked pipe P-δ_c relationship, with small amounts of crack growth, and the through-wall-cracked pipe P-δ_c relationship can be predicted, the degree of the instability can be approximated. (Note that, for simplicity, only one through-wall-cracked pipe curve was shown in Figure 2.9.5. In reality carbon and stainless steel pipes would show different through-wall-cracked pipe curves.)

Figure 2.9.6 schematically shows the effect of increasing compliance for a pipe with a short surface crack. With compliance C_1 in Figure 2.9.6, the surface crack would grow to a through-wall crack of the same length as the original surface crack. Compliance C_2 in Figure 2.9.6 would result in a greater amount of crack growth. Compliance C_3 would result in a DEGB.

An important consideration is that the system compliance must be taken from the higher load of the surface-cracked pipe's P-δ_c relationship and not from the through-wall-cracked pipe's P-δ_c relationship.

Additional considerations on the predictions of the crack growth during an instability are discussed in a following section.

Instability Analysis of Pipes with Long Surface Cracks

For a 360-degree surface-cracked pipe, a slightly different procedure is used to predict the resultant length of the through-wall crack after the surface-crack instability. In this case, when the surface crack breaks through, it resembles the complex-crack geometry (Figure 2.9.7). Since the complex-cracked pipe P-δ_c curve is significantly lower than the simple through-wall-

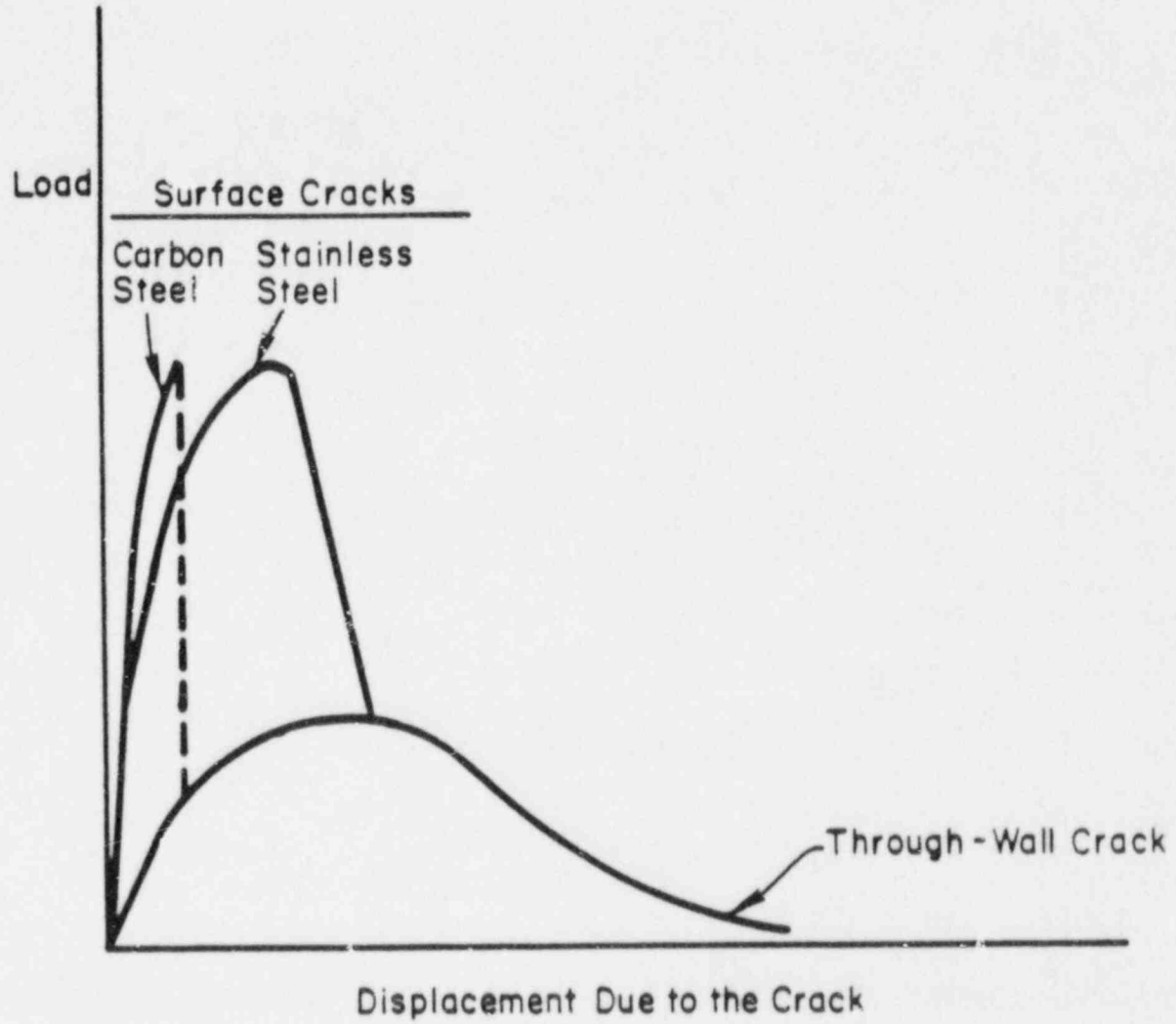

Figure 2.9.5 Typical load versus displacement records from surface- and through-wall cracked pipe experiments.

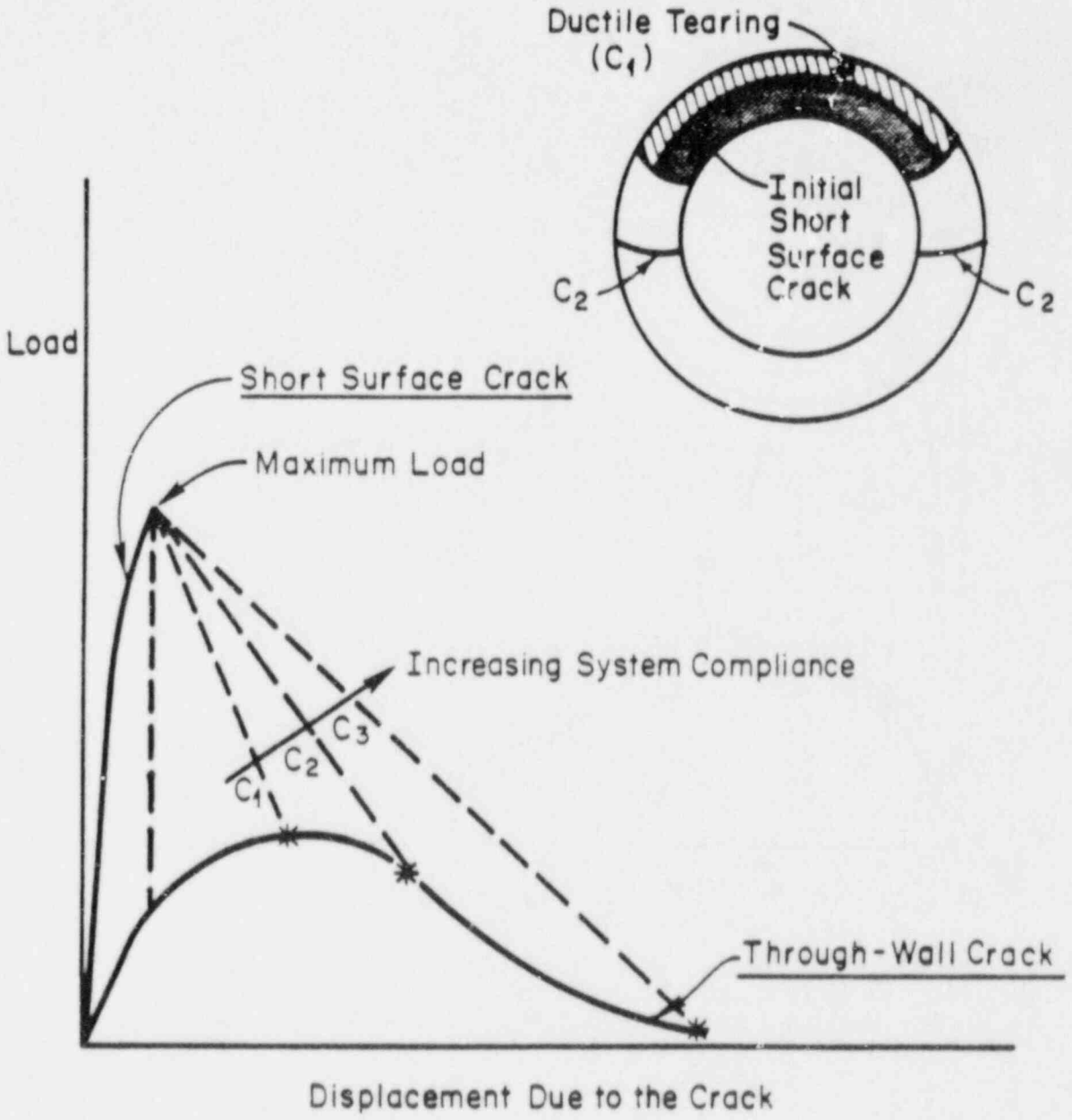

Figure 2.9.6 Schematic showing system compliance effects on instability of pipe with short circumferential cracks.

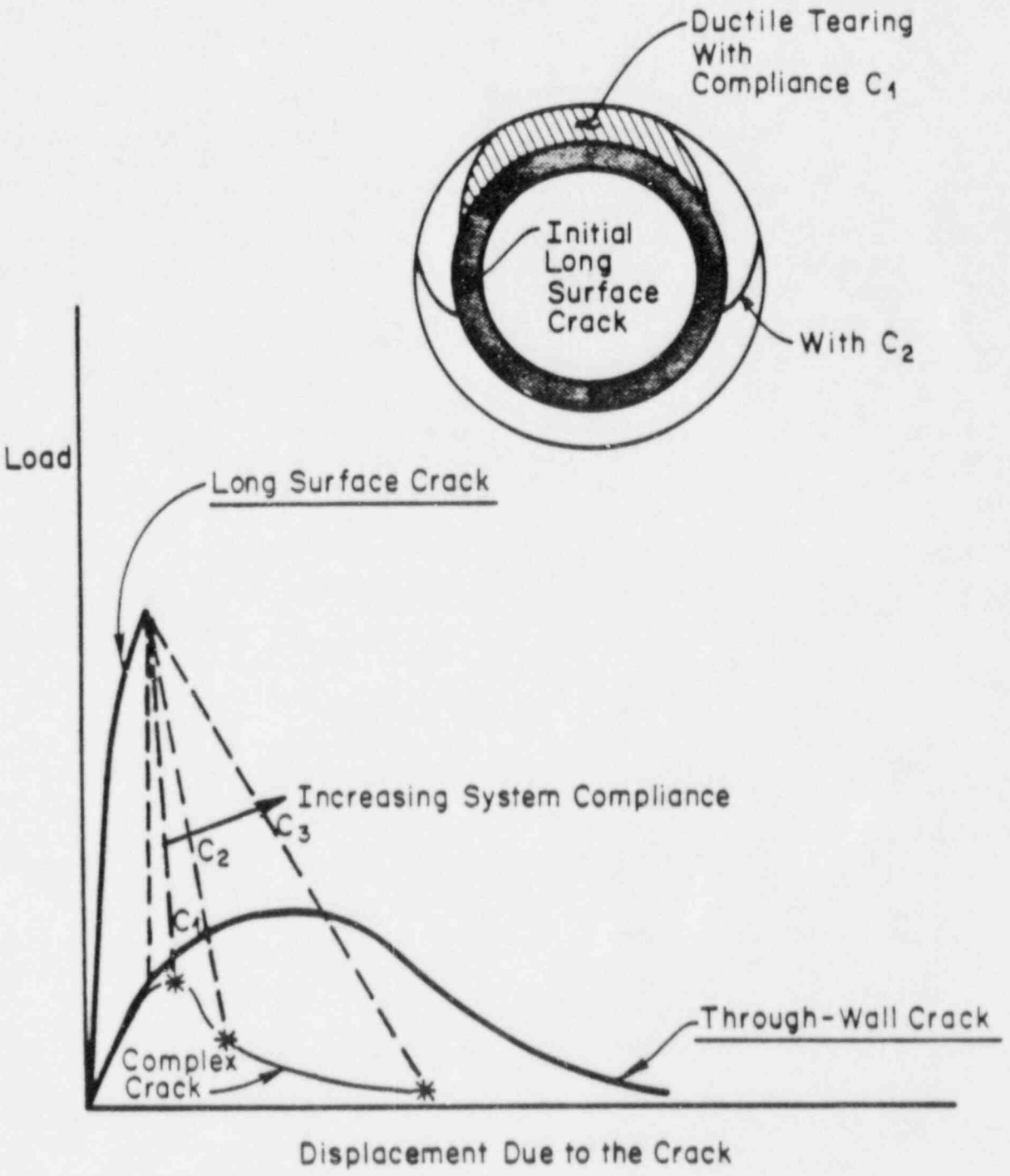

Figure 2.9.7 Schematic showing system compliance effect on instability of pipe with a long circumferential surface crack.

cracked pipe curve, circumferential crack growth will always be greater with a long surface crack than with a short surface crack in a compliant instability. For instance, with the system compliance C_1 in Figure 2.9.7, the crack might jump a small distance around the pipe. With compliance C_2, the crack might grow further. This amount of crack growth would be much greater than in the short surface-crack case (using the simple through-wall crack curve in Figure 2.9.7). A system compliance of C_3 (again in Figure 2.9.7) would produce a DEGB. Note that the compliance for the 360-degree flaw for a complete break is much less than that for either a short surface-cracked or a through-wall-cracked pipe.

A critical aspect in this analysis is determining what initial length of the through-wall part of the complex crack is used to determine the pipe's P-δ_c relationship. This can be determined experimentally from low-compliance pipe tests. An alternative would be to use a circumferential length that is 20 percent of the circumference. Pan (Ref. 2.9.5) showed that with this crack length, $T_{applied}$ is a maximum for a through-wall-cracked pipe.

Instability Analysis of Pipes with Intermediate-Length Surface Cracks

For circumferential cracks of less than 360 degrees, the above two procedures are combined. As shown in Figure 2.9.8, once an intermediate-length surface crack in a low-compliance pipe breaks through, it resembles a complex crack with a short through-wall-crack length. (Note that a complex crack does not necessarily have a 360-degree surface crack, it simply has a surface crack extending from the ends of the through-wall crack.) This crack would grow under increasing displacement to the end of the surface crack length. From that point, it would grow according to the simple through-wall cracked pipe P-δ_c relationship. Hence, by combining the appropriate noncompliant surface-cracked, complex-cracked, and simple through-wall-cracked pipe P-δ_c relationships, this method can be used to predict the degree of the crack instability for any surface-crack geometry.

An Energy Balance Approach to Estimating the Magnitude of Ductile Crack Growth After an Instability

To better estimate the magnitude of the ductile crack growth from an instability, the energy balance approach is used. For instance, if a system compliance of C_1 exists at the start of the instability, the pipe system's elastic potential energy is

$$E_{System} = \tfrac{1}{2}P_1(\delta_2-\delta_1) = A_1 \qquad (2.9.1)$$

(Figure 2.9.9a). However, the energy absorbed by the ductile fracture process

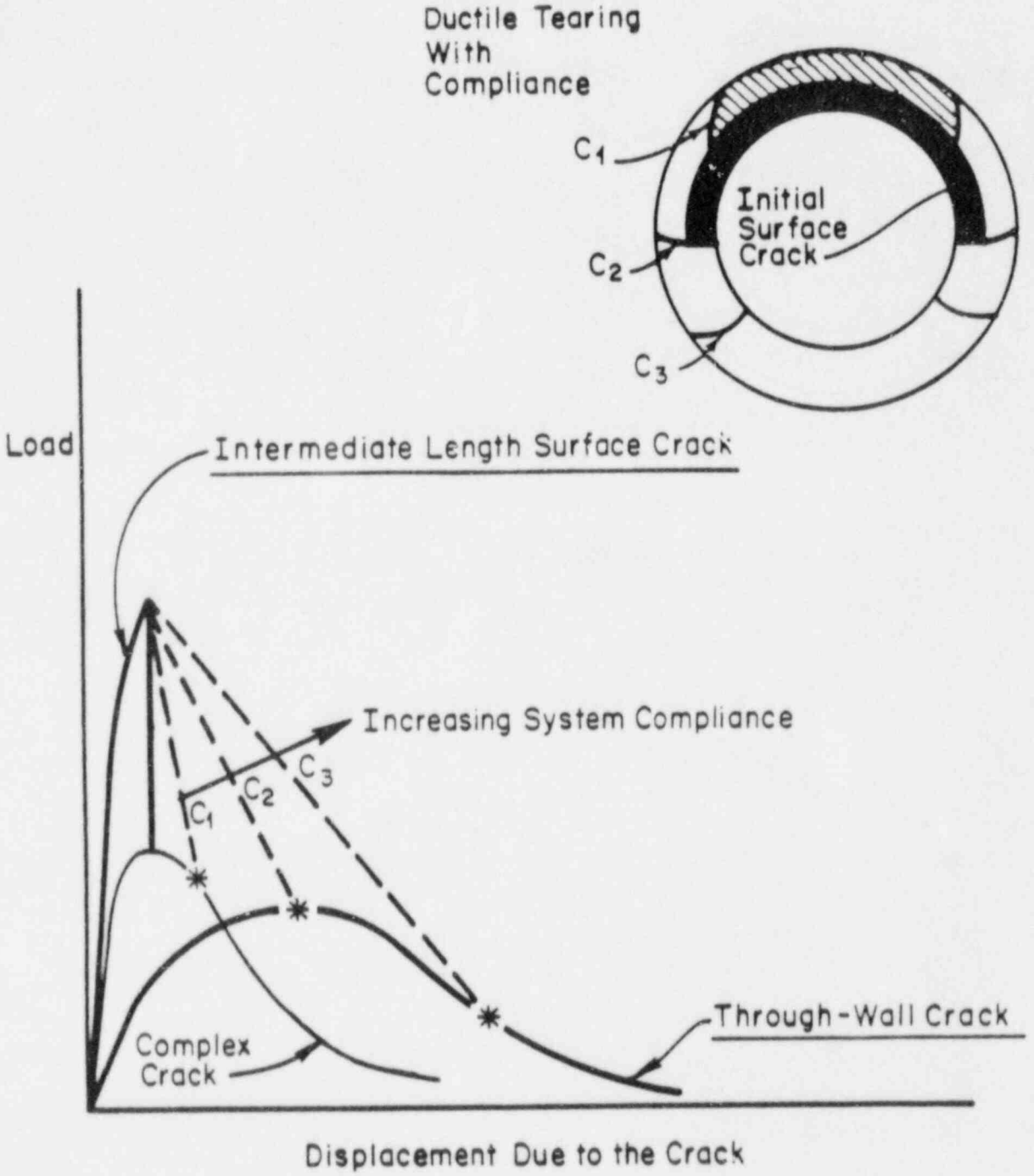

Figure 2.9.8 Schematic showing system compliance effects on instability of pipe with an intermediate length surface crack.

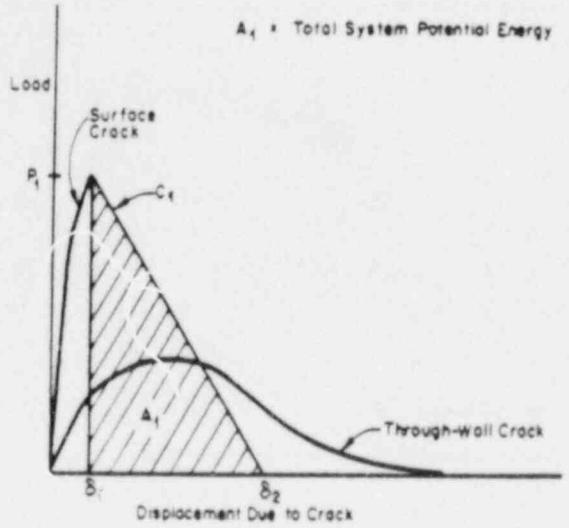

(a) Illustration of system total potential energy at the start of a surface crack instability.

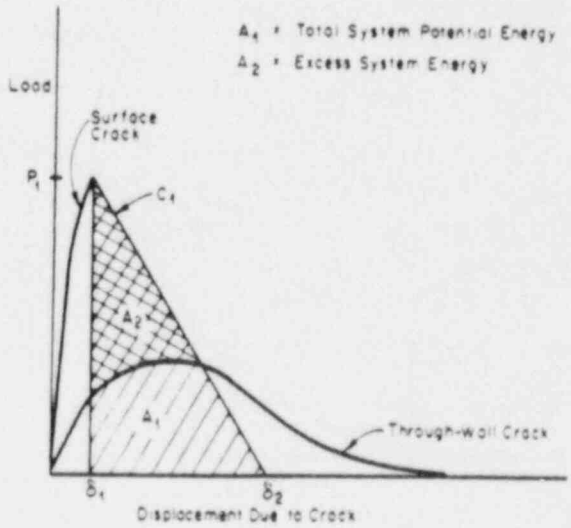

(b) Illustration of energy absorbed due to fracture process versus excess system energy.

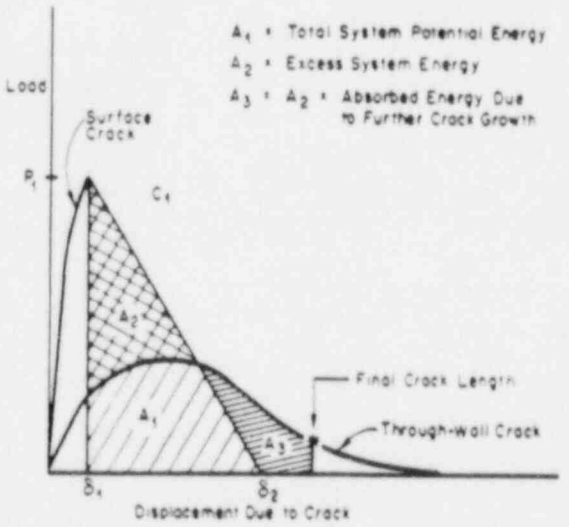

(c) Illustration of energy balance used to predict final crack jump.

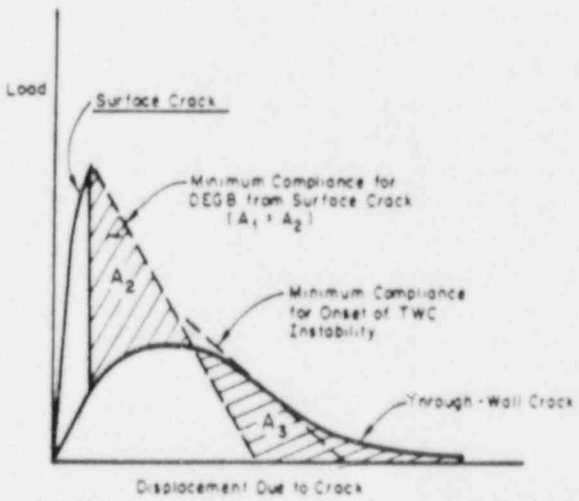

(d) Prediction of minimum compliance to produce a DEGB.

Figure 2.9.9 Energy balance method to predict crack growth after a compliant instability.

is schematically shown in Figure 2.9.9b as $A_1 - A_2$. The energy represented by A_2 is the excess system potential energy. This accelerates the crack growth and moves the pipe, which in turn causes the crack to grow further. If all the excess system potential energy (A_2) drives the crack further, then the energy absorbed in resisting the crack growth is A_3 (Figure 2.9.9c), where in general, $A_3 = A_2$. Consequently, the final crack is much larger because of the excess system energy. The minimum compliance for a DEGB is, therefore, one in which the excess system energy, A_2 in Figure 2.9.9d, just equals the remaining fracture energy the structure can absorb (see A_3 in Figure 2.9.9d). Hence, the minimum compliance for a DEGB in a surface-cracked pipe is much less than that determined in a through-wall-cracked pipe analysis.

In the absence of more sophisticated and accurate models for predicting crack jump length, the above energy balance approach represents a useful engineering tool.

Combined Compliant and Load-Controlled Instability Predictions

For combined displacement-controlled and load-controlled stresses, the method developed in this section can easily be used. Such combined conditions frequently occur. For example, thermal expansion stresses (displacement controlled) frequently coexist with dead-weight or pressure-induced axial stresses (load controlled). For dynamic loading, the inertial stresses are frequently considered load controlled, whereas the seismic anchor motion stresses are displacement controlled. Figure 2.9.10 depicts displacement-controlled stresses for a system compliance equal to C_1. If the load-controlled stresses are equal to P_1 then a DEGB will occur once the surface-crack instability starts. This is because $P_1 > P_M$, where P_M is the maximum load for the resulting through-wall-cracked pipe (Figure 2.9.10). For a low load-controlled stress like P_2 in Figure 2.9.10, the system compliance may cause the crack to jump to P_c, but it would not become unstable unless the displacement was increased to δ_2.

The magnitude of load-controlled tension stresses from internal pressure can be put in terms of an equivalent bending stress for use in a $P\text{-}\delta_c$ relation for a cracked pipe in pure bending. This can be done by simple linear interpolation or by using the detailed nonlinear analysis procedures being assessed in Section 2.8.1 of this report (Figure 2.9.11).

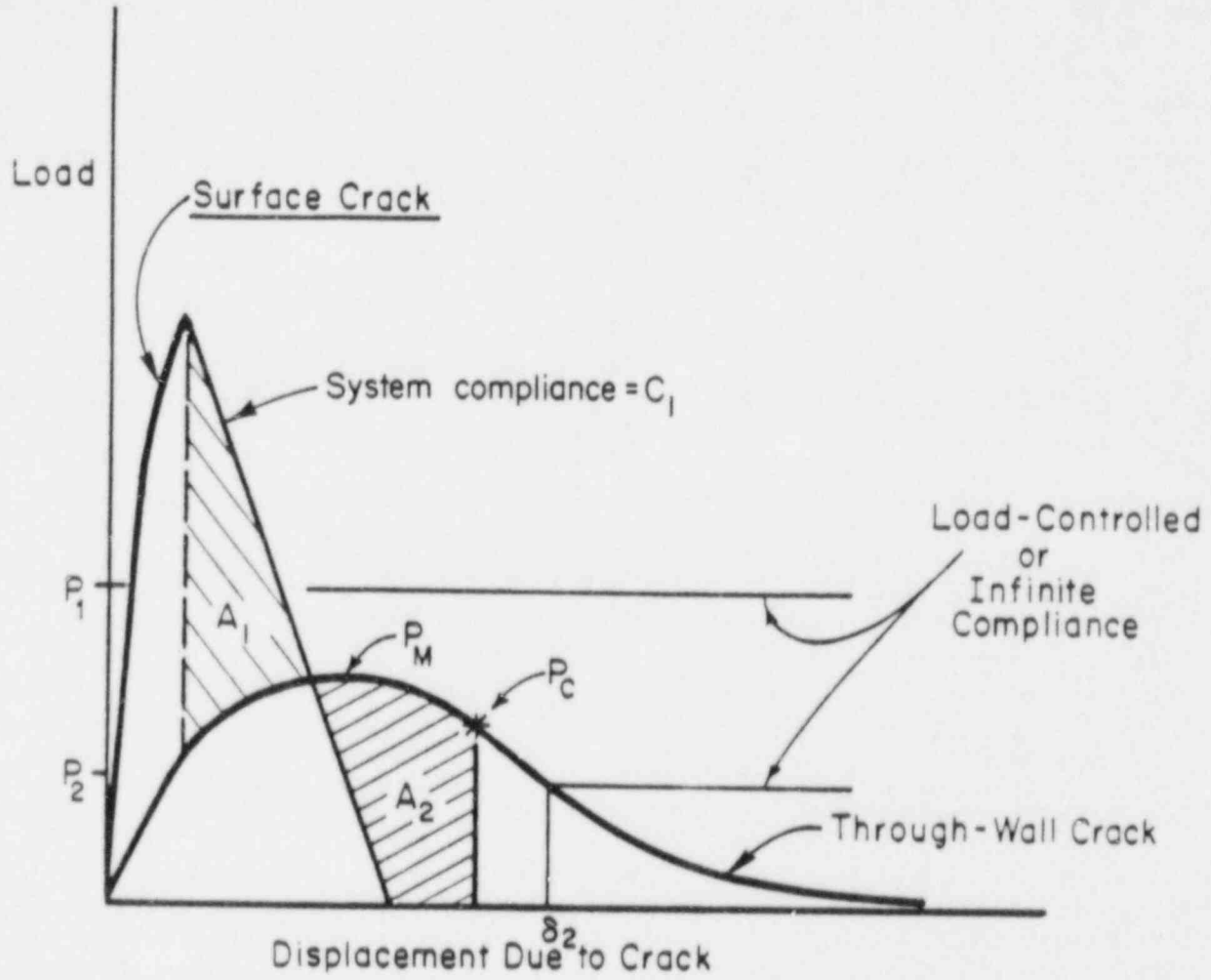

Figure 2.9.10 Load-controlled and compliant stress interactions on instability.

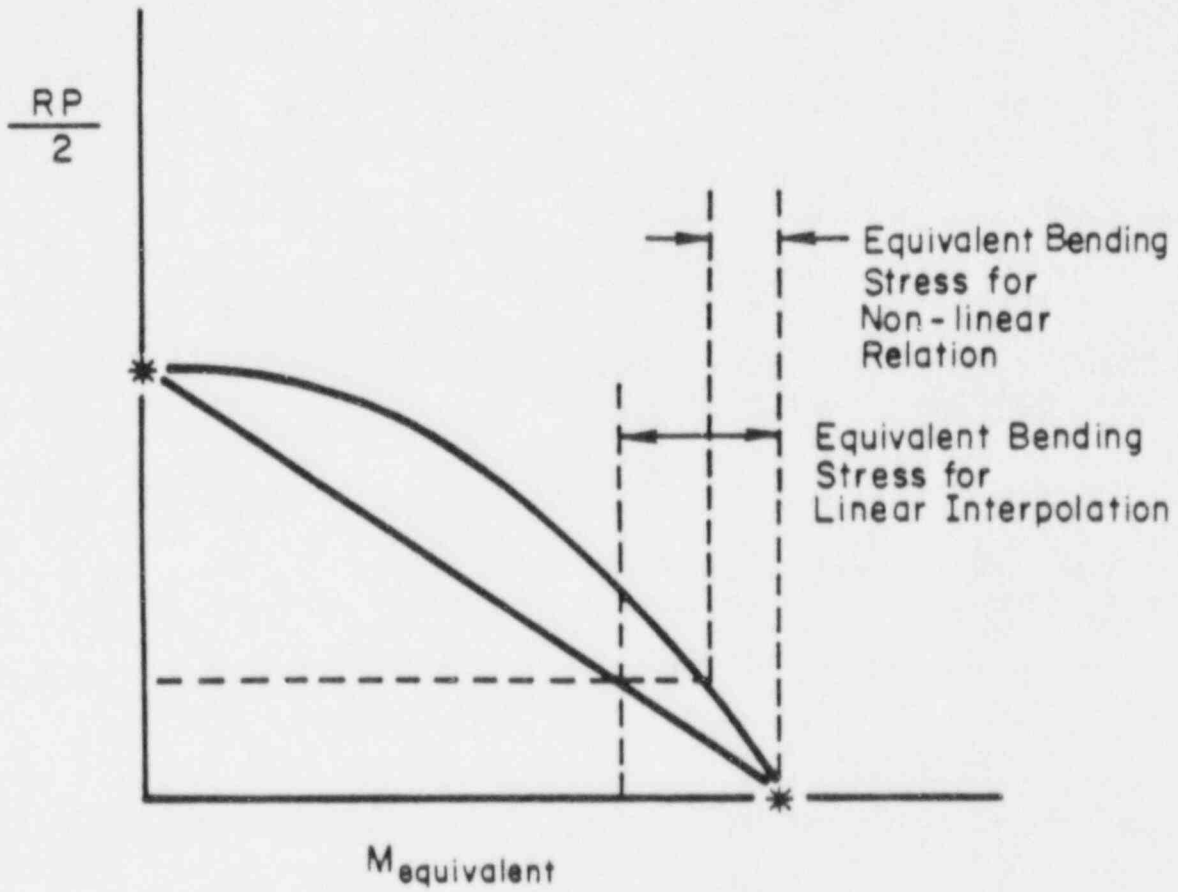

Figure 2.9.11 Tension versus bending load interactions for pipe with identically sized flaws. (P = axial tension load, R = pipe radius.)

Other Considerations

Several second-order improvements could be made in this approach:

- It includes no evaluation of fracture speed during the instability. (This may be important for a dynamic event.)
- The thrust forces from the crack opening may tend to close the crack, unless the crack is near a support, such as a vessel nozzle.
- Reverse unloading during a seismic event could reduce the cracked pipe P-δ_c relation since cyclic plasticity may reduce the J-R curve.
- Dynamic loadings may increase the cracked pipe P-δ_c relationship because the fracture resistance and materials strain-hardening would be increased by the increasing strain rate. This would tend, in turn, to increase the absorbed fracture energy, thereby decreasing the crack jump length. Conversely, a material susceptible to DSA toughness degradation may experience a further crack jump under seismic loading conditions (Section 3.1.2 of this report).

An additional improvement to the previous method involves ensuring that continuum mechanics requirements are satisfied at the stabilized condition immediately after the crack jump. Note that the pipe can be modeled by a small pipe section, V_1, containing the crack and two springs connected to the section (Figure 2.9.12). In this instance, the plastic deformation is assumed to be confined within section V_1. The modeled compliance, C, of the spring includes the compliance of the entirely elastic part of the pipe, V_2, in addition to the load system compliance. At End B, the controlled rotation (ϕ), which is constantly maintained during the fast crack run, is applied. In the energy balance approach, the following conditions are assumed:

1. After the surface crack jump, the surface crack becomes a short through-wall crack, which will then propagate around the pipe circumference. The load-displacement behavior of the developed through-wall crack is approximately consistent with that of an initial through-wall crack of a length identical to the surface crack's initial length.
2. The energy dissipation during the surface crack propagation and the associated plastic deformation is considered to be negligible in comparison with the energy available to drive the through-wall crack.
3. During the crack jump, dynamic effects such as the high strain rate effects on the material properties are not considered. However, kinetic energy is not neglected. Instead, it is postulated that kinetic energy is absorbed by further growth of the through-wall crack.

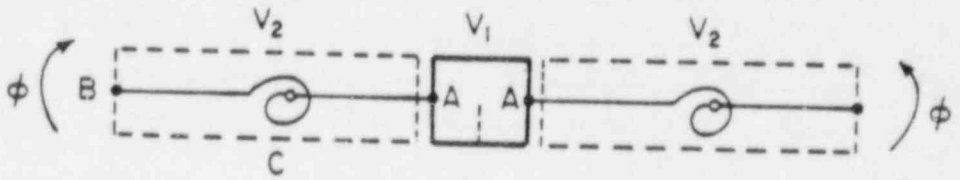

Figure 2.9.12 Modeling pipe deformation.

M-5/86-F5

In this approach, generalized loads are denoted "load", "moment", and so forth, and generalized displacements are denoted "displacement", "rotation", and so forth. At the stabilized equilibrium state immediately after the surface crack jump, the following conditions must be satisfied from the continuum mechanics point of view:

1. The generalized displacements at A on the body V_1 side and the body V_2 side must be the same, which satisfies a compatibility condition.

2. The generalized loads acting at A on the body V_1 side and the body V_2 side must be equal, which satisfies equilibrium conditions.

3. The excessive energy released from the compliance system is totally absorbed into the V_1 section for growing the through-wall crack.

   This excessive applied energy is equal to the absorbed plastic energy from crack growth in the energy balance.

Based on the assumptions and conditions mentioned above, the generalized load (P) versus displacement (δ) caused by the crack relationships are schematically shown in Figure 2.9.13. The following discussion delineates the improvements made to the energy balance approach. In Figure 2.9.13, the curve OA represents the P-δ_c relationship for the surface-cracked pipe section V_1 prior to the crack jump. The curve OEDB shows the through-wall-cracked pipe P-δ_c relationship. The straight line AD corresponds to the total compliance, C, of the piping system. Suppose the onset of instability occurs at the peak load at A in Figure 2.9.13. If the system or the pipe has no elastic compliance, the load will be equilibrated at E after crack growth. However, if compliance exists at all, the P-δ_c state must stay on curve AD at the equilibrated condition immediately after the crack jump is arrested. This equilibration point is designated by C in Figure 2.9.13; the available energy (the area FEADCGF) must be equated to the required energy to grow the through-wall crack (namely the area FEDBCGF). Subtracting the common energy area FEDCGF, the energy balance is given by $W_1 = W_2$. Note that Line CB is an elastic unloading compliance of Section V_1 with the through-wall crack. From the present model, with a nonzero compliance, the possible equilibrated state C after the surface crack jump always resides on the unloading side of the through-wall-crack P-δ_c curve.

Although many additional improvements could be made, the above approach, using the superposition of P-δ_c relationships (for through-wall-, surface-, and complex-cracked pipe) from elastic-plastic fracture estimation schemes and the energy balance approach to predict crack jumps, now provides a general methodology for accurate and simple instability analyses of real flaw geometries in complex pipe systems.

A most important point in this approach is that the accuracy of the method can be established by checking the load-displacement predictive capability of the J-estimation schemes. This has been done extensively in this program for simple through-wall-cracked pipe (Refs. 2.9.6 and 2.9.7) and complex-cracked pipe (Ref. 2.9.8). For surface-cracked pipe (see Section 2.2.1), an analysis

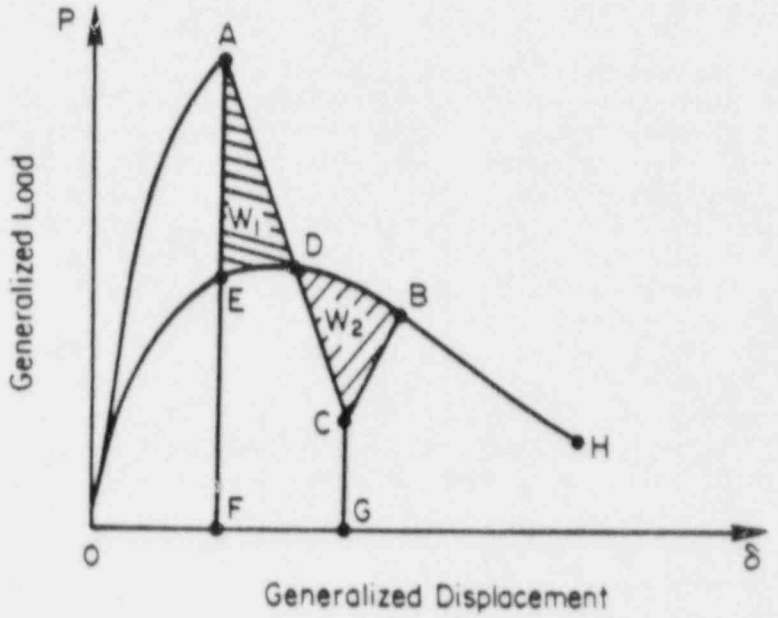

Figure 2.9.13 Schematic of generalized load (P) versus displacement (δ) for energy balance instability predictions.

M-5/86-F6

procedure has been developed, but the displacement prediction capability has not been extensively evaluated. However, it should be noted that the P-δ_c relationship for a surface-cracked pipe from the J-estimation scheme analysis need only account for a small amount of crack growth since the load starts to drop rapidly after passing the maximum load.

Finally, it should also be noted that the through-wall, complex-, and surface-cracked pipe P-δ_c relationships frequently used in the accompanying figures are actual traces from experiments conducted in the Degraded Piping Program. The accuracy of this analysis method is highly dependent on how the estimation schemes (using J, CTOA, or T_p*) can predict the P-δ_c relationship for a noncompliant pipe system.

2.9.2 Verification of the Energy Balance Approach for Surface Cracked Pipe

The experimental test matrix for this subtask contains seven pipe fracture experiments on internally surface-cracked carbon steel and stainless steel pipe. These pipes were tested in four-point bending without internal pressure at 550 F (288 C). The test matrix summarized in Table 2.9.1 shows essentially three sets of experiments. The first was for a finite-length surface crack in a ferritic pipe. The second was for a finite-length surface crack in a stainless steel pipe. The last was for a 360-degree surface crack in a stainless steel pipe. Generally the plan was to conduct experiments with the same size cracks but different compliances for each set to see if the failure could be changed from staple ductile tearing to either limited instability or a DEGB.

The results of these experiments are summarized in Table 2.9.2 and discussed briefly below.

Finite-Length Surface Cracks in Ferritic Steel Pipe

These experiments were conducted on a 10-inch- (254-mm-) diameter Schedule 100 SA-333 Grade 6 ferritic pipe. The pipe was machined in the crack area to obtain a constant thickness; actual thicknesses are given in Table 2.9.1. Two experiments were conducted on this pipe.

Experiment 4115-1 was conducted with crack depth of 70 percent of the thickness and a length of 42 percent of the circumference. The length of the test system and the test results are given in Table 2.9.2. This was considered to be a relatively low-compliance experiment and resulted in a limited instability (Figure 2.9.14). Once maximum load was reached, the surface crack popped through the wall thickness in an unstable manner. The resultant through-wall crack was only slightly longer than the initial surface crack. In this case, the crack propagated less than 0.3 inch (7.6 mm) past each end of the machined surface crack.

Table 2.9.1. Test matrix for instability experiments on surface-cracked pipe.

	Actual Pipe Diameter, inches	(mm)	Pipe Wall Thickness, inch	(mm)	Material	Crack Length/ Circumference	Crack Depth/ Wall Thickness	Compliance Level
				Finite Length Carbon Steel Experiments				
4115-1	10.440	(265.2)	0.680	(17.3)	SA-333 Gr. 6	0.420	0.700	Low
4115-2	10.710	(272.0)	0.674	(17.1)	SA-333 Gr. 6	0.430	0.710	Med
				Finite Length Stainless Steel Experiments				
4115-4	6.627	(168.3)	0.587	(14.9)	SA-376 TP304	0.520	0.490	Low
4115-5	6.620	(168.2)	0.590	(15.0)	SA-376 TP304	0.415	0.600	Low
				360-Degree Surface-Cracked Stainless Steel Experiments				
4115-7	6.614	(168.0)	0.549	(13.9)	SA-376 TP304	1.000	0.647	High
4115-8	6.612	(167.9)	0.553	(14.0)	SA-376 TP304	1.000	0.626	Low
4115-9	6.630	(168.4)	0.551	(14.0)	SA-376 TP304	1.000	0.655	Med

Tests conducted at 550 F (288 C).

Table 2.9.2. Results of surface-cracked pipe instability experiments.

Experiment Number	Outside Diameter, inches (mm)	Wall Thickness, inches (mm)	Material	Initial Crack Dimensions 2c/πD	Initial Crack Dimensions d/t	Test Compliance	Outer Span, inches (m)	Inner Span, inches (m)	Initiation Load, pounds (kN)	Maximum Load, pounds (kN)	Crack/Length/ Circumference (After Instability)
Finite Length Carbon Steel Experiments											
4115-1	10.44 (265.2)	0.680 (17.3)	SA-333 Grt	0.420	0.700	Medium	175 (4.95)[a]	64 (1.63)	65,400 (291)	70,500 (314)	0.44
4115-2	10.71 (272.0)	0.674 (17.1)	SA-333 Grt.	0.430	0.710	Medium	454 (11.5)[b]	132 (3.36)	22,300 (99)	25,800 (115)	0.43
Finite Length Stainless Steel Experiments											
4115-4	6.627 (168.3)	0.587 (14.9)	SA-376 TP304	0.520	0.490	Medium	100 (2.54)[a]	48 (1.22)	(e)	97,800 (435)	(f)
4115-5	6.620 (168.2)	0.590 (15.0)	SA-376 TP304	0.415	0.600	Medium	92 (2.34)[a]	48 (1.22)	(e)	52,300 (233)	0.42
360-Degree Surface-Cracked Stainless Steel Experiments											
4115-7	6.614 (168.0)	0.549 (13.9)	SA-376 TP304	1.000	0.647	High	92 (2.34)[a]	48 (1.22)	48,750 (217)	52,500 (233)	0.95
4115-8	6.612 (167.5)	0.553 (14.0)	SA-376 TP304	1.000	0.626	Low	60 (1.52)[c]	24 (0.61)	61,860 (275)	63,900 (285)	(g)
4115-9	6.630 (168.4)	0.551 (14.0)	SA-376 TP304	1.000	0.655	Medium	40 (1.02)[d]	24 (0.61)	141,750 (630)	178,300 (793)	0.60

(a) Pipe strongback used for test frame.
(b) Large strongback used for test frame.
(c) 130,000-pound (579 kN) MTS machine used for test frame.
(d) 200,000-pound (890 kN) Baldwin machine used for test frame.
(e) Data were not of sufficient quality to determine crack initiation load unambiguously.
(f) Experiment stopped prior to crack penetrating the thickness.
(g) Stable ductile tearing throughout this experiment.

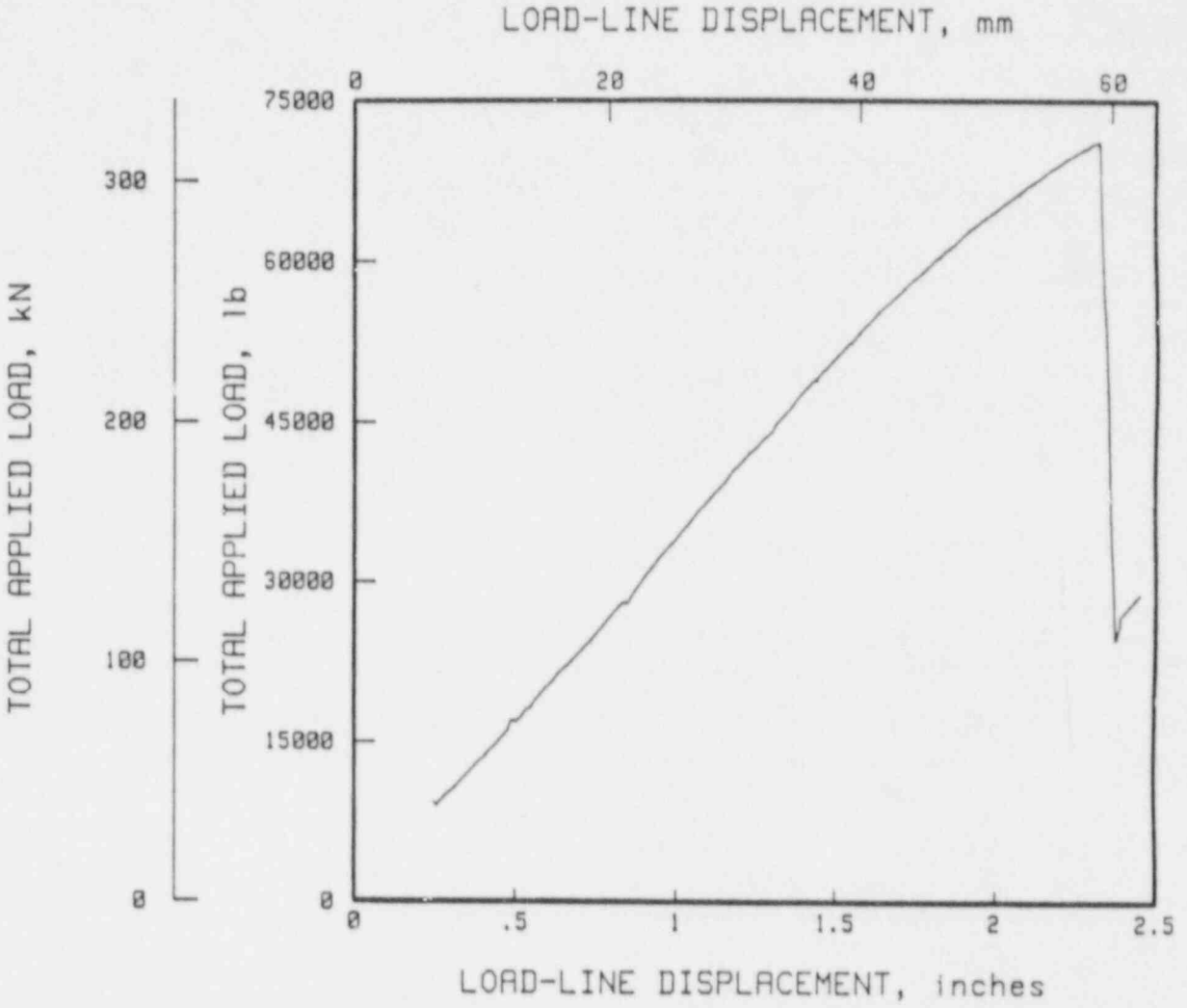

Figure 2.9.14 Load-displacement relationship of an internally surface-cracked carbon steel pipe (Experiment 4115-1).

SA-12/87-F2.9.14

One intermediate-compliance, finite-length surface-cracked pipe experiment conducted as part of this effort was Experiment 4115-2. The load versus load-line displacement record for this experiment is shown in Figure 2.9.15. The outer span length for 4115-2 was about 2.6 times that for the companion low-compliance test, Experiment 4115-1. This choice of span length was based on pretest design calculations indicating this specimen span length should result in enough compliance to promote unstable crack propagation in the test specimen once the crack initiated under quasistatic loading. The exact span lengths were chosen such that the resultant through-wall crack after the instability event would be well in excess of the initial surface crack length, but somewhat less than a complete DEGB.

Unfortunately, this did not occur. Once the crack broke through the wall during the instability event, it arrested at the two ends of the machined surface crack, which was a slightly shorter length of crack growth than in the prior lower-compliance pipe test. One reason for the more stable behavior in the second test was that two different pipe test machines were used because of the different pipe lengths involved. A posttest analysis showed that the machine compliance was found to be significantly higher in the first test than in the second test. The exact values of machine compliance will be documented in the final report. Consequently, a significantly longer section of pipe or a more compliant test frame would have been needed to drive the crack to the desired length. No additional tests are planned at this time.

Finite-Length Surface Cracks in Stainless Steel Pipe

Two experiments were conducted in this series. Experiment 4115-4 involved an internal surface crack with a depth of 50 percent of the pipe thickness and a length of 52 percent of the pipe circumference. This was shallower than the other surface-cracked pipe experiments conducted in this program. No significant crack growth was obtained in this experiment. The experiment was stopped after excessive plastic deformation of the pipe occurred far from the crack. A posttest metallographic examination of the crack plane revealed that the surface crack had initiated and grown a small amount. Hence, it was close to the maximum load. As a result of this experiment, the ratio of crack depth to wall thickness in the next experiment, Number 4115-5, was increased from 50 to approximately 60 percent of the pipe thickness.

Experiment 4115-5 was successfully conducted with the depth of the internal surface crack at 60 percent of the pipe thickness. The length of pipe and the center span length are given in Table 2.9.2. Because the test machine used had a relatively high compliance, this test may be considered an intermediate-compliance test. The total load versus load-point displacement from this experiment is shown in Figure 2.9.16. As shown in this figure, once the maximum load was exceeded, a limited instability occurred. The crack propagated approximately 0.3 inches (7.6 mm) past the end of the initial crack length. A higher-compliance test was not conducted to force a DEGB for this crack geometry.

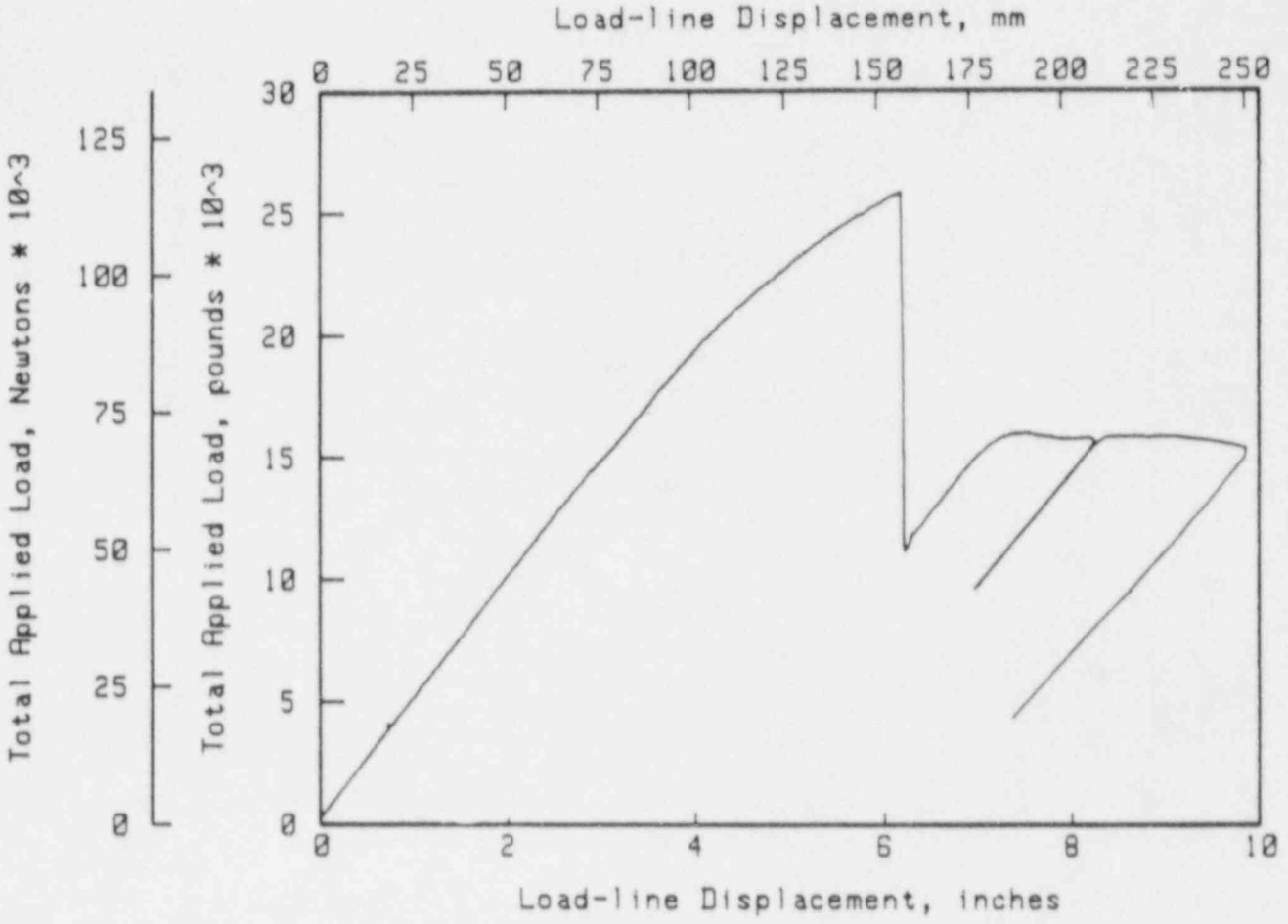

Figure 2.9.15 Load-line displacement from Experiment 4115-2 for an internal 180-degree surface crack on 10-inch- (254-mm-) diameter A333 Grade 6 pipe.

SA-12/87-F2.9.15

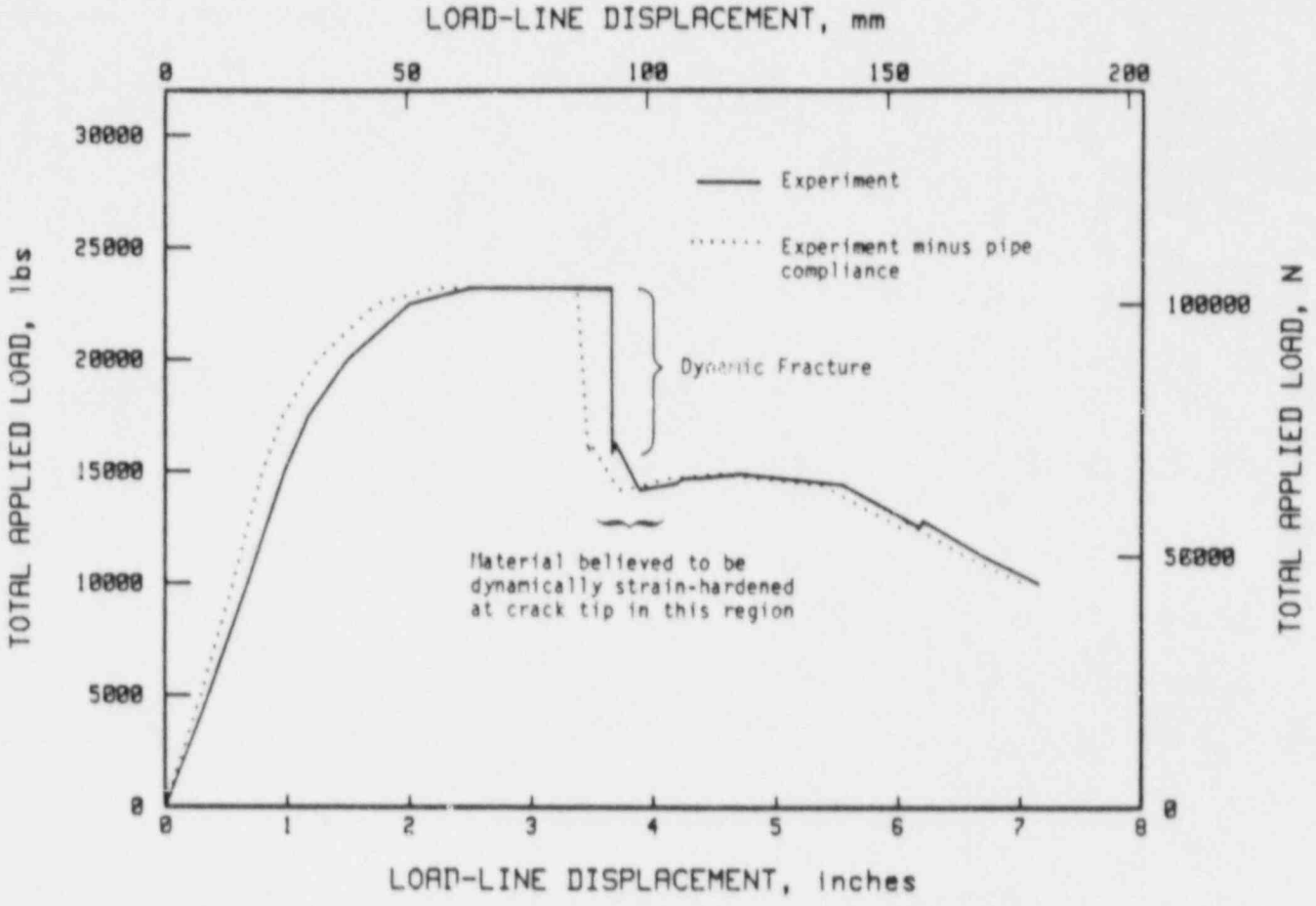

Figure 2.9.16 Load-displacement relationship of an internally surface-cracked stainless steel pipe (Experiment 4115-5).

SA-6/86-F2.9.4

Stainless Steel 360-Degree Surface Crack Experiments

Three experiments with different compliances were conducted on the same 6-inch (152-mm) nominal diameter pipe used in the finite-length surface-cracked pipe instability experiments. The results are summarized in Table 2.9.2.

Experiment 4115-7 was the first of the series conducted and it produced some initially unexpected results. This experiment almost resulted in a DEGB (Figure 2.9.17), even though the experiment was conducted on a fairly short length of pipe. In retrospect, this behavior was suggested by the energy balance approach (see Figure 2.9.7). As noted earlier, after penetrating the wall thickness, a long internal surface crack acts much like a complex crack. The complex-crack geometry constrains the plasticity in the pipe, which effectively reduces the crack growth resistance of the pipe.

As a result of Experiment 4115-7, the remaining companion experiments were conducted with stiffer test frames and shorter lengths of pipe to reduce system compliance. For Experiment 4115-9, the inner and outer spans were 24 and 40 inches (0.610 and 1.016 m), respectively. A dynamic instability was experienced just past the maximum load (Figure 2.9.18). After the instability, the crack length was visually examined and found to be 60 percent of the pipe circumference. The specimen was then reloaded, and the crack grew stably under further applied displacements. The pipe specimen was occasionally unloaded during the further applied displacements to mark the crack front.

The objective of the third experiment, 4115-8, was to obtain completely stable crack growth. This required considerable care in determining how to reduce the compliance further from Experiment 4115-9. An instability compliance analysis showed that, for the inner spans used, if the outer spans were increased, then the system compliance (which includes both the machine compliance and the compliance of the uncracked pipe) would first decrease before it increased. For the particular test frame used and for the center span used and the pipe sized tested, a minimum compliance occurs for a specific outer span length. This is illustrated in Figure 2.9.19, which shows the total compliance - that is, the compliance of the machine and the compliance of the uncracked pipe - as a function of outer span. The inner and outer spans for Experiment 4115-8 were 24 and 60 inches (0.610 and 1.52 m), respectively. These span lengths were chosen because pretest analysis indicated that the cracked pipe would be more stable at these lengths. This system compliance, however, would be on the verge of an instability.

Figure 2.9.20 is the load versus load-line displacement record for Experiment 4115-8. Of note is the fact that no instability was associated with this experiment: the surface crack slowly tore through the wall thickness. This agreed well with our pretest analysis. Further details of this analysis procedure will be provided in the final report to this program.

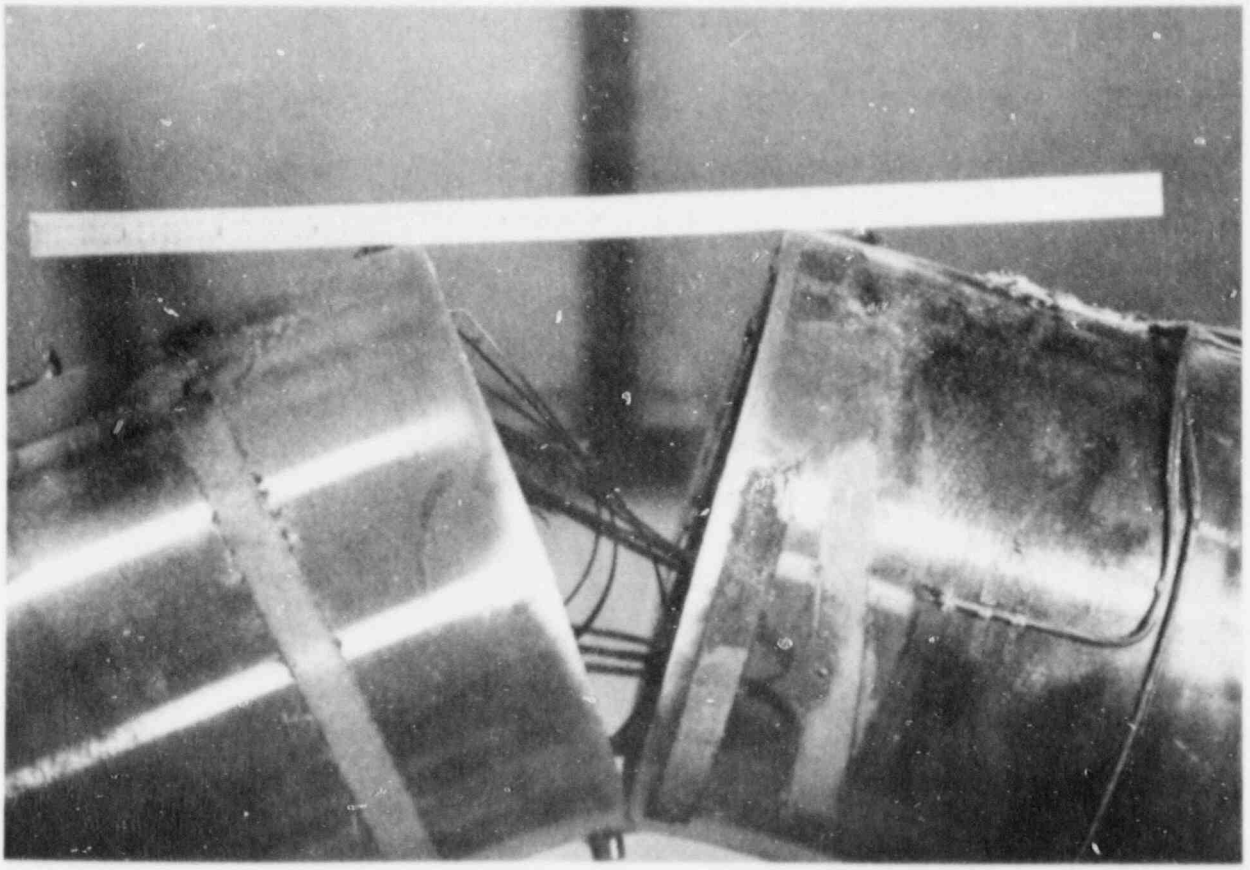

Figure 2.9.17 Photograph of the results of a 360-degree surface-cracked instability experiment on relatively low-compliance SA-376 TP304 stainless steel pipe tested at 550 F (288 C).

SA-6/86-F2.9.6

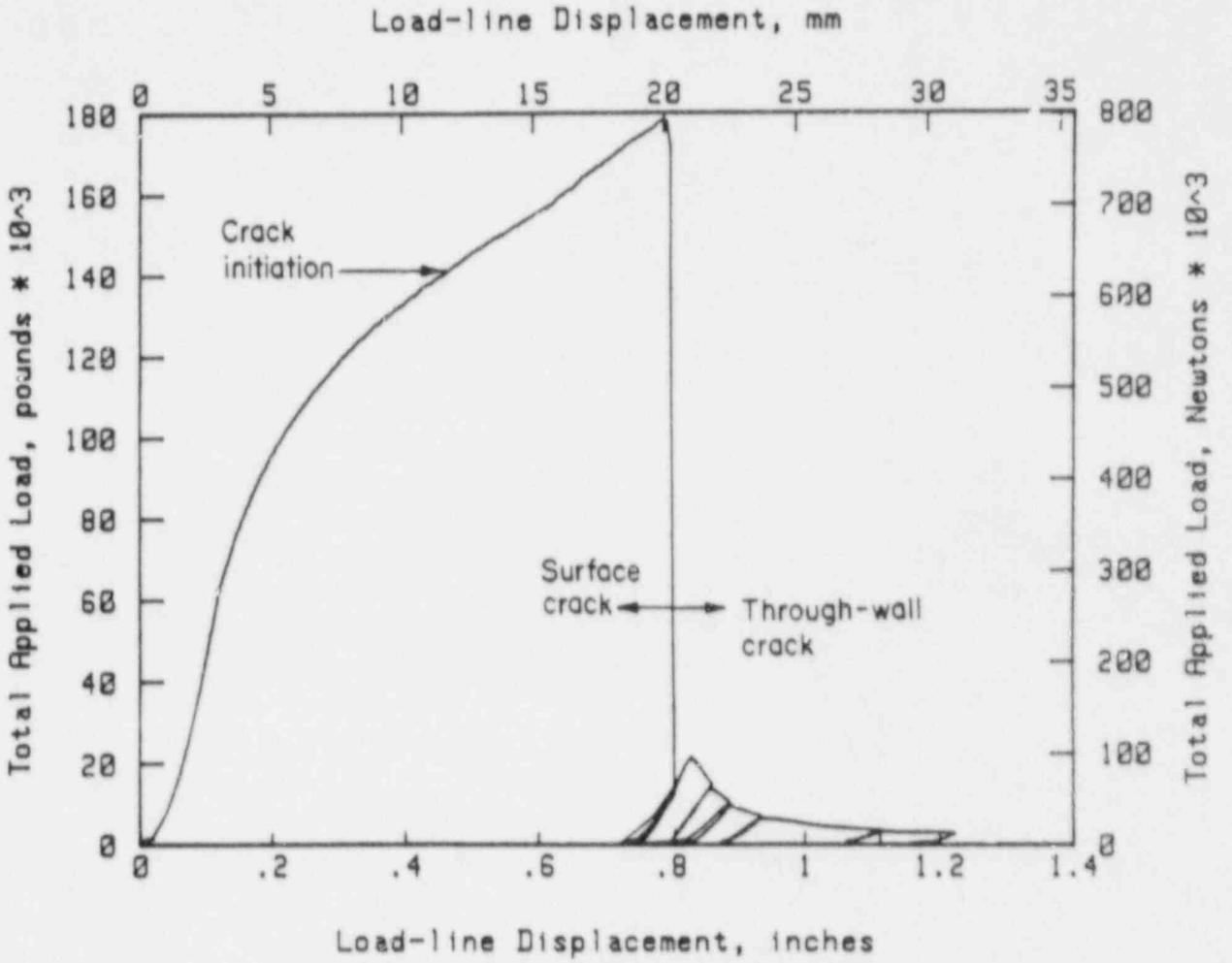

Figure 2.9.18 Load versus load-line displacement from Experiment 4115-9 for an internal 360-degree surface crack in a 6-inch- (152-mm-) diameter Type 304 stainless steel pipe with intermediate compliance.

DRB-1.2.1.19-F11

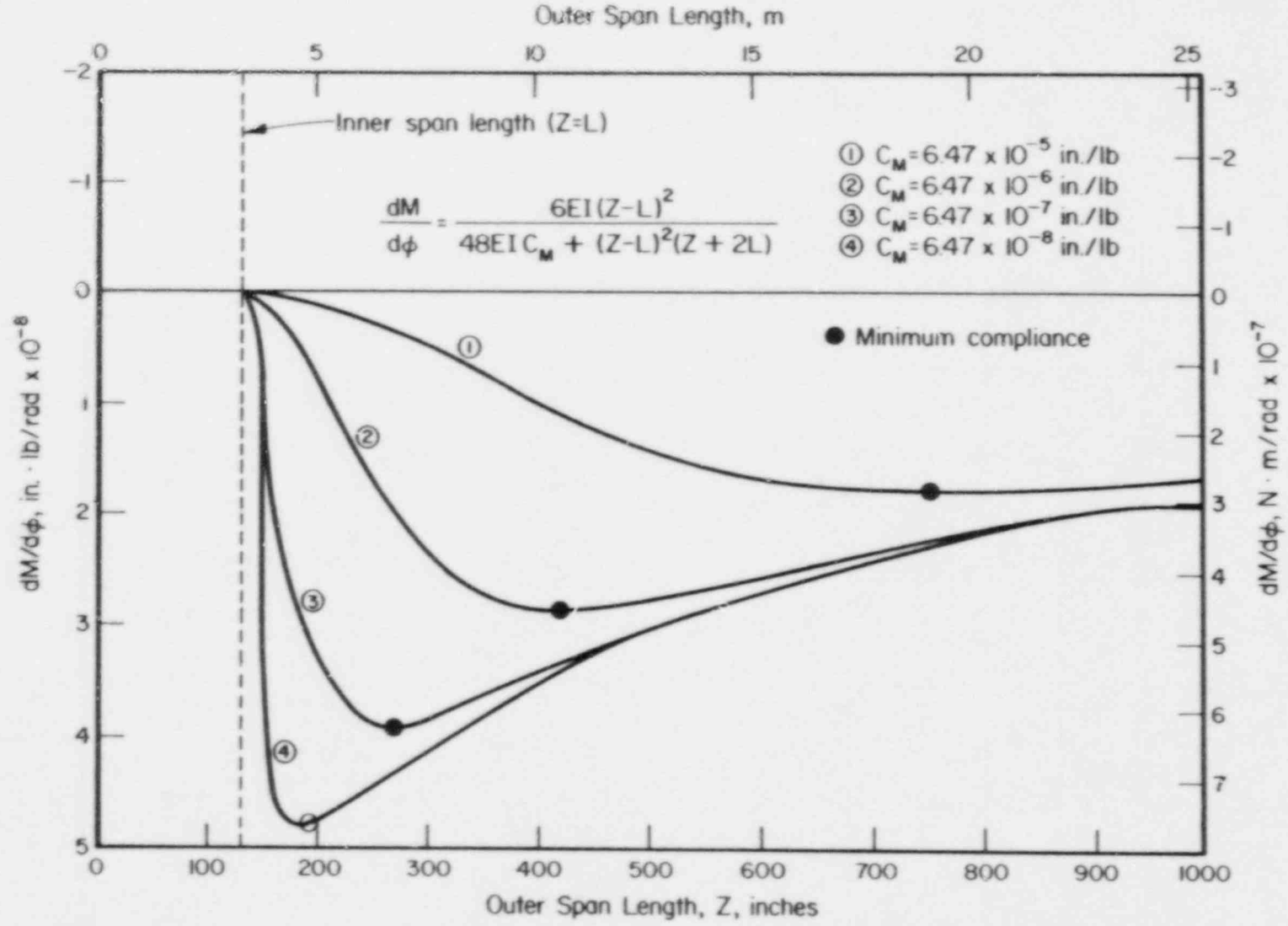

Figure 2.9.19 Examples of total system stiffness calculations showing that a maximum stiffness (minimum compliance) exists for various machine compliances.

SA-12/87-F2.9.19

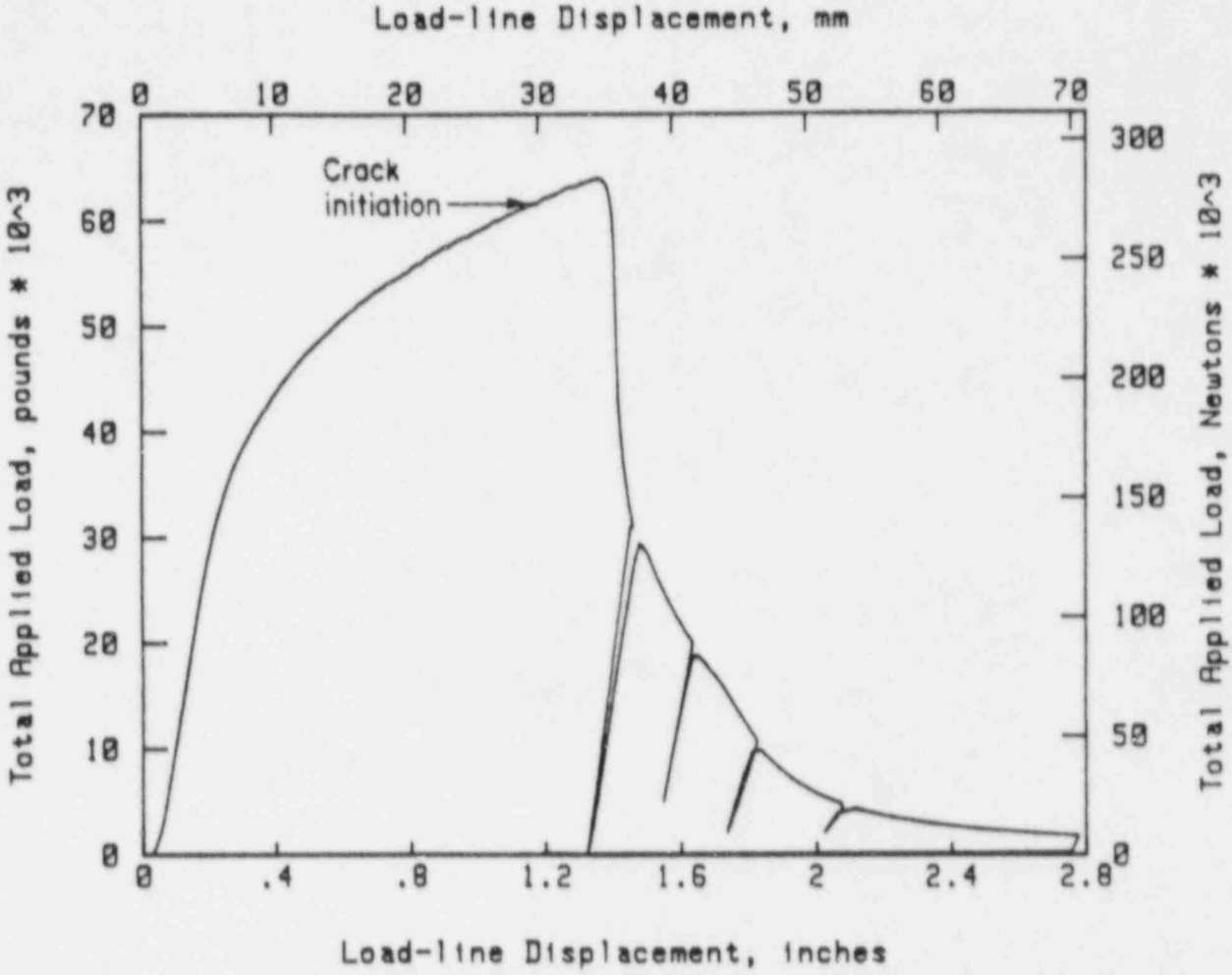

Figure 2.9.20 Total load versus load-line displacement for a 360-degree internal surface-cracked Type 304 stainless steel pipe with low compliance (Experiment 4115-8).

DRB-1.2.1.18-F10

References for Section 2.9

2.9.1 Wilkowski, G. M., and others, "Degraded Piping Program - Phase II", Semiannual Report, April 1985-September 1985, NUREG/CR-4082, Vol. 3, March 1986.

2.9.2 U.S. Nuclear Regulatory Commission Pipe Study Group, "Evaluation of the Potential for Pipe Breaks", NUREG-1061, Vol. 3, November 1984.

2.9.3 Joyce, J. A., "Instability Testing of Compact and Pipe Specimens Utilizing a Test System Made Compliant by Computer Control", ASTM STP 803, 1983, pp. II-348 to II-463.

2.9.4 Scott, P. M., and Brust, F., "An Experimental and Analytical Assessment of Circumferential Through-Wall-Cracked Pipes Under Pure Bending", NUREG/CR-4574, September 1986.

2.9.5 Pan, J., and Wilkowski, G. M., "Application of Tearing Instability Analysis for Complex Crack Geometries in Nuclear Piping", in Proceedings of the CSNI Specialist Meeting on Leak-Before-Break in Nuclear Reactor Piping, NUREG/CP-0051, August 1984.

2.9.6 Brust, F. W., "Approximate Methods for Fracture Analyses of Through-Wall-Cracked Pipes", NUREG/CR-4853, February 1987.

2.9.7 Wilkowski, G. M., and others, "Analysis of Experiments on Stainless Steel Flux Welds", NUREG/CR-4878, April 1987.

2.9.8 Kramer, G., and Papaspyropoulos, V., "An Assessment of Circumferentially Complex-Cracked Pipe Subjected to Bending", NUREG/CR-4687, October 1986.

2.10 Carbon Steel Flux Welds
(C. Marschall, P. Scott, and G. Wilkowski)

The objectives of this effort are to evaluate the fracture behavior of prototypical carbon steel weldments at LWR temperatures and to verify limit-load and EPFM estimation schemes for cracked pipes. These results are directly related to the development of flaw assessment criteria, such as the proposed ASME Section XI IWB-3650 criteria, as well as to pipe fracture analyses. Some results were reported in our last semiannual report (Ref. 2.10.1). The results from earlier semiannual reports are summarized below. Following that section, the status of current work and plans for future work are given.

2.10.1 Summary of Results Reported in Past Semiannual Reports

In the Second Semiannual Report (Ref. 2.10.2), the results of a series of FWFN(T) tests were reported. FWFN(T) specimens are used to simulate the fracture behavior of surface-cracked pipe; that is, the orientation of the crack is in the L-R direction and the ligament is essentially in tension. In this evaluation, stainless steel and carbon steel specimens were tested, each including cracks in the base metal, the SAWs, and the HAZ of the SAW. The objective of this series of tests was to determine the effect of notch acuity on the fracture behavior.

For the A516 Grade 70 carbon steel weld metal tested at 550 F (288 C), a fracture instability (crack pop-in) occurred with very little prior plastic deformation, as is indicated in Figure 2.10.1. Three additional FWFN(T) tests of the same weldment showed similar behavior: crack instabilities occurred with relatively little prior plastic deformation, at or before the maximum load point in the test. It should be noted that the procedure used to make the welds was obtained from a U.S. pressurized-water reactor (PWR) vendor and that the weldment was stress relieved. Hence, this behavior was observed for a prototypical weld.

The reason for the fracture instabilities observed in 550 F (288 C) FWFN(T) tests of SAWs in A516 Grade 70 steel is not known with certainty. Similar instabilities have been observed after ductile tearing in other tests of carbon steel specimens at 550 F (288 C), including pipe fracture tests and compact specimen tests. It is currently thought that this behavior is associated with DSA (see Section 3.1.2).

More recent efforts have involved evaluation of large crack growth predictions from small compact specimens. Both base metal and weld tests were conducted. The results of the carbon steel weld tests were reported in Reference 2.10.2. These tests involved the same SAW procedure used in the FWFN(T) tests discussed above. The results of 1T, 3T, and 9.5T planform size, 1-inch-(25.4-mm-) thick specimens are shown in Figure 2.10.2. For the 1T C(T) specimens, the initiation toughness of approximately 350 in-lb/in^2 (0.061 MJ/m^2) was the lowest initiation toughness value obtained on any

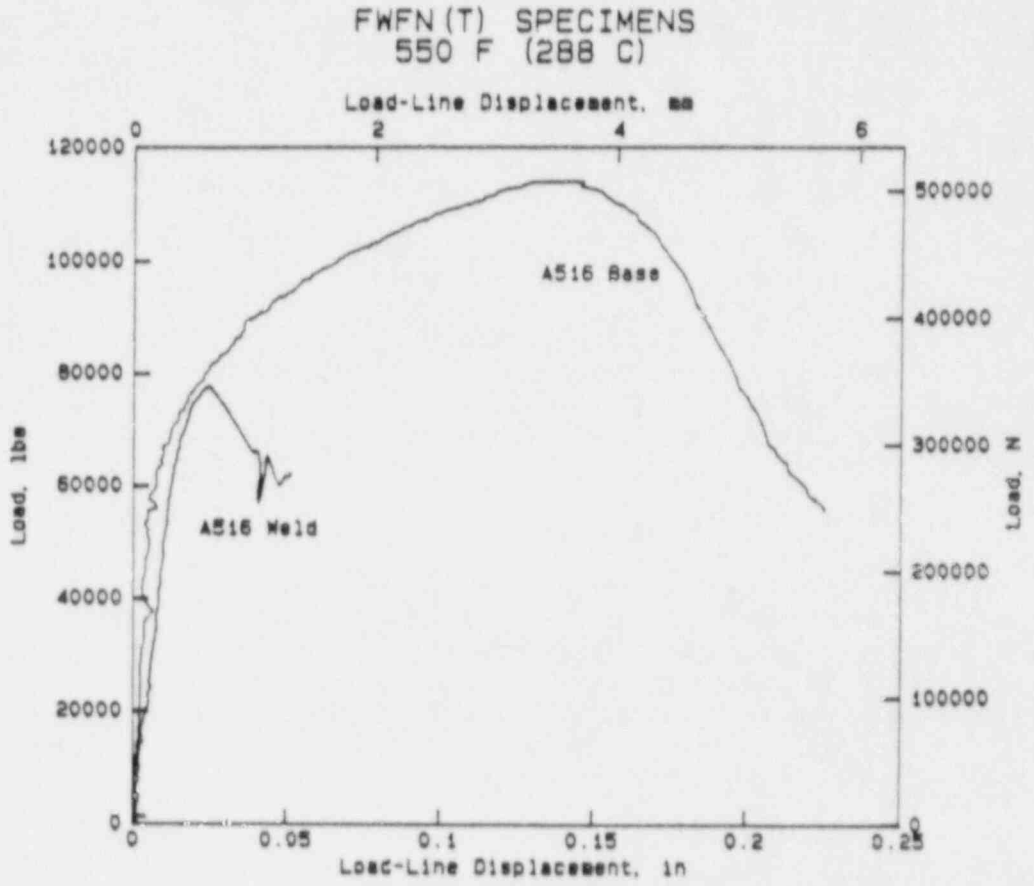

Figure 2.10.1 Comparison of 550 F (288 C) A516 Grade 70 base metal and Linde 44 SAW FWFN(T) specimen data.

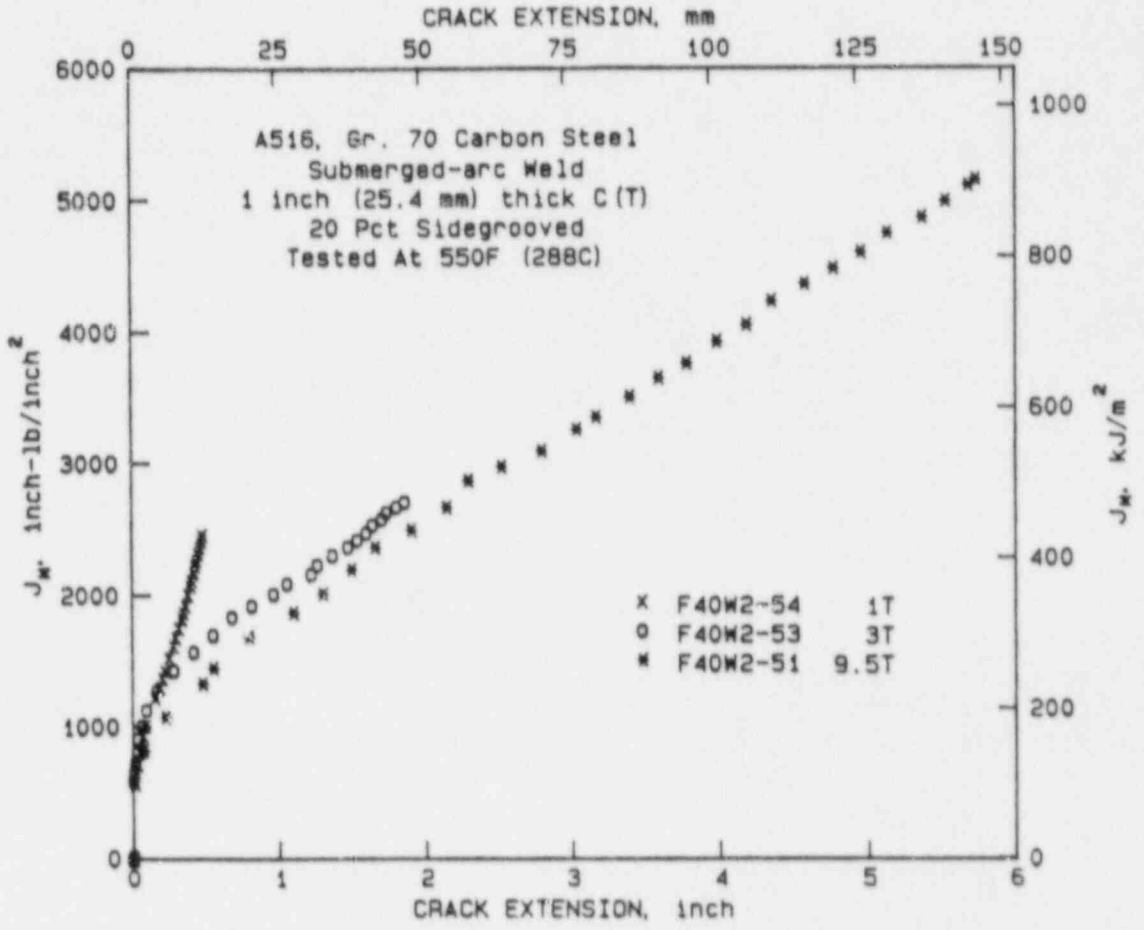

Figure 2.10.2 J_M-R curves for ferritic SAW compact specimens of different planform sizes.

SA-6/86-F3.3.4

material in this program. In addition, the 1T C(T) specimen resulted in a significantly higher tearing resistance than the 3T or 9.5T specimens (Figure 2.10.2). In stainless steel TIG welds, the smaller of variously sized C(T) specimens also gave much higher tearing resistance than the larger planform size specimens (Ref. 2.10.3). These results imply the possibility of a minimum planform C(T) specimen size necessary to obtain J-R curves for extrapolation to larger amounts of crack growth (see Section 3.3 of this report).

In the Fifth Semiannual Report from this program (Ref. 2.10.1), the results from a series of tests evaluating the fracture toughness and tensile properties of the cold-leg pipe shop weld were reported. Figure 2.10.3 shows a section through the cold-leg weld. Note that it is a double-vee weld, and the etched appearance varies from the inside to the outside of the weld. Because of the different appearance in the metallographic section, side-grooved 1-3/8 C(T) specimens containing a sharp machined notch were machined from the top and bottom of the weld. The resulting modified J-R curves from the testing of these specimens are shown in Figure 2.10.4. Note that the inside weld metal was significantly higher in toughness than the outside weld metal. Furthermore, both the inside and outside weld metal toughnesses were significantly higher than that of the SAW shown in Figure 2.10.2.

2.10.2 Progress Since Last Report

Since the last semiannual report was issued, progress in this subtask has been focused in two primary areas. The first was the characterization of material properties for a cold-leg weld, and the second was the preparation of a pipe fracture experiment. During this period, a series of 4T C(T) weld tests were conducted at Materials Engineering Associates (MEA). The weld evaluated in this series of tests was a shop-fabricated, pipe-to-elbow weld from a section of cold-leg pipe. The 4T planform size was selected for testing since it was the largest specimen that could be machined from a pipe of this diameter and wall thickness. For these particular specimens, the thickness was approximately 80 percent of the pipe wall thickness. It was believed that the fracture behavior of specimens of this thickness would reasonably represent full-thickness behavior. Choosing near-full-thickness specimens for this particular weld procedure was especially important since it was a double-vee weld, whose inside weld metal was significantly higher in toughness than its outside weld metal (Figures 2.10.3 and 2.10.4). In addition, by evaluating the larger 4T specimen, the resultant J-R curves should be usable for extrapolation to larger amounts of crack growth. As noted previously, some minimum planform C(T) specimen size may exist to get J-R curves for extrapolation to larger amounts of crack growth (see Section 3.3).

The J-R curves for these 4T C(T) weld specimens are shown in Figure 2.10.5. For Specimens F34W-W1 and F34W-W2 the values of J at crack initiation are 2,180 in-lb/in^2 (382 MJ/m^2) and 2,485 in-lb/in^2 (435 MJ/m^2), respectively.

In addition to evaluating the fracture resistance of the 4T weld specimens, the other major effort associated with this subtask was the preparation of a

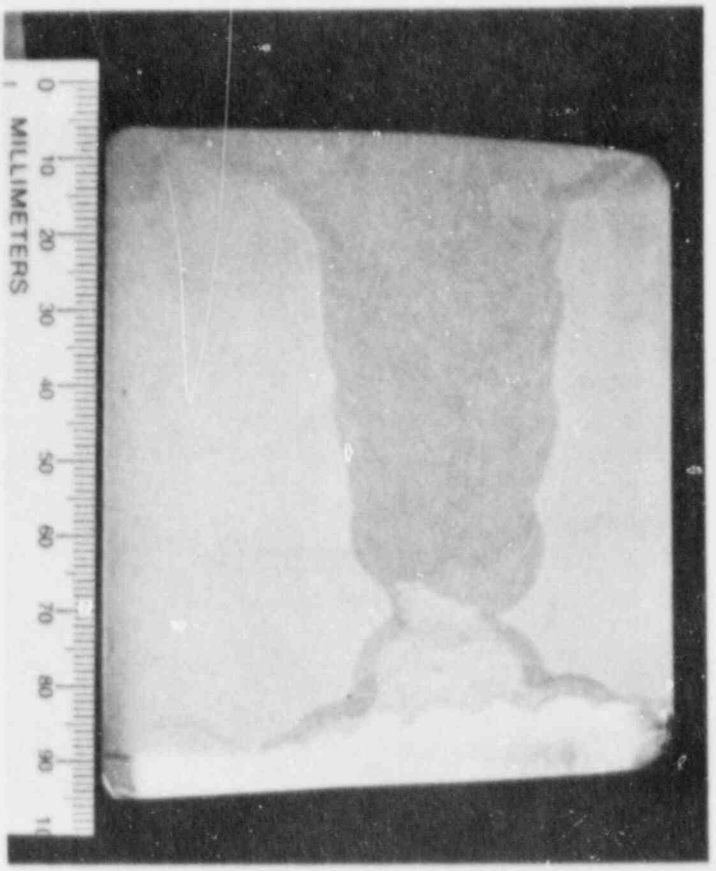

8M428

Figure 2.10.3 Photograph of cross section of a submerged-arc pipe-to-elbow weld in a 37-inch (940 mm) diameter ferritic steel cold-leg pipe.

SA-12/86-F2.10.3

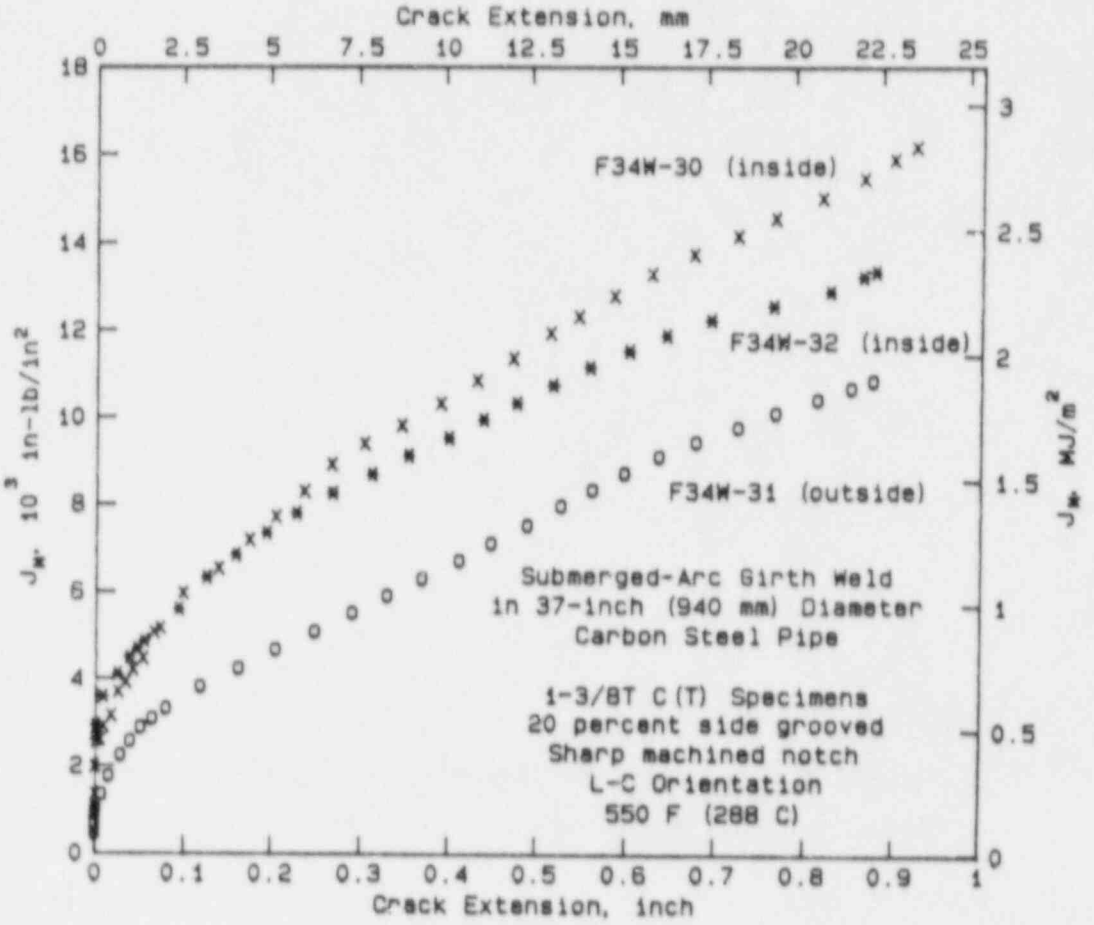

Figure 2.10.4 J_M-resistance curves illustrating the differences between inside and outside regions of a submerged-arc girth weld in a cold-leg pipe.

SA-12/86-F2.10.4

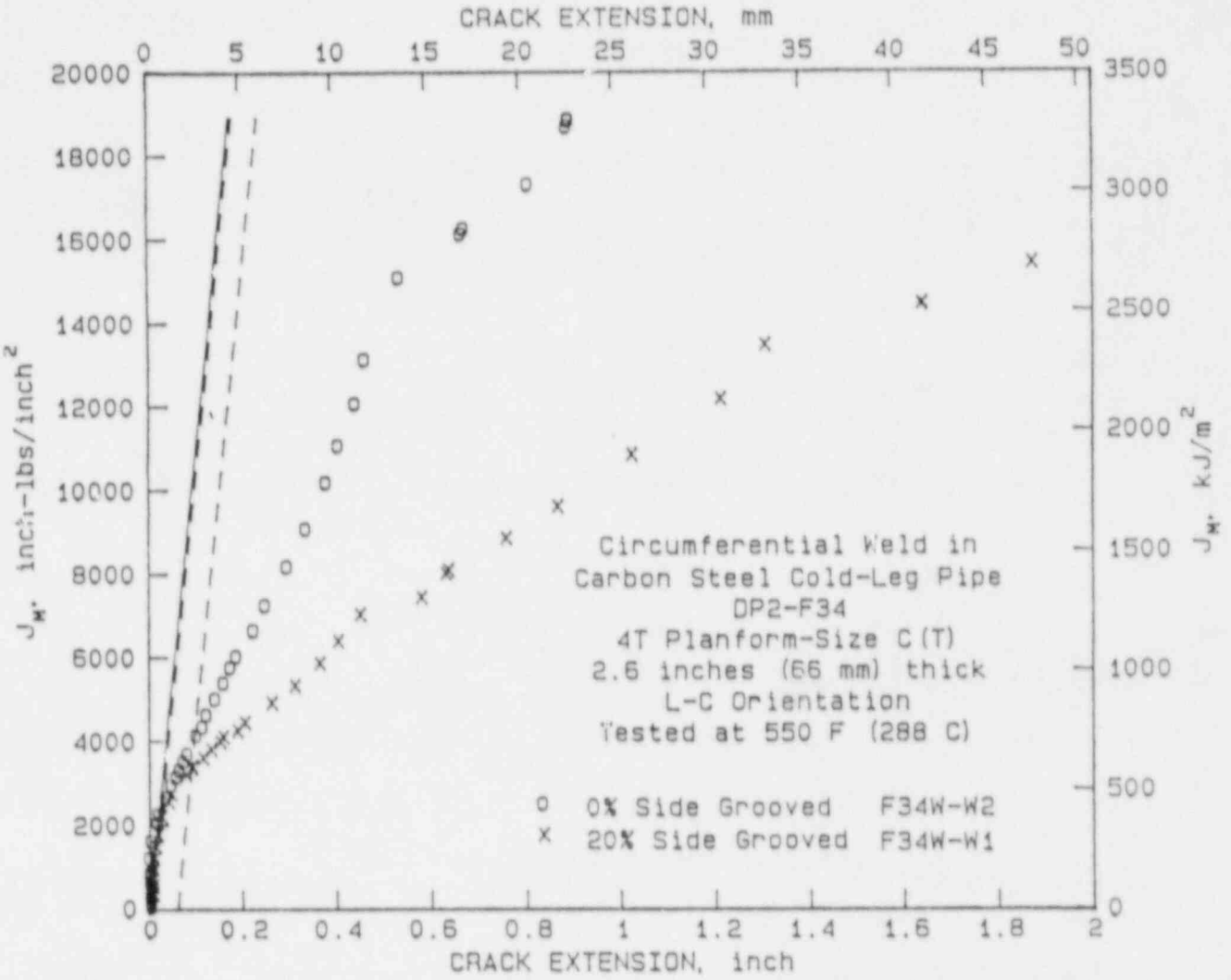

Figure 2.10.5 J-R curves for 4T planform C(T) specimens removed from a shop-fabricated pipe-to-elbow weld of cold-leg pipe. (Data from MEA.)

SA-12/87-F2.10.5

cold-leg weld pipe fracture experiment. The test specimen for this experiment is a section of a cold-leg pipe that was removed from a cancelled PWR plant. The pipe material is A516 Grade 70; the outside diameter of the test specimen is 36.75 inches (933 mm), and the wall thickness is 3.4 inches (86.4 mm). The flaw for this experiment is a circumferential through-wall crack centered in a circumferential shop-fabricated weld. The loading conditions for this experiment will be four-point bending. The test temperature will be 550 F (288 C).

2.10.3 Future Plans

In addition to the cold-leg weld experiment discussed above, two other carbon steel welded pipe fracture experiments are planned. The test specimens will be fabricated from a section of 16-inch- (406-mm-) diameter, Schedule 100, A106 Grade B carbon steel pipe. The test welds for both of these experiments will be fabricated using the same SAW procedure used in the FWFN(T) tests and the planform C(T) tests discussed above. This is a much lower-toughness weld than the cold-leg pipe weld. One experiment will evaluate a circumferential surface crack in the center of the SAW. The other will involve a circumferential through-wall crack in the center of the SAW. The loading conditions for both experiments will be combined pressure and four-point bending. The test temperature for both experiments will be 550 F (288 C). For the through-wall-cracked pipe experiment, a special high-temperature bladder will be used to seal the internal pipe pressure.

These experiments are important in that they will evaluate the material with the lowest toughness level observed to date as part of this program. Consequently, these experiments will provide important data for validating the carbon steel flaw assessment criterion currently being developed in the ASME Section XI Pipe Flaw Evaluation Task Group.

References for Section 2.10

2.10.1 Wilkowski, G. M., and others, "Degraded Piping Program - Phase II", Semiannual Report, April 1986-September 1986, NUREG/CR-4082, Vol. 5, April 1987.

2.10.2 Wilkowski, G. M., and others, "Degraded Piping Program - Phase II", Semiannual Report, October 1984-March 1985, NUREG/CR-4082, Vol. 2, July 1985.

2.10.3 Nakagaki, M., Marschall, C., and Brust F., "Analysis of Cracks in Stainless Steel TIG Welds", NUREG/CR-4806, November 1986.

2.11 Centrifugally Cast Stainless Steel
(G. Kramer, M. Rosenfeld, and G. Wilkowski)

The objectives of this effort are to evaluate the failure behavior of prototypical centrifugally cast stainless steel pipe at LWR conditions. Cast stainless steel is used in elbows, whereas centrifugally cast stainless steel is used for straight pipe. Centrifugally cast stainless steel pipe has been used in Westinghouse primary coolant piping and in Combustion Engineering surge lines.

Centrifugally cast stainless steels are unusual because of their duplex microstructure consisting of ferritic and austenitic grains. The ferritic structure tends to embrittle at high temperatures over a long period of time; this is known as thermal aging. Thermal aging is a concern near the end of material life and for plant life extension. The objectives of this effort are to verify limit-load and EPFM estimation schemes for both aged and unaged centrifugally cast pipes. The aging efforts have been conducted cooperatively with Framatome and Argonne National Laboratories.

The initial efforts in this area are described in the following sections.

2.11.1 Initial Efforts

Thermal aging of cast stainless steel pipe is one of the final efforts to be evaluated within the Degraded Piping Program. Prior work has shown that centrifugally cast stainless steel with high ferrite and molybdenum content is susceptible to thermal aging at 600 F (316 C). Similar findings have been reported by Argonne National Laboratories (Ref. 2.11.1). In laboratory specimen tests at Argonne, a significant reduction in the J-resistance curve was found in aged cast stainless steel material compared with unaged material.

Westinghouse (Ref. 2.11.2) has also evaluated thermal aging of cast stainless steel. In this study, 4-inch- (102-mm-) diameter pipe fracture experiments containing through-wall cracks were conducted in both the aged and unaged conditions. However, for this small pipe size, fully-plastic conditions were easily satisfied (Ref. 2.11.3), even though the fracture toughness of the material was lowered by thermally aging. For larger-diameter pipe sizes in which contained plasticity may occur, the lower toughness of the thermally aged material may significantly lower the load-carrying capacity of the pipe.

Two different CF-8m centrifugally cast stainless steel pipes will be evaluated within this subtask. The first is a 39.4-inch (1-m) length of thermally aged pipe donated to the program by Framatome of France. This material has been aged to simulate 40 years of service for a hot-leg pipe. The pipe has a 15.75-inch (400-mm) outer diameter and a wall thickness of 1.97 inch (50 mm). Tensile data and fracture toughness data taken from a plate aged at the same time are listed in Table 2.11.1. Unaged material property data are currently being assembled by Framatome and will be made available for comparison with the aged data.

Table 2.11.1. Material property data for thermally aged cast stainless steel.

	Framatome Material[a]	Combustion Engineering Surge Line
Tensile Data		
Yield Stress, psi (MPa)	29,900 (206)[b]	23,900 (165)[c]
Ultimate Stress, psi (MPa)	87,500 (603)[b]	62,400 (430)[c]
Young's Modulus, psi (MPa)	25.3×10^6 (1.747×10^5)	N/A
Elongation, percent	N/A	31.7[c]
Reduction in Area, percent	N/A	50.4[c]
Fracture Toughness Data		
Charpy V-Notch, ft-lb (J)	17.7 (24)[d]	N/A
J_{IC}, in-lb/in^2 (kJ/m^2)	565-662 (99-116)[b]	N/A
dJ/da, in-lb/in^3 (MJ/m^3)	27,200-41,800 (121-186)[b]	N/A

(a) Data for similar material aged at same time as pipe.
(b) Tested at 572 F (300 C) in aged condition.
(c) Tested at 550 F (288 C) in unaged condition.
(d) Tested at 68 F (20 C) in aged condition.

The second pipe material that will be evaluated is a surge line from a cancelled Combustion Engineering plant. Three separate sections of pipe, totaling approximately 58 feet (17.7 m) in length, were procured for use in this subtask. Two of the lengths also contain cast stainless steel elbows. The pipe material is 12-inch- (305-mm-) diameter, Schedule 160, SA 351 Grade CF-8m. The elbow material is thought to be the same, but verification of this fact has not been completed. Table 2.11.1 presents the results of tensile tests on the pipe; Table 2.11.2 lists a chemical analysis conducted on both the pipe and elbow.

The majority of this second material is unaged, but several specimens are currently being thermally aged at Argonne National Laboratories. The aged specimens include pipe base metal, a pipe-to-pipe girth weld, and several pieces of a 45-degree elbow. At the time of this writing, these sections had been aged at 750 F (399 C) for nearly 20,000 hours to simulate approximately 40 to 50 years of service in a cold leg, or 14 to 20 years of service in a hot leg. Aging of the specimens will continue until approximately January of 1988.

2.11.2 Future Plans

To evaluate the effects of aging on full-scale pipe behavior, the four pipe fracture experiments listed in Table 2.11.3 are scheduled for this subtask. The first experiment will be conducted on the aged Framatome pipe, the final three on the surge line pipe and a pipe-to-pipe weld. A constant crack geometry will be evaluated in each of the three surge line pipe fracture experiments. The unaged pipe experiment will therefore provide baseline data for evaluating both the aged base metal and the aged weld experiments. In this way, an assessment can be made of the reduction in fracture toughness caused by thermally aging. Fabrication of the surge line pipe fracture experiments will begin in early 1988. Future work involves calculating an appropriate flaw size for the Framatome pipe experiment. R-6 curve evaluations provided by Framatome will be carefully reviewed in the design of this experiment, and the final flaw size will be coordinated with researchers at Framatome before final approval from the NRC contract monitor.

References for Section 2.11

2.11.1 Chopra, O. K., and Chung, H. M., "Investigations of the Mechanisms of Thermal Aging of Cast Stainless Steels", presented at the ACRS Metal Components Subcommittee Meeting, Columbus, OH, July 2, 1987.

2.11.2 Bamford, W. H., and Landerman, E. I., "Thermal Analysis of Cast Stainless Steel and Its Impact on Piping Integrity", Circumferential Cracks in Pressure Vessels and Piping, Vol. II, ASME PVP, Vol. 95, 1984, pp. 137-172.

2.11.3 Wilkowski, G. M., and others, "Degraded Piping Program - Phase II", Semiannual Report, April 1985-September 1985, NUREG/CR-4082, Vol. 3, March 1986.

Table 2.11.2. Chemical analysis for thermally aged SA-351 CF-8m cast stainless steel pipe and elbow.

Element	A37-Elbow	A37-Pipe
C	0.04	0.04
Mn	0.84	0.93
Cr	19.23	17.88
Ni	9.66	8.80
Mo	3.12	3.37
Si	0.69	0.63
P	0.019	0.019
S	--	--
Al	--	--
Ti	<0.01	0.012
V	0.07	0.07
Cu	0.08	0.07
Nb	--	--
Zr	--	--
W	--	--
Co	0.07	0.06

Table 2.11.3. Test matrix for cast stainless steel pipe fracture experiment.

Experiment Number	Pipe Diameter, inch (mm)	Nominal Wall Thickness, inch (mm)	Base Metal or Weld	Aged or Unaged	Source	Initial Crack Length, % Circumference	Initial Crack Depth, % Wall
4143-1	15.73 (400)	1.968 (50.0)	Base Metal	Aged	Framatome	(a)	(a)
4143-2	12.75 (324)	1.312 (33.3)	Base Metal	Aged	Surge Line	50	67
4143-3	12.75 (324)	1.312 (33.3)	Weld	Aged	Surge Line	50	67
4143-4	12.75 (324)	1.312 (33.3)	Base Metal	Unaged	Surge Line	50	67

All tests conducted at 550 F (288 C); crack geometry = surface crack; loading method = pressure and bend.

(a) To be determined.

3. SUPPORTING RESEARCH ACTIVITIES

Besides the extensive full-scale fracture investigations and related pipe fracture analytical developments described in Section 2, the Degraded Piping Program includes supporting research activities. These are conducted to establish the characteristics of the materials being investigated and to provide baseline data for various experiments and analytical developments. Other related analytical tasks essential to the overall goals of the program were also pursued. These activities included

- Characterization of the properties of the pipe materials used in the program and transfer of data to other programs
- Investigation of the effect of anisotropy causing crack turning in carbon steels
- Study of the possible role of dynamic strain aging (DSA) in carbon steel fracture at light-water reactor (LWR) temperatures
- Examination of specimen geometry effects on J-R curves
- Application of the results of small test specimens in predicting the large crack growth behavior exhibited by full-scale piping materials
- Development of a user-friendly J-estimation scheme computer code
- Documentation of round-robin efforts.

3.1 Characterization of Material Properties for Pipe Used in Pipe Fracture Experiments (C. Marschall, M. Landow, and G. Wilkowski)

In the full-scale pipe fracture test matrix, there are approximately 70 experiments that are tests of materials ranging from carbon steel base metal, stainless steel base metal, Inconel 600 base metal, and centrifugally cast stainless steel base metals to carbon steel and austenitic stainless steel weld metal. Each of the pipes used in the pipe-fracture experiments is being characterized to provide data for the analysts and for the U.S. Nuclear Regulatory Commission (NRC) computerized pipe material property database being developed at Materials Engineering Associates (MEA). In addition, material property data for pipe from past or current pipe fracture programs were generated in several cases.

This effort resulted in two unexpected findings, the most significant of which were the turning of cracks from the circumferential direction in carbon steels (possibly due to material anisotropy), and dynamic crack jumps in carbon steels (possibly due to dynamic strain aging). The material characterization efforts and the investigations of unanticipated fracture behavior are summarized in the following sections.

3.1.1 Summary of Material Characterization Tests Conducted in Support of Pipe Fracture Experiments

Each pipe that is subjected to a pipe fracture test in this program is characterized according to the following data:

1. Chemical composition.

2. Tensile stress-strain behavior to the point of fracture at 72, 300, and 550 F (22, 149, and 288 C), using specimens oriented with their tensile axes parallel to the pipe axis.

3. Ductile-to-brittle transition behavior as determined from Charpy V-notch impact specimens machined in the L-C orientation and tested over a range of temperatures. Data obtained include absorbed energy, lateral expansion, and percent shear of the fracture surface, each as a function of temperature. Only ferritic steels are subjected to these tests. In pipes whose wall thickness is not sufficient for a full-size Charpy specimen, subsize Charpy specimens are used.

4. J-R curves from precracked compact or bend specimens at 300 and 550 F (149 and 288 C) with L-C specimen orientation.

5. J-R curves from sharp machine-notched compact, bend, or full-width-face-notched (tension) FWFN(T) specimens at 550 F (288 C) or at the temperature of the pipe test. The tests are designed to simulate the pipe test. If the pipe test uses a circumferential through-wall

flaw, the characterization test will use a compact or a bend specimen having the L-C orientation. If the pipe test uses a circumferential surface flaw, the characterization test will use an FWFN(T) specimen having the L-R orientation. Both specimen types are illustrated in Figure 3.1.1.

For the mechanical property tests described above, specimens are removed from the pipe without flattening them. This is illustrated in Figure 3.1.1. The dimensions of the fracture toughness specimens are determined by the pipe diameter and wall thickness. Obviously, the test specimen thickness must be less than the pipe wall thickness if flattening is not used. A rule of thumb employed is to use specimen thicknesses that are no less than 80 percent of the pipe wall thickness, in the belief that the behavior at this thickness will be reasonably representative of full-thickness behavior. The maximum attainable width of the specimen will depend on the inside pipe diameter (D), the pipe wall thickness (t), and the ratio of specimen thickness to pipe wall thickness (A), according to the relation

$$\text{specimen width} = 2[tD(1-A) + t^2(1-A^2)]^{0.5} \qquad (3.1.1)$$

It is recognized that the J-R curves being developed in this subtask may not meet the ASTM requirements for J_{Ic} testing, as set forth in E813-87, or for J-R curve testing, as described in ASTM E1152-87, Standard Test Method for Determining J-R Curves. Specifically, specimen sizes used in this program usually are not sufficiently large to meet the following requirements set forth by ASTM:

$$J_{Ic} \leq B\sigma_f/25 \qquad (3.1.2a)$$

and

$$J \leq B\sigma_f/20 \qquad (3.1.2b)$$

where B is specimen thickness and σ_f is flow strength (the average of yield and tensile strength). Assuming flow strengths of 45,000 to 50,000 psi (310 to 345 MPa) at 550 F (288 C) for the pipe materials under investigation, the maximum allowable J_{Ic} value for a 1-inch- (25.4-mm)-thick specimen would be approximately 2,000 in-lb/in^2 (350 kJ/m^2) and the maximum allowable J value during crack growth would be approximately 2,500 in-lb/in^2 (440 kJ/m^2). Actual specimen thicknesses generally are less than 1 inch (25.4 mm), and sometimes are as small as 0.2 inch (5 mm). Even for the larger thickness, observed J values in this investigation frequently exceed 2,000 to 2,500 in-lb/in^2 (350 to 440 kJ/m^2) and, hence, often do not satisfy ASTM validity requirements.

Additionally, the amount of crack growth investigated here greatly exceeds the 10 percent of the remaining ligament that is the limit recommended by ASTM for so-called J-controlled crack growth. Typically, in fracture toughness tests conducted in this program, cracks are allowed to grow approximately 40 to 60 percent of the original ligament.

General Guidelines for Machining Specimens

1. Much of the machining will involve preparing flat specimens from pipe. In no instance should the pipe be flattened or mechanically deformed in any way.

2. Five different types of specimens are to be machined from pipe, as illustrated schematically below. The specimens will be of various sizes that will depend on the pipe dimensions.

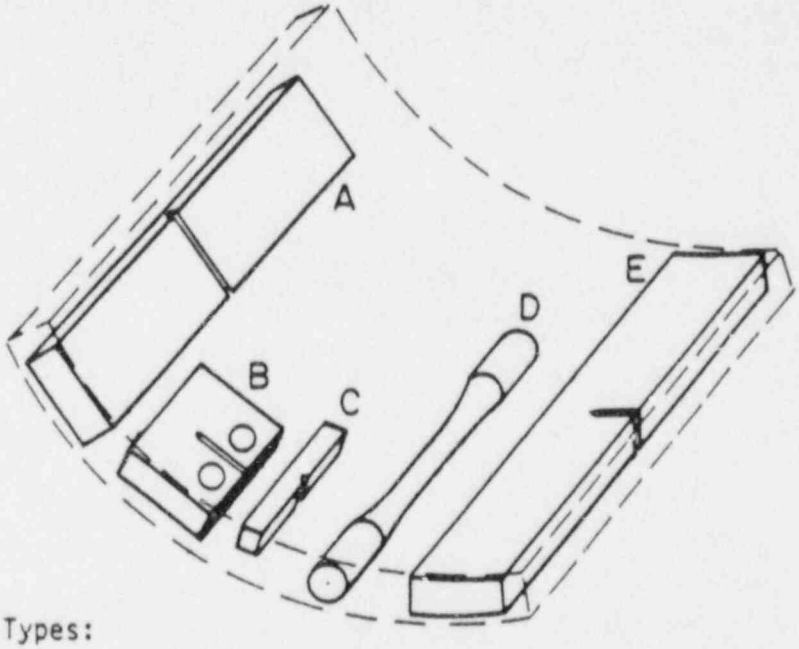

Specimen Types:

A	Full-width-face-notch (tension) - FWFN(T)	L-R orientation
B	Compact (tension) - C(T)	L-C orientation
C	Charpy V-notch-CVN	L-C orientation
D	Tension - T	Axial orientation
E	Bend - SE(B)	L-C orientation

3. The A specimens should be notched on the face that corresponds to the inner wall surface of the pipe.

4. The notch in the A, B, & C specimens should match that used in full-scale pipe experiments, except where fatigue cracks are explicitly requested.

5. The notch in Specimen C must be oriented as shown in sketch.

Figure 3.1.1 Instruction sheet for machining test specimens from pipe.

SA-12/85-F3.1.1

The rationale for testing specimens that do not meet specimen size criteria and for permitting large amounts of crack growth can be stated simply. The fracture resistance data being developed here are not to be used to characterize a certain material under conditions of plane strain, but rather to characterize a pipe material in a thickness approximately equal to its wall thickness. The crack is allowed to grow far in excess of 10 percent of the original ligament because pipe tests typically have large amounts of crack growth. Thus, meeting validity criteria established to define a material property is of less concern than the ability to characterize the behavior of a specific pipe.

During the current reporting period, progress was made in the following material-characterization areas: (1) data reduction for 300 F (149 C) compact-specimen tests and for 72 and 300 F (22 and 149 C) tensile-specimen tests, (2) data reduction for 550 F (288 C) compact-specimen tests on two welds, and (3) preparation of material characterization inputs to Pipe Fracture Data Record Books.

Tables 3.1.1 and 3.1.2 summarize material property data for austenitic and ferritic materials, respectively, through November 30, 1987.

3.1.2 Data Transfer to MEA

During the current reporting period, Battelle has transferred material characterization data for all pipes tested in the Degraded Piping Program to MEA. Information transferred included results of chemical analyses, tensile tests, Charpy V-notch impact tests, and fracture toughness tests. The transfer was accomplished by copying data from Battelle's storage files onto hard disks in a format prescribed by MEA. MEA, in turn, is placing the data in the NRC Pipe Material Data Base.

3.1.3 Observations of Dynamic Strain Aging in Carbon-Steel Pipe

Many carbon steels are susceptible to strain aging, including those carbon steels used in nuclear plant piping. Strain aging in these materials is a change in the stress-strain response resulting from the interaction of dislocations and interstitial solute atoms, primarily nitrogen and carbon, in the steel. In static strain aging, the property changes occur after plastic deformation and depend on the temperature and time (aging) after the deformation has occurred. In dynamic strain aging, on the other hand, the property changes occur during plastic deformation.

Figure 3.1.2 illustrates static strain aging in a tensile specimen. First, assume that the specimen is loaded and then unloaded such that curve OABC is produced. If it is reloaded immediately, it will follow curve CBD; the BD portion of the curve will be the same as if the specimen had not been unloaded. If, however, the specimen is allowed to age for some time after unloading to point C, reloading will produce a curve similar to CEF. Static strain aging increases the yield strength, causes the Luders strain to reappear, increases the ultimate strength, and decreases the fracture elongation. Strain aging

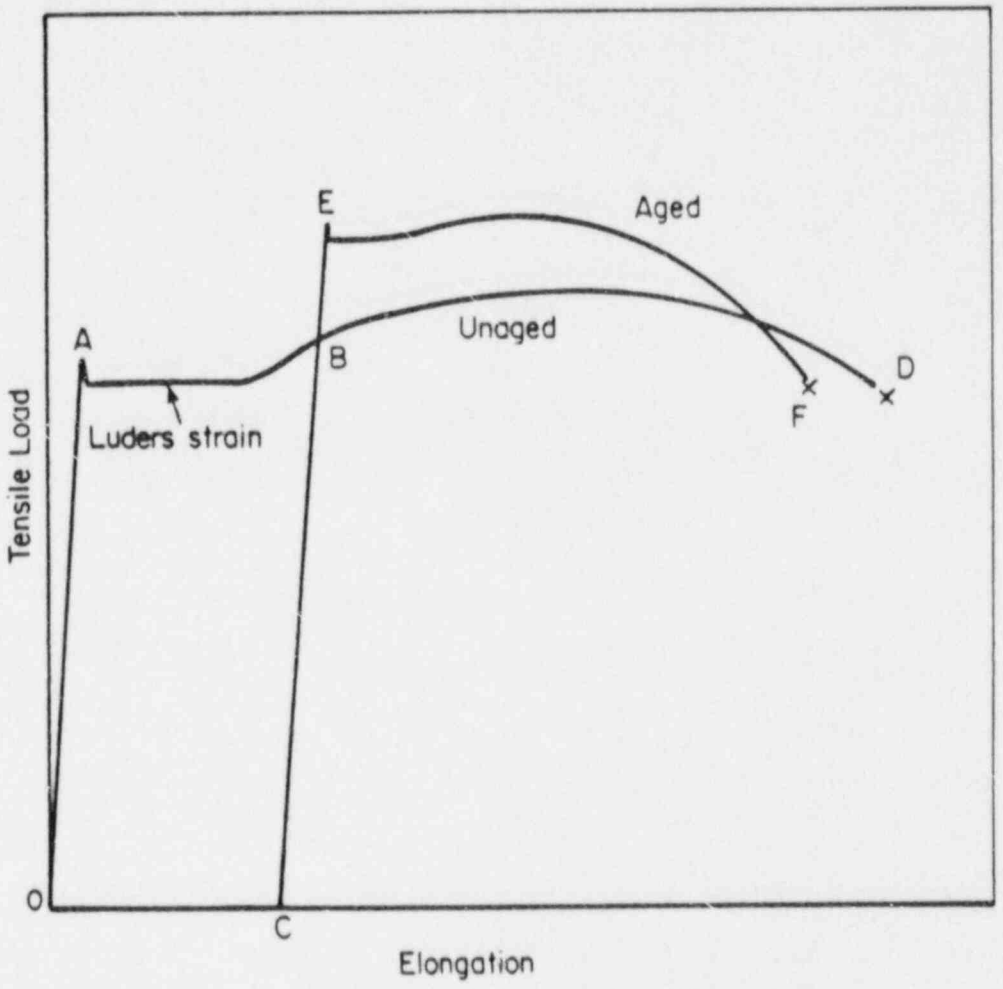

Figure 3.1.2 Static strain aging in a tensile specimen.

SA-6/86-F3.1.10

Table 3.1.1 Material characterization data for austenitic pipe materials.

Pipe I.D.	Pipe Mat.	Pipe size Dia. in.	Wall in.	Charpy V Notch Spec size	USE,ft-lb	FATT, F	Test Temp.,F	Average YS, ksi	UTS, k
DP2-A23	SA376-304	6	0.562				72	36.0	87.
							300	25.5	67.
							550	20.1	65.
							550		
							550		
							550		
							550		
DP2-A5	SA358-316L	16	0.375				72	36.4	89.
							300	28.2	73.
							300		
							550	24.2	68.
							550		
							550		
							550		
DP2-A45W	304(SAW)	Plate	1.0				550	47.1	67.
							550		
							550		
							550		
							550		
DP2-A35	SA376-304	6	0.864				75	36.5	91.
							300	26.4	71.
							300		
							550	21.9	69.
							550		
							550		
DP2-A7	SA376-304	6	0.280				79	31.4	86.
							300	25.5	67.
							550	21.3	65.
							550		
							550		
DP2-A8	SA358-304	16	1.031				72	42.8	105.
							300	31.0	69.
							300		
							550	26.1	66.
							550		
							550		
							550		
							550		

Tensile Properties			Fracture Toughness Data								
si	% Elong.	Gage Length, inches	% Red of Area	Spec. Type	Notch Type	% Side-grooves	Orientation	W, inches	B, inches	No. of Tests	Ji, ave. in.-lb/in.^2	dJm/da, ave. in.-lb/in.^3
7	97.7	0.5	73.6									
7	59.7	0.5	71.7	C(T)	FC	0	L-C	1.0	0.5	2	N.D.	N.D.
2	53.8	0.5-1.0	71.4	C(T)	FC	0	L-C	1.0	0.5	2	>7700	N.D.
				C(T)	FC	20	L-C	1.0	0.5	2	6900	47600
				C(T)	SMN	0	L-C	1.0	0.5	1	6110	78300
				C(T)	SMN	20	L-C	1.0	0.5	1	6220	50300
				FWFN(T)	SMN	10	L-R	0.44	1.60	2	13400	89900
5	68.8	1.0	79.6									
7	47.5	1.0	74.3	C(T)	FC	0	L-C	2.0	0.27	1	3520	38410
				C(T)	FC	20	L-C	2.0	0.27	1	1810	43970
2	39.5	1.0	72.8	C(T)	FC	0	L-C	2.0	0.27	1	2250	41400
				C(T)	FC	20	L-C	2.0	0.27	1	2180	34200
				C(T)	SMN	0	L-C	2.0	0.29	2	3270	49600
				FWFN(T)	SMN	10	L-R	0.29	2.00	2	6497	69640
6	31.5	0.5	44.2									
				C(T)	FC	0	WCL	2.0	1.00	2	616	15800
				C(T)	SMN	0	WCL	2.0	0.92	2	561	18410
				C(T)	FC	0	WCL	19.0	1.16	1	2987	10070
				FWFN(T)	SMN	10	WCL	1.02	3.5	2	1073	20930
6	78.9	1.00	80.6									
0	55.3	1.00	81.0	C(T)	FC	0	L-C	2.00	0.64	1	7210	68380
				C(T)	FC	20	L-C	2.00	0.64	1	4830	70440
2	48.5	1.00	75.0	C(T)	FC	0	L-C	2.00	0.64	1	3965	81780
				C(T)	FC	20	L-C	2.00	0.64	1	3270	63640
				FWFN(T)	SMN	10	L-R	0.69	1.99	2	8630	172100
2	80.1	0.5	79.7									
3	55.2	0.5	78.1	C(T)	FC	0	L-C	0.8	0.23	2	12460	56830
1	43.3	0.5	63.6	C(T)	FC	0	L-C	0.80	0.23	2	8846	N.D.
				C(T)	FC	20	L-C	0.80	0.23	1	4985	41940
				FWFN(T)	SMN	10	L-R	0.22	0.98	2	8633	69055
2	76.5	1.0	76.7									
5	49.2	1.0	80.2	C(T)	FC	0	L-C	2.0	0.90	1	11780	88180
				C(T)	FC	20	L-C	2.0	0.90	1	5400	82470
5	46.4	1.0	74.5	C(T)	FC	0	L-C	2.0	0.90	1	4050	88500
				C(T)	FC	20	L-C	2.0	0.90	1	3555	76000
				C(T)	SMN	20	L-C	2.0	0.90	1	8540	83200
				FWFN(T)	FC	10	L-R	0.80	3.47	1	9195	95600
				FWFN(T)	SMN	10	L-R	0.80	3.5	1	6675	220000

8805060305-04

Table 3.1.1 (Continued)

Pipe I.D.	Pipe Mat.	Pipe size Dia. in.	Wall in.	Charpy V Notch Spec size	USE,ft-lb	FATT, F	Test Temp.,F	Average YS, ksi	Average UTS, k
DP2-A12	SA358-304	42	0.250				72 72	31.9	98.9
DP2-A34	SA312-304	2	0.250				72	35.7	95.2
DP2-A25WO	TIG overlay;304SS	6	0.562				550	37.5	63.2
DP2-A45	SA240-304	Plate	1.0				550 550	22.8	68.3
DP2-A45WA	Anr.l'd SAW;304SS	Plate	1.0				550	28.3	67.5
DP2-A36	304	4.5	0.25				72	35.8	91.3
DP2-A37	SA316 (CF8M)	12	1.312				72	33.4	84.7
							300	27.9	67.0
							550 550	23.9	62.4
DP2-A46	304	Plate	0.39				550 550 550	22.5	68.1
DP2-A46W	TIG Weld 304	Plate	0.39				550 550 550	43.2	64.9
DP2-A47	304	4	0.35				72	40.1	92.0
DP2-I1	Inconel-600	6	0.432				77	34.6	93.5
							300	31.2	87.8
							550 550	28.5	88.4

Tensile Properties			Fracture Toughness Data								
i % Elong.	Gage Length, inches	%, Red of Area	Spec. Type	Notch Type	% Side-grooves	Orientation	W, inches	B, inches	No. of Tests	Ji, ave. in.-lb/in.^2	dJm/da, ave. in.-lb/in.^3
83.2	1.0	75.4	C(T)	FC	0	L-C	2.0	0.20	2	3122	33950
			C(T)	SMN	0	L-C	2.0	0.20	2	3892	39400
63.0	1.0	N.D.	3Pt-Bend	SMN	0	L-C	0.65	0.18	3	2957	155700
30.8	0.5	66.6	FWFN(T)	FC	10	L-R	0.79	2.0	2	4500	52000
47.3	1.0	79.0	C(T)	FC	0	L-T	2.0	1.0	1	12500	78600
			C(T)	FC	20	L-T	2.0	1.0	1	7830	95700
34.5	0.5	47.0	C(T)	SMN	0	WCL	2.0	1.0	2	970	25600
71.9	1.0	80.1	3PtBend	SMN	0	L-C	1.0	0.24	2	10100	62000
62.3	1.0	77.2									
35.7	1.0	63.4	C(T)	FC	0	L-C	3.0	0.93	2	4390	41480
31.7	1.0	50.4	C(T)	FC	0	L-C	3.0	0.97	2	3940	26690
			C(T)	SMN	0	L-C	3.0	0.91	2	5975	27195
39.7	1.0	70.8	C(T)	FC	0	L-T	1.0	0.38	2	2075	27575
			C(T)	FC	0	L-T	3.0	0.39	1	3100	19890
			C(T)	FC	0	L-T	6.0	0.39	1	3820	12875
31.5	1.0	73.6	C(T)	FC	0	WCL	1.0	0.34	2	4100	56960
			C(T)	FC	0	WCL	3.0	0.48	1	7315	32240
			C(T)	FC	0	WCL	6.0	0.48	1	6155	25410
60.8	0.5	81.6									
63.9	0.5	73.5									
58.5	0.5	71.4	C(T)	FC	20	L-C	1.0	0.36	1	11010	69300
58.6	0.5	66.2	C(T)	FC	0	L-C	1.0	0.36	1	9310	60950
			C(T)	FC	20	L-C	1.0	0.36	1	10390	73290

Table 3.1.2 Material characterization data for ferritic pipe mater

Pipe I.D.	Pipe Mat.	Pipe size Dia. in.	Wall in.	Charpy V Notch Spec size	USE,ft-lb	FATT, F	Test Temp.,F	Average YS, ksi	Average UTS,
DP2-F29	A106B	16	1.021	Full	75	68	72	40.1	75.2
							300 300	36.5	87.5
							550 550 550	34.1	88.5
DP2-F9	SA333-Gr6	10	0.719	Full	115	-4	72	40.8	65.7
							300 300	39.8	70.0
							550 550 550 550 550	34.7	76.5
DP2-F30	A106B	6	0.562	Full	110	100	77	45.6	75.4
							300	44.7	91.1
							550 550 550	46.4	90.0
DP2-F26	A155	28	0.875	Full	122	60	72	39.1	63.6
							300 300	38.9	76.3
							550 550 550 550	33.5	78.9
DP2-F32	API-5LX65	42	0.875	Full	72	-50	72	63.0	82.4
DP2-F1	A106B	6	0.280	0.58	70	-140	75	42.8	68.1
							300	37.2	62.3
							550 550 550	30.8	67.8
DP2-F40	A516,Gr.70	Plate	1.0				550 550	34.1	79.6
DP2-F40W2	SAW;A516,Gr.70	Plate	1.0	Full	58	68	550 550 550 550 550 550 550 550 550	64.2	104.5

ials.

Tensile Properties			Fracture Toughness Data								
si % Elong.	Gage Length, inches	%, Red of Area	Spec. Type	Notch Type	% Side-grooves	Orientation	W, inches	B, inches	No. of Tests	Ji, ave. in.-lb/in.^2	dJm/da, ave. in.-lb/in.^3
29.6	1.0	61.4									
18.6	1.0	44.5	C(T)	FC	0	L-C	2.00	0.85	1	660	11020
			C(T)	FC	20	L-C	2.00	0.85	1	295	10750
24.0	1.0	41.4	C(T)	FC	0	L-C	2.00	0.85	1	635	16410
			C(T)	FC	20	L-C	2.00	0.85	1	850	12910
			FWFN(T)	SMN	10	L-R	0.71	1.6	2	2025	60950
39.1	1.0	73.0									
24.8	1.0	63.6	C(T)	FC	0	L-C	2.00	0.55	1	861	23490
			C(T)	FC	20	L-C	2.00	0.55	1	966	8700
27.3	1.0	60.0	C(T)	FC	0	L-C	2.00	0.55	1	885	31950
			C(T)	FC	20	L-C	2.00	0.55	1	900	19180
			C(T)	SMN	0	L-C	2.00	0.52	1	1700	22950
			C(T)	SMN	20	L-C	2.00	0.52	1	1120	10500
			FWFN(T)	SMN	10	L-R	0.57	2.4	4	1160	74500
38.6	0.5	62.2									
23.6	0.5	37.6	C(T)	FC	0	L-C	1.0	0.36	2	732	19350
24.0	0.5	34.4	C(T)	FC	0	L-C	1.00	0.36	2	680	19650
			C(T)	FC	20	L-C	1.00	0.36	2	588	15550
			FWFN(T)	SMN	10	L-R	0.44	1.60	2	1456	33025
34.3	1.0	69.5									
22.8	1.0	51.6	C(T)	FC	0	L-C	2.00	0.76	1	610	20670
			C(T)	FC	20	L-C	2.00	0.76	1	628	13650
29.8	1.0	53.6	C)T)	FC	0	L-C	2.00	0.76	1	1030	N.D.
			C(T)	FC	20	L-C	2.00	0.76	1	1240	19500
			C(T)	SMN	0	L-C	2.00	0.83	1	1483	N.D.
			C(T)	SMN	20	L-C	2.00	0.83	1	1180	18200
25.1	1.0	66.9	3Pt Bend	SMN	0	L-C	3.50	0.53	1	2275	37000
38.7	0.5	64.6									
32.8	0.5	70.9	C(T)	FC	0	L-C	0.80	0.23	2	2095	32260
25.0	0.5	54.7	C(T)	FC	0	L-C	0.80	0.23	2	2303	40390
			C(T)	FC	20	L-C	0.80	0.23	2	1388	23350
			FWFN(T)	SMN	10	L-R	0.22	1.00	2	1960	109600
33.0	1.0	69.5	C(T)	FC	0	L-T	2.0	1.00	1	1645	35300
			C(T)	FC	20	L-T	2.0	1.00	1	1305	20800
31.0	0.5	43.4	C(T)	FC	0	WCL	2.0	1.0	1	335	8900
			C(T)	FC	20	WCL	2.0	1.0	1	356	8370
			C(T)	SMN	0	WCL	2.0	1.0	1	735	N.D.
			C(T)	SMN	20	WCL	2.0	1.0	1	690	N.D
			C(T)	FC	0	WCL	19.0	1.0	1	1010	7900
			C(T)	FC	20	WCL	19.0	1.0	1	564	2230
			C(T)	FC	0	WCL	6.0	1.1	1	534	10070
			C(T)	FC	20	WCL	6.0	1.1	1	537	6240

Table 3.1.2 (Continued)

Pipe I.D.	Pipe Mat.	Pipe size Dia. in.	Wall in.	Charpy V Notch Spec size	USE, ft-lb	FATT, F	Test Temp., F	Average YS, ksi	Average UTS, k
DP2-F45	A106B	10	0.718	Full	94	78	72	45.1	79.
							300	43.6	94.
							550	40.2	92.
DP2-F13	A106B	16	0.5	Full	73	0	72	48.0	76.
							300 300	47.4	90.
							550 550 550	38.0	88.
DP2-F2	A106B	6	0.864	Full	100	60	77	41.0	74.
							300	36.7	77.
							550 550 550	37.5	82.
DP2-F11	SA333,Gr.6	4	0.337	0.75	97	-38	72	42.2	73.
							300 300		
							550 550	28.7	71.
DP2-F34	A516,Gr.70	37	3.25	Full Full Full Full	106 148(I) 97(M) 106(O)	37 60 53 60	72	38.3	73.
							300	34.7	65.
							550 550 550 550	30.1 33.4(I) 30.5(M) 38.3(O)	73. 70. 73. 71.
							550 550		
DP2-F34W	Pipe-To-Elbow Weld A516, Gr.70	37	3.25	Full Full Full	>150(I) 172(M) 123(O)	-45 -30 0	550 550 550 550	66.6 74.6(I) 73.5(M) 74.8(O)	91. 98. 97. 95.
DP2-F6	SA333,Gr. 6	24	1.531	Full	153	-36	550 550 550 550	30.4	76.

Tensile Properties				Fracture Toughness Data								
si	% Elong.	Gage Length, inches	%, Red of Area	Spec. Type	Notch Type	% Side-grooves	Orientation	W, inches	B, inches	No. of Tests	Ji, ave. in.-lb/in.^2	dJm/da, ave. in.-lb/in.^3
9	28.6	1.0	65.1									
6	17.8	1.0	46.1	C(T)	FC	0	L-C	2.0	0.51	2	1015	17740
9	24.4	1.0	43.1									
6	28.9	1.0	63.2									
3	18.4	1.0	48.2	C(T)	FC	0	L-C	2.0	0.37	1	525	11810
				C(T)	FC	20	L-C	2.0	0.37	1	340	8990
7	26.0	1.0	52.0	C(T)	FC	0	L-C	2.0	0.37	1	950	20000
				C(T)	FC	20	L-C	2.0	0.37	1	790	12100
				FWFN(T)	SMN	10	L-R	0.4	2.5	2	1490	115200
5	44.6	0.5	50.7									
4	26.6	0.5	47.2	C(T)	FC	20	L-C	1.6	0.7	2	585	11700
7	30.1	0.5	48.8	C(T)	FC	0	L-C	2.0	0.6	2	1580	30900
				C(T)	FC	20	L-C	1.6	0.7	2	1030	20600
				FWFN(T)	SMN	10	L-R	0.57	1.8	2	1550	43700
2	33.0	1.0	69.6									
				C(T)	FC	0	L-C	0.8	0.21	1	950	28215
				C(T)	FC	20	L-C	0.8	0.21	1	780	19230
6	30.3	1.0	69.2	C(T)	SMN	0	L-C	0.8	0.27	2	1910	N.D.
				C(T)	FC	20	L-C	0.8	0.27	1	560	26400
5	32.7	1.0	65.8									
1	29.6	1.0	67.7	C(T)	FC	20	L-C	2.0	1.0	2	1705	23950
1	28.4	1.0	63.7	C(T)	FC	20	L-R	2.0	1.0	2	635	13600
3(I)	32.5(I)	2.0	64.4(I)	C(T)	FC	20	L-C	2.0	1.0	2	1055	25900
9(M)	N.D.	2.0	N.D.	FWFN(T)	FC	10	L-R	1.0	3.0	2	1615	76000
7(O)	30.2(O)	2.0	63.7(O)	FWFN(T)	FC	10	L-C	1.0	3.0	2	1275	58100
				C(T)	FC	0	L-C	8.0	2.6	1	480	31600
				C(T)	FC	20	L-C	8.0	2.6	1	1095	22000
1	32.0	0.5	60.2	C(T)	SMN	20	L-C	2.75	1.28	2	2650(I)	33050(I)
0(I)	45.5(I)	0.31	54.0(I)	C(T)	SMN	20	L-C	2.75	1.28	1	975(O)	30330(O)
3(M)	53.4(M)	0.32	58.9(M)	C(T)	FC	0	L-C	8.0	2.6	1	2480	20920
5(O)	45.9(O)	0.32	59.2(O)	C(T)	FC	20	L-C	8.0	2.6	1	2180	18360
1	32.0	2.0	71.9	C(T)	SMN	0	L-C	1.0	0.3	2	1760	135900
				C(T)	SMN	20	L-C	1.0	0.3	2	2190	32310
				C(T)	SMN	0	L-C	2.0	0.6	1	2590	55450
				C(T)	SMN	20	L-C	2.0	0.6	1	1860	42290

can also cause a significant decrease of fracture toughness, although this decrease is not shown in Figure 3.1.2.

Figure 3.1.3 illustrates the occurrence of DSA in quasi-static tensile tests of a low-carbon steel (Ref. 3.1.1). In the absence of DSA, it would be expected that the tensile strength would diminish with increasing test temperature. However, as shown in Figure 3.1.3, with DSA, both the tensile strength and the rate of strain hardening increase with increasing temperature, up to a certain temperature, before starting to diminish. Even at the highest temperature shown, 655 F (346 C), the tensile strength is about the same as at 122 F (50 C). Also evident at certain temperatures within the DSA range in Figure 3.1.3 are serrated load-elongation curves; these, too, are manifestations of DSA.

The temperature range over which DSA occurs depends on the strain rate. Increasing the strain rate moves the temperature range upward; this behavior is illustrated in Figure 3.1.4 for the appearance of serrations on stress-strain curves in a low-carbon steel.

Most of the carbon-steel pipe materials tested in the Degraded Piping Program have behaved in a manner similar to that shown in Figure 3.1.3. They exhibited serrated stress-strain curves at 300 F (149 C) but not at room temperature or at 550 F (288 C), and they exhibited higher strain hardening rates and higher tensile strengths at 300 F (149 C) than at room temperature. Furthermore, in another program, tensile tests at 550 F (288 C) on one of the Degraded Piping Program steels at a strain rate of about 1 s^{-1} revealed serrated stress-strain curves that were not observed at a strain rate of 4×10^{-4} s^{-1}. Thus, it can be concluded that most carbon steel pipes used in U.S. nuclear plants are susceptible to DSA.

None of the above observations about DSA is, in itself, of concern relative to the performance of nuclear piping. In fact, the observation that the tensile strength at 550 F (288 C) is similar to that at room temperature because of DSA could be considered a positive aspect of DSA. Nonetheless, concerns do exist about DSA lowering the steel's fracture resistance. Work reported by Miglin, et al. (Ref. 3.1.2) suggests that this is, indeed, the case. Those investigators found that J_{Ic} values reached a minimum value at about 400 F (205 C) in two heats of A106 C carbon steel, both of which were susceptible to DSA. Additionally, in two other heats of carbon steel, both A515 Grade 70, only one of which was susceptible to DSA, the susceptible heat exhibited a more pronounced decrease in the slope of the J-R curve (proportional to the tearing modulus, T) with increasing temperature than did the nonsusceptible heat.

Perhaps an even greater source of concern related to DSA is the observation that many of the carbon steel pipe materials in the Degraded Piping Program exhibited a series of unstable fractures at 550 F (288 C). Both compact-specimen tests and full-scale pipe tests displayed this behavior. An example for a compact specimen is shown in Figure 3.1.5. The net result of the rapid crack jumps was a lowering of the load-displacement curve and a reduction in the slope of the J-R curve. The possibility that DSA was responsible for the

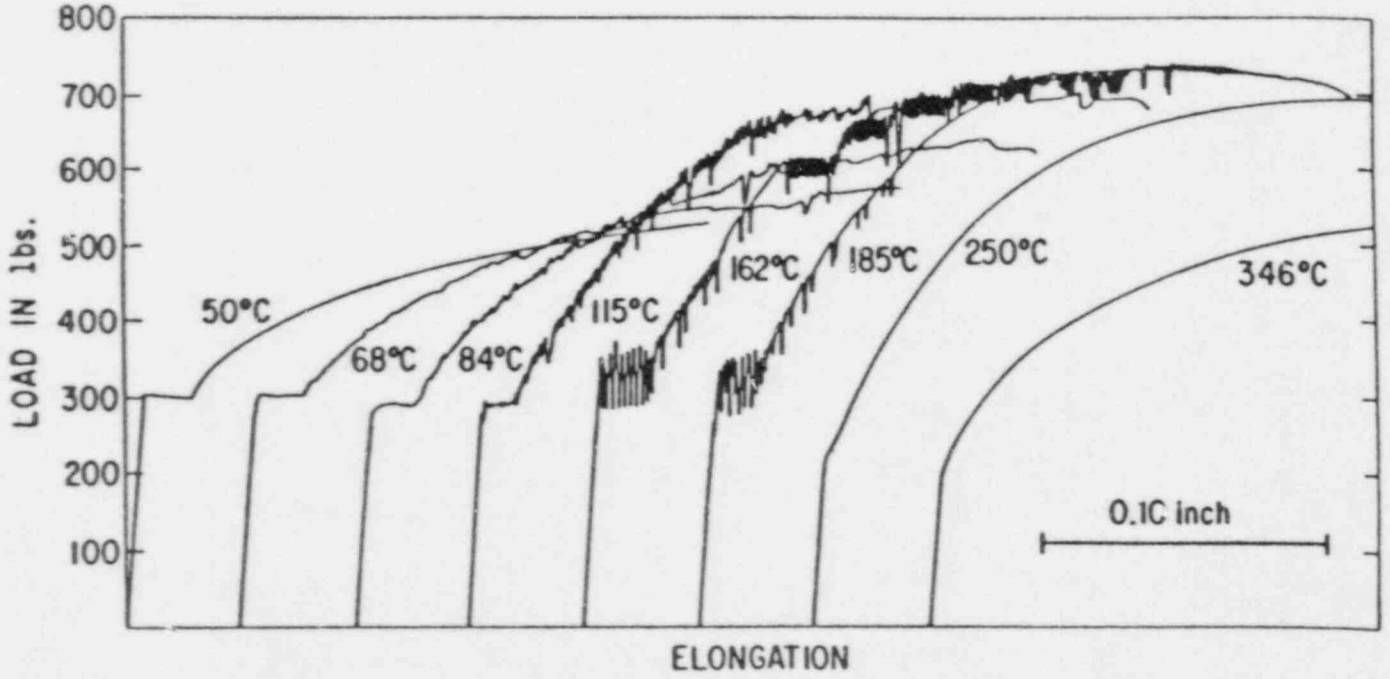

Figure 3.1.3 Load-elongation curves of a 0.35 percent C steel strained in tension at crosshead speed of 0.0025 in/min (cross section area ~ 0.014 in^2, gage length = 1.00 in). (Ref. 3.1.4, Keh et al., 1968, copyright McGraw-Hill Book Company, used by permission.)

SA-6/86-F3.1.11

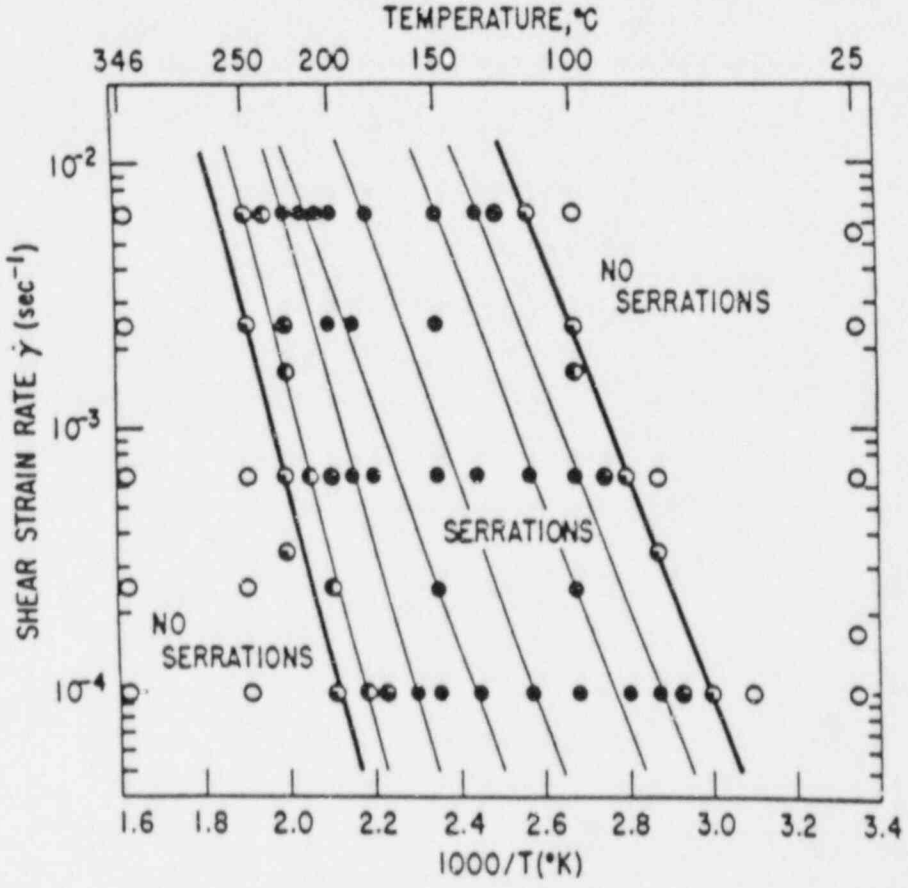

Figure 3.1.4 Dependence of stress-strain curve serrations on temperature and strain rate for 0.03 percent carbon steel, quenched from 480 F (250 C). (Ref. 3.1.1, Keh et al., 1968, copyright McGraw-Hill Book Company, used by permission.)

SA-6/86-F3.1.12

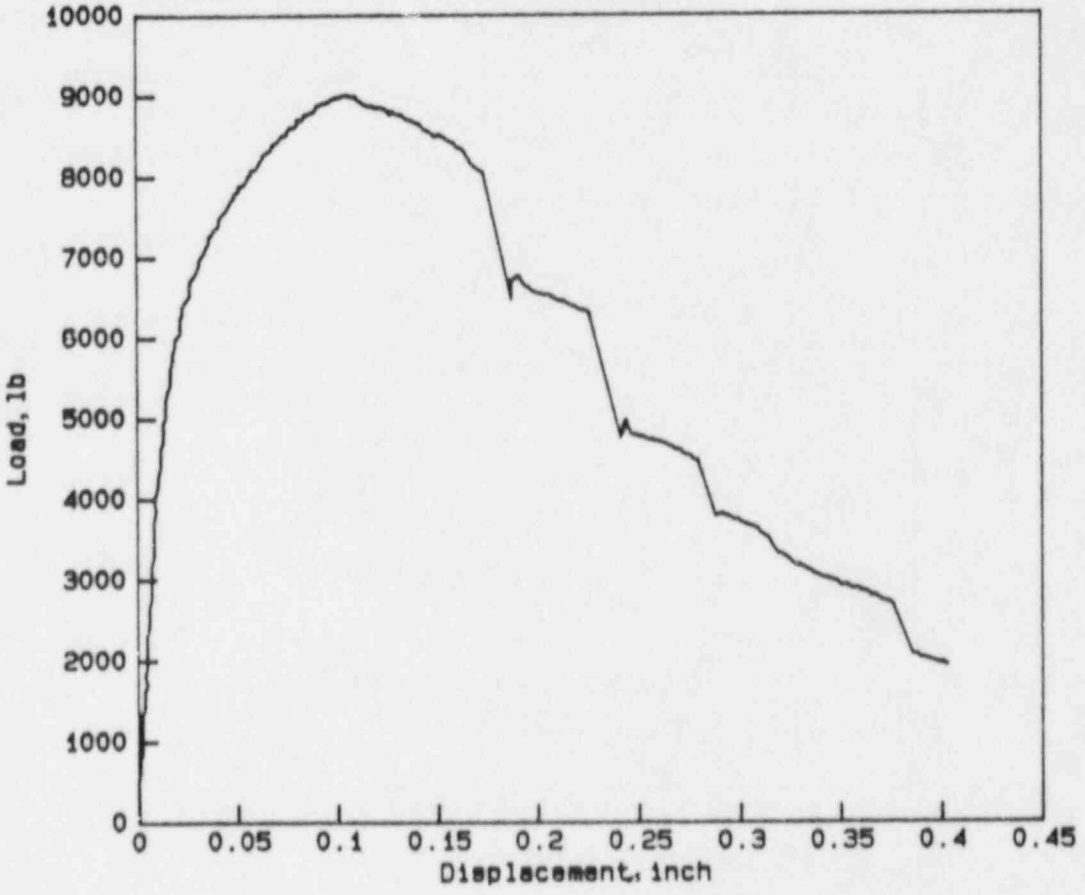

Figure 3.1.5 Load-displacement record for a carbon steel compact specimen that displayed several bursts of unstable crack growth at 550 F (288 C).

SA-6/86-F3.1.9

crack growth instabilities was considered in Reference 3.1.3. However, at least one puzzling aspect remains; compact specimen tests at 300 F (149 C) did not display crack growth instabilities, even though that temperature is in the range of DSA. An attempt was made in Reference 3.1.3 to rationalize this behavior in terms of crack-tip strain rate. Since the effective crack-tip strain rate is likely several orders of magnitude greater than the average bulk strain rate, the material at the growing crack tip may not be experiencing DSA at 300 F (149 C).

A question that remains unanswered is the effect of high strain rates, such as might be associated with a seismic event, on crack-growth instabilities and fracture toughness at 550 F (288 C).

3.1.4 Anisotropy Effects in Carbon Steel Pipes

An unexpected observation in the Degraded Piping Program was the growth of cracks at an angle to the intended growth direction in carbon steel pipes. This behavior was observed both in a pipe containing through-wall circumferential flaws and in compact specimens machined from the pipe in the same (L-C) orientation. For each specimen, it was observed that the crack grew at an angle of approximately 60 degrees to the circumferential direction (30 degrees to the pipe axis). This angle varies for other pipes. In an attempt to learn more about this unexpected result, one of the carbon steel pipes that displayed this behavior was subjected to metallographic examination and to additional compact specimen testing.

Metallographic Examination

The pipe investigated was identified as DP2-F11. Its diameter was 4 inches (102 mm) and its wall thickness was 0.34 in (8.6 mm). It was purchased to ASTM Specification A333, Grade 6, which permits the pipe to be either seam welded or seamless. To determine which type it was, a cross section normal to the pipe axis (i.e., in the r-θ plane, using cylindrical-coordinate terminology, Figure 3.1.6) was metallographically polished and etched and examined under a microscope at magnifications of 7X to 100X. Inasmuch as no evidence of a seam weld was found, it was concluded that the pipe was seamless.

Two other metallographic sections were then prepared, one in the r-z plane and the other in the z-θ plane (Figure 3.1.6). Both sections were examined first in the as-polished condition to reveal the shape and distribution of nonmetallic inclusions prior to etching, to reveal the microstructure.

As was expected, the inclusions viewed on the r-z plane were flattened and elongated in the z direction. After etching, the microstructure seen on that plane was a banded structure made up of both ferrite and pearlite. The banding was pronounced from the inside diameter of the pipe to well beyond midwall, but gave way to an essentially equi-axed structure near the outside diameter.

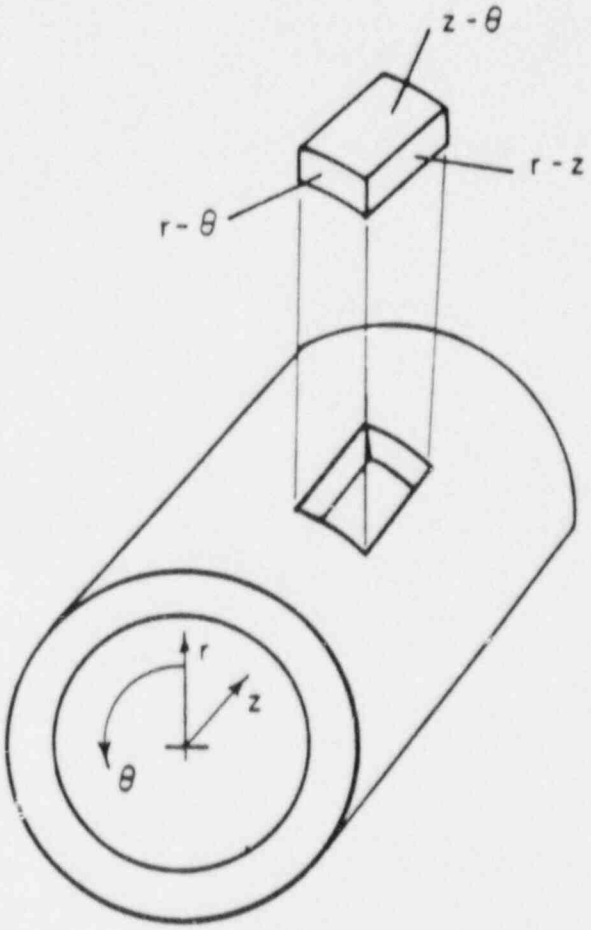

Figure 3.1.6 Schematic illustration showing cross sections of pipe DP2-F11 that were examined metallographically.

M-11/85-FA1

The most interesting finding was associated with the z-θ plane. On that plane, the inclusions were found to be elongated and clustered, not in the expected z-direction, but at an angle of approximately 20 to 30 degrees to the z direction (see Figure 3.1.7). Since it is the nonmetallic inclusions that are largely responsible for orientation effects in steel products, the above observation may help to explain the tendency of the cracks to grow away from the r-θ plane both in pipe fracture experiments and in compact-specimen tests. The source of the inclusion orientation at an angle to the z direction stems from the process used to produce seamless pipe; apparently it is not uncommon for seamless pipe to develop a twist during the hot forming as it is being manufactured[1]. Except for the inclusion shape and orientation, there is little physical evidence of such a helical deformation from the hot forming process. The findings of the metallographic study indicate that Pipe DP2-F11 was twisted during forming.

Testing of Compact Specimens

Four additional compact specimens of 0.4T planform-size and about 0.27 inch (6.9 mm) thick were machined from pipe DP2-F11 to study possible orientation effects. Two were oriented with the notch plane parallel with the pipe axis (i.e., the notch plane was the r-z plane) and two with the notch plane at 30 degrees to the pipe axis. As was the case for the specimens tested earlier that had their notch planes parallel with the circumferential direction (the r-θ plane), each contained a sharp machined notch of radius 0.005 inch (0.125 mm) and each was tested at 550 F (288 C).

The results confirmed that a definite orientation effect exists in pipe DP2-F11. As is shown in Figure 3.1.8, regardless of the initial orientation of the notch plane in the compact specimens, the crack tended to grow on a plane oriented about 20 to 30 degrees from the pipe axis, corresponding with the inclusion orientation revealed metallographically. The existence of an orientation effect is indicated also by values of J at crack initiation, J_i. As is shown in Table 3.1.3, notches oriented in the circumferential direction produced J_i values several times those for the other two orientations investigated.

Discussion

The results of this limited study indicate that the particular seamless pipe examined underwent some twisting as it was being manufactured. This resulted in the nonmetallic inclusions being oriented at an angle of 20 to 30 degrees to the pipe axis. The resistance to fracture was found to be significantly lower in the direction of inclusion orientation than in the circumferential direction.

---

[1] D. N. Williams, Battelle, private communication.

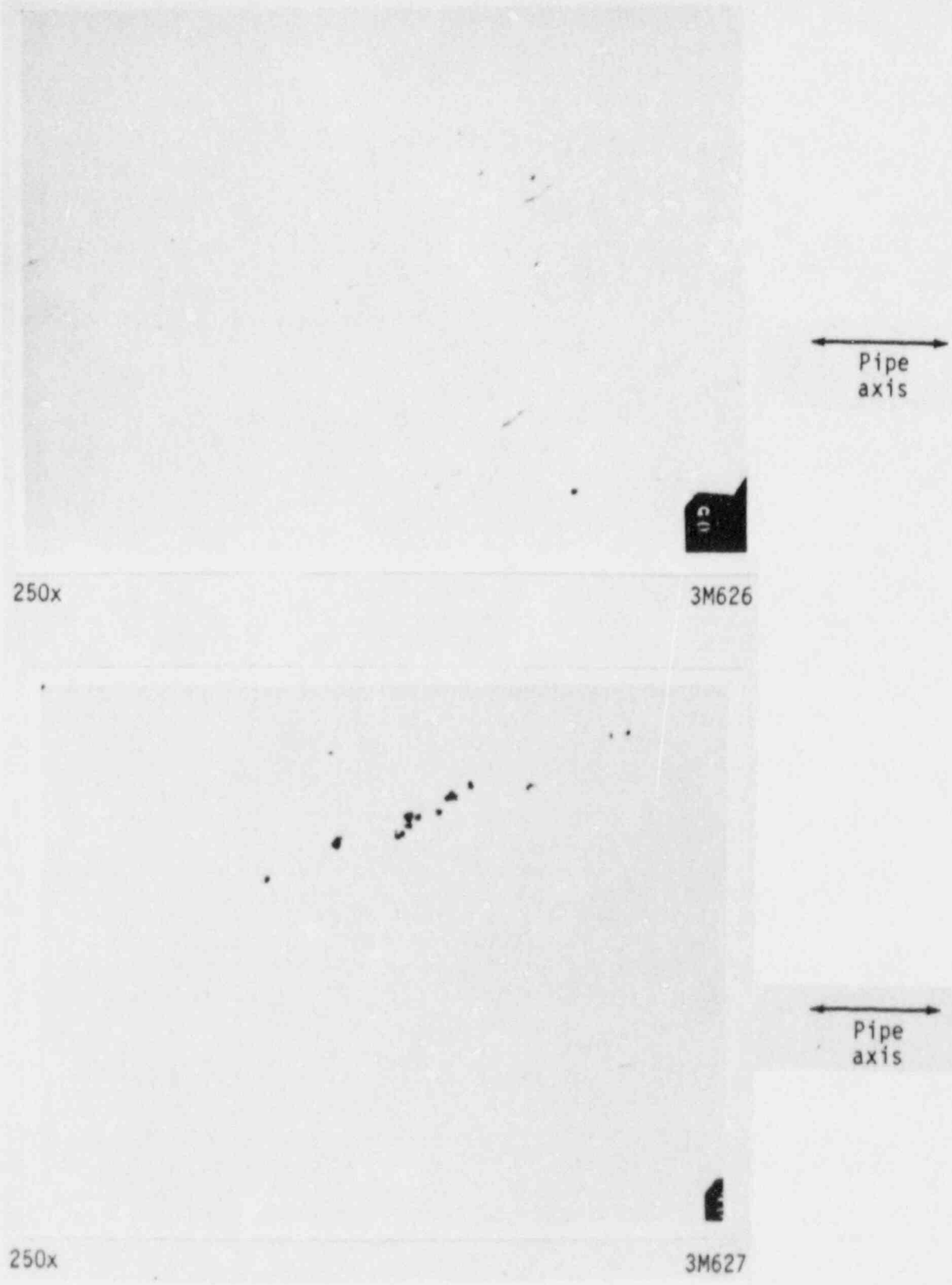

Figure 3.1.7 Photomicrographs of nonmetallic inclusions in Pipe DP2-F11 as viewed on the z-y plane (refer to Figure 3.1.6).

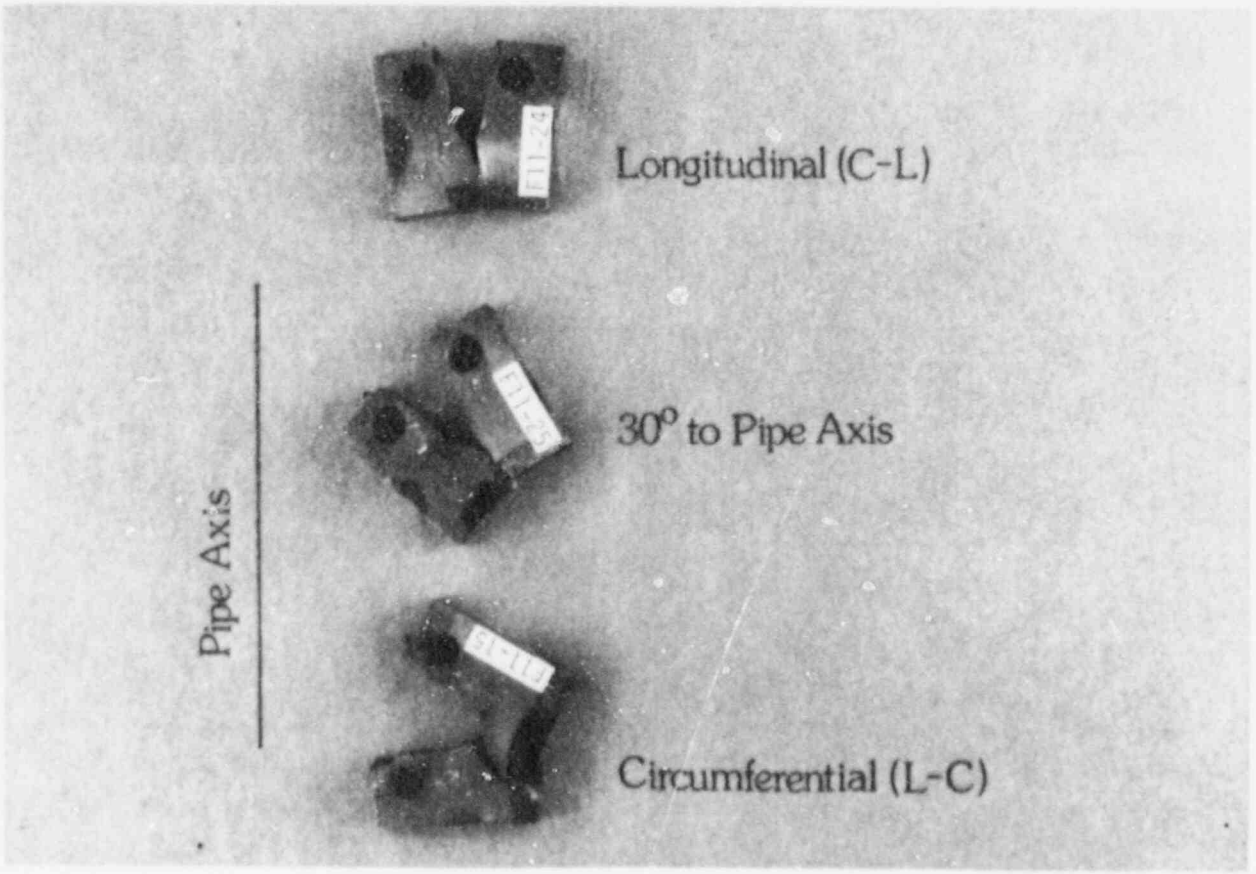

1615-12

Figure 3.1.8 Photograph of tested compact specimens to illustrate tendency of crack to grow along a plane oriented at 30 degrees to the pipe axis.

M-11/85-FA3

Table 3.1.3. Effect of specimen orientation on J_i values for pipe DP2-F11.

Specimen Ident. Number	Notch Orientation	J_i(a) in-lb/in^2	kJ/m^2
F11-17	Circumferential	1680	(294)
F11-18	Circumferential	2140	(375)
F11-23	Longitudinal	408	(71)
F11-24	Longitudinal	461	(81)
F11-25	30 degree to pipe axis	430	(75)
F11-26	30 degree to pipe axis	599	(105)

Material: SA333, Gr. 6 pipe; 4-inch (100-mm) diameter, Schedule 80

Specimen Type: 0.4T planform-size compact, thickness 0.27 inch (6.9 mm)

Test Temperature: 550 F (288 C)

(a) At onset of crack growth, as determined from point of deviation from a straight line in a graph of d-c E.P. versus displacement.

The lower fracture resistance at 20 to 30 degrees from the pipe axis may be the explanation for the crack turning away from the circumferential direction. The opportunity for turning arises early in the test when a plastic hinge, associated with the formation of shear lips, forms at the notch tip; the crack initially follows the boundary of the hinge at an angle of about 45 degrees from the intended plane of fracture. Once growing at a large angle to the intended plane, the crack may continue growing with relative ease along the plane of low toughness.

One troublesome observation is that, on occasion, the two crack tips in the through-wall cracked pipe do not grow in the same direction. Figure 3.1.9 is a schematic illustration of crack growth in a pipe. The lower sketch shows clearly that only the crack on the right end of the starting flaw is following the direction of the nonmetallic inclusions; the other crack is growing at a sizable angle to the inclusion direction. Thus, the inclusions oriented at 20 to 30 degrees to the pipe axis in Pipe DP2-F11 may actually have had nothing to do with the crack turning from the circumferential direction. Perhaps the crack would have turned even without oriented inclusions.

Another possible explanation for the crack turning may be the relationship between double-shear and single-shear fracture. As was noted above, a plastic hinge forms at the notch tip in the early stages of shear lip development. Crack growth at the specimen surface initially follows the hinge boundary, both above and below the notch, as shown schematically in Figure 3.1.10. Eventually either crack direction A or direction B predominates on each surface. If the same crack growth direction is established on both the front and back surfaces, a double-shear crack will form and will grow at a large angle to the original notch (Figure 3.1.11a). If opposite crack growth directions are established on the two surfaces, a single shear crack will form and the crack will grow in the same direction as the original notch, though the plane of fracture will be tilted (Figure 3.1.11b). In compact specimens, the likelihood of double shear appears to be about the same as that for single shear. However, in pipe tests, some as-yet-unknown factor may strongly favor the occurrence of double shear fracture and, hence, cracks that turn from the circumferential direction.

Additional study will be required to establish a more certain explanation for crack turning.

3.1.5 Future Material Characterization Efforts

Material characterization efforts are essentially completed within this program. Of the new pipe fracture experiments planned within this program, only the centrifugally cast stainless steel pipe data need to be generated. These efforts are being coordinated with Argonne National Laboratories and Framatome. Consequently the efforts at Battelle will involve assembling the data from the different organizations.

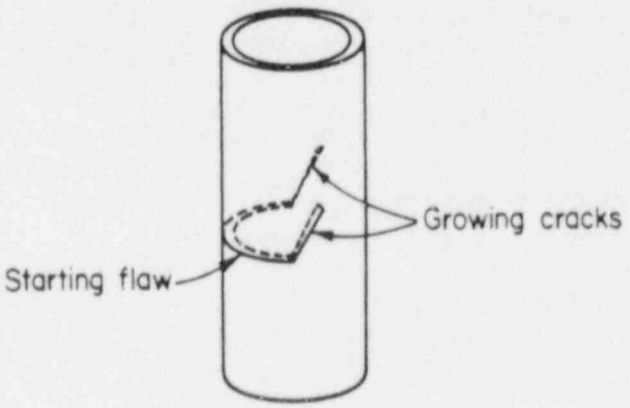

a. After Testing

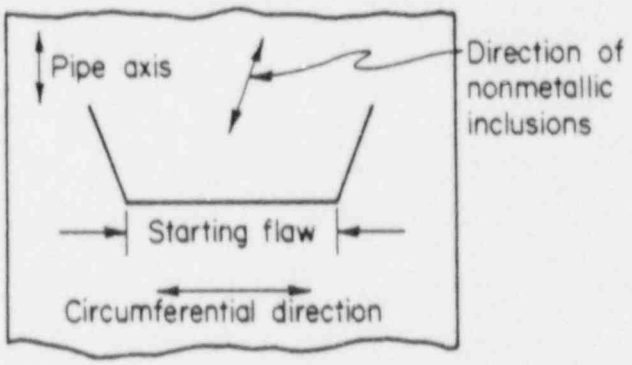

b. After Cutting and Flattening

Figure 3.1.9 Schematic illustration of crack growth in carbon steel pipe.

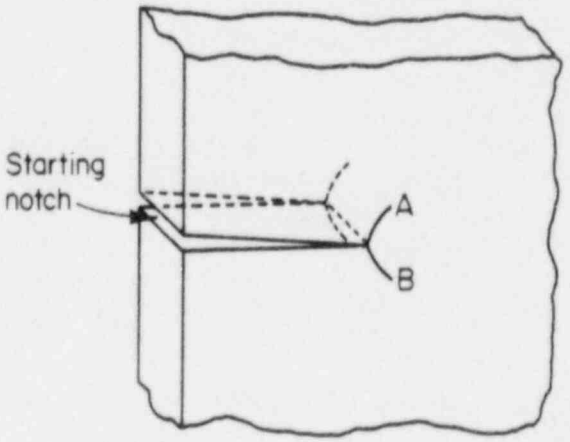

SA-12/87-F3.1.10

Figure 3.1.10 Surface crack formation in specimens that develop shear lips.

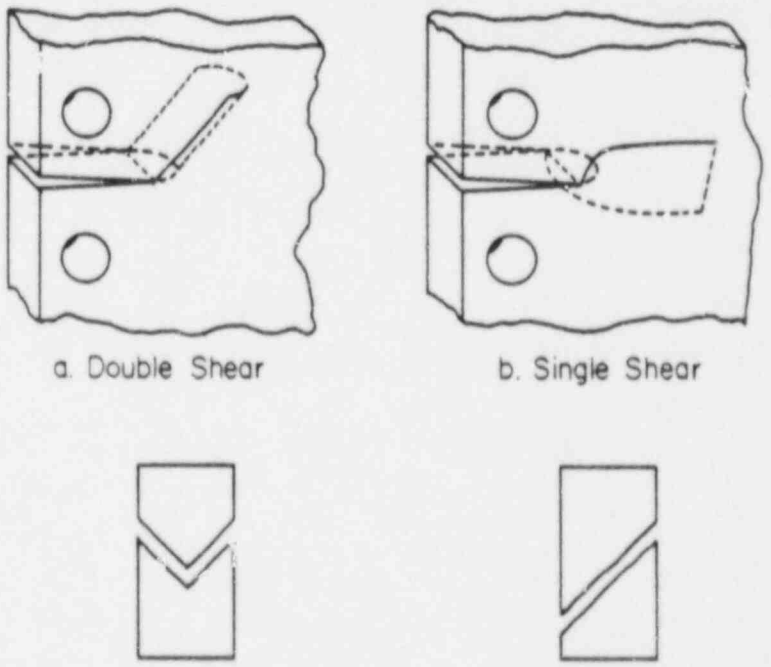

SA-12/87-F3.1.11

Figure 3.1.11 Double shear versus single shear fractures observed in carbon steel compact specimens.

References for Section 3.1

3.1.1 Keh, A. S., Nakada, Y., and Leslie, W. C., "Dynamic Strain Aging in Iron and Steel", in A. R. Rosenfield and others (eds.), Dislocation Dynamics, McGraw-Hill Book Co., New York, 1968, pp. 381-408.

3.1.2 Miglin, M. T., and others, "Effects of Strain Aging in the Unloading Compliance J-Test", in E. T. Wessel and F. J. Loss (eds.), Elastic-Plastic Fracture Test Methods, The User's Experience, ASTM STP 856, American Society for Testing and Materials, pp. 150-165.

3.1.3 Wilkowski, G. M., and others, "Degraded Piping Program - Phase II", Semiannual Report, October 1985-March 1986, NUREG/CR-4082, Vol. 4, September 1986.

3.2 Progress on the Effect of Laboratory Specimen Geometry on J-R Curves

(C. Marschall, M. Landow, V. Papaspyropoulos, J. Ahmad, N. Ghadiali, and G. Wilkowski)

An important feature of the Degraded Piping Program is the characterization of each pipe using laboratory specimens machined from the pipes. For fracture toughness specimens, latitude exists in choosing the type of specimen and its dimensions. For example, to model a circumferential through-wall crack in a pipe test, either a compact specimen or a three-point-bend specimen (L-C orientation) could be selected. A circumferential surface crack, on the other hand, might be modeled with an FWFN(T) specimen (L-R orientation) or, if the pipe diameter and wall thickness are large, with a compact or bend specimen (L-R orientation).

Whichever specimen is selected, its maximum dimensions will be dictated by the pipe dimensions. Within that restriction, however, it is possible to choose a relatively thick, narrow specimen or a wide, thin specimen. The effort described here was undertaken to determine possible effects of specimen size and geometry on J-R curves in both ferritic and austenitic steels.

The following efforts were conducted toward this objective:

- Development of test techniques for the FWFN(T) specimen
- Evaluation of compact (tension) [C(T)], bend bar, and FWFN(T) specimens of different sizes
- Evaluation of C(T) and FWFN(T) specimens from a heavy-wall, cold-leg, carbon steel pipe
- Transfer of data to the David Taylor Research Center (DTRC) for an investigation of specimen size effects on J_D- and J_M-R curves.

A related topic involved the evaluation of different size C(T) specimens that have the same thickness. These nonstandard thickness C(T) specimens are referred to as planform C(T) specimens. Significant efforts were undertaken in these evaluations; consequently they are described separately in Section 3.3.

3.2.1 Development of the FWFN(T) Test

Laboratory specimen tests to characterize the fracture resistance of pipes are designed to simulate as closely as possible the conditions existing in pipe fracture tests. Pipe test conditions that are maintained in laboratory tests include

- Notch tip radius
- Notch orientation and crack growth direction

- Thickness (specimen thickness is at least 80 percent of pipe-wall thickness)

  Temperature

- Rate of loading and load history.

With respect to notch orientation and crack growth direction, either a compact specimen or a 3-point bend specimen would be selected to model a through-wall circumferential crack in a pipe test (see Figure 3.1.1). However, if the same two types of specimen were used to model a circumferential surface crack, the specimens would, of necessity, be quite small, except in the case of large diameter pipes with very thick walls. In an attempt to model the conditions existing in a circumferential-surface-crack pipe test more closely, Battelle devised a specimen called the FWFN(T) specimen. It is shown schematically in Figure 3.1.1.

The principal advantages of the FWFN(T) specimen are that the crack plane and direction of growth are the same as in a surface-cracked pipe and that both the pipe and FWFN(T) specimen experience tensile stresses throughout the uncracked ligament. In addition, the FWFN(T) specimen has a relatively long crack front and relatively high constraint against strain in the circumferential direction.

The usefulness of the FWFN(T) specimen to model the behavior of a surface-cracked pipe has not yet been firmly established. The principal question pertains to the validity of calculating J for a test in which the grips are not free to rotate and in which the entire relatively short ligament may undergo yielding prior to crack initiation. Finite element modeling of the FWFN(T) specimen has been conducted during the current reporting period to shed further light on the usefulness of this test. These analytical efforts are described in Section 3.2.5.

3.2.2 Summary of Specimen Size Effect and Geometry Effect Study

The effort described here was undertaken to determine possible effects of specimen size and geometry on J-R curves in both a ferritic and an austenitic steel.

The test matrix is described in Reference 3.2.1. Briefly, the approach was to fabricate and test compact, bend, and FWFN(T) specimens in a range of sizes, with and without side-grooves, from one ferritic pipe and one austenitic pipe. Both were relatively large pipes, permitting a wide range of specimen sizes. The ferritic pipe was 24-inch (610-mm) diameter SA-333 Grade 6 carbon steel having a wall thickness of 1.53 inches (38.9 mm). The austenitic pipe was 16-inch (406-mm) diameter SA-358 Type 304 stainless steel having a wall thickness of 1.03 inches (26.2 mm). The range of specimen sizes investigated included those that could be machined from small-diameter, thin-walled pipe to those from large-diameter, thick-walled pipe.

An additional set of experiments to investigate specimen geometry and specimen orientation effects was conducted on a very large-diameter [37 inches (940 mm)], thick-walled [3.25 inches (83 mm)] ferritic steel pipe from a cold-leg pipe loop. The pipe wall was sufficiently thick so that both compact and FWFN(T) specimens could be machined in two different orientations, L-C and L-R. Results of those experiments are presented in Section 3.2.3.

Specimen testing to study the size and geometry effects on J-R curves was completed during the previous reporting period. During the current reporting period, progress was limited to reduction of data for most of the tests which had not been analyzed earlier. Data reduction for FWFN(T) tests is awaiting the completion of J-calculation procedures (see Section 3.2.5). Detailed analysis of all the size- and geometry-effect studies also remains to be completed.

Test analysis results to date were described in the Third and Fourth Semiannual Reports (Refs. 3.2.2 and 3.2.1, respectively). Briefly, they indicate the following:

1. When preliminary J-calculation procedures were employed, FWFN(T) specimens displayed greater J_i values than did compact specimens of the same material; however, some of this difference may disappear when an improved method is used to calculate J_i, as is discussed in Section 3.2.5.

2. FWFN(T) specimens tended to exhibit J_i values that increased with increasing specimen width in the ferritic steel but not in the austenitic steel; the ratio of thickness to ligament length, which might be viewed as a constraint factor, did not appear to have a strong effect on J_i.

3. No strong effect on J_i of compact specimen size or of side-grooving was found; however, any effects of those variables were masked by large data scatter associated with experimental uncertainty in defining the actual point of crack initiation. Data obtained in other tasks indicated that side grooving tends to lower J_i and increasing specimen size tends to increase J_i.

During the final reporting period all test data for compact, bend, and FWFN(T) specimens will be reduced, and the effects of specimen geometry and specimen size on J-resistance curves will be assessed.

3.2.3 Study of Size, Geometry, and Orientation Effects in Cold-Leg Pipe

In the Fourth Semiannual Report (Ref. 3.2.1), experiments to measure the fracture toughness of a large diameter, thick-walled, cold-leg pipe were described. The pipe, identified as DP2-F34, was an A516, Grade 70 carbon steel having a diameter of about 37 inches (940 mm) and a wall thickness of about 3.25 inches (83 mm).

The large thickness of the pipe permitted both 1T compact specimens and FWFN(T) specimens to be machined in two different orientations, L-C and L-R. Specimens having the L-C orientation were machined such that the midthickness plane coincided approximately with the midwall position in the pipe and the crack would extend circumferentially. Specimens having the L-R orientation were machined so that the initial crack tip was located at the midwall position and the crack would extend radially from the inside to the outside of the pipe.

As was noted in Reference 3.2.1, duplicate tensile specimens machined from the pipe and tested at 550 F (288 C) showed a sizable variability in yield strength: 26.7 and 33.4 ksi (184 and 230 MPa). That result suggests a nonhomogeneous structure in the thick-walled pipe.

The results of the fracture toughness tests on 1T compact specimens reported in Reference 3.2.1 showed clearly that the L-C orientation was more resistant to stable crack growth than was the L-R orientation. J_i values for the L-C orientation were about 65 percent greater than the L-R orientations. The dJ_M/da values were about 100 percent greater for the L-C orientation. In sharp contrast to the compact specimen results were the results for the FWFN(T) specimens. Not only was the orientation effect much less pronounced, it was the opposite of that observed in the C(T) specimens. Both J_i and dJ_M/da for the L-C orientation were, on average, 20 to 25 percent less than those for the L-R orientation. No satisfactory explanation is yet available for the different orientation effects observed for the two specimen types.

During the current reporting period, additional testing of the cold-leg pipe has been conducted at MEA. MEA fabricated 4T planform-size compact specimens of 2.6 inch (66 mm) thickness, having the L-C orientation, from both base metal and a circumferential weld. Results of J-R curve tests at 550 F (288 C) are presented in Table 3.2.1, along with results obtained at Battelle for 1T and 1-3/8T specimens of the same orientation.

The results for base metal tests in Table 3.2.1 show excellent agreement between the 20-percent side grooved 4T planform-size specimen and the 20-percent side grooved 1T specimens. The J_i value for the zero-percent side grooved 4T specimen was unexpectedly lower than for the other specimens. That result probably reflects experimental uncertainty from unloading compliance results early in the J-R curve.

For the circumferential weld metal tests, the 1-3/8T planform-size specimens showed an effect of location within the weld on J_i. Specimens that were machined from near the root of the weld (near the pipe I.D.) had a higher J_i value than did a specimen machined from near the weld crown (near the pipe O.D.). That result makes comparisons between the 1-3/8T and the 4T specimens difficult, because the larger specimen sampled both regions of the weld. Nonetheless, J_i values from side grooved 1-3/8T and 4T planform-size specimens agree reasonably well when the smaller specimen results are from near the bottom of the weld, even though different notch types were used

Table 3.2.1. Comparison of J results from compact specimens of different sizes machined from a large diameter, thick-walled cold-leg pipe, DP2-F34.
Pipe Material: A516 Grade 70 Carbon Steel
Specimen Orientation: L-C
Test Temperature: 550 F (288 C)

Specimen Identification Number	Location	Specimen Dimensions, inches (mm) W	Specimen Dimensions, inches (mm) B	Percent Side Grooves	Notch Type(a)	J at Initiation, in-lb/in^2 (kJ/m^2)	dJ_M/da, in-lb/in^3 (MJ/m^3)
F34-19	Base Metal	2.0 (50.8)	1.0 (25.4)	20	FC	1020 (179)	26,300 (181)
F34-20	Base Metal	2.0 (50.8)	1.0 (25.4)	20	FC	1090 (191)	25,500 (176)
F34-B1(b)	Base Metal	8.0 (203)	2.6 (66)	20	FC	1095 (192)	22,000 (152)
F34-B2(b)	Base Metal	8.0 (203)	2.6 (66)	0	FC	480 (84)	31,600 (218)
F34W-31(c)	Circular Weld	2.75 (69.9)	1.28 (32)	20	SMN	975 (170)	30,300 (209)
F34W-30(d)	Circular Weld	2.75 (69.9)	1.28 (32)	20	SMN	2125 (370)	38,400 (265)
F34W-32(d)	Circular Weld	2.75 (69.9)	1.28 (32)	20	SMN	3180 (560)	27,700 (191)
F34-W1(b)	Circular Weld	8.0 (203)	2.6 (66)	20	FC	2180 (382)	18,360 (127)
F34-W2(b)	Circular Weld	8.0 (203)	2.6 (66)	0	FC	2485 (435)	20,920 (144)

(a) FC = fatigue crack.
SMN = sharp machined notch.
(b) Specimens were fabricated and tested at Materials Engineering Association.
(c) Specimen was machined from top part of weld.
(d) Specimen was machined from bottom part of weld.

3.2.4 Transfer of Data to DTRC for J_M Versus J_D Study

As part of its work for the NRC, the DTRC is conducting a study of the relative merits of J_D and J_M as parameters for characterizing the ductile crack growth resistance of reactor materials. To aid DTRC in its study, Battelle has provided data from eight series of experiments conducted in the Degraded Piping Program. Each series included test results for three different planform-size compact specimens tested at 550 F (288 C). Table 3.2.2 is a summary of the eight series of tests.

3.2.5 J-Resistance Curves Using FWFN(T) Specimens

For surface crack growth predictions, the material's J-resistance (J-R) curve, corresponding to the radial crack growth direction, is the most appropriate resistance curve to use. FWFN(T) specimens are being used to obtain data which can be analyzed to establish such J-R curves. The specimens are machined from pipes. A schematic illustration of the specimen and grips is shown in Figure 3.2.1. This specimen design was selected to simulate the extension of a crack through the pipe wall in a surface-cracked pipe. The specimen orientation is L-R. The dimension in which the crack is to extend is the maximum achievable from the nominal wall thickness of the pipe. Side-grooves of 5 percent depth per side and having a root radius of about 1/16 inch (1.5 mm) are introduced to minimize crack tunneling. A sharp notch is machined at midlength using an electric-discharge machining (EDM) process and an 0.008-inch (0.20-mm) diameter wire electrode to produce a notch-tip radius of about 0.005-inch (0.13-mm). The notch mouth is located on the inside-diameter surface of the specimen to simulate an internal surface crack in the pipe. Typically, the initial notch depth is such that a/W is approximately 0.5.

The specimens are tested at a displacement rate that is designed to cause crack initiation in about 5 to 20 minutes, similar to that required for crack initiation in Battelle's pipe-fracture tests. The data obtained are load, load-line displacement measured on one side of the specimen, direct-current electric potential (U), and two measures of crack-opening displacement obtained from a dual clip-gage located at the front edge of the specimen, as illustrated in Figure 3.2.1. Crack growth initiation is estimated from the direct-current electric potential data. To accomplish this, graphs of U versus LLD, U versus P, and U versus COD are examined for points of slope change prior to maximum load. Engineering judgment is applied to estimate U_o, the value of U at crack initiation. Crack growth beyond initiation is estimated from the ratio U/U_o using the Johnson expression (Ref. 3.2.3). The expression has been shown in calibration studies at Battelle to provide reasonable estimates of crack extension in FWFN(T) specimens in the absence of plastic deformation.

To calculate J as a function of crack-extension (Δa) using the experimental load, load-line displacement, and crack-extension data, an expression for J

Table 3.2.2. Compact specimen test data provided to DTRC for its J_M versus J_D study. All tests were at 550 F (288 C)

Material	C(T) Specimen Sizes	Thickness, inch	Sidegrooved	FEM Analysis	References
304 Stainless Base	1T, 3T, 10T	1.0	No	1T, 3T, 10T	• NUREG/CR-4575 Sections 2-4 • NUREG/CR-4573 • NUREG/CR-4082 Vol. 4, Sect. 3.1.3
304 Stainless Base	1T, 3T, 10T	1.0	Yes	----	• NUREG/CR-4575 Sections 2 and 3
A516 Gr 70 Base	1T, 3T, 10T	1.0	Yes	----	• NUREG/CR-4575 Sections 2 and 3
A516 Gr 70 Base	1T, 3T, 10T[a]	1.0	No	----	• NUREG/CR-4575
304 Stainless Steel TIG	0.5T, 1.5T, 3T	0.38	No	0.5T, 3T	• NUREG/CR-4806 Sections 4 and 5
304 Stainless Base	0.5T, 1.5T, 3T	0.38	No	3T	• NUREG/CR-4806 Sections 4 and 5
304SS-SAW	1T, 3T, 9.5T	1.0	No	1T, 9.5T	• NUREG/CR-4082 Volume 4, Sect. 3.3 • NUREG/CR-4878 Section 3.0
Carbon Steel SAW	1T, 3T, 9.5T	1.0	Yes	---	• NUREG/CR-4082 Volume 4, Sect. 3.3

(a) Only J_i values for 3T and 10T exist since crack turned 90 degrees.

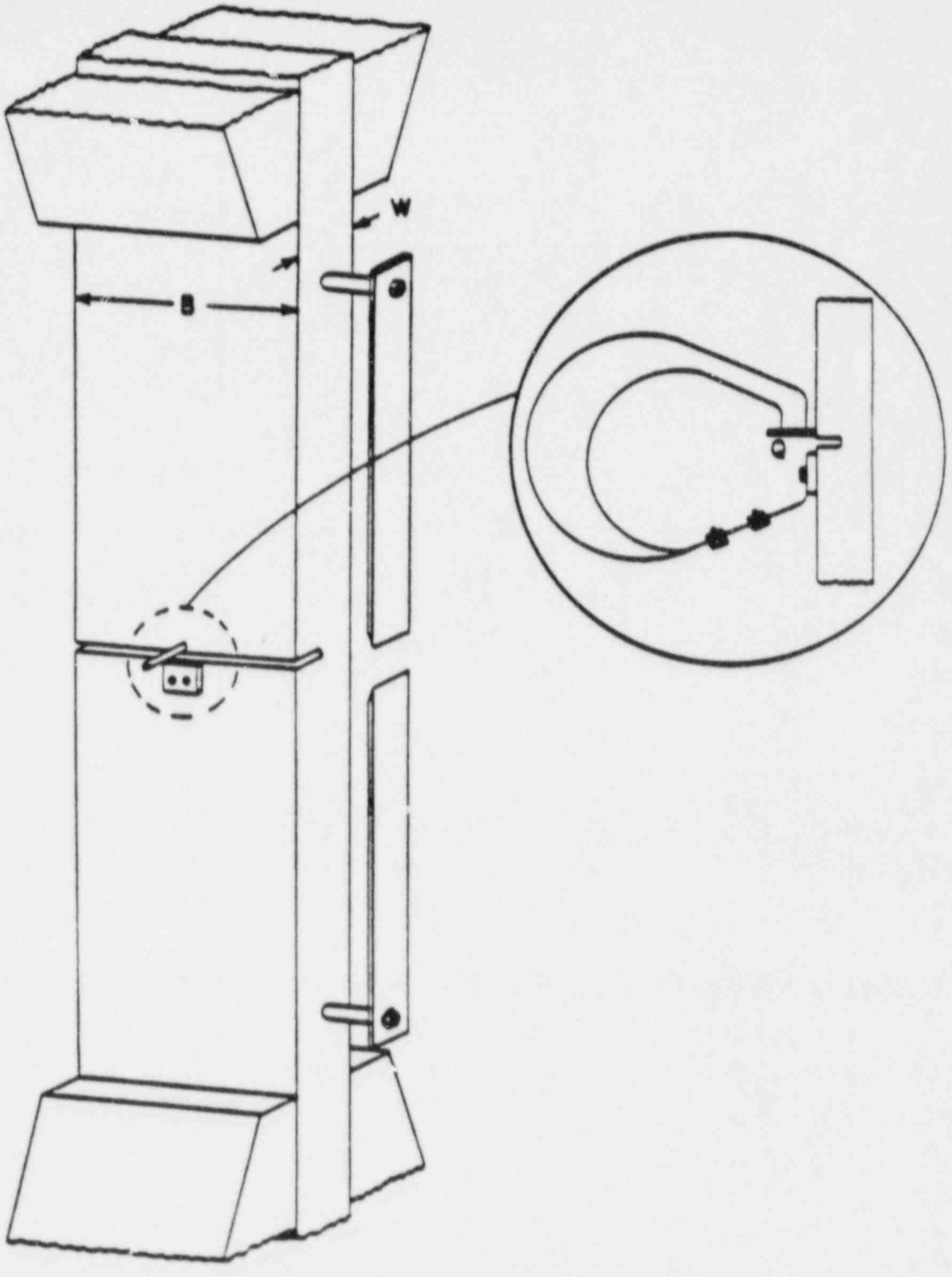

Figure 3.2.1 Schematic illustration of FWFN(T) specimens showing wedge grips and attachments for measurement of displacements.

has been developed assuming a fixed-grip boundary condition across the sections containing the load-line displacement gages. With reference to Figure 3.2.2, showing the specimen dimensions and the uniform remote displacement boundary conditions, Eqs. 3.2.1 to 3.2.22 were used in calculating J.

$$J = J_e + J_p \tag{3.2.1}$$

where J_e is elastic component of J and J_p is the plastic component of J.

The key to obtaining estimates of both the elastic and the plastic components of J is the normal stress distribution across the edge of the specimen, which is assumed to have uniform normal displacement. This stress distribution was obtained by using the elastic relation between compliance and J (see Ref. 3.2.4) together with the fixed grip boundary condition. Details of this derivation are to appear in a forthcoming NUREG Report on the assessment of FWFN(T) specimen. The derivation gives

$$\frac{J_e E' W}{P^2} = \pi \left(\frac{a}{W}\right) (f_1 - 6\, \xi_4\, f_2)^2 \tag{3.2.2}$$

where

$E' = E$ for plane stress

$= E/(1-\nu^2)$ for plane strain

E = Young's modulus

ν = Poisson's ratio

P = load/thickness

$$J_p = \frac{\eta}{b} \int_0^{\Delta_p^c} P \, d\Delta_p^c \tag{3.2.3}$$

where

Δ_p^c = plastic component of displacement due to the crack; that is,

$$\Delta_p^c = \Delta - \Delta_e - \Delta_p^{nc} \tag{3.2.4}$$

where Δ is the total (experimental) displacement, Δ_e is the elastic component of displacement, and Δ_p^{nc} is the plastic component of displacement without the presence of a crack. These are given by

$$\frac{\Delta_e E'}{P} = \frac{H}{W} + (\xi_1 - \xi_2 \xi_4) \tag{3.2.5a}$$

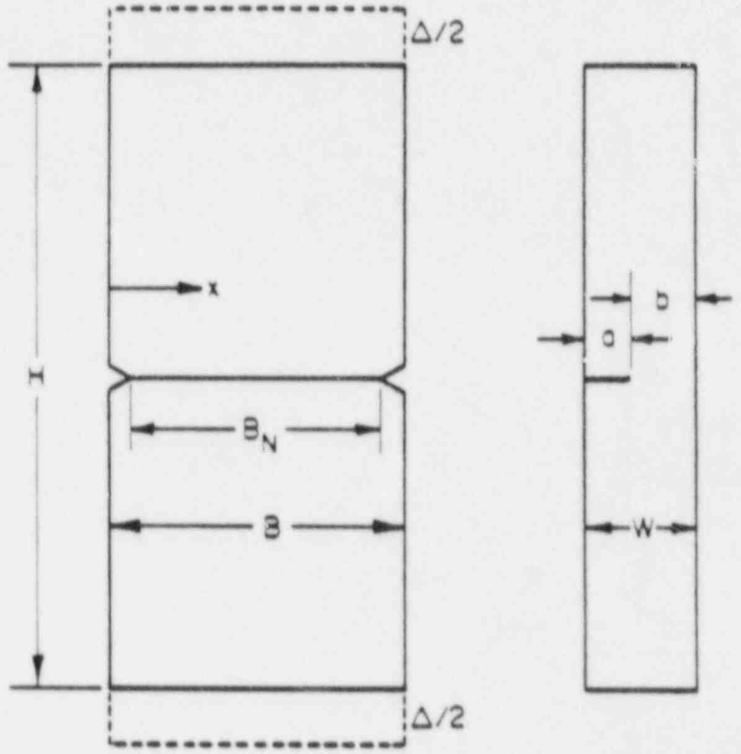

Figure 3.2.2 Schematic drawing of the FWFN(T) specimen with side-grooves.

T-4072-F-C-2

and

$$\frac{\Delta_p^{nc_E}}{p} = H \cdot \left(\frac{\varepsilon E}{p} - \frac{1}{W}\right) \qquad (3.2.5b)$$

where ε is the strain (from the material's uniaxial stress-strain data) corresponding to the stress of p/W. If the applied load is such that the corresponding stress results in purely elastic strain, then by Eq. 3.2.5(b), Δ_p^{nc} is zero. However, this is not always the case.

The factor η of Eq. 3.2.3 is found by using the following equations:

$$\eta = \frac{1}{\alpha}\left[\alpha + \frac{2b\alpha}{2\alpha+g}\left\{\frac{W}{b^2} - \frac{Wf}{3b^2} + \frac{1}{3}\left(\frac{W}{b} - 1\right)\beta\right\}\right] \qquad (3.2.6)$$

$$g = \frac{2W}{b} - \frac{2f}{3}\left(\frac{W}{b} - 1\right) - 2 \qquad (3.2.7)$$

$$f = \frac{6W}{(W-b)}\xi_4 \qquad (3.2.8)$$

$$\alpha = \frac{-g + \sqrt{g^2+4}}{2} \qquad (3.2.9)$$

$$\beta = \frac{6W\xi_4}{(W-b)^2} + \frac{(226.195)\ \xi_4 f_2}{\xi_2 W}\left(6\,\xi_4\, f_2 - f_1\right) \qquad (3.2.10)$$

In the above, if $a = a_1 \leq 0.6\ W$, then

$f_1 = f_{11}$
$f_2 = f_{21}$
$\xi_1 = \xi_{11}$
$\xi_2 = \xi_{21}$
$\xi_3 = \xi_{31}$
$\xi_4 = \xi_{41}$

and if $a = a_2 > 0.6\ W$, then

$$f_1 = f_{12}$$
$$f_2 = f_{22}$$
$$\xi_1 = \xi_{11} + \xi_{12}$$
$$\xi_2 = \xi_{21} + \xi_{22}$$
$$\xi_3 = \xi_{31} + \xi_{32}$$
$$\xi_4 = \xi_{41} + \xi_{42}$$

where

$$f_{11} = 1.12 - 0.231 \left(\frac{a_1}{W}\right) + 10.55 \left(\frac{a_1}{W}\right)^2 - 21.72 \left(\frac{a_1}{W}\right)^3 + 30.39 \left(\frac{a_1}{W}\right)^4 \quad (3.2.11)$$

$$f_{21} = 1.122 - 1.4 \left(\frac{a_1}{W}\right) + 7.33 \left(\frac{a_1}{W}\right)^2 - 13.08 \left(\frac{a_1}{W}\right)^3 + 14.0 \left(\frac{a_1}{W}\right)^4 \quad (3.2.12)$$

$$\xi_{11} = 2\pi \left(\frac{a_1}{W}\right)^2 \left[0.627 - 0.172 \left(\frac{a_1}{W}\right) + 5.92 \left(\frac{a_1}{W}\right)^2 - 10.705 \left(\frac{a_1}{W}\right)^3 + 31.578 \left(\frac{a_1}{W}\right)^4 - 67.476 \left(\frac{a_1}{W}\right)^5 + 139.124 \left(\frac{a_1}{W}\right)^6 - 146.682 \left(\frac{a_1}{W}\right)^7 + 92.355 \left(\frac{a_1}{W}\right)^8\right] \quad (3.2.13)$$

$$\xi_{21} = 72\pi \left(\frac{a_1}{W}\right)^2 \left[0.629 - 0.609 \left(\frac{a_1}{W}\right) + 4.93 \left(\frac{a_1}{W}\right)^2 - 11.097 \left(\frac{a_1}{W}\right)^3 + 26.757 \left(\frac{a_1}{W}\right)^4 - 48.997 \left(\frac{a_1}{W}\right)^5 + 81.82 \left(\frac{a_1}{W}\right)^6 - 77.953 \left(\frac{a_1}{W}\right)^7 + 42.546 \left(\frac{a_1}{W}\right)^8\right] \quad (3.2.14)$$

$$\xi_{31} = 12\pi \left(\frac{a_1}{W}\right)^2 \left[0.629 - 1.047 \left(\frac{a_1}{W}\right) + 4.602 \left(\frac{a_1}{W}\right)^2 - 9.975 \left(\frac{a_1}{W}\right)^3 + 20.295 \left(\frac{a_1}{W}\right)^4 - 32.933 \left(\frac{a_1}{W}\right)^5 + 47.041 \left(\frac{a_1}{W}\right)^6 - 40.693 \left(\frac{a_1}{W}\right)^7 + 19.6 \left(\frac{a_1}{W}\right)^8\right] \quad (3.2.15)$$

$$\xi_{41} = \frac{\xi_{21}}{\xi_{31} + 12\pi} \quad (3.2.16)$$

$$f_{12} = \frac{1 + 3\left(\frac{a_2}{W}\right)}{2\left(1 - \frac{a_2}{W}\right)^{3/2} \left(\frac{\pi a_2}{W}\right)^{1/2}} \quad (3.2.17)$$

$$f_{22} = \frac{0.375 \left(\frac{W}{a_2}\right)^2}{\left(\frac{W}{a_2} - 1\right)^{3/2}} \quad (3.2.18)$$

$$\xi_{12} = \frac{21\left(\frac{a_2}{W}\right) - 9\left(\frac{a_2}{W}\right)^2 - 8}{\left(1 - \frac{a_2}{W}\right)^2} - 4.5 \log_e \left(1 - \frac{a_2}{W}\right) - 12.62 \quad (3.2.19)$$

$$\xi_{22} = \frac{3.99\, W\, (3a_2 - W)}{(W - a_2)^2} - 19.95 \quad (3.2.20)$$

$$\xi_{32} = \frac{15.9\, W^2}{(W - a_2)^2} - 99.38 \quad (3.2.21)$$

$$\xi_{42} = \frac{\xi_{22}}{\xi_{32} + 12\,\frac{H}{W}} \qquad (3.2.22)$$

The elastic-plastic finite element method was used in assessing the accuracy of the results of the J-estimation method represented by Eqs. 3.2.1 through 3.2.13. These are discussed below.

Finite Element Method Analyses

Thus far, two detailed finite element method analyses have been performed. As shown in Table 3.2.3, these correspond to specimens with widely different height-to-width ratios. The finite element meshes for the two specimens are shown in Figures 3.2.3a and 3.2.3b. The material for the two specimens is A106 Grade B at 550 F (288 C). However, since the two specimens were fabricated from different pipes, their uniaxial stress-strain properties are somewhat different. Figures 3.2.4a and 3.2.4b show the stress-strain curves corresponding to the materials of specimen numbers DP2-f29-25b and DP2-f6-31, respectively. Tables 3.2.4 and 3.2.5 contain the load, displacement and crack extension data for the two specimens.

Table 3.2.3 FWFN(T) specimen dimensions.

Dimension	Specimen No. DP2-f6-31 inch	(mm)	DP2-f29-25b inch	(mm)
W	1.180	(29.97)	0.712	(18.08)
B	2.502	(63.55)	1.614	(40.99)
H	6.000	(152.4)	10.000	(254.0)
a	0.594	(15.09)	0.357	(9.06)

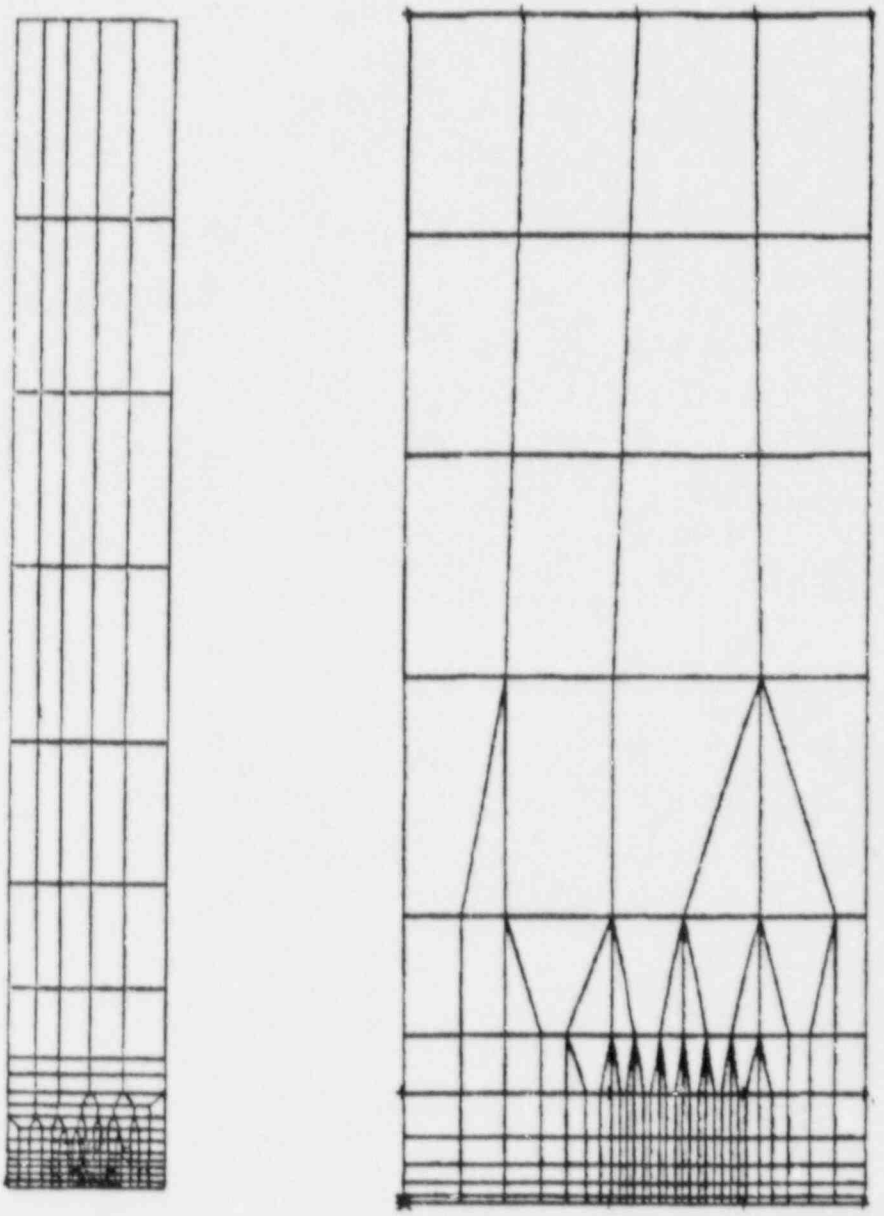

(a) H/W = 14 (b) H/W = 5.085

Figure 3.2.3 Finite element models for FWFN(T) specimens

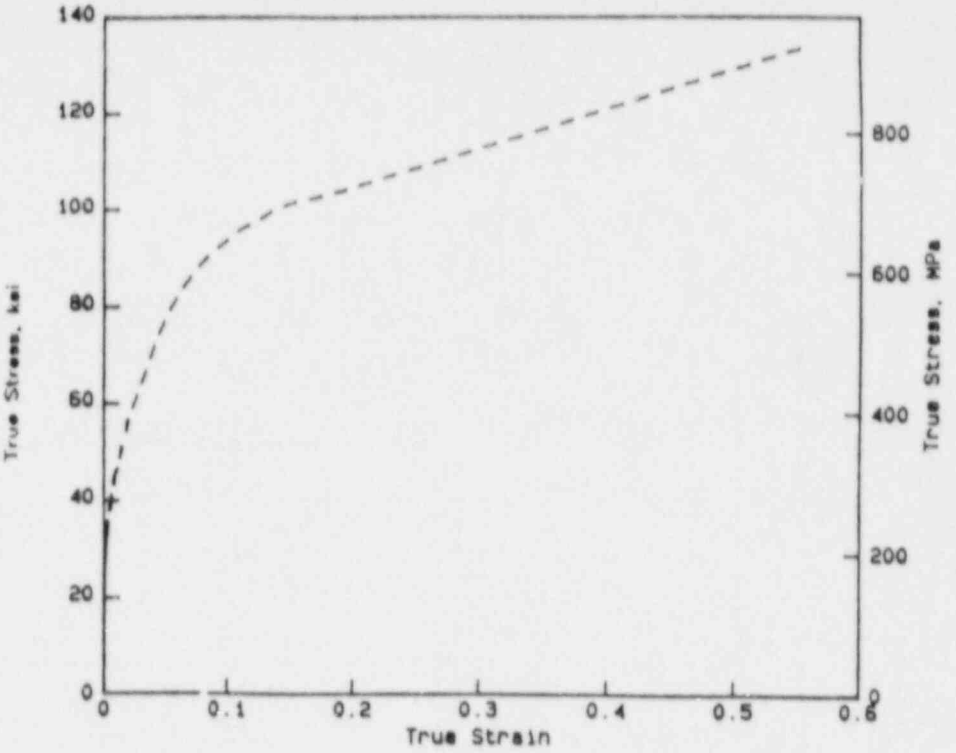

(a) Large strain data

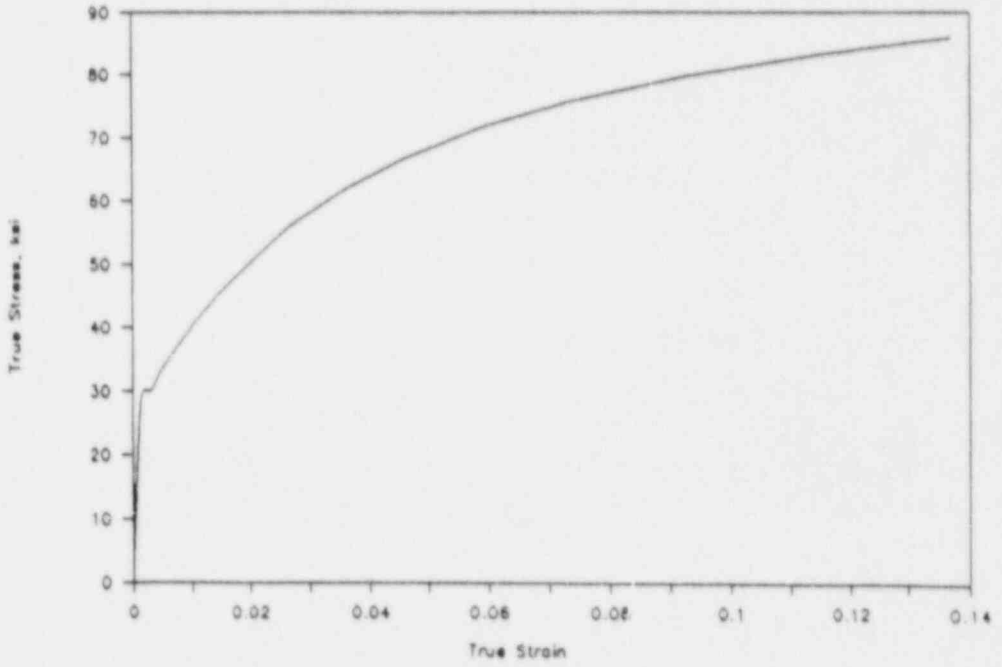

(b) Small strain data

Figure 3.2.4 True stress-true strain for Pipe F29, A106 Grade B carbon steel at 550 F (288 C).

SA-12/87-F3.2.4

Table 3.2.4 Experimental data for conducting finite element method analysis (see Figure 3.2.4a)

Load		Displacement		Crack Extension	
lbs	N	inches	mm	inches	mm
764.6	3401	0.00029	0.0073	0.0000	0.0000
2276	10124	0.00096	0.0243	0.0000	0.0000
4087	18179	0.0017	0.0432	0.0000	0.0000
5725	25465	0.00237	0.0602	0.0000	0.0000
7295	32448	0.00309	0.0784	0.0000	0.0000
8906	39614	0.00397	0.1008	0.0000	0.0000
10720	47682	0.00503	0.1277	0.0000	0.0000
12330	54844	0.00616	0.1564	0.0000	0.0000
13920	61916	0.00726	0.1844	0.0000	0.0000
15530	69077	0.00853	0.2166	0.0000	0.0000
16930	75304	0.00978	0.2484	0.0000	0.0000
18540	82466	0.01134	0.2880	0.0000	0.0000
20070	89271	0.01317	0.3345	0.0000	0.0000
21530	95765	0.01488	0.3779	0.0000	0.0000
22820	101503	0.01683	0.4275	0.0000	0.0000
23960	106574	0.01864	0.4734	0.0000	0.0000
25200	112089	0.02115	0.5372	0.0000	0.0000
26310	117027	0.02391	0.6073	0.0014	0.0355
27280	121341	0.02647	0.6723	0.0027	0.0685
28040	124722	0.02887	0.7333	0.0055	0.1397
28800	128102	0.03131	0.7953	0.0068	0.1727
29590	131616	0.03426	0.8702	0.0095	0.2413
30210	134374	0.0369	0.9373	0.0122	0.3098
30790	136954	0.03973	1.0091	0.0175	0.4445
31170	138644	0.04261	1.0823	0.0227	0.5765
31230	138911	0.04635	1.1773	0.0368	0.9347
31110	138377	0.04913	1.2479	0.0479	1.2166
31000	137888	0.04984	1.2659	0.0503	1.2776

Table 3.2.5 Experimental data for conducting finite element method analysis (see Figure 3.2.4b)

Load		Displacement		Crack Extension	
lbs	kN	inches	mm	inches	mm
678.216	3.017	0.00162	0.0411	0.00000	0.0000
5652.370	25.143	0.00166	0.0422	0.00000	0.0000
10500.600	46.709	0.00246	0.0625	0.00000	0.0000
15881.500	70.644	0.00349	0.0886	0.00000	0.0000
21077.400	93.756	0.00438	0.1113	0.00000	0.0000
25876.600	115.104	0.00537	0.1364	0.00000	0.0000
31107.900	138.374	0.00689	0.1750	0.00000	0.0000
36106.000	160.607	0.00727	0.1847	0.00000	0.0000
40865.700	181.779	0.00819	0.2080	0.00000	0.0000
45452.800	202.183	0.01091	0.2771	0.00000	0.0000
50031.200	222.549	0.01339	0.3401	0.00000	0.0000
54469.900	242.293	0.01614	0.4100	0.00000	0.0000
58598.800	260.659	0.02039	0.5179	0.00000	0.0000
62703.600	278.918	0.02436	0.6187	0.00000	0.0000
66959.100	297.847	0.02870	0.7290	0.00000	0.0000
70929.000	315.506	0.03295	0.8369	0.00000	0.0000
74800.100	332.726	0.03750	0.9525	0.00000	0.0000
78460.700	349.009	0.04243	1.0777	0.00000	0.0000
82003.400	364.768	0.04781	1.2144	0.00000	0.0000
85187.400	378.931	0.05397	1.3708	0.00000	0.0000
88071.800	391.761	0.05994	1.5225	0.00000	0.0000
90628.700	403.135	0.06641	1.6868	0.00000	0.0000
93110.100	414.172	0.07306	1.8557	0.00640	0.1626
94850.000	421.912	0.08071	2.0500	0.01950	0.4953
94376.700	419.806	0.08922	2.2662	0.04080	1.0363
93520.600	415.998	0.09643	2.4493	0.06120	1.5545
94276.700	419.362	0.10393	2.6398	0.07850	1.9939
93207.400	414.605	0.11136	2.8285	0.10400	2.6416
92517.500	411.536	0.11889	3.0198	0.12330	3.1318
89927.000	400.013	0.12554	3.1887	0.15210	3.8633
86082.400	382.912	0.13002	3.3025	0.18060	4.5872
85505.500	380.346	0.13408	3.4056	0.19730	5.0114
82732.900	368.012	0.14009	3.5583	0.22110	5.6159
78678.700	349.979	0.14402	3.6581	0.23410	5.9461
77632.100	345.323	0.14951	3.7976	0.25380	6.4465
73963.100	329.003	0.15294	3.8847	0.27010	6.8605

Finite element method analyses were performed using the experimental data contained in Figures 3.2.4a and 3.2.4b and Tables 3.2.4 and 3.2.5. In these computations, crack extension was modeled according to the experimental displacement versus crack length data. Throughout the incremental solution procedure, J values were computed using the path-independent contour-integral definition. The results for the two specimens are shown in Figures 3.2.5 and 3.2.6. Figure 3.2.5 shows the calculated J-R curve for Specimen DP2-F29-25b. Figure 3.2.6 shows the calculated J versus applied displacement up to crack initiation for Specimen DP2-F6-31. For both specimens, J is calculated by finite element method analysis as well as by the estimation scheme represented by Eqs. 3.2.1 through 3.2.13.

To judge whether the agreement between finite element method and estimation method J-R curves should be considered acceptable or not, we look at a similar comparison for a 1T C(T) specimen results obtained earlier in the DP^{3}II Program. These are shown in Figure 3.2.7. It is found that the J-estimation method for the FWFN(T) specimen provides results which show approximately the same degree of agreement with finite element method results as that obtained by the ASTM E813-81 J-estimation method used in calculating the estimated J-R curve of Figure 3.2.7 for C(T) specimen.

References for Section 3.2

3.2.1 Wilkowski, G. M., and others, "Degraded Piping Program - Phase II", Semiannual Report, October 1985-March 1986, NUREG/CR-4082, Vol. 4, September 1986.

3.2.2 Wilkowski, G. M., and others, "Degraded Piping Program - Phase II", Semiannual Report, April 1985-September 1985, NUREG/CR-4082, Vol. 3, March 1986.

3.2.3 Johnson, H. H., "Calibrating the Electric Potential Method for Studying Slow Crack Growth," Materials Research and Standards, Vol. 5, 1965, p. 422.

3.2.4 Tada, H., Paris, P., and Irwin, G., The Stress Analysis of Cracks Handbook, Del Research Corporation, Hellertown, PA, 1973.

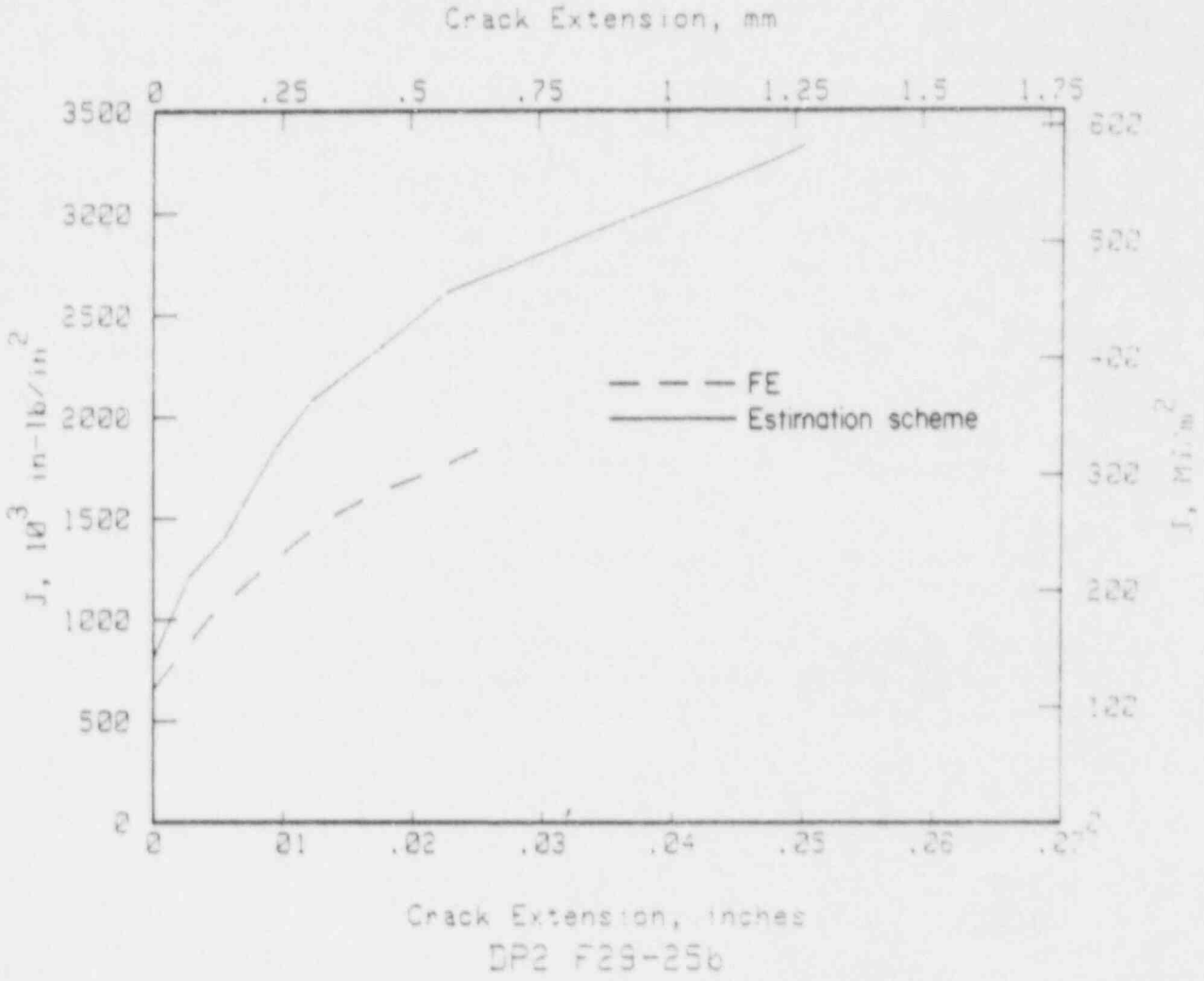

Figure 3.2.5 J-R curve for specimen DP2-F29-25b [FWFN(T)].

SA-12/87-F3.2.5

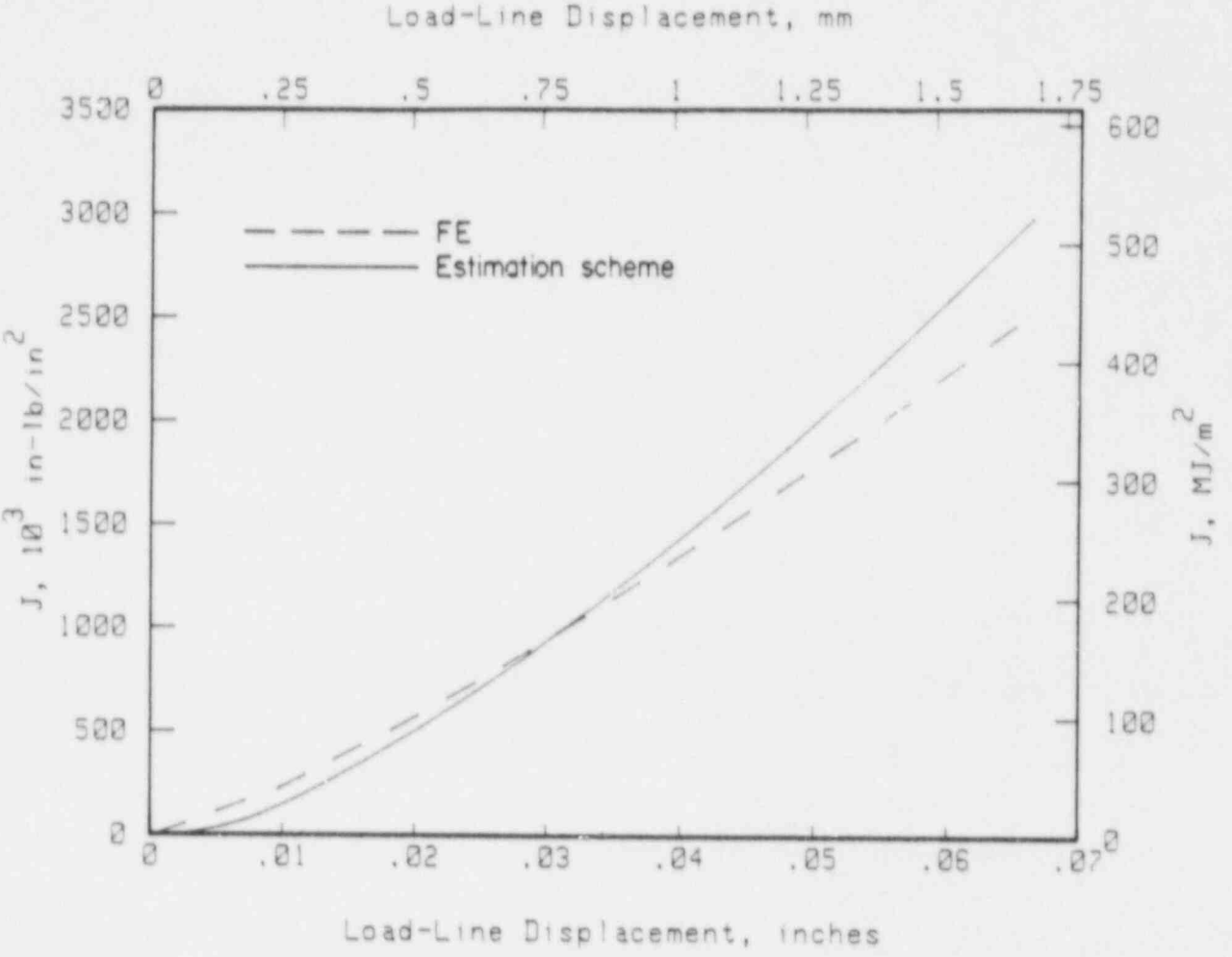

Figure 3.2.6 J versus load-line displacement up to crack initiation for specimen DP2-F6-31 [FWFN(T)].

SA-12/87-F3.2.6

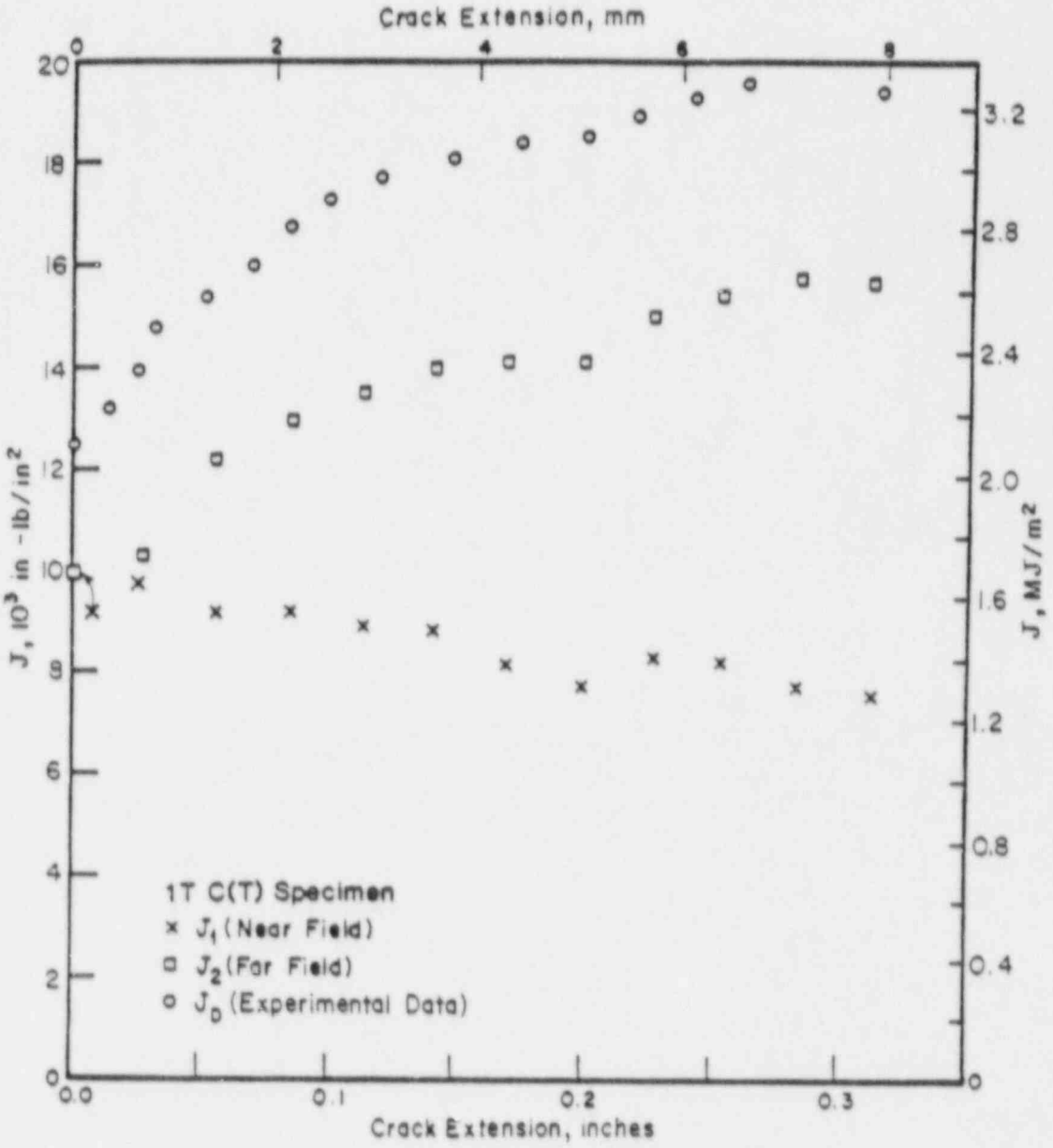

Figure 3.2.7 J-resistance curve for nonside-grooved 1T Type 304 stainless steel compact (tension) specimen.

T-4575-F4.14

3.3 Assessment of Large Crack Growth Using Planform Size Compact Specimens

(C. Marschall, V. Papaspyropoulos, M. Landow, M. Nakagaki, and G. Wilkowski)

One of the problems in predicting fracture instability in pipes is that J-R curves for large amounts of crack growth often are needed. Such data are impossible to obtain from laboratory specimens machined from the pipe because the pipe curvature permits only relatively small specimens to be fabricated. Consequently, a need exists either to verify existing methods or to develop improved methods for extrapolating small-specimen J-R curve data to large amounts of crack growth.

The approach taken in the Degraded Piping Program was to compare J-R curve data obtained from constant thickness but different planform size C(T) specimens [typically 1-inch (25.4-mm) thick 1T, 3T and 9.5T or 10T planform-size compact specimens], to determine if curves from smaller specimens can be extrapolated in a manner that duplicates results from large specimens. Experimental details and results for 1-inch (25.4-mm) thick Type 304 stainless steel and A516 Grade 70 ferritic steel base metal specimens were presented in the following topical report.

> "Predictions of J-R Curves with Large Growth from Small Specimen Data" by V. Papaspyropoulos, C. Marschall, and M. Landow, NUREG/CR-4575.

For a Type 304 stainless steel base metal and tungsten-inert-gas (TIG) weld a similar evaluation on 0.38-inch (9.5 mm) thick 0.5T, 1.5T, and 3T planform C(T) specimens was reported in the following topical report.

> "Analysis of Cracks in Stainless Steel TIG Welds" by M. Nakagaki, C. Marschall, and F. Brust, NUREG/CR-4806.

For ferritic and austenitic flux weld metal specimens, the welding procedures, the experimental procedures, and the results were presented in the Fourth Semiannual Report (Ref. 3.3.1). The austenitic weld results were also published in the following topical report.

> "Analysis of Experiments on Stainless Steel Flux Welds" by G. Wilkowski, J. Ahmad, F. Brust, D. Guerrieri, G. Kramer, G. Kulhowvick, M. Landow, C. Marschall, M. Nakagaki, V. Papaspyropoulos, and P. Scott, NUREG/CR-4878.

The results from these investigations are summarized in the following sections. This includes nine different sets of planform C(T) specimen tests conducted at 550 F (288 C).

3.3.1 Review of Planform C(T) Specimen Test Results

The use of a planform specimen for evaluation of piping materials was first pursued by Paris and others (Ref. 3.3.2). The logic for conducting these nonstandard tests was that the large planform specimens would more closely

simulate the plane stress conditions that probably exist for a through-wall-cracked pipe in bending.

During the course of this program, several series of planform C(T) specimen tests have been conducted. Table 3.3.1 summarizes all of the series. The objective in developing these data was that specimens machined from pipes have the limitation in size due to the curvature of the pipe, hence making it necessary to extrapolate J-R curve data. Typically in the Degraded Piping Program, the procedure for fabricating specimens from pipes has been that the thickness of the specimen should not be less than 80 percent of the pipe thickness, and the specimen size is the largest planform C(T) that can be made. The largest specimen possible is used so that the amount of crack growth data is maximized (see Section 3.1.1 of this report). The effect of different planform specimen sizes on the J-R curves, however, was not known. Consequently, these series of experiments were vital to understanding the possible geometry effects.

Initial Efforts on Stainless and Ferritic Steel Base Metals

Initial efforts from this program are reported in Reference 3.3.3. These efforts involved tests on Type 304 stainless steel base metal and A515 Grade 70 base metal. Each material was 1 inch (25.4 mm) thick. The tests were conducted at 550 F (288 C). The orientation of these specimens from the plate material was the same as if the plate had been seam welded into pipe, with the rolling direction in the pipe axis, and the crack growing in the circumferential direction. Each material was tested with and without side-grooves. Of these data, the Type 304 stainless steel specimen data were analyzed using finite element analyses. The results of this investigation showed the following:

- The crack in the nonside-grooved 3T and 10T C(T) A516 Grade 70 ferritic steel specimens quickly turned 90 degrees from the intended crack plane. This was the low toughness direction in the plate. This was similar to the fracture behavior observed in the cold-leg (also an A516 Grade 70 ferritic steel) circumferential through-wall-cracked pipe test reported in Section 2.1 of our Fifth Semiannual Report (Ref. 3.3.4). This crack turning made it impossible to calculate the J-R curve from the C(T) experiments. Only the J_i values could be determined.

- For the carbon steel specimens, the J_i values were clearly dependent on the specimen size. The stainless steel specimens showed less effect of specimen size on J_i, but generally were more sensitive to side-grooving. With the exception of one specimen, all of the side-grooved specimens from both materials had a lower J_i than the nonside-grooved specimens. These data are shown in Figure 3.3.1.

- For the side-grooved A-516 Grade 70 ferritic steel, both J_D and the modified J, J_M, resistance curves were calculated. The specimens had a total side-grooving depth of 20 percent of the thickness. The J_D-R curves showed significant size dependency, the trend being that

Table 3.3.1. Compact specimen test data provided to DTRC for its J_M versus J_D study. All tests were at 550 F (288 C).

Material	C(T) Specimen Sizes	Thickness, inch	Sidegrooved	FEM Analysis	References
304 Stainless Base	1T, 3T, 10T	1.0	No	1T, 3T, 10T	• NUREG/CR-4575 Sections 2-4 • NUREG/CR-4573 • NUREG/CR-4082 Vol. 4, Sect. 3.1.3
304 Stainless Base	1T, 3T, 10T	1.0	Yes	----	• NUREG/CR-4575 Sections 2 and 3
A516 Gr 70 Base	1T, 3T, 10T	1.0	Yes	----	• NUREG/CR-4575 Sections 2 and 3
A516 Gr 70 Base	1T, 3T, 10T(a)	1.0	No	----	• NUREG/CR-4575
304 Stainless Steel TIG	0.5T, 1.5T, 3T	0.38	No	0.5T, 3T	• NUREG/CR-4806 Sections 4 and 5
304 Stainless Base	0.5T, 1.5T, 3T	0.38	No	3T	• NUREG/CR-4806 Sections 4 and 5
304SS-SAW	1T, 3T, 9.5T	1.0	No	1T, 9.5T	• NUREG/CR-4082 Volume 4, Sect. 3.3 • NUREG/CR-4878 Section 3.0
Carbon Steel SAW	1T, 3T, 9.5T	1.0	Yes	---	• NUREG/CR-4082 Volume 4, Sect. 3.3

(a) Only J_i values for 3T and 10T exist since crack turned 90 degrees.

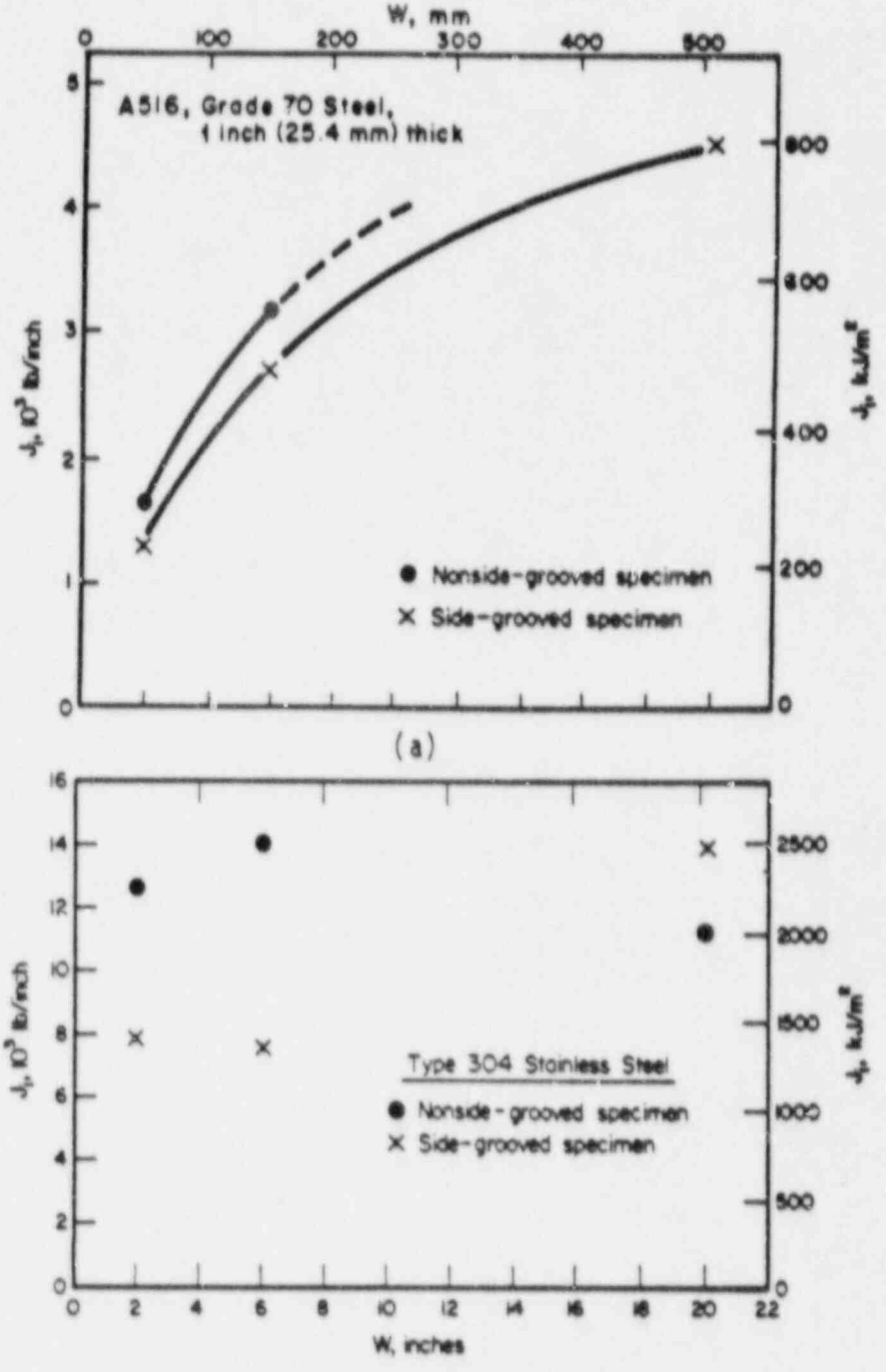

Figure 3.3.1 Effect of specimen width and side-grooves on J at crack initiation in 1-inch- (25.4-mm)-thick compact (tension) specimens tested at 550 F (288 C).

T-4575-F3.1

the smaller the specimen the lower the J_D-R curve (Figure 3.3.2). The J_M-R curves showed much less size dependency, and after 0.25 inch (6.3 mm) of crack growth all of the different specimen J_M-R curves were virtually identical (Figure 3.3.3). Note that for the 1T C(T) specimens, this amount of crack growth is about 25 percent of the ligament which far exceeds the ASTM limit of 10 percent of the ligament.

- For the nonside-grooved Type 304 stainless steel specimens, the J_D-R curves showed slight specimen size dependence (Figure 3.3.4). The 1T C(T) specimen J_D-R curve was very close to the 3T C(T) specimen J_D-R curve. The J_M-R curves indicate that the smaller specimens tend to display higher slopes than for the larger specimens (Figure 3.3.5). This could result in a non-conservative extrapolation of the J-R curve from the smaller specimens.

- The finite element contour integral J_I values were quite close to those calculated from the experimental data and the ASTM approach. This was encouraging in that the ASTM standard specifically excludes stainless steels. Hence, the ASTM standard technique could be expanded to include stainless steels.

- Finite element analyses were performed for all nonside-grooved Type 304 stainless steel specimens, and the J-R curves were calculated by the contour integral J. The finite element J-R curves were path independent for up to 10 percent and 15 percent of the initial crack ligament for the 3T and 10T specimens, respectively. Path dependence was observed immediately after crack initiation for the 1T specimen. The loss of path dependence is the point generally believed to be the limit of validity of the deformation theory J. In the ASTM J-R curve procedure, the limitation on the crack growth is 10 percent of the ligament. Our finite element computations indicate that this limit may vary with specimen size. The 10 percent limit in the ASTM standard was adopted using an approximate analysis. In this analysis, the condition for the applicability of J was defined in terms of the parameter w, given by the equation below:

$$w = \frac{b}{J}\frac{dJ}{da} \gg 1 \qquad (3.3.1)$$

where b is the length of the uncracked ligament.

- In general, the far field J-R curves from the finite element analysis compared well with the J_M-R curves (Figure 3.3.6). The agreement between the far-field J-R curves and the J_D-R curves was poor with large crack growth.

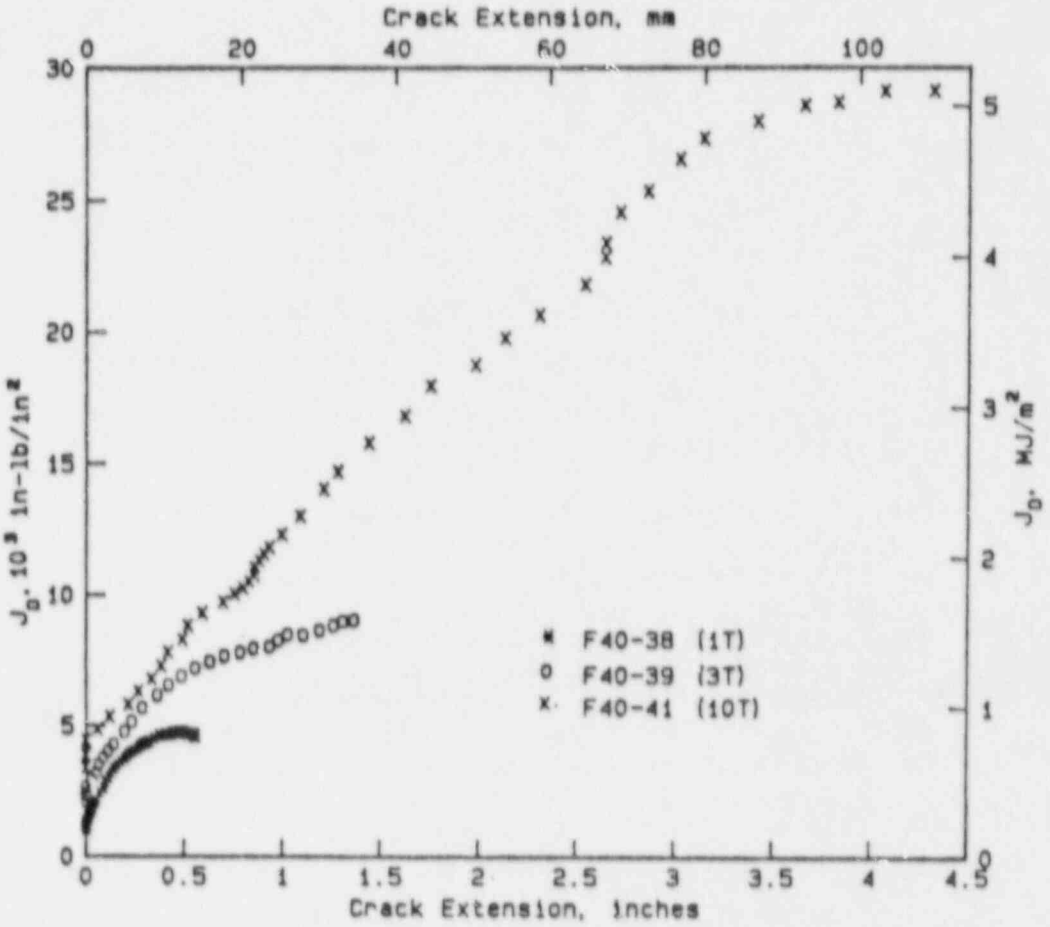

Figure 3.3.2 J_D versus Δa for 1T, 3T, and 10T, 1-inch- (2.54-mm)-thick side-grooved compact (tension) specimens of A516 Grade 70 carbon steel tested at 550 F (288 C).

SA-12/87-F3.3.2

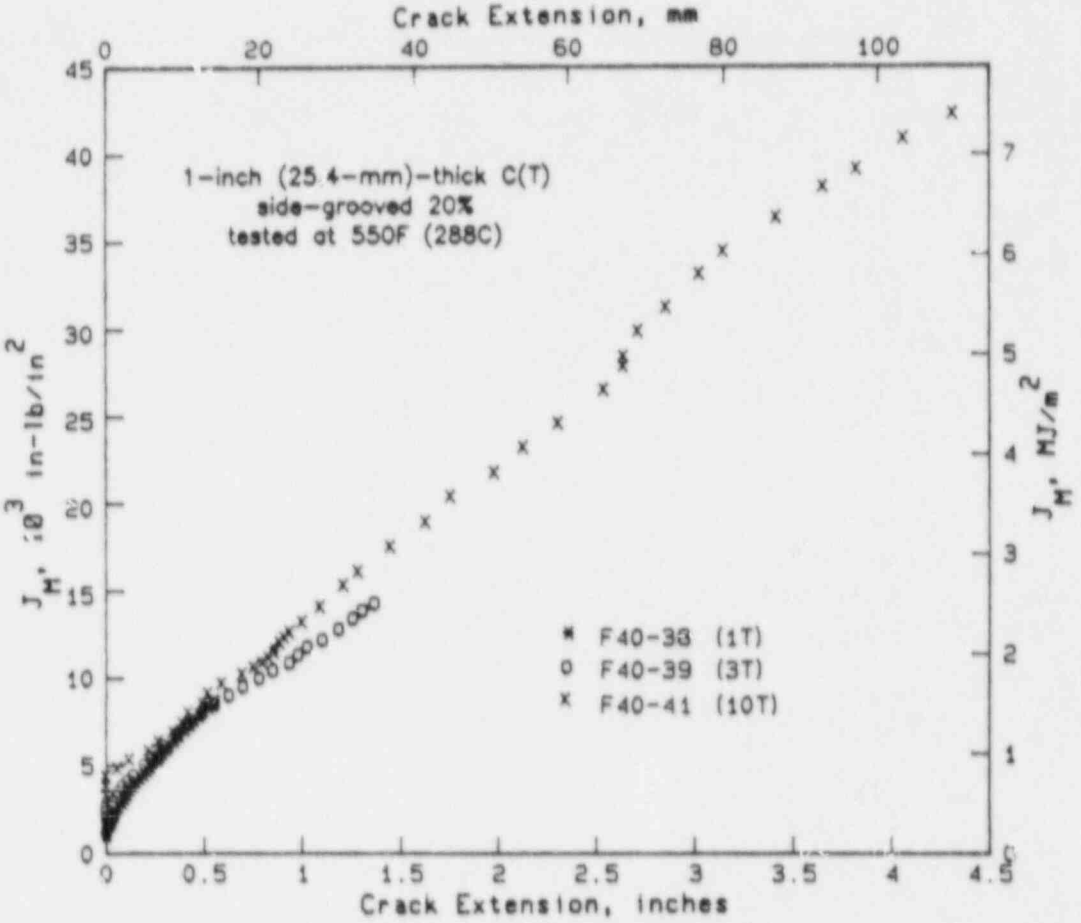

Figure 3.3.3 J_M versus Δa for 1T, 3T, and 10T planform-sized side-grooved compact (tension) specimens of A516 Grade 70 steel tested at 550 F (288 C).

T-4575-F3.7

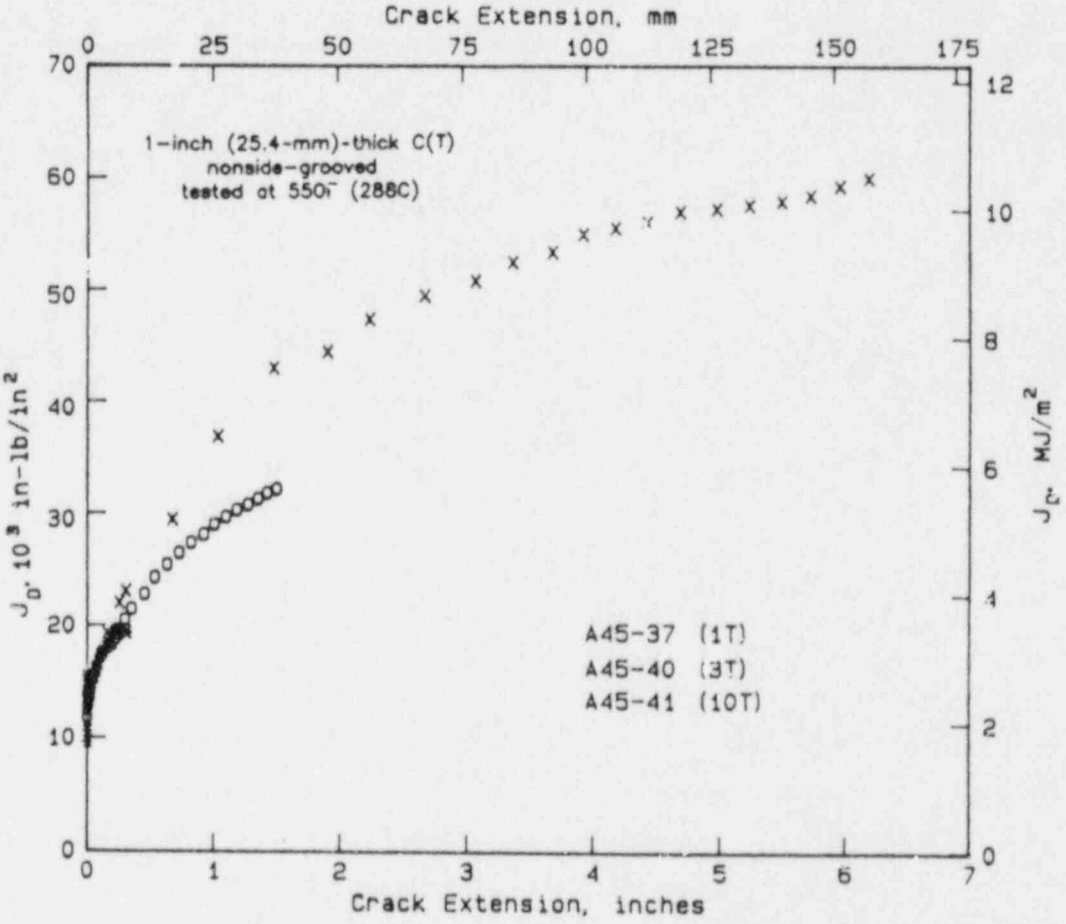

Figure 3.3.4 J_D versus Δa for 1T, 3T, and 10T planform-sized nonside-grooved compact (tension) specimens of Type 304 stainless steel tested at 550 F (288 C).

T-4575-F3.2

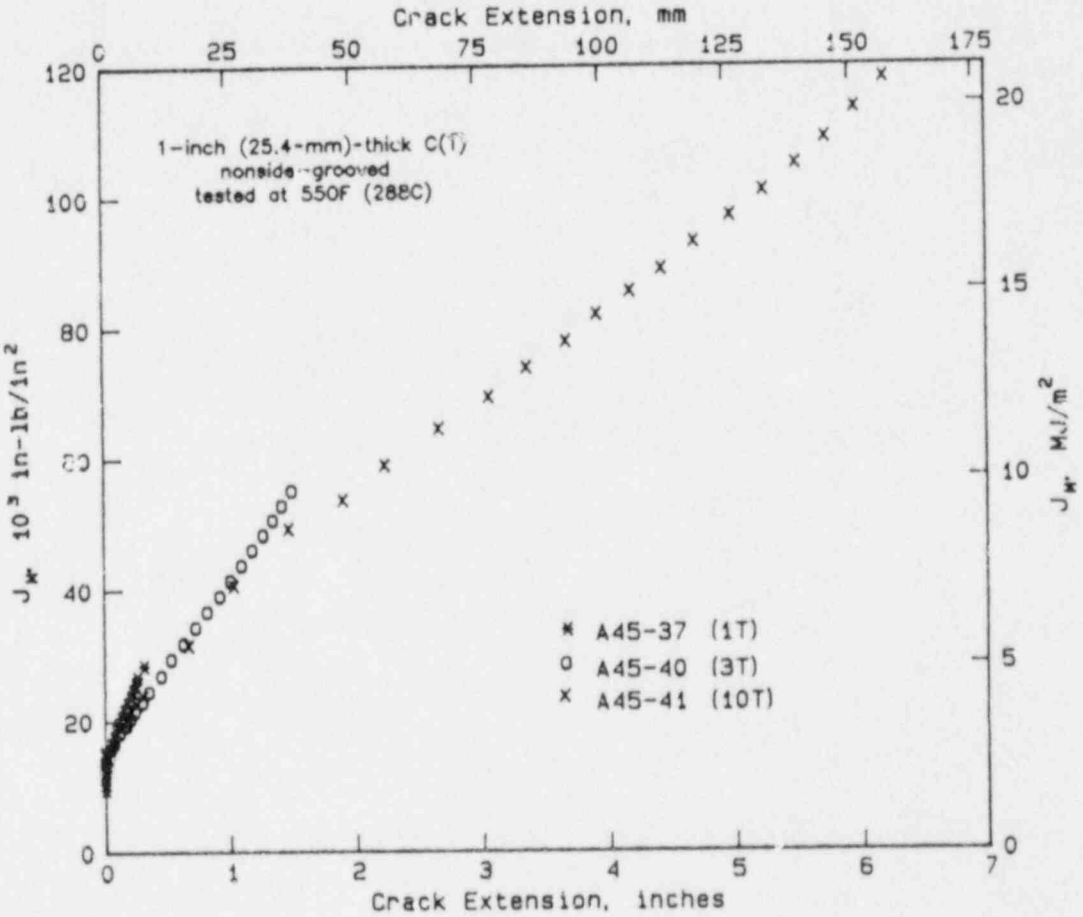

Figure 3.3.5 J_M versus Δa for various planform-sized Type 304 stainless steel compact (tension) specimens.

T-4575-F3.4

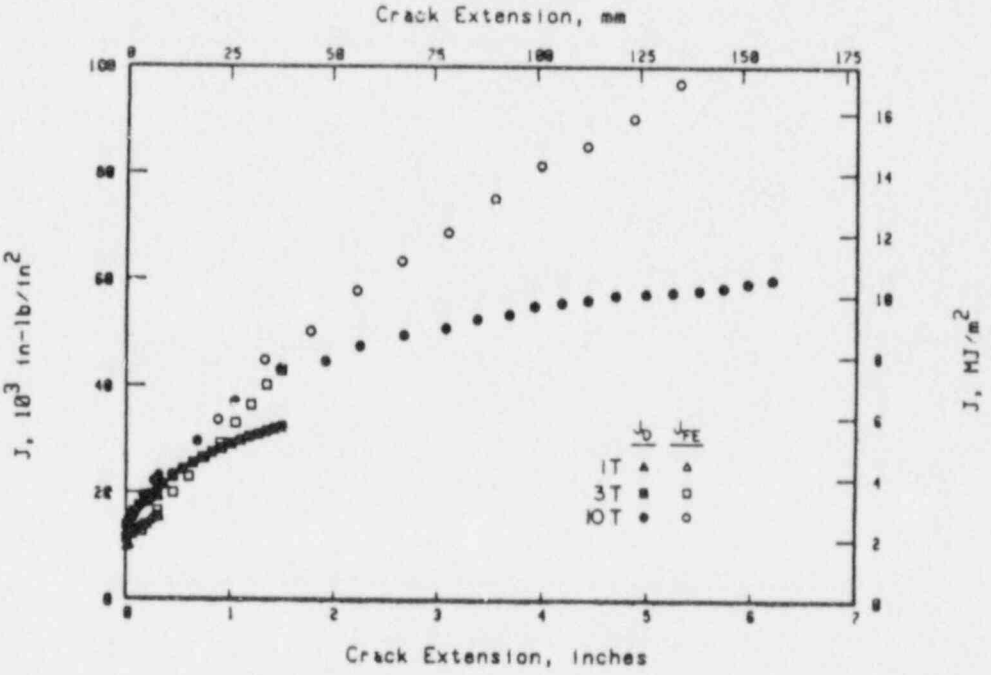

(a) J_D versus finite element method

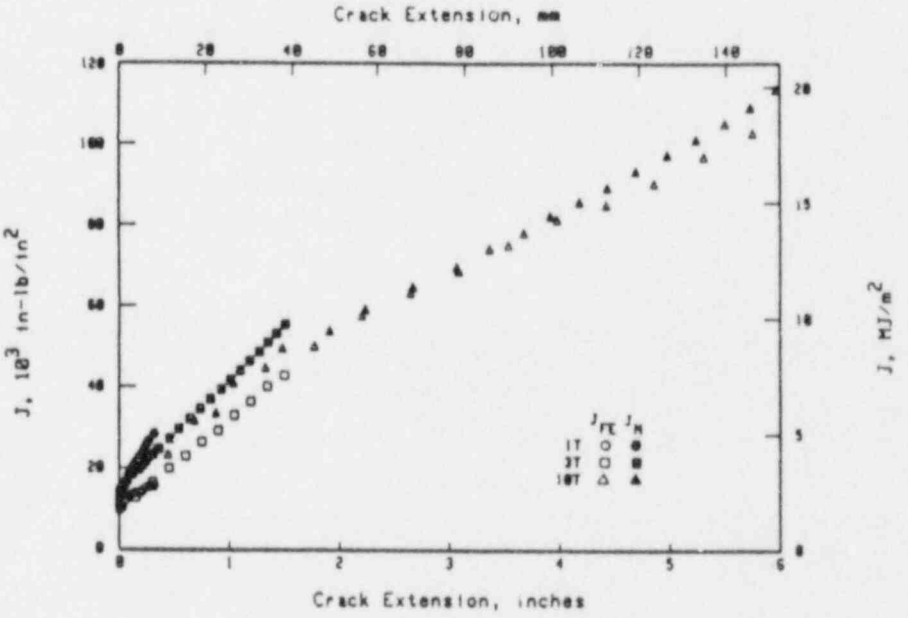

(b) J_M versus FEM

Figure 3.3.6 Comparison of far-field J-resistance curves from finite element analysis J-R curves, J_{FE}, to η-factor analysis, J_D and J_M, for the nonside-grooved Type 304 stainless steel compact (tension) specimens.

T-4575-F4.18

- The 10T nonside-grooved Type 304 stainless steel C(T) specimen data were used in a calculational round-robin that confirmed that all NRC contractors were calculating J_D- and J_M-R curves from experimental data in the same way. These results are given in Section 3.5.2 of this report.

- The 10T C(T) nonside-grooved Type 304 Stainless steel C(T) specimen data were used in a finite element round-robin. These results are given in Section 3.5.4 of this report.

- The side-grooved Type 304 stainless steel C(T) specimen J_M-R curves are shown in Figure 3.3.7. With large crack growth, the 1T specimen J-R curve reaches a maximum and then decreases. This is frequently seen when the crack growth data are well beyond the ASTM limits. The 3T specimen J-R curve agreed with the 10T specimen J-R curve until crack growth exceeded 30-percent of the ligament.

- The side-grooved J_M-R curves are shown in Figure 3.3.8. As with the nonside-grooved specimens, the 1T specimen shows a steeper slope than the larger specimens do. The 10T specimen slope is significantly less than even the 3T specimen in this test series.

Stainless Steel TIG Weld and Base Metal Evaluations

The next series of planform C(T) specimen J-R curves were developed in an evaluation of stainless steel TIG weld specimens (Section 2.6). Base metal Type 304 stainless steel specimens were also tested for comparison to the weld specimens. All specimens were nonside-grooved. The thickness of these specimens was 0.38 inch (9.5 mm). The planform specimen sizes were 0.5T, 1.5T, and 3T. All specimens were tested at 550 F (288 C). Finite element analyses were conducted on the 0.5T and 3T C(T) specimens. The results showed the following:

- For the base metal specimens, the 0.5T specimens had a lower J_i than the larger specimens. These J_i values were significantly lower than the J_i values for the 1-inch- (25.4-mm)-thick specimens cited in the first series of planform C(T) specimen testing. Whether this difference is due to thickness or normal variations in toughness for Type 304 stainless steel is not known.

- For the base metal specimens, the J_D-R curves showed significant geometry dependence (Figure 3.3.9). The geometry dependence in this case was much greater than for the 1-inch (25.4-mm) thick Type 304 stainless steel specimens.

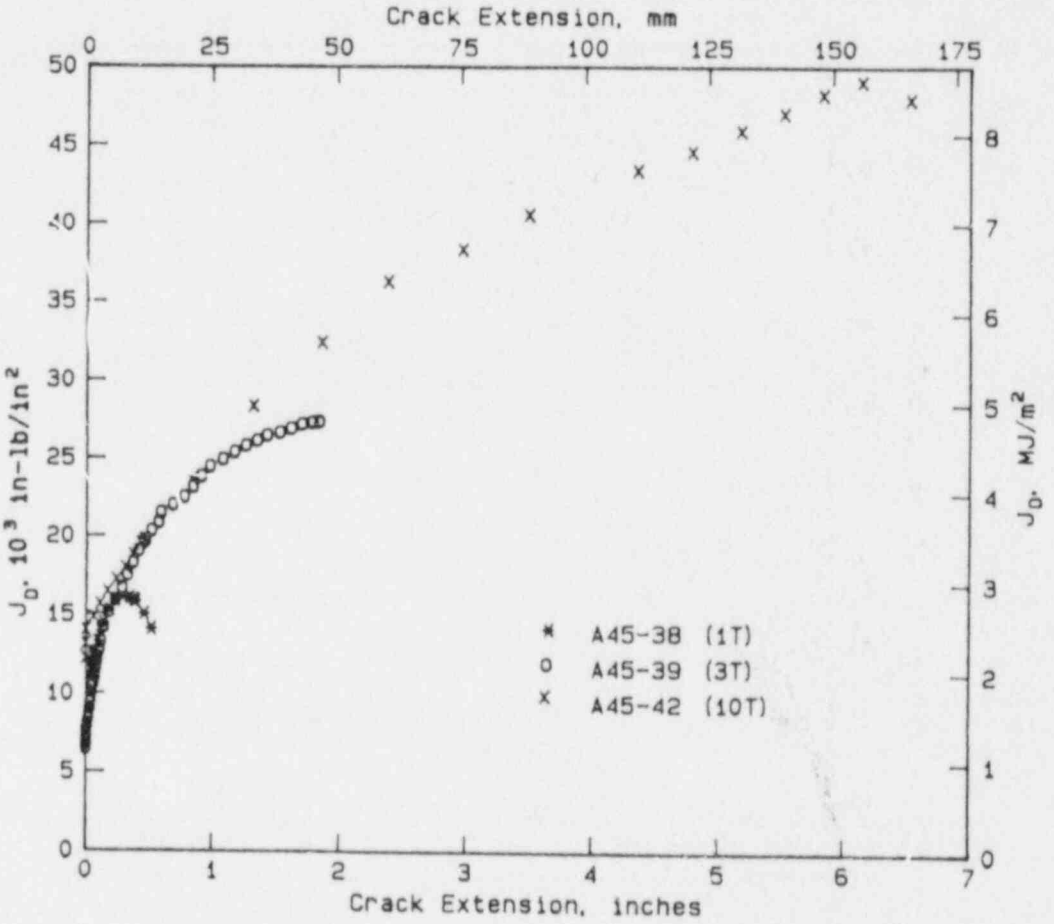

Figure 3.3.7 J_D versus Δa for 1T, 3T, and 10T, 1-inch- (2.54-mm)-thick, side-grooved compact (tension) specimens of Type 304 stainless steel specimens tested at 550 F (288 C).

T-4575-F3.3

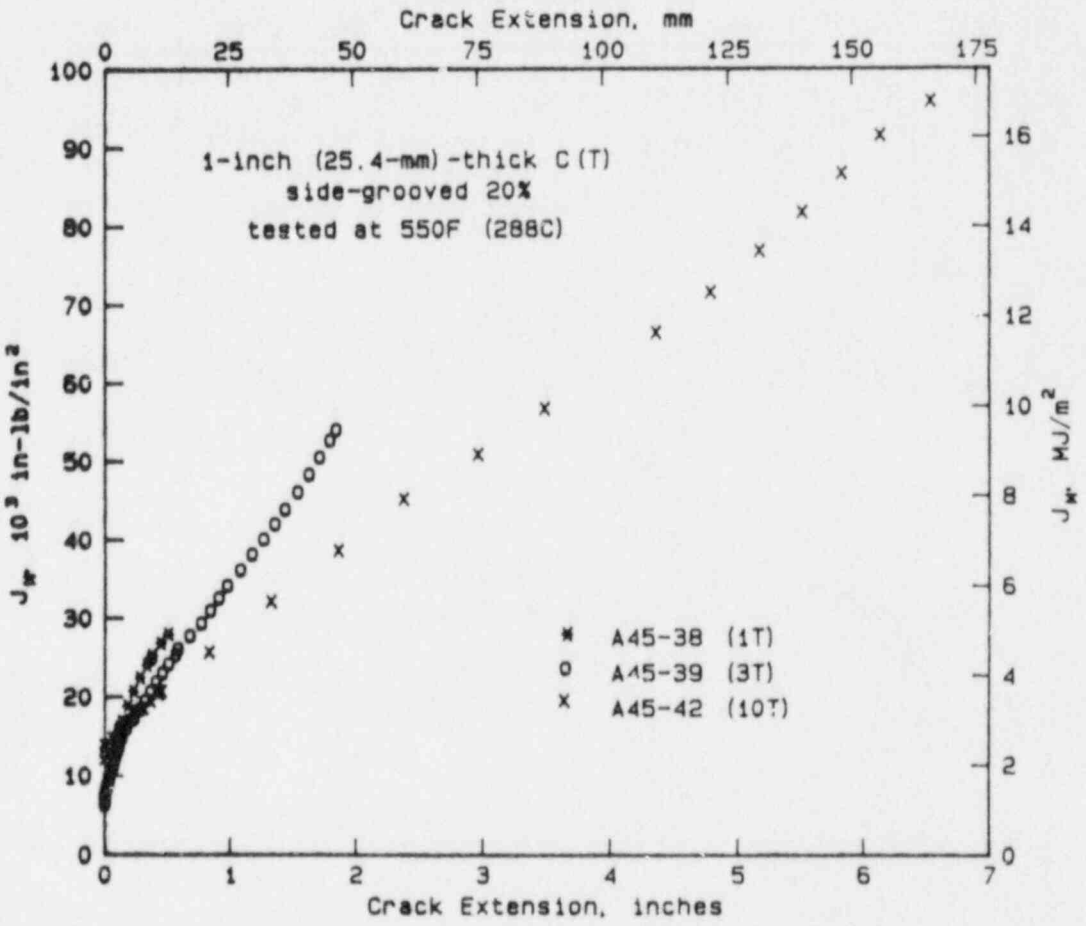

Figure 3.3.8 J_M versus Δa for various planform-sized Type 304 stainless steel compact (tension) specimens.

T-4575-F3.5

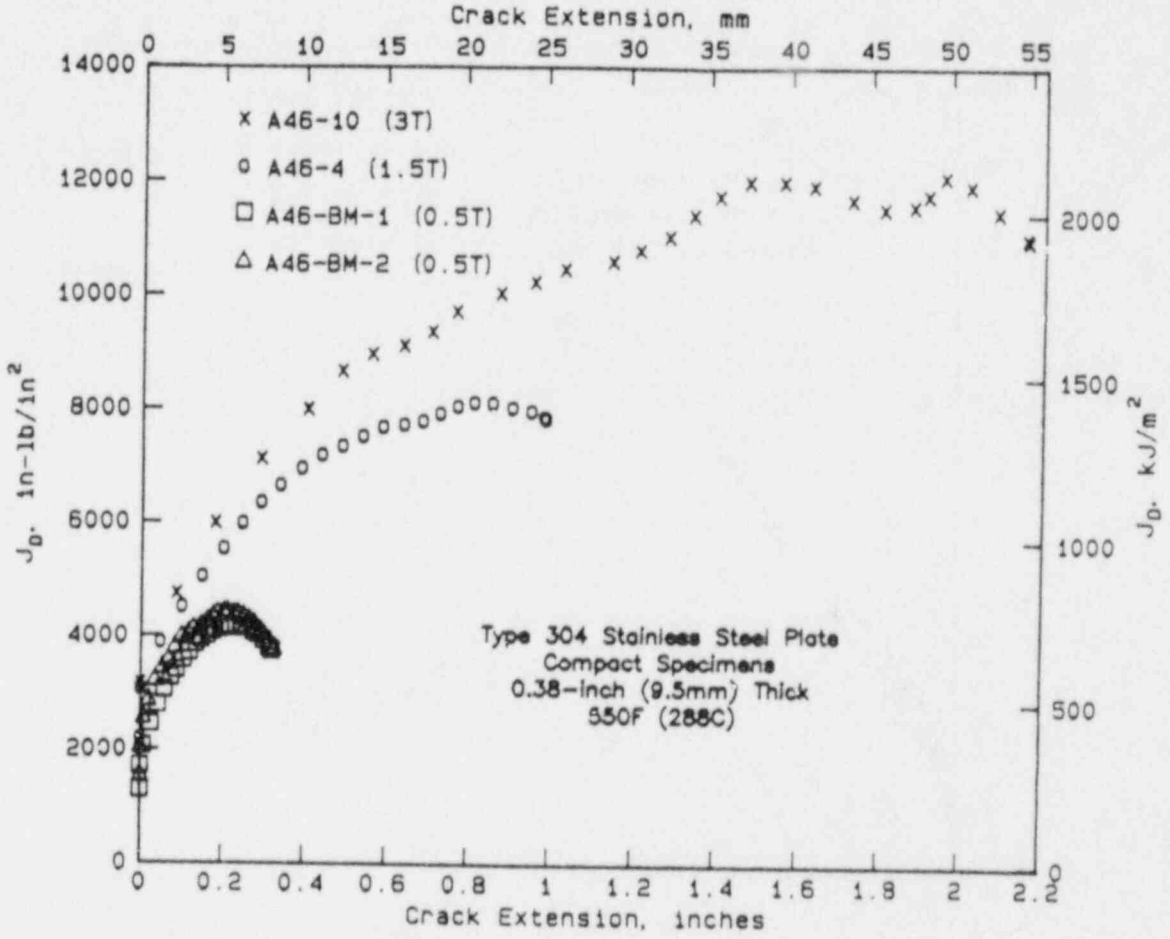

Figure 3.3.9 J_D versus crack extension for TP 304 stainless steel base metal.

T-4806-F7

- The J_M-R curves showed less geometry dependence than the J_D-R curves (Figure 3.3.10). The smallest specimen showed a greater slope than the larger specimens, which is a non-conservative trend.

- For the TIG weld specimens, the 0.5T C(T) specimens had a lower J_i than the larger specimens, with the 1.5T C(T) specimen having the highest value. The 0.5T C(T) specimen had the weld crown machined off, whereas the larger specimens had the weld crown left on. Since J-R curves from these specimens were to be compared to welded pipe test J-R curves with a weld crown left on, it was desired to have the weld crown left on the larger specimens.

- For the TIG weld specimens, the general shape of the J_D-R curves was not as well ordered with the specimen size. This was perhaps due to the influence of the weld and the weld crown left on the larger specimens (Figure 3.3.11). The initial slope of the 0.5T C(T) specimens was steeper than that for the larger specimens, which is consistent with the previously discussed base metal J-R curves.

- For the TIG weld specimens, the J_M-R curves were much steeper for the 0.5 T C(T) specimens, (Figure 3.3.12). The 0.5T specimens also showed an upward hooking, which was a concern raised at a recent J_M-R curve workshop (Ref. 3.3.5). The 3T J-R curve was quite close to the pipe J-R curves from an η-factor analysis and a finite element analysis of a pipe experiment (Figure 3.3.13). Note that the 3T specimen J_D-R curve is shown in this figure; however, for the amount of crack growth in this figure, there is little difference between the 3T C(T) J_D- and J_M-R curves.

- Finite element analysis of the base metal and TIG weld metal 0.5T and 3T C(T) specimens was also conducted. These results showed good agreement between contour integral and virtual crack extension (VCE) J values from the finite element analysis and the ASTM procedure calculated J-R curve. As with the first series of stainless steel planform experiments, this shows that the ASTM procedure could be used for stainless steels.

Stainless Steel SAW Tests

The next series of planform C(T) specimen tests were on a stainless steel submerged arc weld (SAW). The weld procedure used came from a boiling-water reactor (BWR) specification. The plate material in the welded specimens was the same as used in the first series of tests described on 1-inch (25.4-mm) thick Type 304 stainless steel. Only nonside-grooved specimens of 1T, 3T, and 9.5T planform size were tested. The weld crown was left on 3T and 9.5T specimens. All specimens were tested at 550 F (288 C). The 1T and 9.5T C(T)

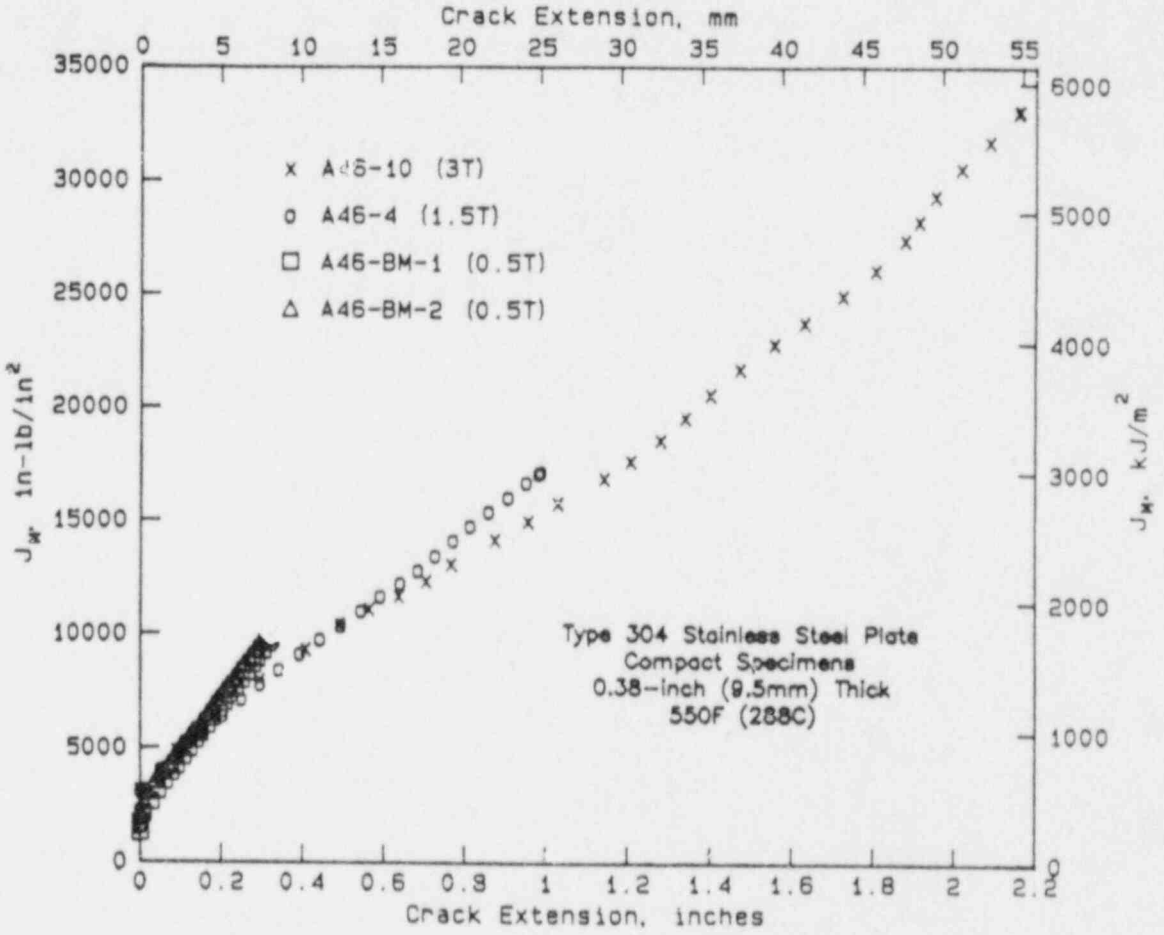

Figure 3.3.10 J_M versus crack extension for TP 304 stainless steel base metal.

T-4806-F9

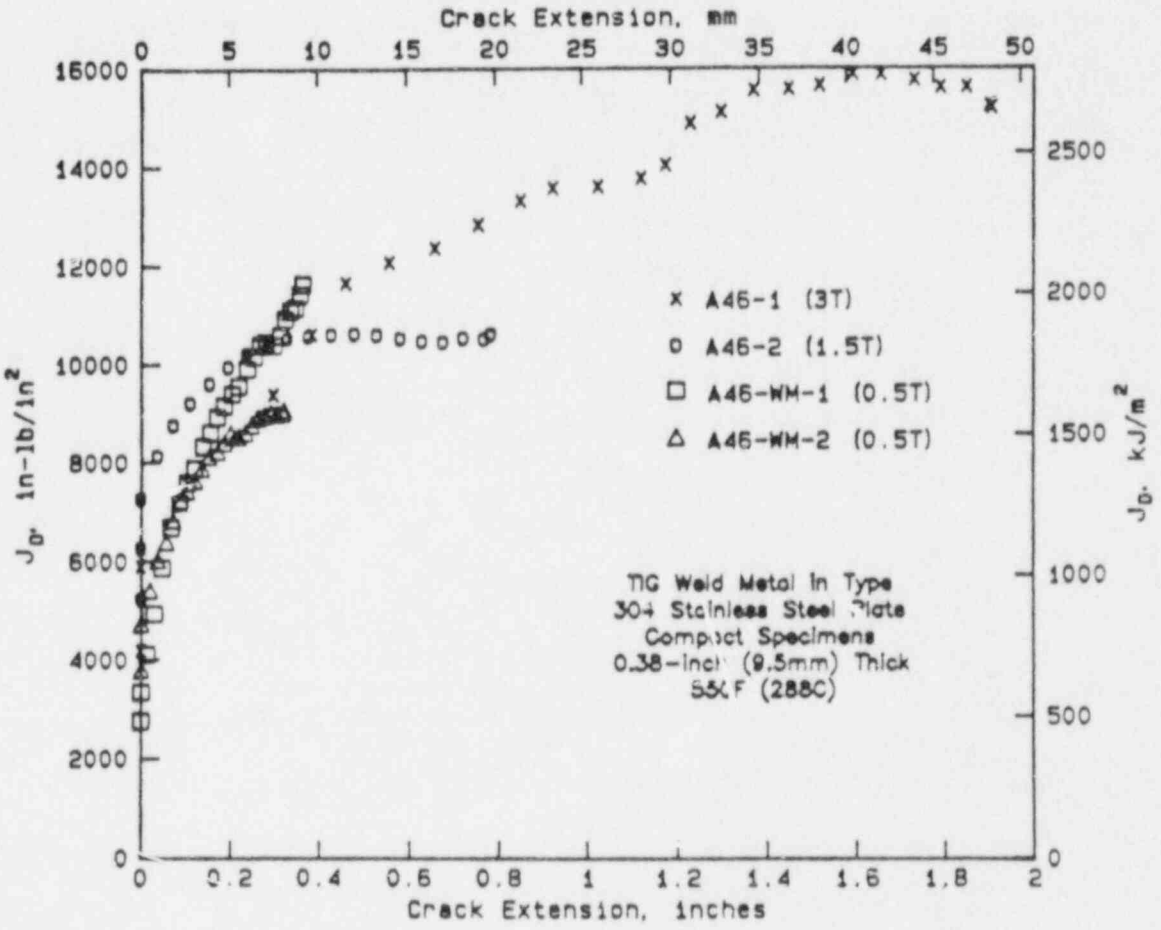

Figure 3.3.11 J_D versus crack extension for a stainless steel TIG weld.

T-4806-F8

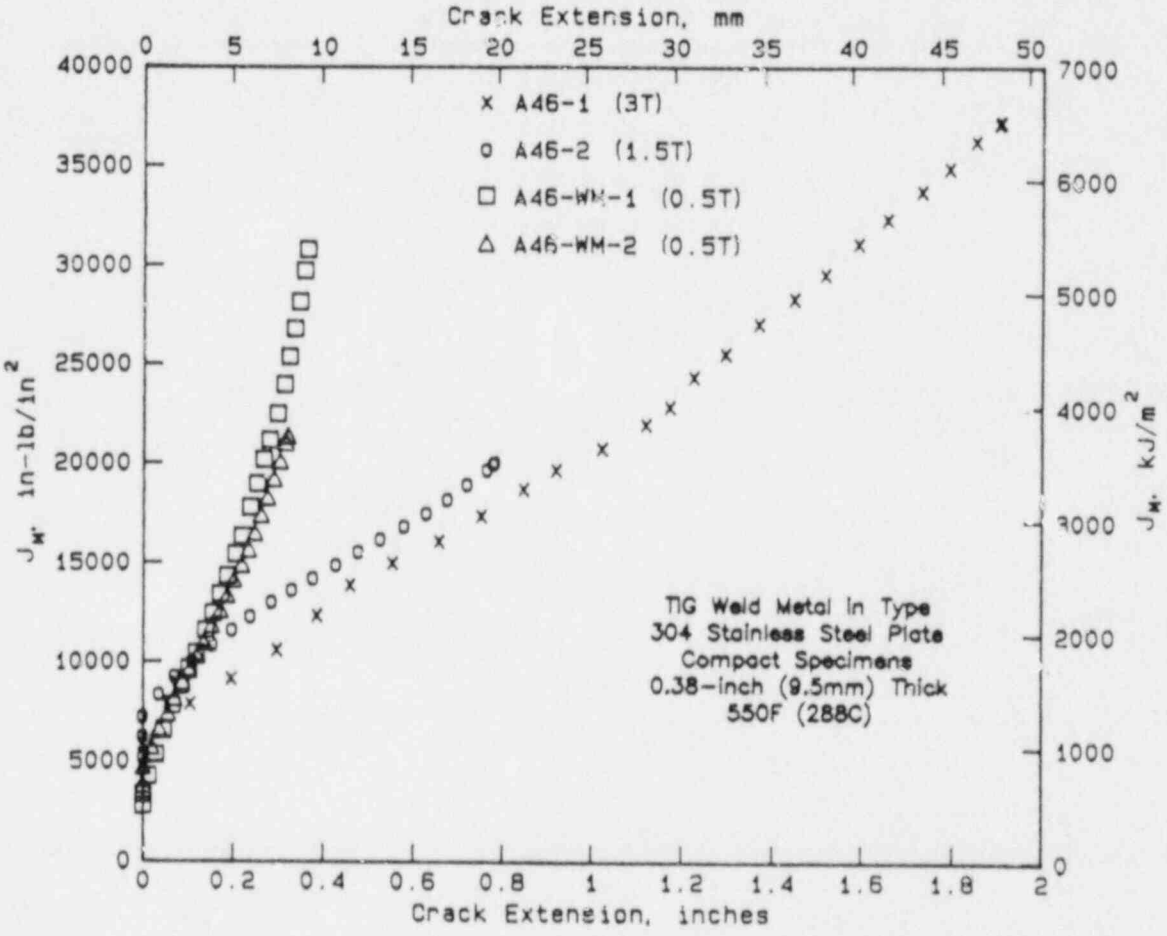

Figure 3.3.12 J_M versus crack extension for a stainless steel TIG weld.

T-4806-F10

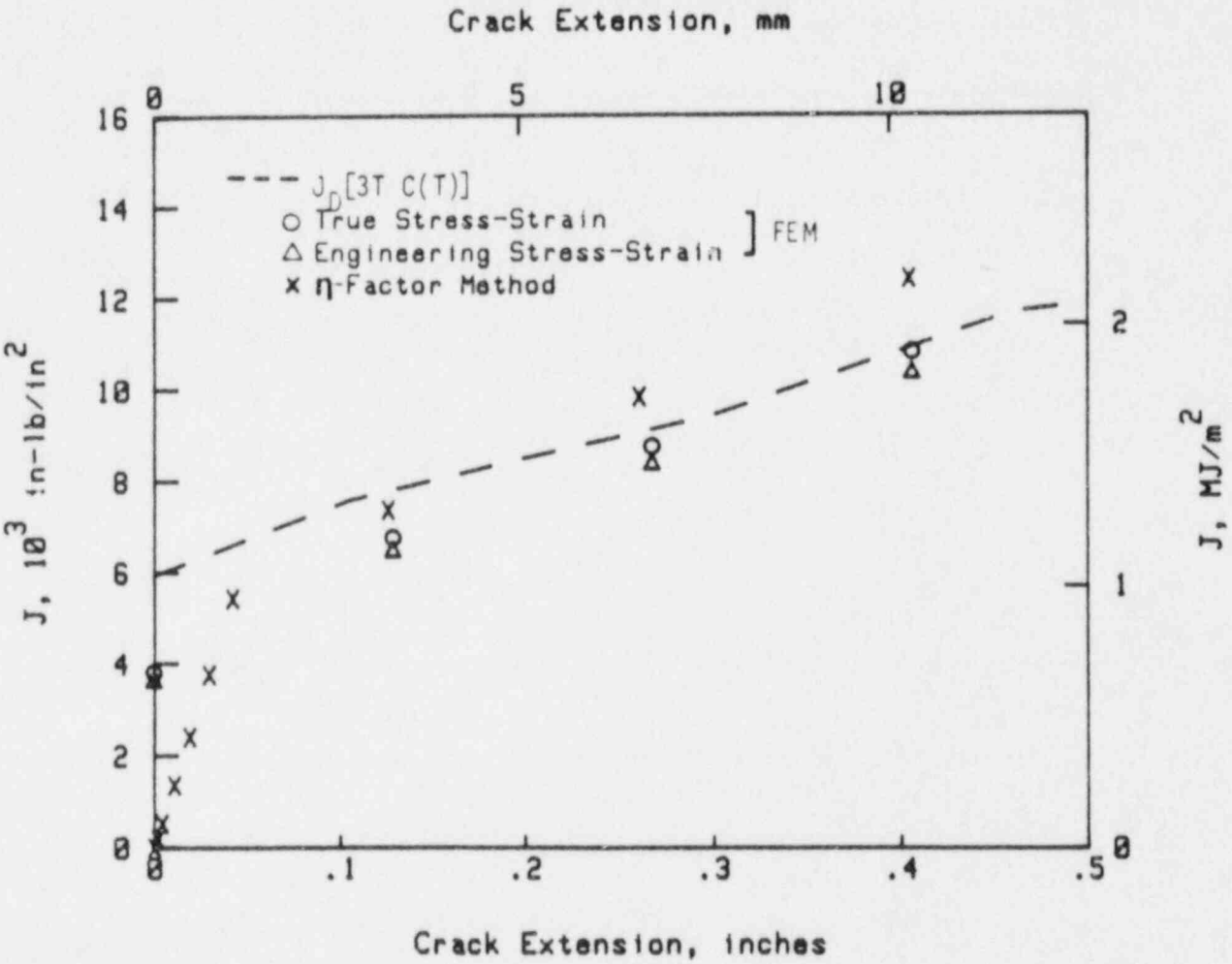

Figure 3.3.13 J-R curves for crack in TIG weld of stainless steel pipe tested at 550 F (288 C); Experiment No 2.

T-4806-F21

specimens were analyzed using the finite element method. These results are summarized below.

- The larger planform specimens had a higher J_i. This is the general trend of the other data.
- With large amounts of crack growth, there was significant geometry dependence of the J_D-R curves (Figure 3.3.14).
- Once the crack growth was greater than 0.25 inch (6.3 mm), the J_M-R curves agreed more closely (Figure 3.3.15). The 1T C(T) specimen J-R curves in this case had a lower slope, which is not consistent with the general trend of the other planform specimen test series.
- The C(T) specimen J_M-R curves agreed quite well with a 16-inch (406-mm) diameter through-wall cracked pipe test using the same weld procedure and the same pipe thickness (Figure 3.3.16). A 6-inch-(152-mm)-diameter pipe with a smaller thickness showed a much higher toughness, probably due to the higher percentage of the tougher TIG weld metal in the thinner weld (Section 2.7).
- The finite element results showed good agreement with the ASTM J_D-R curve during crack growth up to 20 percent of the ligament. (Crack growth in the finite element analysis was limited to 20 percent of the uncracked ligament.) Hence once again this shows that the ASTM testing method is applicable to stainless steels. Additionally, the J_D- and J_M-R curves showed little difference over this crack growth range for these materials.

A516 Grade 70 SAW Tests

This weld was made using a procedure obtained from a U.S. pressurized-water reactor (PWR) vendor. The weldments were made in the same plate used in the first series of planform C(T) specimens described in this section. The 3T and 9.5T specimens were tested with the weld crown left on. All specimen sizes were tested without side-grooves. The test temperature was 550 F (288 C). The results of these tests are summarized below.

- The J_D-R curves are shown in Figure 3.3.17. This was the lowest toughness material tested in the Degraded Piping Program. The initiation toughness of the larger specimens was higher than for the smaller specimens. This is consistent with the other planform C(T) series.
- The 1-T C(T) specimen J_D-R curve agreed well with the 9.5T C(T) specimen J-R curve.

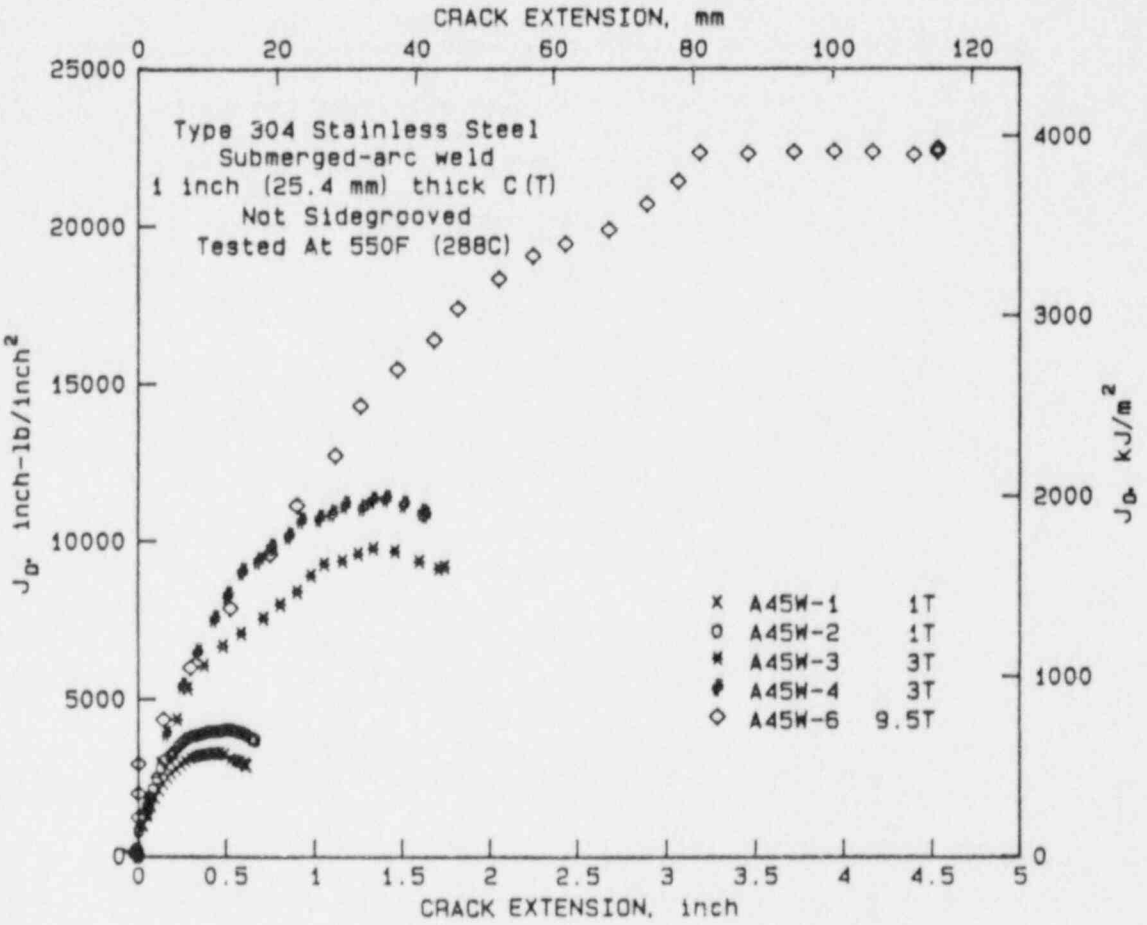

Figure 3.3.14 J_D-R curves for austenitic submerged arc weld metal compact specimens of different planform sizes.

SA-6/86-F3.3.1

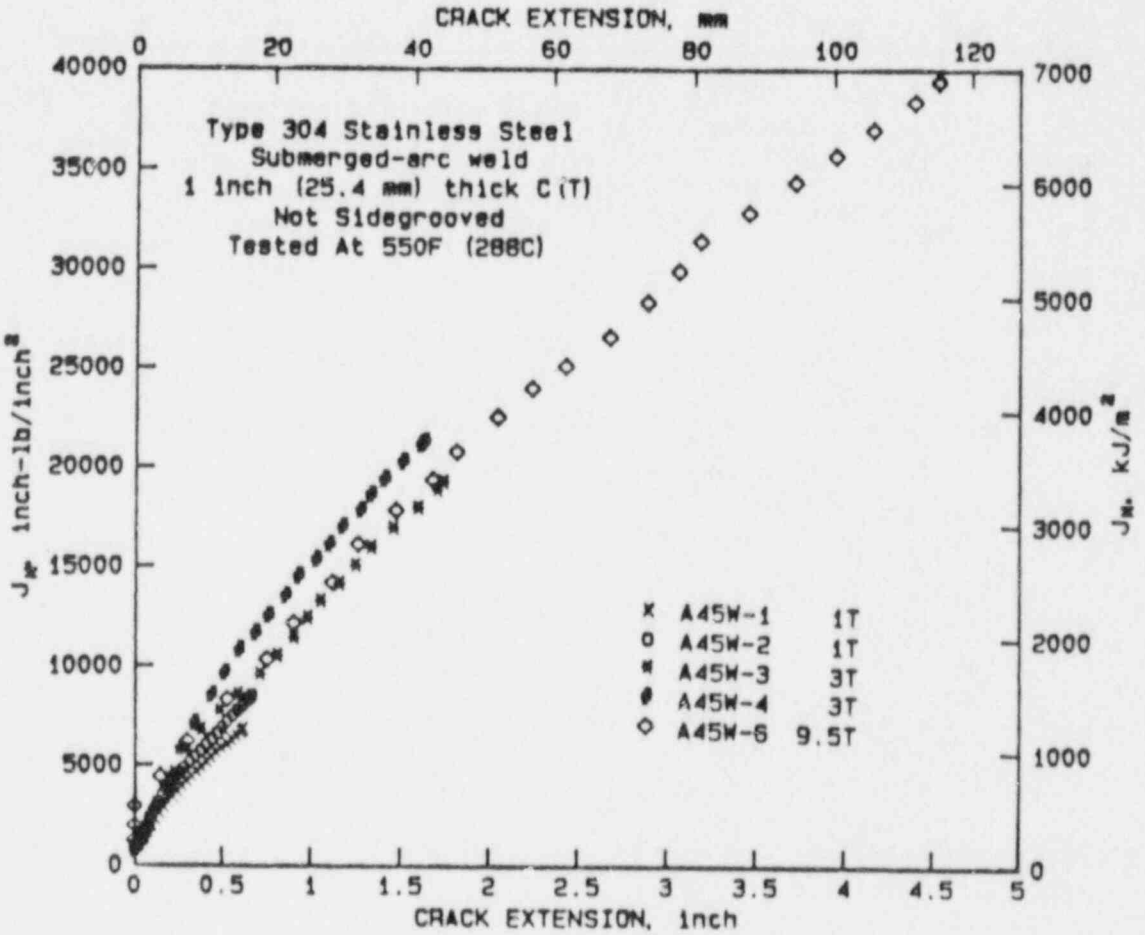

Figure 3.3.15 J_M-R curves for austenitic submerged arc weld compact specimens of different planform sizes.

SA-6/86-F3.3.2

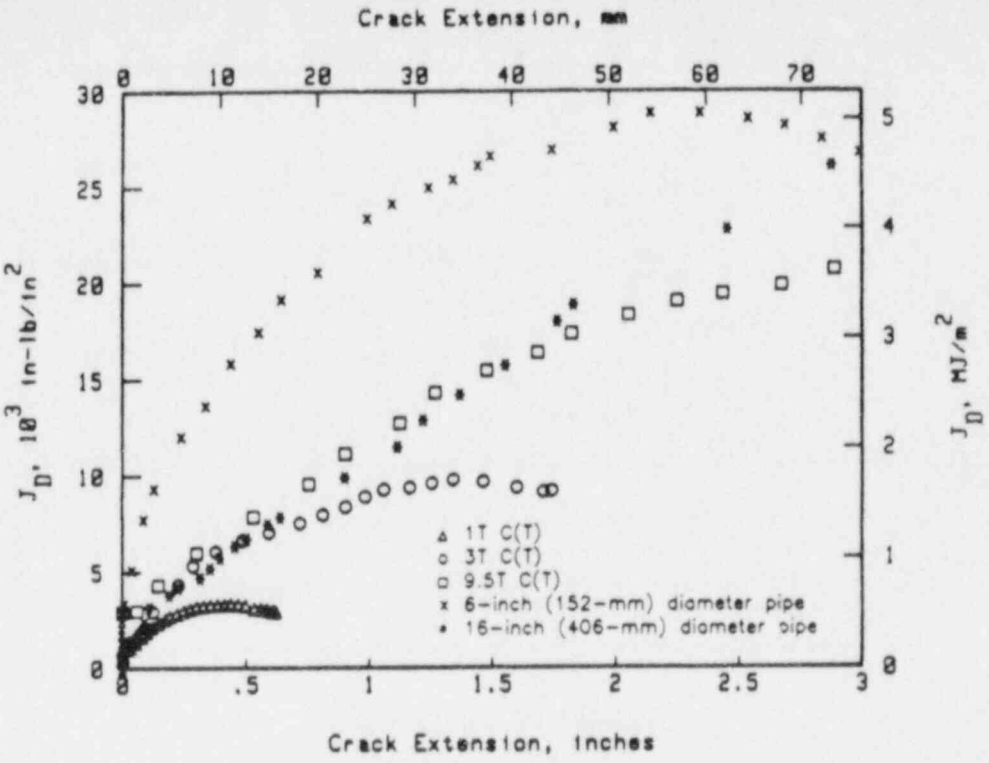

(a) J_D-R curves at 550 F (288 C)

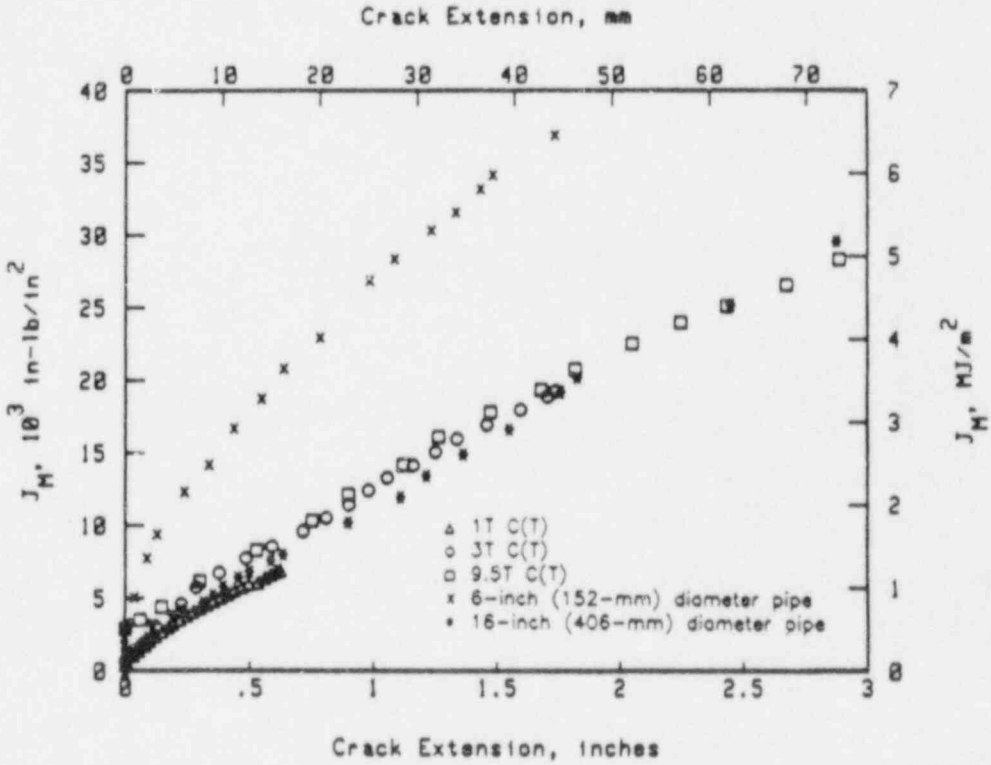

(b) J_M-R curves at 550 F (288 C)

Figure 3.3.16 Comparison of as-welded SAW J-R curves from various size C(T) specimens and pipe experiments.

T-4878-F6.9

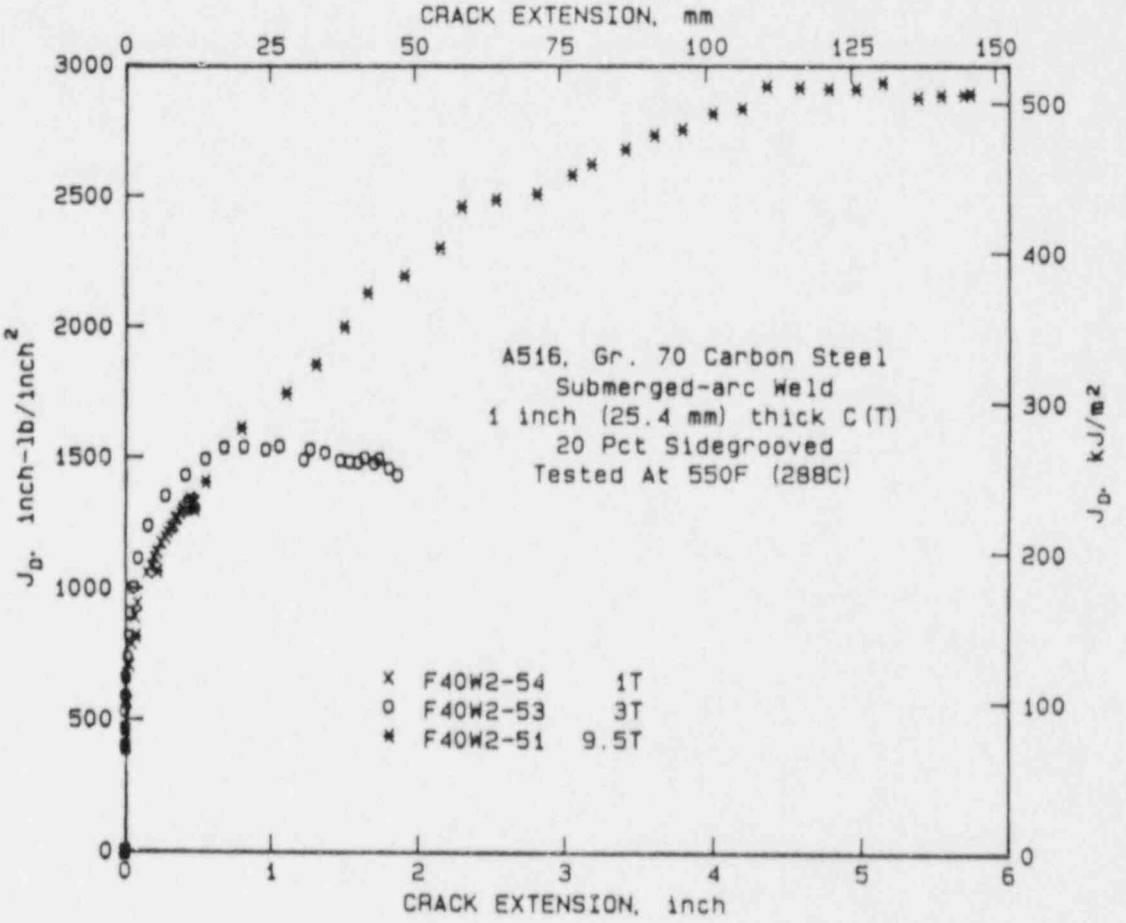

Figure 3.3.17 J_D-R curves for ferritic submerged arc weld compact specimens of different planform sizes.

SA-6/86-F3.3.3

- For the J_M-R curves, the initial slopes of the J-R curves were in agreement. With more than 0.2 inch (5.1 mm) of crack growth, the 1T specimen J_M-R curve was considerably steeper than for the larger specimens (Figure 3.3.18). This is potentially non-conservative behavior, depending on how the through-wall-cracked pipe behaves. A pipe test is currently planned to assess this effect (Section 2.10). It can also be noted in this figure that the 1T specimen J_M-R curve is hooking upward, which is a concern with other J_M-R curve data (Ref. 3.3.5). This upward hooking of J_M-R curves occurs with large crack growth, above the ASTM limits. It was observed in low and high toughness materials (e.g., see the high toughness TIG weld data).

3.3.2 Discussion of Planform C(T) Specimen Results

All of the planform C(T) specimen testing planned for this program has been completed. From the above summary the following trends and observations can be made.

1. In general, the smaller the specimen, the lower the J_i value.

2. In general, J_M did a better job of eliminating the specimen geometry effects than did J_D; however, the J_M analysis was not as good as desired.

3. For J_M, the larger specimens generally gave a lower tearing resistance.

4. The finite element J-values agree well with those calculated by ASTM procedures. Hence the ASTM procedure could be extended to include stainless steels.

5. For the cases where there were pipe tests on the same material the following were found:

   - The TIG weld results showed that the larger planform specimens agreed better with the pipe test J-R curve.

   - The stainless steel SAW results showed that there was little difference between the J_M tearing resistance of the different specimen sizes.

To confirm the trend observed with the TIG weld tests, a ferritic SAW pipe test is to be conducted (see Section 2.10 in this report).

It appears that the prudent approach would be to use a smaller (standard) size specimen to obtain a lower J_i, and a larger specimen to obtain a lower J-R curve slope. The smaller specimen J_i value may be especially important for evaluation of a surface crack in a pipe where there is little crack growth

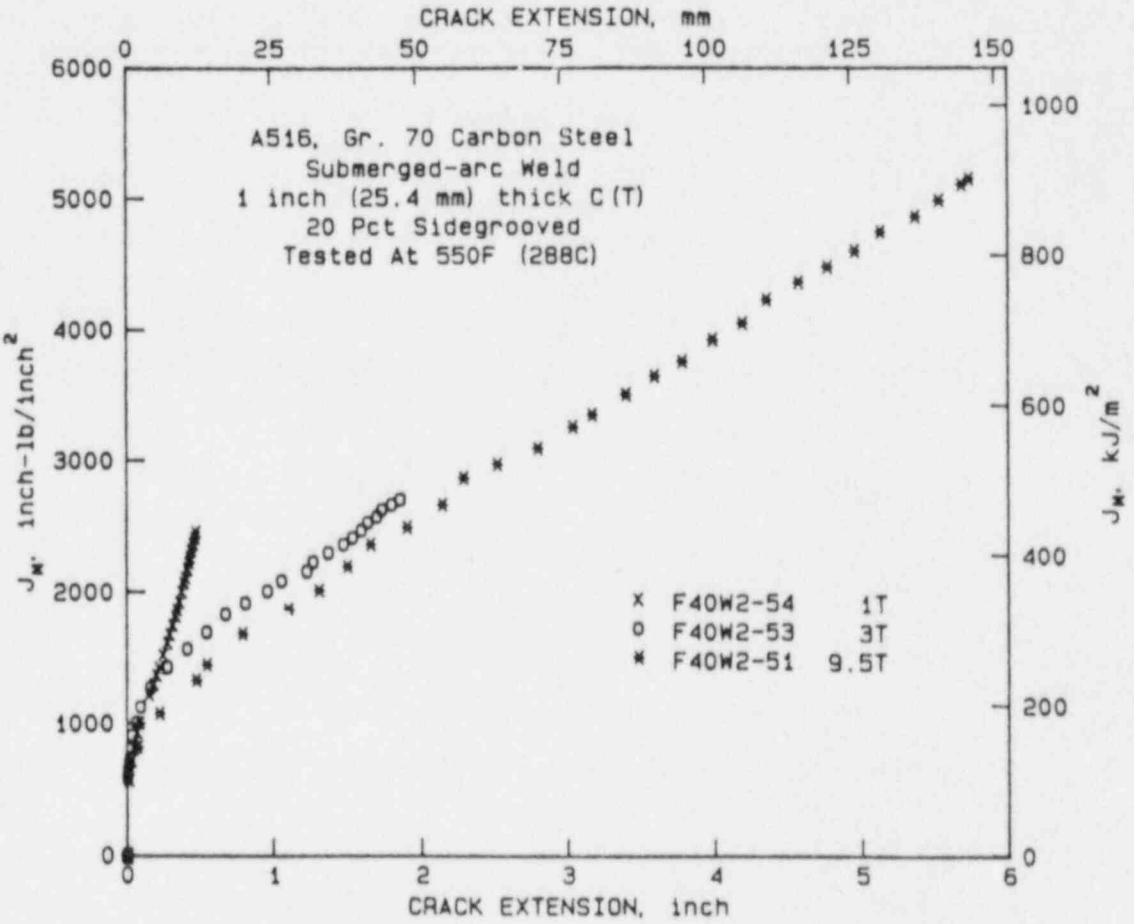

Figure 3.3.18 J_M-R curves for ferritic submerged arc weld compact specimens of different planform sizes.

SA-6/86-F3.3.4

from initiation to maximum load (also see Section 3.5.5). To assess how large a specimen may be needed to get a lower tearing resistance, the data in this section were plotted in a normalized manner. This involved normalizing the tearing resistance of any specimen by that from the largest specimen tested in its series. This normalized tearing resistance was then plotted versus specimen size normalized by the standard size for that specimen thickness. This normalized graph is shown in Figure 3.3.19. The data suggest that a planform specimen of four times the standard size for that thickness should be tested to obtain a lower bound tearing resistance. This is perhaps more important for leak-before-break (LBB) analyses where the stability of a through-wall crack is evaluated.

References for Section 3.3

3.3.1 Wilkowski, G. M.,and others, "Degraded Piping Program - Phase II", Semiannual Report, October 1985-March 1986, NUREG/CR-4082, Vol. 4, September 1986.

3.3.2 Paris, P. C., Burnett, J. V., and Cotter, K. H., "The Effect of Large Crack Extension on the Tearing Resistance of Stainless Steel Piping Materials", in Proceedings of the CSNI Specialist Meeting on Leak-Before-Break in Nuclear Reactor Piping, NUREG/CP-0051, August 1984.

3.3.3 Kramer, G., and Papaspyropoulos, V., "An Assessment of Circumferentially Complex-Cracked Pipe Subjected to Bending", NUREG/CR-4687, October 1986.

3.3.4 Wilkowski, G. M., and others, "Degraded Piping Program - Phase II", Semiannual Report, April 1986-September 1986, NUREG/CR-4082, Vol. 5, April 1987.

3.3.5 Hays, R., and Hackett, E., "Proceedings of the DTRC/NRC Meeting on J_M", To be published as a NUREG report, August 5-6, 1987.

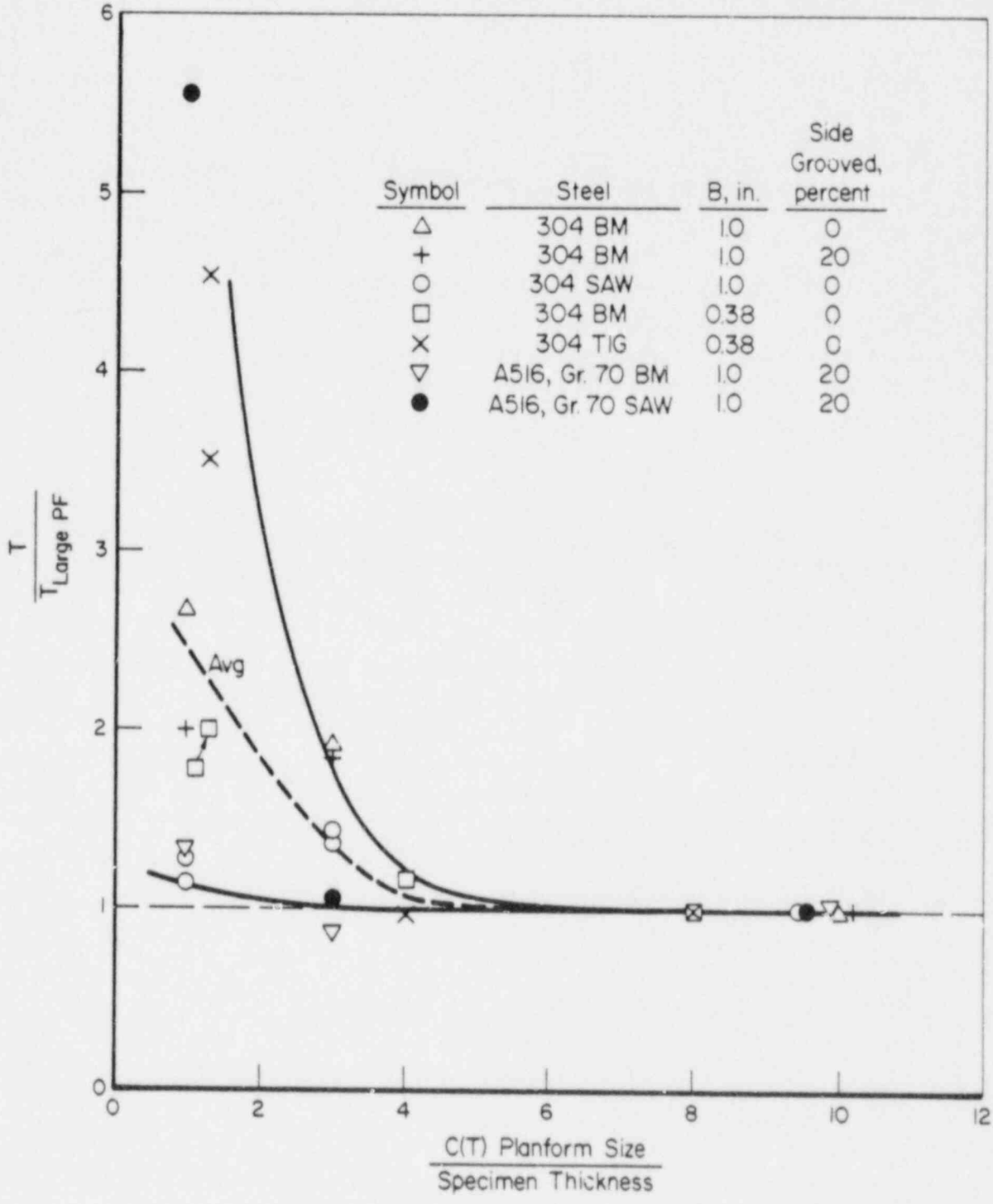

Figure 3.3.19 Graph of normalized tearing modulus (using Modified J) versus normalized planform C(T) specimen size.

3.4 NRCPIPE - A J-estimation Scheme Computer Code for Circumferentially Cracked Pipe

(F. Brust, D. Broek, N. Ghadiali, and G. Wilkowski)

A computer program known as NRCPIPE is being developed specifically for the elastic-plastic fracture mechanics (EPFM) analysis of nuclear power plant piping containing cracks.

At present, the engineering treatment of EPFM is in a stage of development and verification. Many different procedures have been proposed, but all remain largely unvalidated by experimental data. For this reason NRCPIPE includes several analysis procedures. NRCPIPE can, at the user's option, perform the analysis using any of these procedures. In addition, as new procedures are developed, the modular structure of NRCPIPE permits their inclusion. In fact, incomplete blocks of code have been reserved to accommodate new developments.

NRCPIPE is written in BASIC and is available for use on an IBM-PC. In addition, a version of NRCPIPE in BASIC is also available for use on a VAX.

The following sections describe the basic features of the NRCPIPE code.

3.4.1 Objectives of the NRCPIPE Code

Most engineering EPFM techniques are based on the J-integral. The NRCPIPE code is designed to perform EPFM analysis, that is, to establish the fracture-failure conditions of an engineering structure in terms of sustainable load (or stress) or displacement. The analysis procedures focus on circumferentially cracked pipe. Several options are available for different flaw geometries and loading conditions for comparison. This code was used in the analysis efforts throughout the Degraded Piping Program.

The J-integral fracture parameter is used as a basis for this analysis since it is a common fracture parameter in the nuclear industry. The code has two main options. The first is to calculate the loads or displacements for a cracked pipe or specimen, given a J-R curve and tensile test data for the material. The other option is to provide the user with the value of J if the fracture conditions are given as input. In this case, the user provides the program with detailed results of a test.

3.4.2 NRCPIPE Analysis Capabilities

Table 3.4.1 summarizes the crack/structure geometries and loading conditions currently within the scope of NRCPIPE. Both load-control and displacement-control analyses are possible. In these two cases the user supplies a J-resistance curve. In addition, if an experimental load, displacement and crack growth record is available from an experiment, NRCPIPE can calculate the corresponding J-resistance curve for any of the methods.

Table 3.4.1. Estimation scheme methods currently in NRCPIPE.

Structure	Analysis Method Available Within NRCPIPE	Loading[a] Type
Center-Cracked Panel	GE/EPRI	T
Compact-Tension Specimen	GE/EPRI	T
Single-Edge Notch Specimen	GE/EPRI	T
Bend Specimen	GE/EPRI	B
Circumferential Through-Wall Cracked Pipe	GE/EPRI	T,B,T+B
	NUREG/CR-3464	T,B,T+B
	LBB.NRC	T,B,T+B
	LBB.BCL1	T,B,T+B
	LBB.BCL2	T,B,T+B
	Modified GE/EPRI	T,B,T+B
	CEGB.REV. 3	T,B,T+B
Complex-Cracked Pipe	GE/EPRI	T,B,T+B
	NUREG/CR-3464	T,B,T+B
	LBB.NRC	T,B,T+B
	LBB.BCL1	T,B,T+B
	LBB.BCL2	T,B,T+B
	Modified GE/EPRI	T,B,T+B
	CEGB.REV. 3	T,B,T+B
Surface-Cracked Pipe	SC.SEN	B
	SC.Thin	B
	SC.Thick	B
	CEGB. Rev. 3	T,B,T+B

(a) T = Tension, B = Bending, T+B = Tension + Bending.

Currently the code is modified to incorporate the following features:

- Improvement in the user-friendliness of the code
- Improvement of the NUREG/CR-3464, LBB.NRC, LBB.BCL1, and LBB.BCL2 computational times by improving the iteration schemes currently used (It is desired to reduce the calculation time on an IBM-PC to less than one minute.)
- Development of standard check problems using data from the Degraded Piping Program pipe fracture experimental database
- Development of a simplified user's manual with a check problem for the user.

3.5 Round-Robin Activities

(C. Marschall, M. Landow, V. Papaspyropoulos,
F. Brust, M. Nakagaki, J. Ahmad,
N. Ghadiali, and G. Wilkowski)

During the course of the Degraded Piping Program, numerous round-robin activities were undertaken. In most of these cases, Battelle was the organizer, but in some cases Battelle was a participant in NRC contractor round-robin efforts. These efforts were essential to verification of experimental or analytical techniques relative to this program. The major efforts were:

- Tensile testing evaluations using Type 304 stainless steel at room temperature and 550 F (288 C).
- Calculation procedure evaluations for J_D- and J_M-R curves, using given load-displacement-crack growth data from a C(T) specimen.
- A C(T) specimen-testing evaluation of the d-c electric potential method for monitoring the crack initiation and crack growth during a J-R curve test.
- Finite element anlaysis of a 10T C(T) specimen and a circumferential through-wall cracked pipe. (This involved large crack growth in stainless steel base metal.)
- Finite element and J-estimation scheme analysis of a FWFN(T) specimen and a circumferential surface-cracked pipe. [This involved A106 Grade B pipe base metal at 550 F (288 C).]

Of these efforts the finite element round-robin was documented in a topical report in this program:

> Ahmad, J., Nakagaki, M., Brust, F., and Wilkowski, G., "Elastic-Plastic Finite Element Analysis of Crack Growth in Large Compact Tension and Circumferentially Through Wall-Cracked Pipe Specimen", NUREG/CR-4573, October 1986.

The different round-robin efforts and their results are summarized in the following sections.

3.5.1 Tensile-Test Round-Robin

Tensile tests are conducted on nuclear reactor materials to provide strength properties and stress-strain data for fracture analysts. Battelle organized and conducted a tensile-test round-robin to ensure that test results obtained by the various contractors and delivered to the NRC are not laboratory dependent. A detailed description of the procedures and results was presented in the Fourth Semiannual Report (Ref. 3.5.1). A summary of the procedures and findings is presented here.

Participants in the tensile-test round-robin were:

Laboratory	Responsible Individual
Battelle	M. P. Landow
MEA	A. Hiser
DTRC	R. Hays

Each participant received 6 nominally identical tensile specimens machined from a 6-inch (152-mm)-diameter, Schedule 120, SA-376 Type 304 stainless steel pipe. This material was selected because of its high ductility, which can cause problems in obtaining a complete stress-strain curve to fracture. These problems include: (1) exceeding the capacity of the elongation gage, and (2) slippage of the elongation gage during a test, due to large amounts of diameter reduction prior to neck formation.

Specimens were of the round-bar type with threaded ends and were machined such that the tensile axis was aligned with the pipe axis. The reduced section of each specimen had a length of 1.25 inches (31.8 mm) and a diameter of 0.250 inch (6.35 mm). To favor neck formation and fracture at midlength, the reduced section was tapered slightly such that the diameter was 0.001 to 0.002 inch (0.025 to 0.050 mm) smaller at the middle than at the ends. Each laboratory tested 3 specimens at room temperature and 3 specimens at 550 F (288 C), employing procedures that were typical for that laboratory.

The results of the tensile-test round-robin indicated that the tensile properties and stress-strain curves were not significantly laboratory dependent. Figure 3.5.1 shows engineering stress-strain curves obtained by the 3 laboratories at room temperature. For the ultimate tensile strength (UTS), percent elongation, and percent area reduction, standard deviations were less than 3 percent at both test temperatures. A somewhat larger standard deviation was observed for the yield strength: 3.6 percent at room temperature and 6.1 percent at 550 F (288 C). The greater observed variability in yield strength is perhaps to be expected because: (1) the yield strength is more sensitive to small microstructural differences than are the other properties, and (2) more judgment is required in selecting the 0.2 percent offset yield load than for the other properties.

The reproducibility of the data was analyzed in another way that recognizes the attempt of fracture analysts to fit a mathematical expression to the stress-strain data. A commonly used expression is the Ramberg-Osgood equation:

$$\epsilon/\epsilon_0 = \sigma/\sigma_0 + \alpha(\sigma/\sigma_0)^n \qquad (3.5.1)$$

where σ is stress, σ_0 is a reference stress (sometimes yield stress or flow stress is used), ϵ is strain, and ϵ_0 is a reference strain equal to σ_0/E, where E is Young's modulus. This expression will produce a straight line having a slope of n and an intercept of log α if log $(\epsilon/\epsilon_0 - \sigma/\sigma_0)$ is plotted

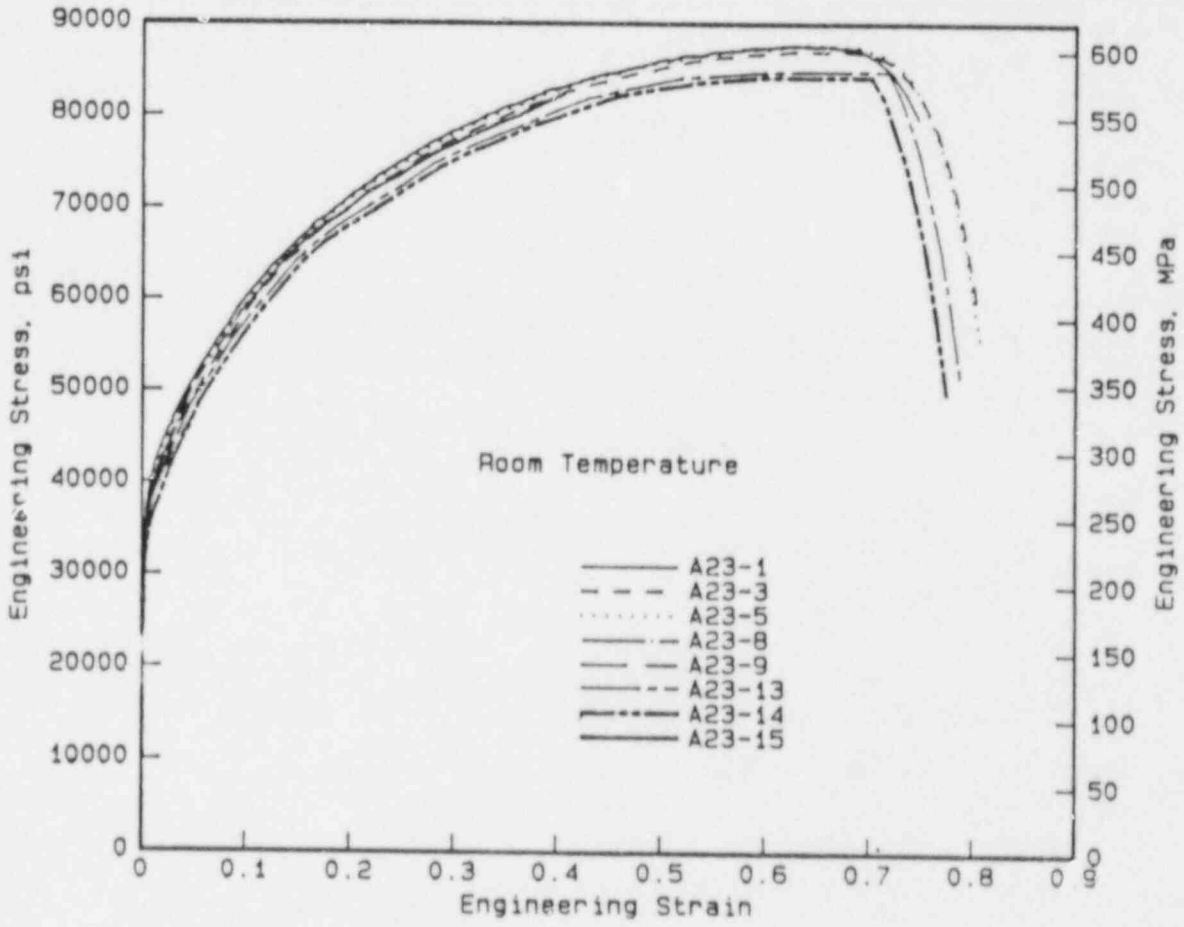

Figure 3.5.1 Stress-strain curves obtained from round-robin for room temperature tests.

SA-6/86-F3.1.4

against log (σ/σ_0). As was noted in the Second Semiannual Report (Ref. 3.5.1), stress-strain curves for austenitic stainless steel tend not to be amenable to good fitting by Eq. 3.5.1 over the entire stress-strain curve. For that reason, the round-robin data were subjected to Ramberg-Osgood analysis over three different regions of strain: (1) the entire curve, (2) the low strain region (up to 5 percent), and (3) the high strain region (greater than 5 percent).

Linear regression analysis was used to fit straight lines to the Ramberg-Osgood graphs and, thereby, to obtain values of the parameters α and n. The graph for the entire stress-strain area is shown in Figure 3.5.2. Good reproducibility of the parameters was found for the high-strain portion of the stress-strain curves (standard deviation about 5 percent) and for the entire stress-strain curves (maximum standard deviation about 7 percent). However, reproducibility was poor, particularly for α (16 to 34 percent standard deviation) when only the low-strain portion of the stress-strain curve was analyzed. This observation probably reflects the fact that the lower ends of the curves in the low-strain region represent very small strain values that are subject to sizable measurement errors on a percentage basis.

On the basis of the tensile-test round-robin, it was concluded that tensile properties determined by the three laboratories were not significantly laboratory dependent. It was concluded also that if fracture analysis should determine that low-strain data ($\epsilon < 5$ percent) are more important than high-strain data in applying tensile curves to the analysis of cracked pipes, additional attention should be given by experimenters to more accurately defining the stress-strain relations in that region.

3.5.2 J-Calculation Round-Robin

Methods used for calculating the ductile fracture resistance parameter J have undergone several changes in the past several years. To check the reproducibility of the various J-values calculated at different laboratories, Battelle organized and conducted a J-calculation round-robin. A detailed description of the round-robin was presented in the Fourth Semiannual Report (Ref. 3.5.1). A summary is presented here.

Participants in the J-calculation round-robin were:

Laboratory	Responsible Individual
Battelle	M. P. Landow
Oak Ridge National Laboratory	R. K. Nanstad
DTRC	R. E. Link
MEA	A. Hiser
Westinghouse	D. McCabe

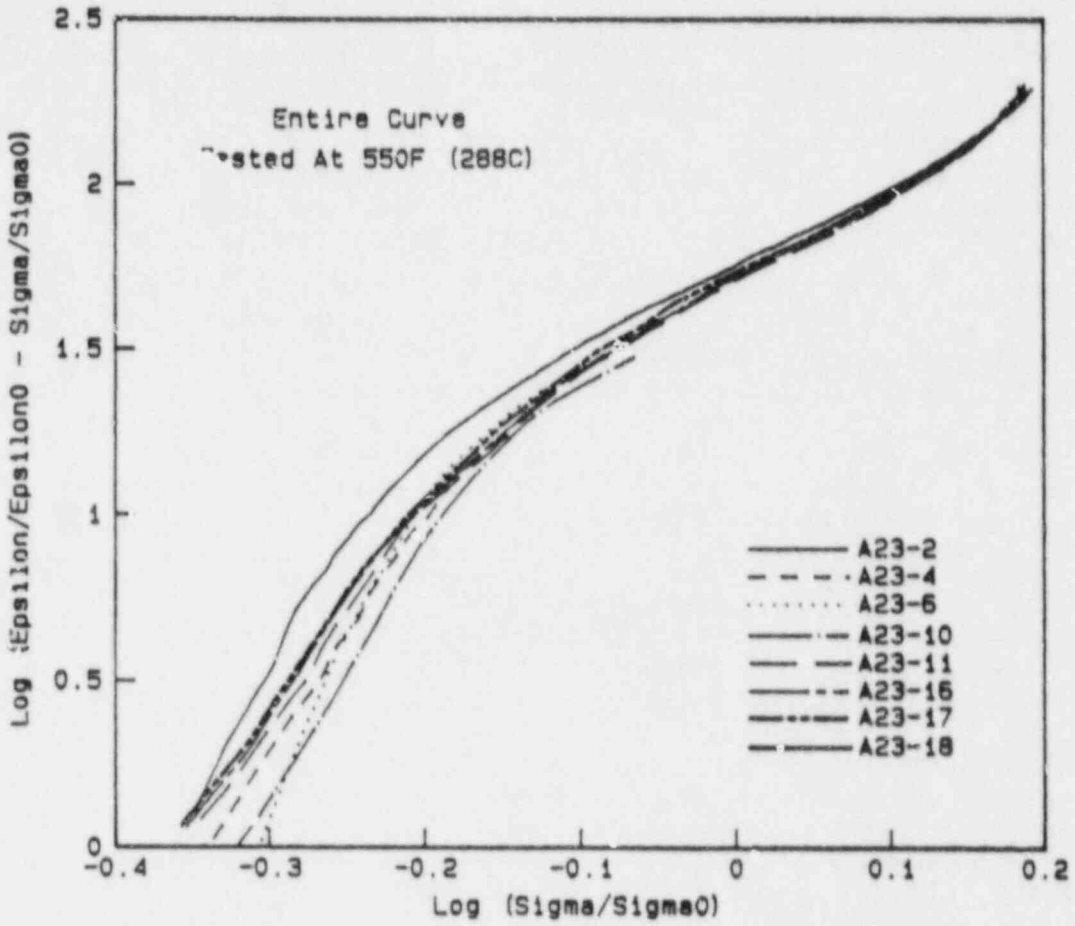

Figure 3.5.2 Logarithmic plot of entire stress-strain curve round-robin data.

SA-6/86-F3.1.6

Each participant received experimental data from a fracture toughness test on a 10T planform-size, 1-inch (25.4mm)-thick compact specimen of Type 304 stainless steel tested at 550 F (288 C). The data sets included load, displacement, crack length, and calculated compliance. Participants were requested to calculate J_D* and J_M; however, each calculated J_D and several calculated J_M* as well. The various J parameters are described below; each parameter accounts for crack growth:

- J_D is deformation J calculated by the method described in ASTM E813-81, Standard Method for J_{IC}, A Measure of Fracture Toughness.
- J_D* is calculated in essentially the same way as J_D, except that J is separated into elastic and plastic portions.
- J_M denotes modified J and was proposed by Ernst (Ref. 3.5.2) as a method for extending the usefulness of J to crack growth values well beyond 10 percent of the original ligament. It differs from J_D primarily in that it contains an extra plasticity term in the calculation; thus, for a growing crack, J_M always exceeds J_D and the magnitude of the difference increases with increasing crack extension.
- J_M* is calculated in the same way as J_M, except that it is divided into elastic and plastic components.

The results of the J-calculation round-robin indicated that even though exact agreement was not found among all five laboratories for any of the J parameters, the differences were sufficiently small to eliminate calculational procedures as a source of concern in accurately determining J-R curves.

3.5.3 Electric Potential Round-Robin

Single-specimen methods for determining J-R curves are gradually replacing the multiple specimen method in many laboratories. One single-specimen method, that employs direct-current electric potential measurements to monitor crack growth, is increasing in popularity. No standard method yet exists for conducting electric potential measurements. Consequently, a variety of methods are in use.

At the direction of the NRC, a round-robin of NRC contractors has been organized and is being conducted by the DTRC. Battelle is one of the participants. During the current reporting period, Battelle tested three carbon-steel and three aluminum-alloy compact specimens that had been machined and precracked at DTRC. The data from those tests were reduced and the results have been sent to DTRC, along with a complete description of the experimental procedures.

3.5.4 Finite Element Round-Robin of a 10T C(T) and Circumferential Through-Wall-Cracked Pipe

The objective of this round-robin effort was to assess the accuracy of finite element methods to calculate the J-R curve for large amounts of ductile crack growth in a very ductile material. The material was Type 304 stainless steel. Two problems were solved. The first was a two dimensional problem that involved determining the J-R curve for a 10T C(T) specimen with 6 inches (152 mm) of crack growth. The second was a three-dimensional problem that involved calculating the J-R curve for a 16-inch (406-mm) diameter circumferential through-wall-cracked pipe in four-point bending. There were also 6 inches (152 mm) of ductile crack growth in the pipe problem.

Nine organizations from five countries participated in this round-robin (Table 3.5.1). The results of this round-robin are published in Reference 3.5.3. These results are briefly reviewed below.

10T C(T) Stainless Steel Finite Element Round-Robin Results

The 10T C(T) specimen was a planform specimen that was 1 inch (25.4 mm) thick, see Section 3.3.1 of this report. The test was conducted at Battelle at 550 F (288 C). The geometry of the specimen is shown in Figure 3.5.3. The material stress-strain curve was given to all of the participants as well as the crack growth versus load-point displacement curve. Table 3.5.2 summarizes the variables used by the different participants in this problem.

The calculated load versus load-line displacement values are compared to the experimental data in Figure 3.5.4. In general there is good agreement up to crack initiation, and more variation during crack growth.

The calculated J-R curves are given in Figure 3.5.5. The ASTM calculated J_D-R curve and the J_M-R curve from the experimental data are also shown. The J_i values from all participants but Participant 5 are in good agreement with each other and those calculated from the experimental data. The finite element J-R curve from Participant 5 was significantly lower than the other curves. The J-R curves from Participants 1, 2, and 4 show a continuously rising J-R curve which is close to the J_M-R curve. These three solutions modeled the growing crack by the node release method.

The J-R curve solution by Participant 3 was much lower and was in closer agreement to the J_D-R curve from the experimental data. This solution modeled the growing crack by using multiple meshes with different crack lengths. Therefore, the results of Participant 3 do not reflect the crack growth history dependence on the computed J-R curve. As expected, these results agree with the deformation theory J-R curve using the experimental data.

In summary, all of the solutions in terms of the computed J-R curves are within 20 percent of each other, with the exception of the solution of Participant 5. The computed J values of this solution are considerably lower, even at crack

Table 3.5.1. List of Participants and Affiliations.

Technical Research Center, Finland
Dr. K. Ikonen Mr. T. Mikkola Dr. H. Talja
Commissariat à l'Energie Atomique, Cadarache, France
Dr. E. de Langre
Gesellschaft für Reaktorsicherheit m.b.H., West Germany
Dr. D. Azodi
Materialprüfungsanstalt Stuttgart, West Germany
Mr. K-H. Herter Dr. A. Sauter
University of Tokyo, Japan
Prof. T. Miyoshi Prof. Y. Yoshida
Central Research Institute of Electric Power, Japan
Dr. K. Kashima Dr. Y. Takahashi
Kawasaki Heavy Industries, Japan
Mr. T. Shimakawa
Yokohama National University, Japan
Prof. M. Shiratori
Battelle Columbus Division, USA
Dr. J. Ahmad Mr. N. Ghadiali Dr. M. Nakagaki Ms. V. Papaspyropoulos Mr. G. Wilkowski

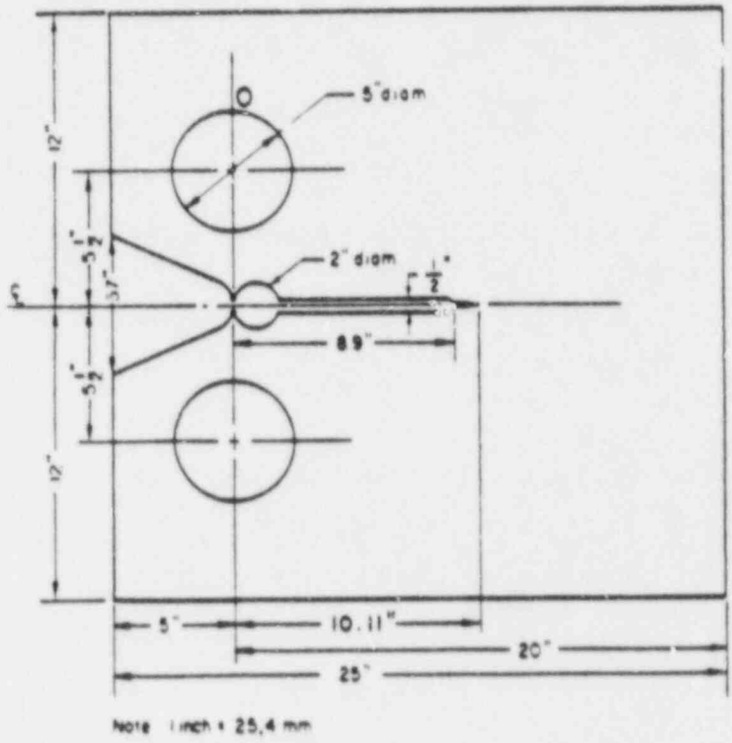

Figure 3.5.3 Geometry of the 1.0-inch- (25-mm)-thick 10T-C(T) specimen.

SA-12/87-F3.5.3

Table 3.5.2 Variables used in the round-robin finite element analyses of the 101 compact specimen (Problem A)

Participant	(3)	(4)	(5)	(2)	(1)
No. & Type of Elements	90 8-noded isoparametric	482 8-noded isoparametric	488 8-noded isoparametric	327 constant strain triangles	263 8-noded isoparametric
No. of nodes	340	482	592	201	879
Integration Order	3x3 Gauss	2x2 Gauss	2x2 Gauss		3x3 Gauss
Type of Analysis and Formulation	2D plane stress small deformations small strains	2D plane stress large deformations small strains	2D plane stress small deformations small strains	2D plane stress small deformations small strains	2D plane stress large deformations large strains
Equilibrium Compensation		Mod. Newton Raphson			Mod. Newton Raphson
Crack Extension Procedure	N.A.•	Node shift & node release	Node shift & node release	Nodal force release	Nodal force release
Yield Surface	Von Mises	Von Mises	Von Mises	Von Mises	Von Mises
Hardening Model	Isotropic	Isotropic	Isotropic	Isotropic	Isotropic
σ-ε Curve	Engineering	True	True	True	True
J-Computation	VCE	VCE	VCE	Contour Integral	Contour Integral

• Multiple analyses performed for 5 different crack lengths

T-4573-T5.1

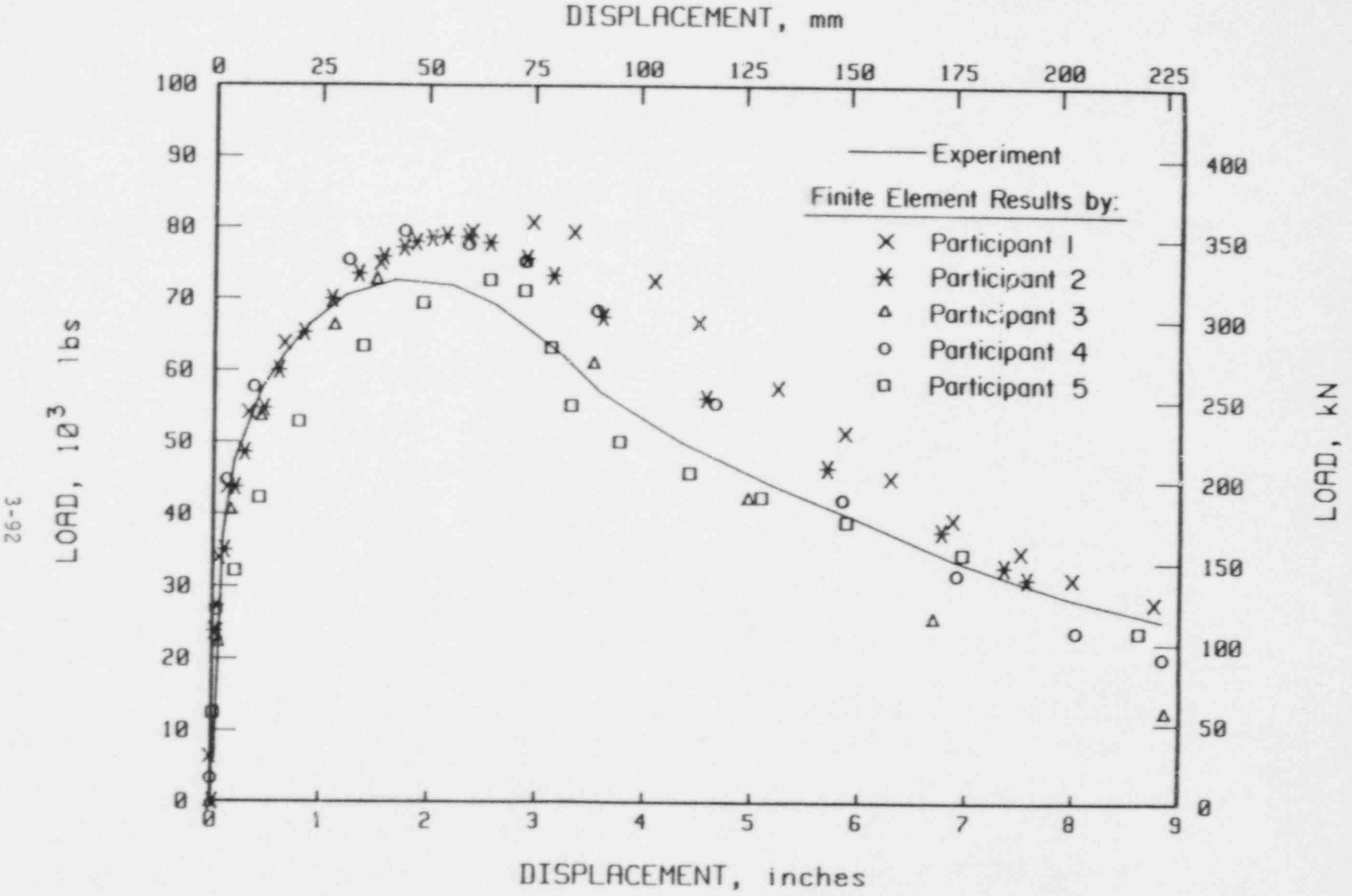

Figure 3.5.4 Comparison of the finite element analysis results for the C(T) specimen (Problem A) with experimental data.

SA-12/87-F3.5.4

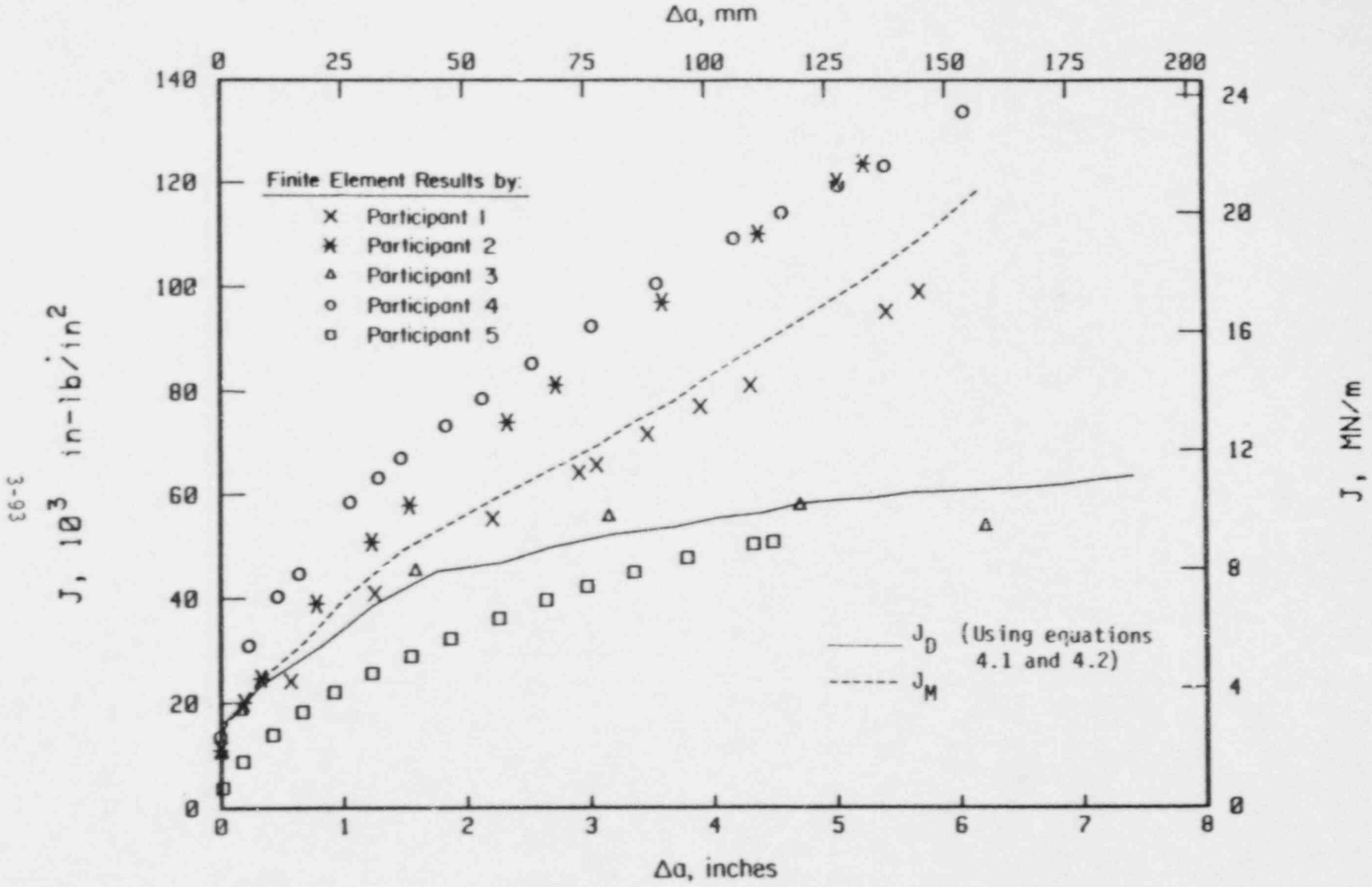

Figure 3.5.5 Comparison of the J (far field) versus crack growth curves computed by finite element analysis with the J_D and J_M resistance curves (Problem A).

SA-12/87-F3.5.5

initiation, compared to the other solutions. This is consistent with the corresponding lower load versus displacement results from Participant 5. A rechecking of these values is in progress.

Finite Element Round-Robin Analysis of Circumferentially Through-Wall-Cracked Pipe

The circumferentially through-wall-cracked pipe problem was on a 16-inch (406-mm) diameter 1.03-inch (26.2-mm) thick Type 304 stainless steel pipe. This pipe test was conducted as part of an Electric Power Research Institute (EPRI) program at Battelle (Ref. 3.5.4). The test was conducted at room temperature. Since this pipe was made from a different material than the material of the plate used in the C(T) specimen, and since this test was run at a different test temperature, the J-R curves from these two problems should not be compared to each other.

A schematic of the test apparatus and the crack geometry is shown in Figure 3.5.6. The participants were given the stress-strain data and the crack growth versus load-point displacement data.

Table 3.5.3 gives the variables used in the finite element analysis by the different participants. Out of the five participants, only one used shell elements. The others used brick elements.

The calculated and experimental load versus load-point displacement is shown in Figure 3.5.7. The agreement is good in the linear-elastic range, but the finite element results underpredict the experimental loads, even at crack initiation. This is typical of all the other comparisons we have made in the Degraded Piping Program, even using experimental data from other sources.

The calculated J versus load-line displacement values are given in Figure 3.5.8. The J_D and J_M values calculated from the experimental data are also given in this figure. The agreement is quite good up to 12 inches (305 mm) of displacement.

The load versus J values are shown in Figure 3.5.9. The finite element values are compared to the J values from J-estimation schemes that use the experimental pipe fracture data. Participant 1 shows reasonable agreement with the estimation scheme results. Subsequent analysis of the solution by Participant 1 showed that when they increased the number of iterations for convergence, their analysis results agreed with the results of the other participants (Ref. 3.5.5). Consequently their refined analysis agreed with the other solutions, but were not as close to the experimental data.

The J-R curves from the finite element and the estimation schemes are shown in Figure 3.5.10. The J at initiation values are very close for all the finite element solutions. Participant 4 only solved the problem up to crack initiation. The J-R curves from Participants 1, 2, 3, and 5 are in reasonable agreement with each other. They differ from the estimation J-R curves at initiation, where the finite element values are higher. This is surprising

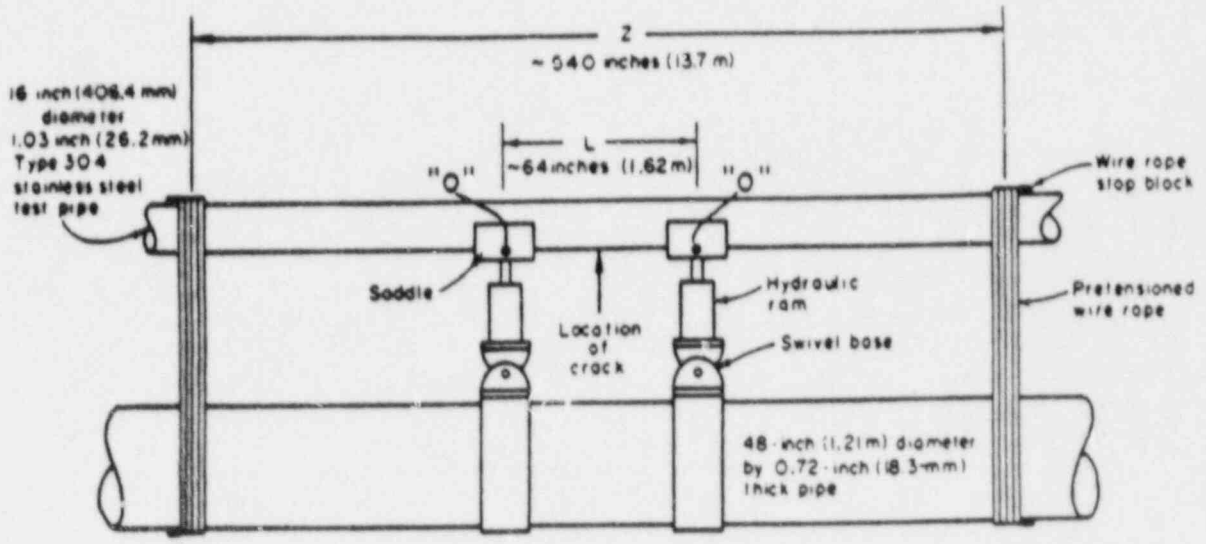

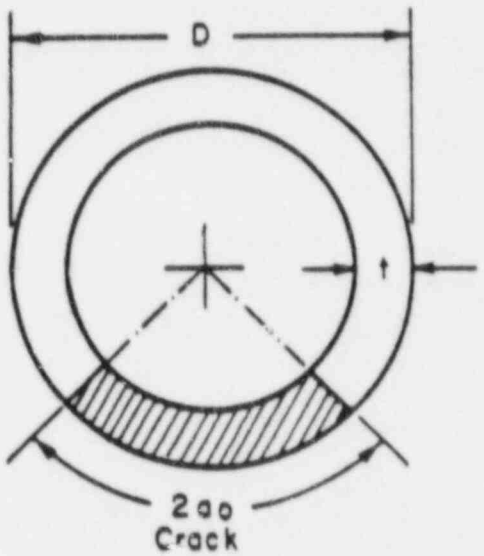

D = 16" (406.4 mm)

t = 1.03" (26.16 mm)

$2a_0/\pi D = 0.3675"$

Figure 3.5.6 The apparatus and cracked pipe geometry for 16-inch (406.4-mm) outside diameter pipe bending experiment.

Table 3.5.3 Variables used in the round-robin finite element analysis of the 16-inch (406 mm) pipe (Problem B)

Participant	(1)	(4)	(2)	(3)	(5)
No. & Type of Elements	142 16-node isoparametric	1107 3-node shell	130 20-node isoparametric	304 thick shell	142/60 20-node Brick/general
No. of nodes	974	616	1133	337	1102
Integration Order	3x3x2 Gauss	1 Gauss	2x2x2 Gauss	1 Gauss	3x3x3 Gauss
Finite Deformation	No	Yes Small strain	Yes Small strain	No	No
Equilibrium Compensation	Yes	No	Mod. Newton-Raphson	Newton-Raphson	Newton-Raphson
Crack Extension Procedure	Node release	No	Node shift & release	Node release	Node release
Yield Surface	Von Mises	Von Mises	Von Mises	Von Mises	Von Mises
Hardening Model	Isotropic	Isotropic	Isotropic	Kinematic	Isotropic
σ-ε Curve	Engineering	Engineering	True	True	Engineering
J--Computation	VCE	VCE	VCE	VCE	VCE

T-4573-T5.2

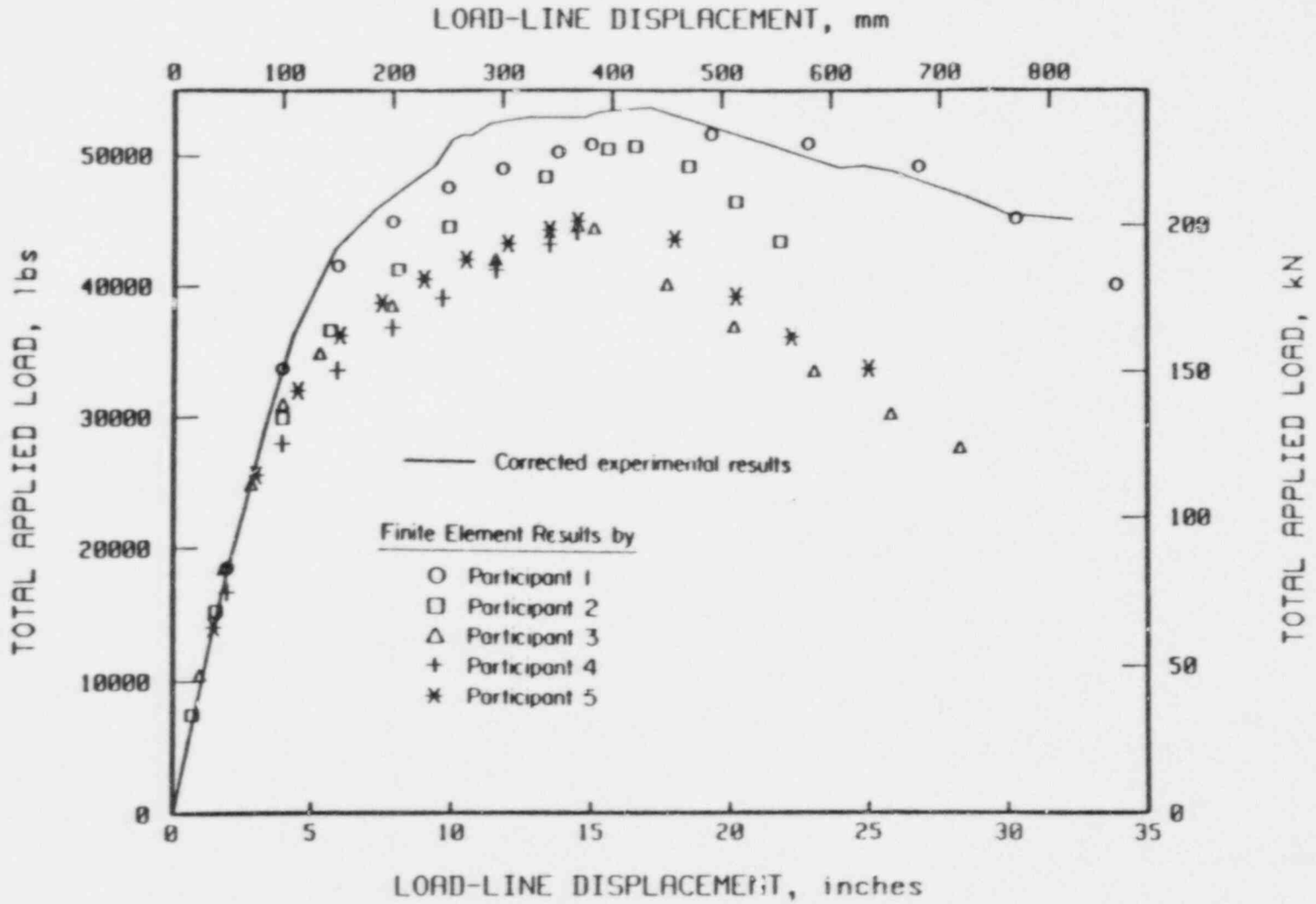

Figure 3.5.7 Comparison of the finite element analysis results for Problem B with experimental data. (Experimental data corrected for machine compliance and dead weight of pipe.)

T-4573-F5.5

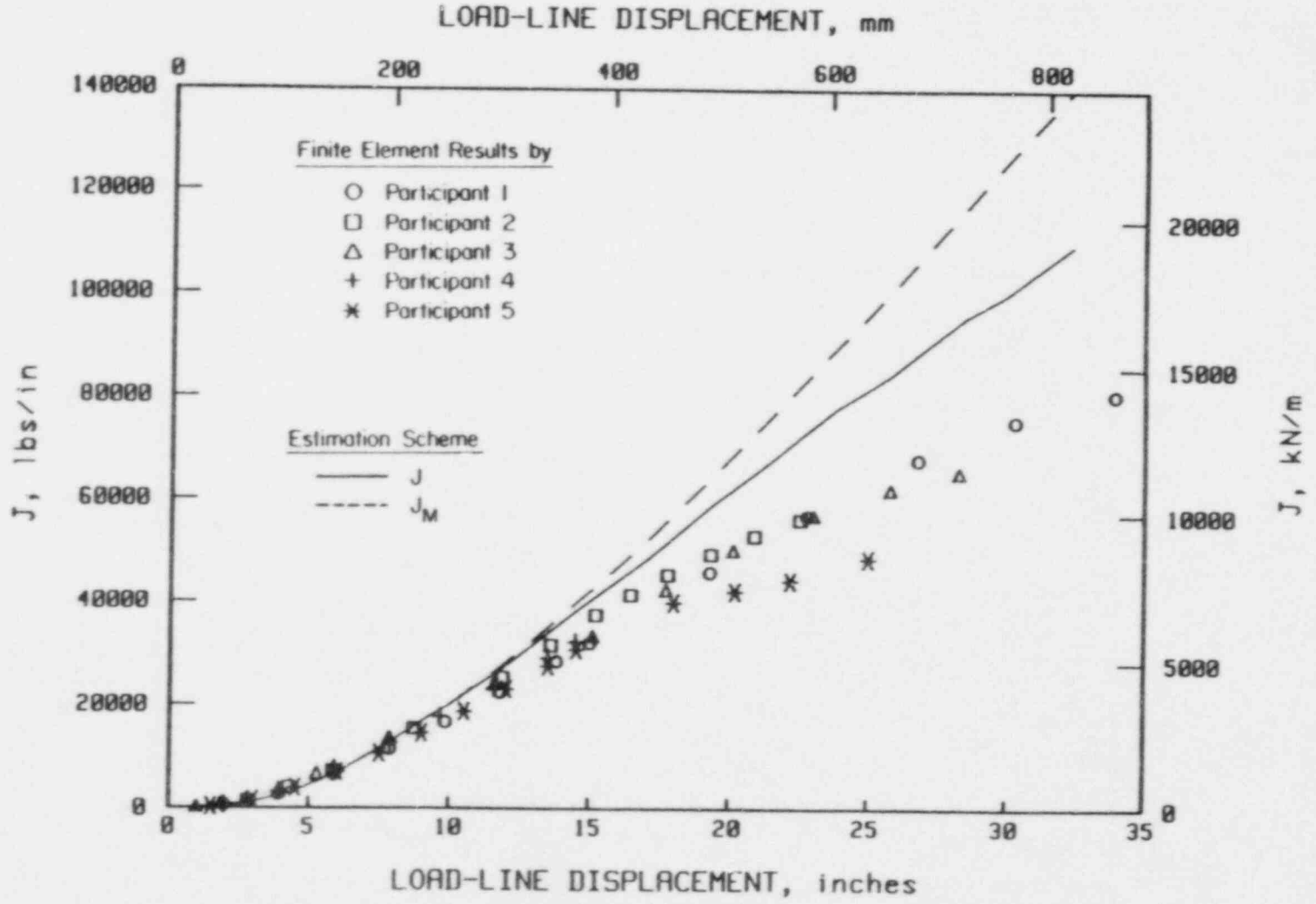

Figure 3.5.8 J versus load-line displacement computed by finite element analysis and by J-estimation scheme for circumferential through-wall cracked pipe problem.

T-4573-F5.6

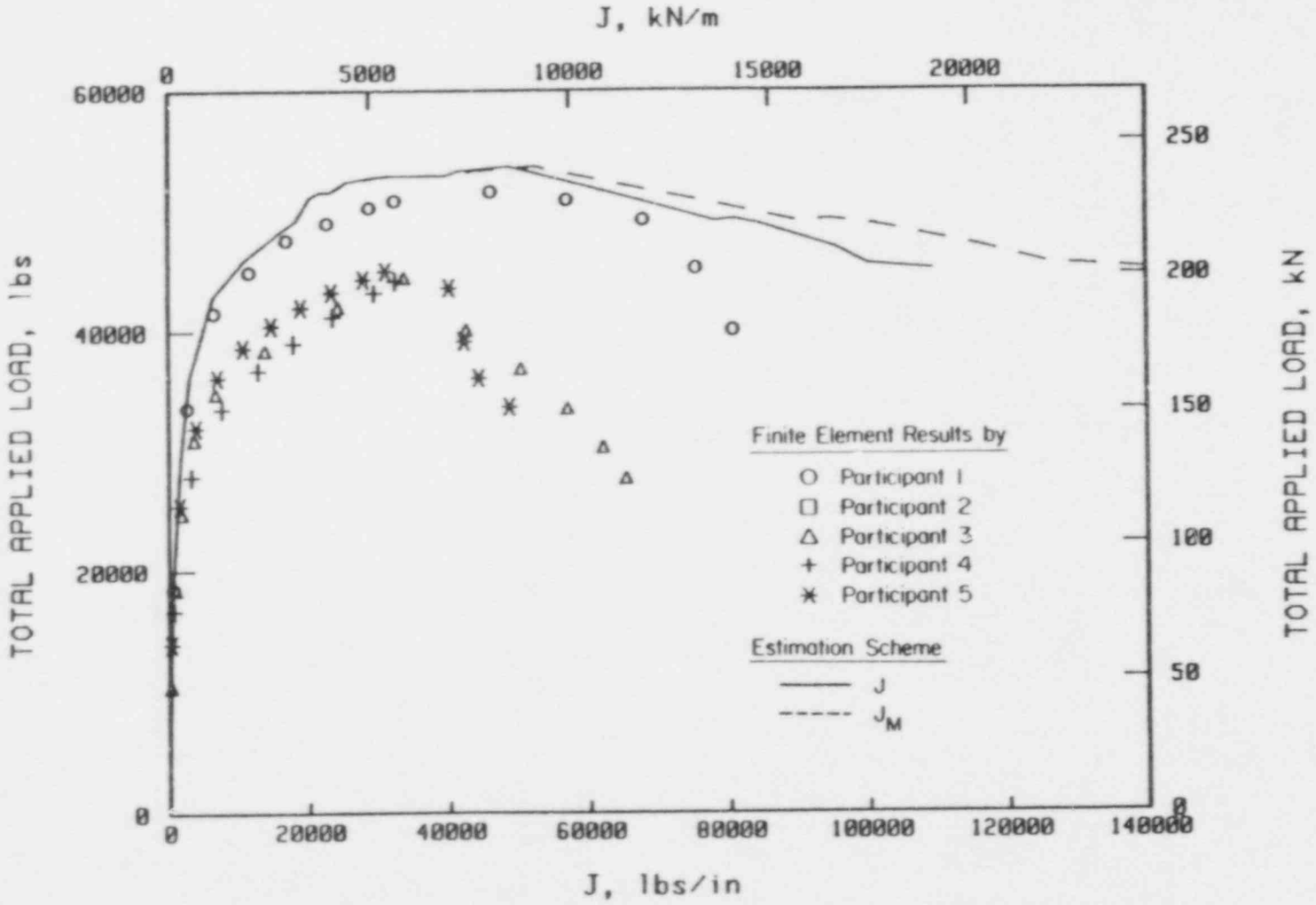

Figure 3.5.9 Load versus J computed by finite element analysis and by J-estimation scheme.

T-4573-F5.7

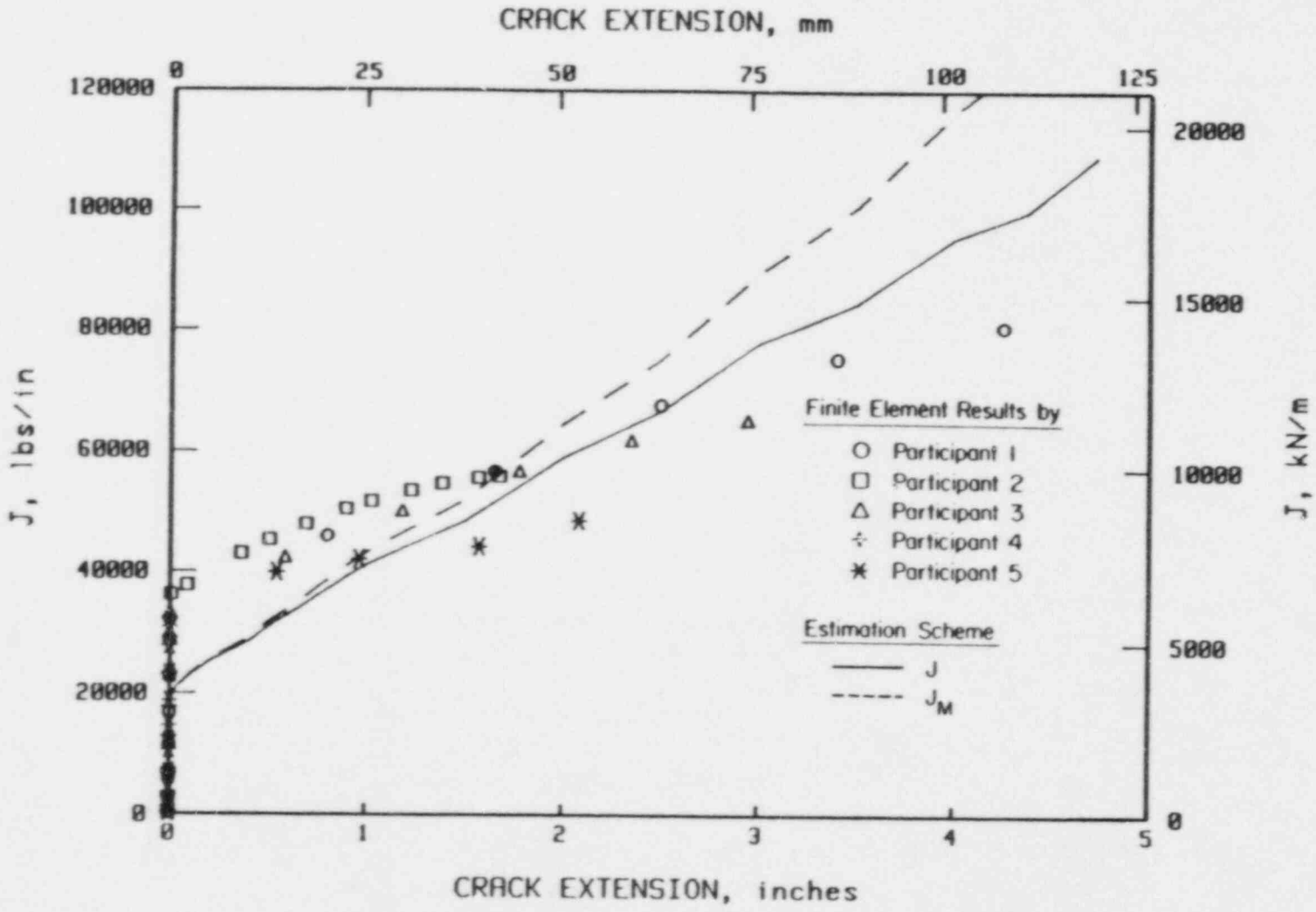

Figure 3.5.10 The J versus crack growth computed by finite element analysis, and by a J-estimation scheme (Problem B).

T-4573-F5.8

since the finite element loads were underpredicting the experimental loads. The slope of the finite element J-R curves is flatter than the J-estimation scheme J-R curves. This is reasonable since the finite element load versus displacement curves are different from the experimental data used in the estimation schemes.

Discussion of Stainless Steel Finite Element Round-Robin Results

These results showed the following:

- If multiple meshes are used in an finite element analysis to model crack growth, then the calculated J-R curve should agree more closely with the deformation theory J-R curve than with the modified J-R curve.

- For the C(T) specimen, the J at initiation was close to the ASTM estimation scheme. This standard currently excludes application to stainless steels. These results show that the standard could be expanded to include stainless steels.

- For the circumferentially through-wall cracked pipe, the loads were consistently underpredicted. This is consistent with other finite element versus pipe fracture data comparisons made in the Degraded Piping Program, even when using data from other organizations. Although this is a conservative trend, from the viewpoint of using finite element analysis for licensing applications, it is not technically satisfying. The reason for this underprediction is not known at this time.

- J-R curves calculated from the far field contours were in good agreement with the J_M-R curves.

3.5.5 Finite Element and J-Estimation Scheme Round-Robin of a FWFN(T) Specimen and a Surface-Cracked Pipe

This round-robin was held in conjunction with the ASME PVP conference in June of 1986. The objective was to assess crack growth resistance in the through-thickness direction of a ferritic nuclear piping steel for a two-dimensional and a three-dimensional problem. In this round-robin, the two dimensional specimen was machined from the pipe, and was tested at the same temperature as the pipe test. The test temperature was 550 F (288 C). The pipe was an A106 Grade B 16-inch (406-mm) diameter Schedule 100 pipe [nominal thickness of 1.03 inch (26.16 mm)].

The two-dimensional specimen was an FWFN(T) specimen. This is essentially a single-edge notched specimen. The objective of using this specimen is that it can be easily machined from a pipe, and it evaluates the J-R curve of the material in the same direction of crack growth as a circumferential surface crack growing through the pipe thickness. Another advantage of this specimen is that the ligament is in tension just as a surface crack in the pipe.

There were 12 participants from 5 countries in this round-robin (Table 3.5.4). The results of this round-robin are summarized below. These results should be considered somewhat tentative since they need to be reconfirmed with all the participants.

FWFN(T) Round-Robin Results

The FWFN(T) specimen geometry is shown in Figure 3.5.11. A unique aspect of this specimen is that it is loaded in constant displacement by wedge grips in the test machine. Hence the normal constant stress J-estimation schemes for a pin-loaded side-edge-notched specimen does not model the boundary conditions properly since the bending of the specimen at the grips is restrained. This restraint of bending is probably a closer simulation of the stresses in a surface-cracked pipe where the curvature of the pipe helps to restrain the through-thickness bending. The engineering and true stress-strain curve data were given to all participants. For the estimation scheme solutions, the participants determined their own Ramberg Osgood fit to the tabulated stress-strain curve data. The crack growth versus load-line displacement data were provided to all participants.

FWFN(T) Finite Element Results

There were four participants that solved this problem. One of them used both a plane stress and a plane strain solution. Table 3.5.5 summarizes the variables in the finite element analyses. Figure 3.5.12 shows the calculated loads versus displacements compared to the experimental data. Data from participants 5 and 6 were the closest to the experimental data. Of the five J-R curve solutions, four of them are in very good agreement (Figure 3.5.13).

The results from Participant 5 are significantly lower than the other results. The results of Participants 4 and 7 are almost identical in the load versus displacement calculations and the J-R curves. (Note that Solution 7-a was for plane stress, whereas 7-b was for plane strain.)

FWFN(T) J-estimation Scheme Results

There were five participants that solved this problem with J-estimation schemes. Participant 3 solved the problem three different ways. Table 3.5.6 summarizes the solution methods. (Some of these solutions are not well defined since details of the solutions were not sent to Battelle.) The J-R curves are shown in Figure 3.5.14. The J_D- and J_M-R curves from a C(T) specimen tested in the usual L-C orientation are also shown in this figure. Compared to the scatter of the finite element solutions, these results are very poor. One observation is that the solutions that used the EPRI/GE estimation scheme had the J-R curves hooking upward. [This was a general trend also observed from C(T) specimen predictions using the EPRI/GE estimation scheme and inputing load versus crack growth to calculate a J-R curve (Section 3.2.5 in Ref. 3.5.6)].

Table 3.5.4. List of Second Analytical Round-Robin Participants.

(12 Participants from 5 Countries)

England

Central Electricity Generating Board

France

Framatome/Novatome

Japan

Central Research Institute for Electric Power Industry
Ishi Kawajima - Harima Heavy Industry
Kawasaki H.I.
Mitsubishi R.I.
University of Tokyo (Yagawa - Ueda)
University of Tokyo (Miyoshi - Yoshida)

USA

Battelle
Electric Power Research Institute
Structural Integrity Associates

West Germany

Gesellschaft für Reaktorsicherheit

W = 0.71 inch (18.03 mm)
B = 1.614 inch (40.99 mm)
h = 10 inch (254 mm)
d = 0.01 inch (0.254 mm)
a_0 = 0.35 inch (8.89 mm)

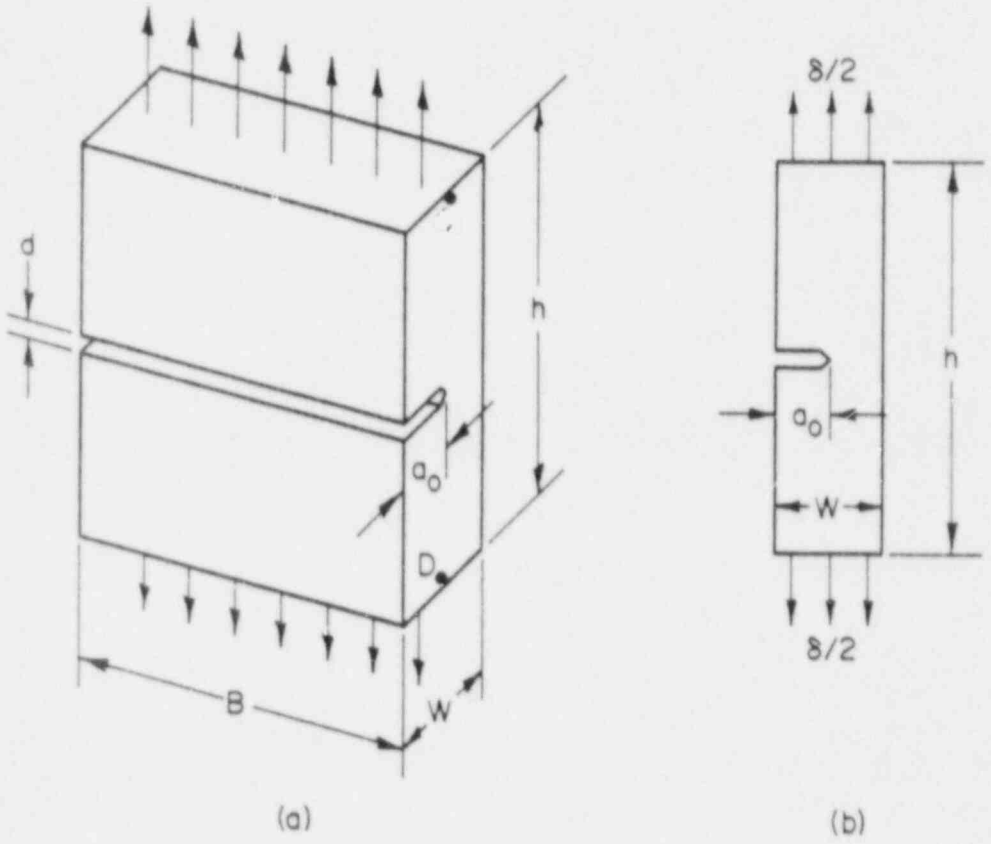

Figure 3.5.11 Geometry of the full-width face-notched, FWFN(T), specimen.

Table 3.5.5. Variables in finite element analyses of FWFN(T) specimens.

Variable	Participant 4	5	6	7
No. & Type of Elements	299 8-Node Isop. Plane Strain	36 10-Node Gen. PE	251 16-Node Brick 3-D	120 8-Node Isop. Plane Strain
No. of Nodes	938	138	1174	407
Integration Order	3x3 Gauss	2x2	3x3x2 Gauss	2x2 Gauss
Yield Surface	Von Mises	Von Mises	Von Mises	Von Mises
Hardening Model	Isotropic	Isotropic	Isotropic	Isotropic
J-E Curve	True	Engineering	Engineering	True
Finite Deformation	No	No	No	Total Lagrange Small Strain
Equilibrium Compensation	Newton-Raphson	Newton	Tangent Stiffness Radical Return	Modified Newton
Crack Extension Procedure	Spring Relaxation	Mesh Distortion	Node Release	Node Shift and Release
J-Computation	Contour J	VCE	VCE	VCE

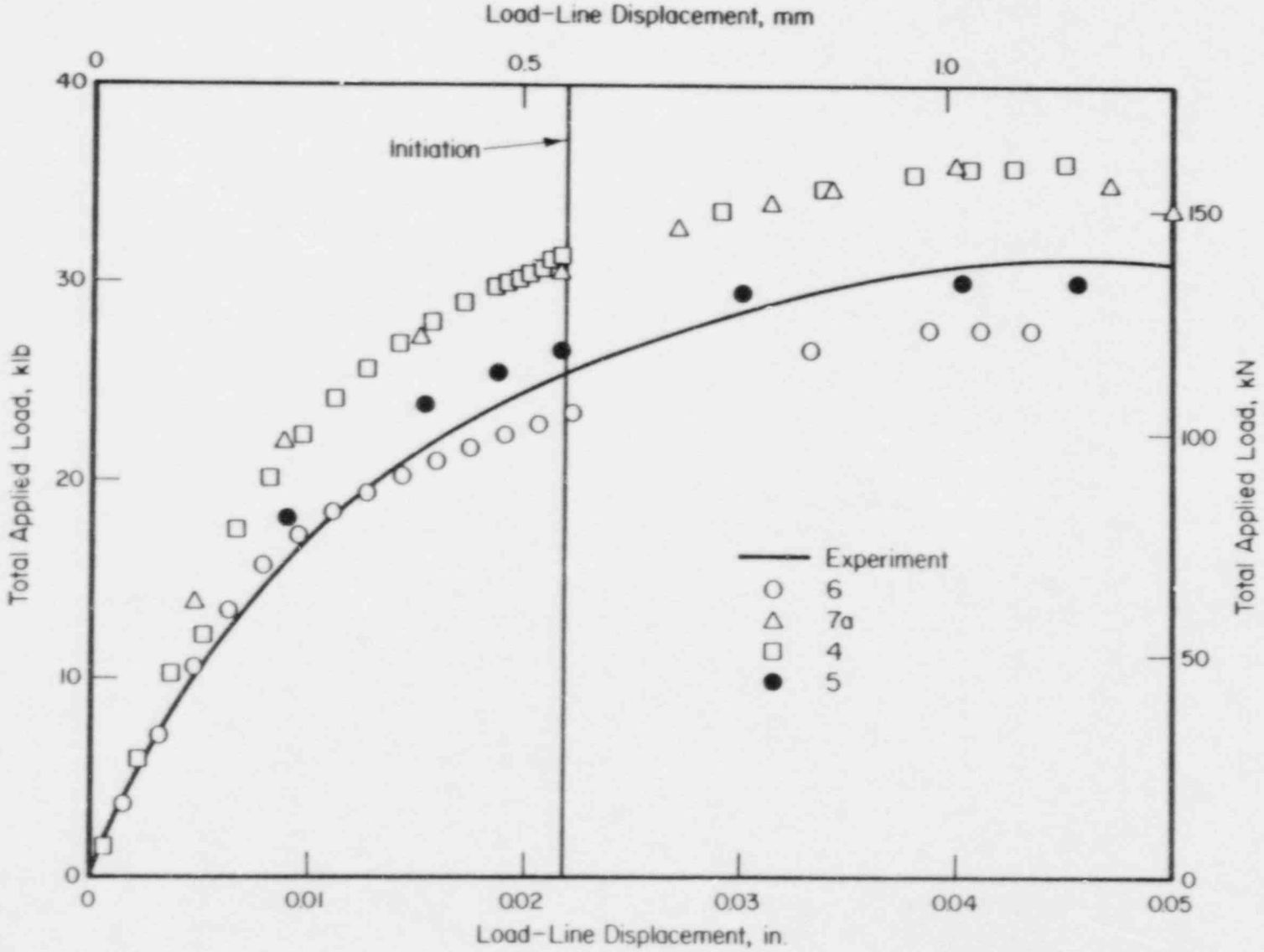

Figure 3.5.12 Comparison of load and displacement predictions for the finite element analyses (FEA).

SA-12/87-F3.5.12

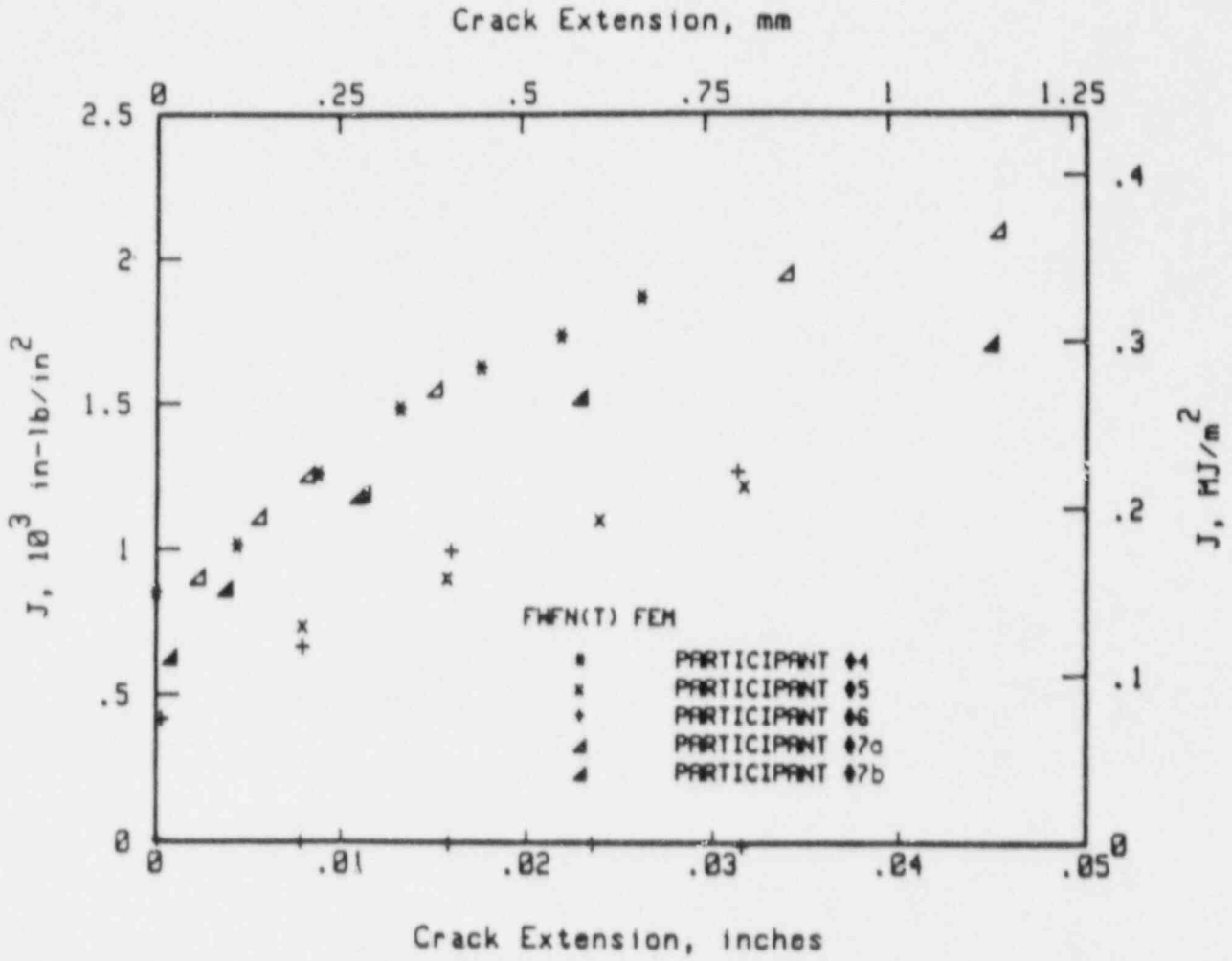

Figure 3.5.13 FEM analysis results for J-resistance curve for FWFN(T) specimen.

WRSRIM-12/86-F5.5

Table 3.5.6. Summary of estimation methods for FWFN(T) problem.

Participant	Description of Method
1	GE/EPRI constant stress edge-cracked specimen solution, Ramberg-Osgood fit unknown at this time.
2	GE/EPRI constant stress edge-cracked specimen solution.
3	Used GE/EPRI method, Ramberg-Osgood constants unknown at this time.
3a	GE/EPRI bending solution.
3b	GE/EPRI combined tension plus bending on edge-notched specimen solution.
3c	GE/EPRI constant stress edge-notched specimen solution.
4	n-factor solution developed from finite element solutions.
5	R6 Rev. 3 using finite element solution for K_r term.
5a	- Solution (a) used elastic J finite element results in K_r term.
5b	- Solution (b) used elastic J finite element results with restrained bending geometry option.
5c	- Solution (c) used elastic J finite element results.

The best results were from Participants 4 and 5. Participant 4 developed an η-factor estimation scheme with the guidance of finite element analyses. Participant 5 used the R6 Rev. 3 method, where the elastic solution for K_r came from finite element results.

The next closest solution used the EPRI/GE estimation scheme for combined tension and bending of an edge-notched specimen, Solution 3-b in Figure 3.5.14. The constant stress edge-notched specimen solutions, from Participant solutions 1 and 3-c, gave very high J-R curves.

Surface-Cracked Pipe Results

The surface-cracked pipe problem represents the first time (that we are aware of) a truly three-dimensional structural analysis problem has been used in a major fracture mechanics finite-element round-robin exercise. The crack geometry and the loading frame of the test system is given in Figure 3.5.15. The crack was an internal surface crack, and the pipe was unpressurized. The test was conducted at 550 F (288 C). The pipe material and test temperature were the same as those used in the FWFN(T) problem; hence the J-R curves are comparable. For this problem, both finite element and estimation scheme results were solicited. The material stress-strain curve data and the load-line displacement versus crack growth data at the center of the surface crack were given to the participants. The experimental load versus load-line displacement curve is shown in Figure 3.5.16. This shows that after a small amount of crack growth, the surface-crack broke through the thickness and became unstable.

Finite Element Method Results

Eight participants solved this problem by the finite element method. Of these, Participant 5 solved the problem using two different computer codes. The participants were asked to calculate the J values up to crack initiation. None of the participants conducted finite element crack growth analyses in this round-robin. Table 3.5.7 summarizes the variables used in the finite element solutions.

The first comparison was the load versus load-line displacement. Particular care was taken to account for the test machine compliance and the dead-weight of the pipe for determining the experimental test record. As shown in Figure 3.5.17, all of the finite element solutions agree well with each other and with the experimental data.

The second comparison was for J versus load-line displacement. The calculated values are shown in Figure 3.5.18, along with the displacement at crack initiation from the experimental data. The calculations are all in good agreement in the linear-elastic region, but they differ tremendously in the elastic-plastic region. At crack initiation, the ratio of the highest J to the lowest J is a factor of 426 percent. This is an unacceptably large difference.

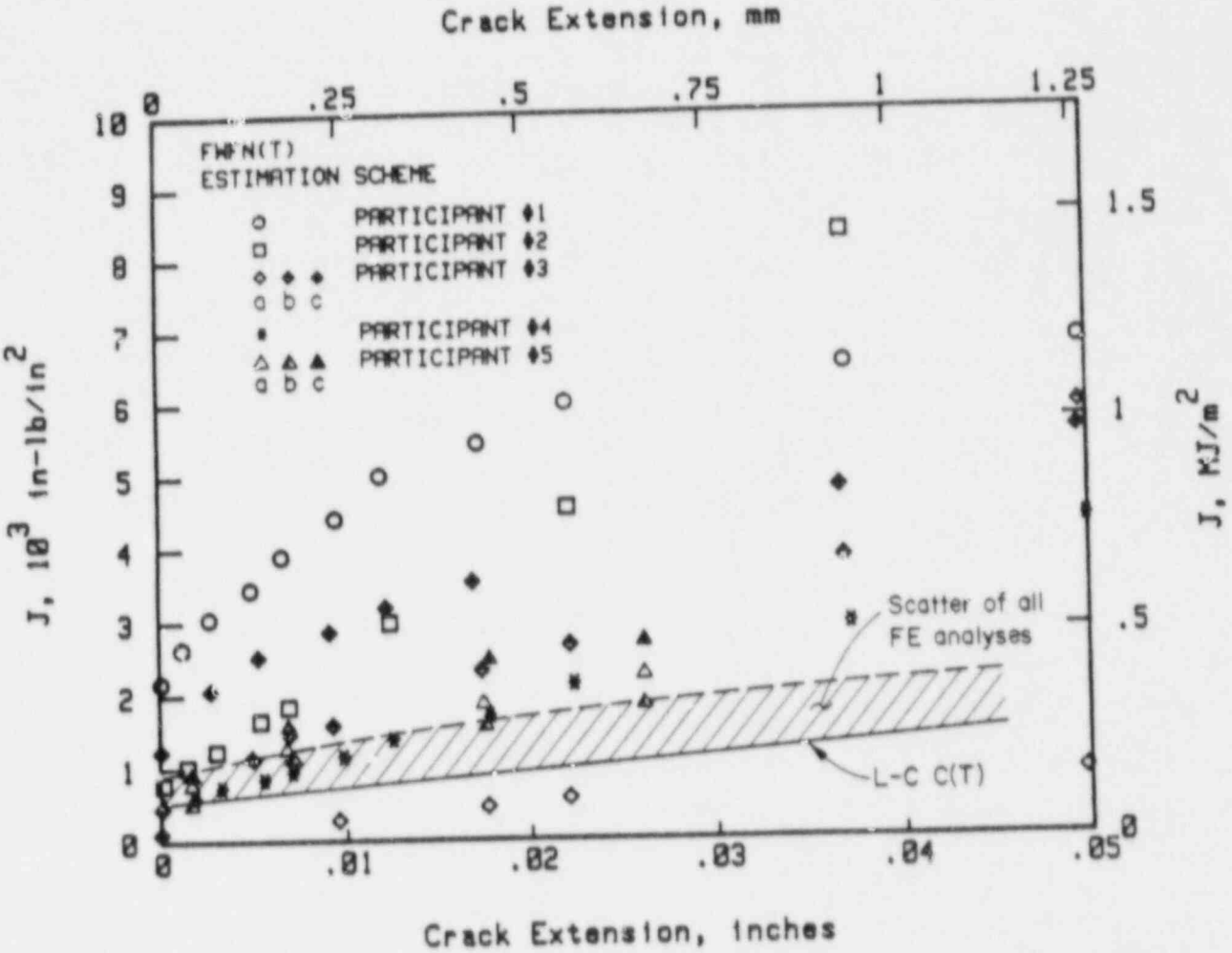

Figure 3.5.14 Comparison of FWFN(T) estimation scheme calculations to FEM values.

SA-12/87-F3.5.14

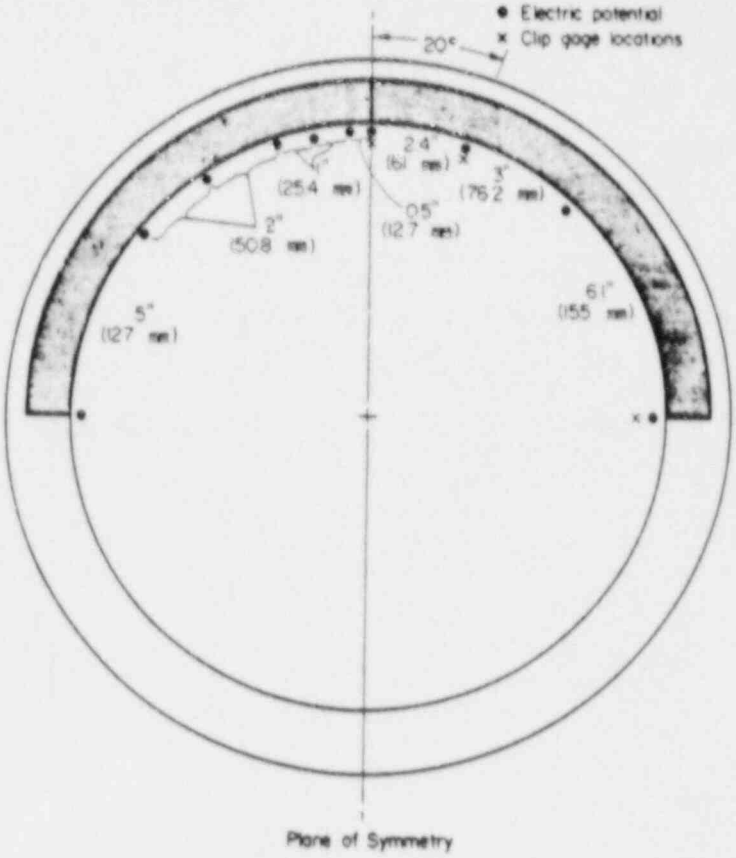

(a) Schematic of crack geometry for Experiment 4112-8

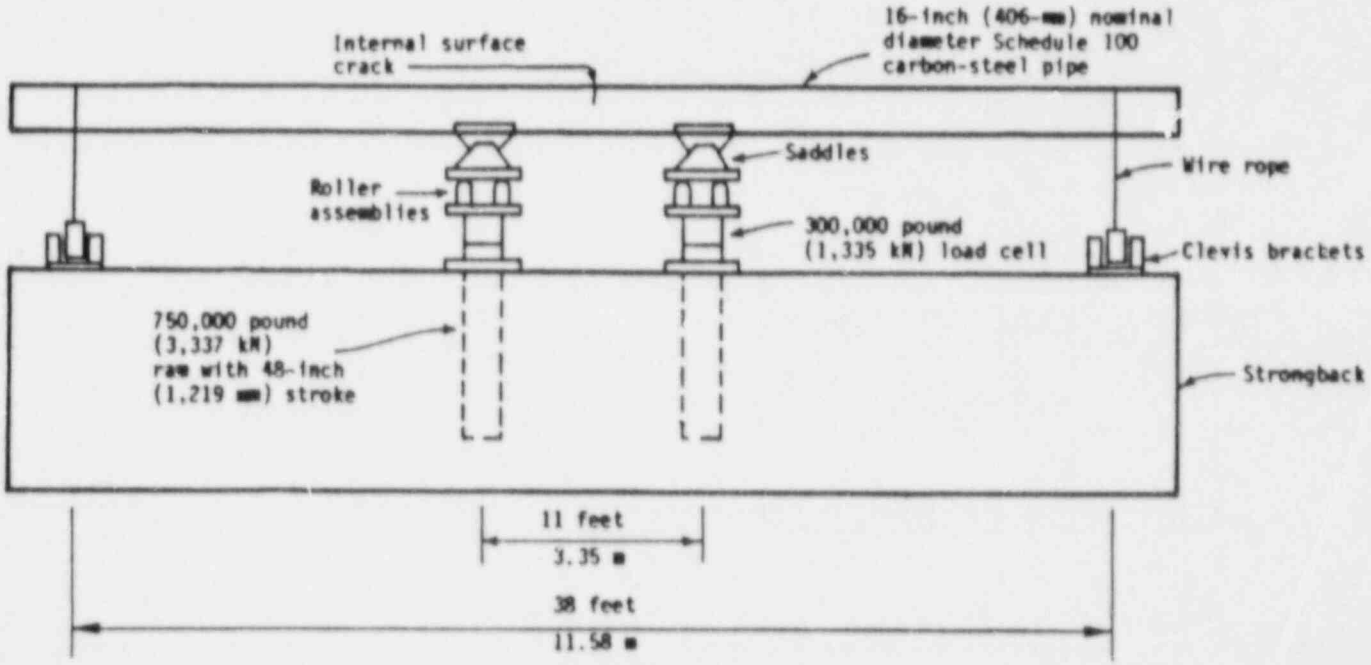

(b) Schematic of test apparatus

Figure 3.5.15 Surface-cracked pipe test dimensions.

SA-12/87-F3.5.15

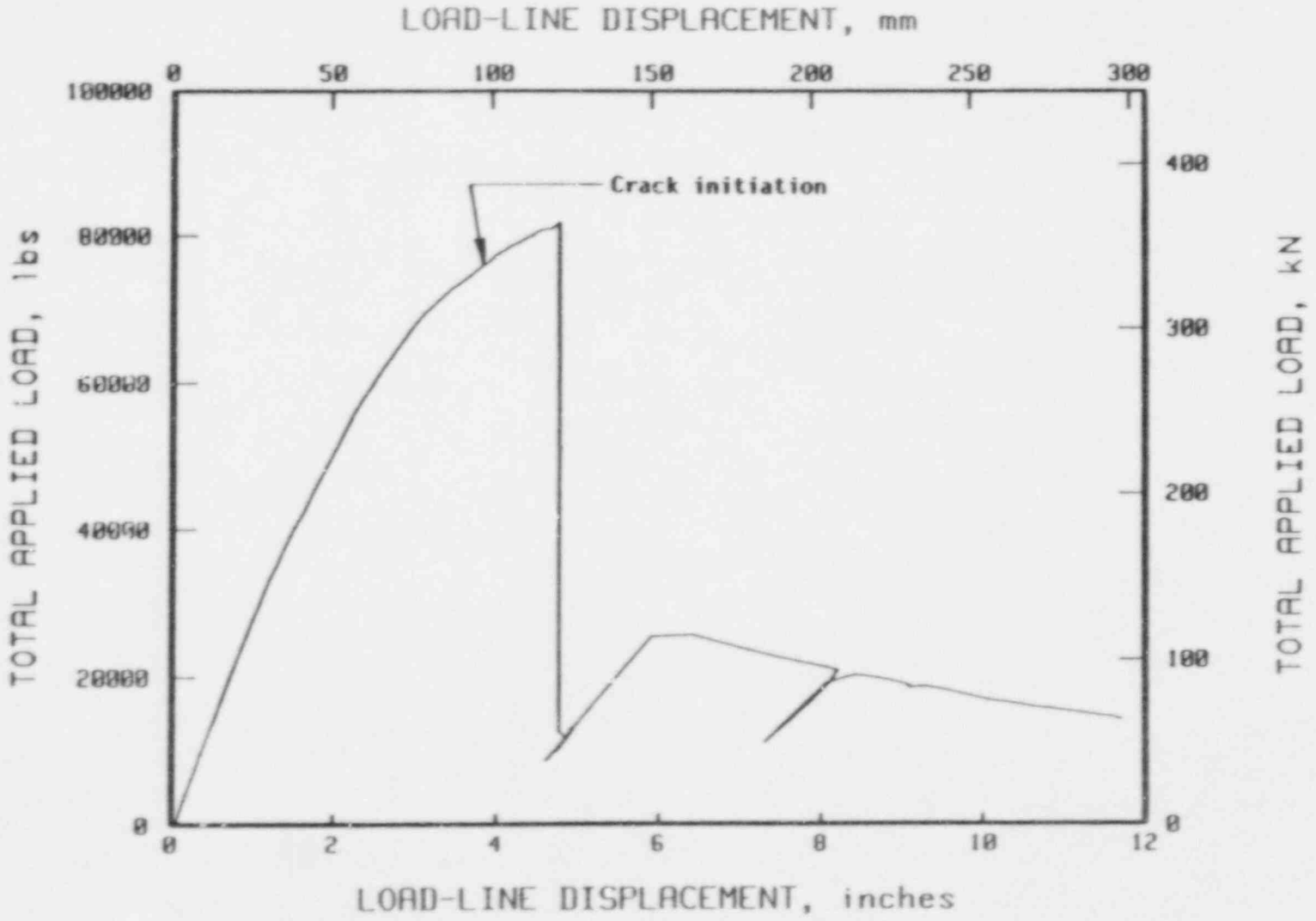

Figure 3.5.16 Total applied load versus load-line displacement for surface cracked pipe experiment (4112-8).

SA-12/87-F3.5.16

Table 3.5.7. Summary of variables in finite element analyses of surface-cracked pipe specimens.

Variable	Participant								
	4	5a	5b	6	8	9	10	11	12
No. & Type of Elements	783 20-Node Brick	348 20-Node Brick & 15-Node Fracture	348 20-Node Brick	300 16-Node Brick	165 20/15-Node Brick	198 20-Node Brick	168 20-Node Brick	150 20-Node Brick	626 16-Node Brick
No. of Nodes	3809	2036	2178	1574	1073	1064	1168	956	2526
Integration Order	2x2x2 Gauss	2x2 reduced	2x2 reduced	3x3x2 Gauss	--	3x3x3 Gauss	3x3x3 Gauss	2x2x2 Gauss	3x3x2/2x2x1 Gauss
Yield Surface	Von Mises	Von Mises	Von Mises	Von Mises	Von Mises	Von Mises	Von Mises	Von Mise	--
Hardening Model	Isotropic	Isotropic	Isotropic	Isotropic	Isotropic	Isotropic	Isotropic	Isotropic	--
σ-ε Curve	True	Engineering	Engineering	Engineering	True	True	Engineering	Engineering	Engineering
Finite Deformation	No	No	No	No	No	No	No	No	No
Equilibrium Compensation	Modified Newton-Raphson	Mixed Newton-Raphson	Newton	Tangent Mod Radial Return	--	Tangent Mod Radial Return	Full Newton-Raphson	Newton	Newton-Raphson
Crack Extension Procedure	None	None	None	None	None	None	None	None	None
J-Computation	VCE	J^*_w Contour Integral	VCE	VCE	VCE	$\bar{J}$	VCE	VCE	VCE

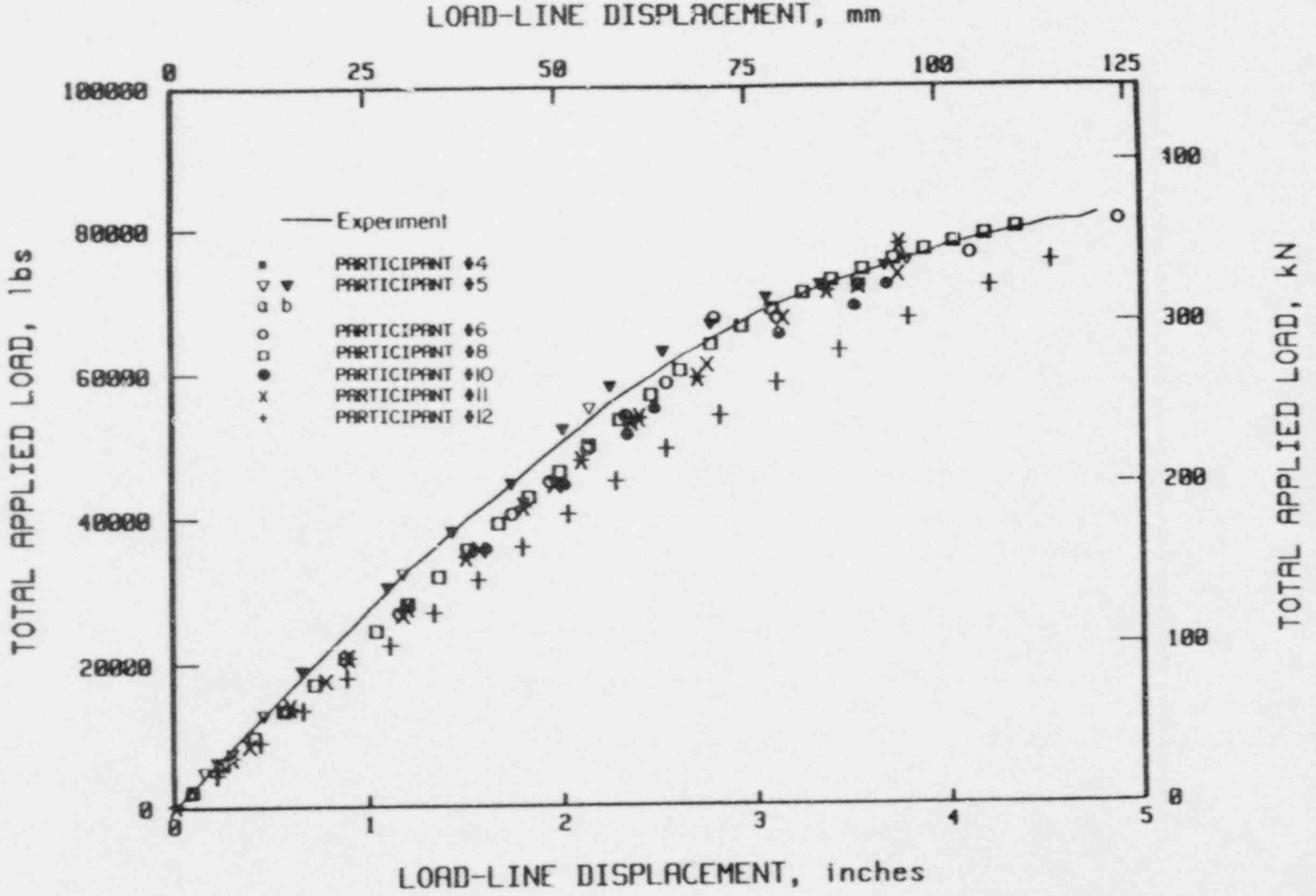

Figure 3.5.17 Comparison of FEM results to surface cracked pipe experimental load-displacement data.

SA-12/87-F3.5.17

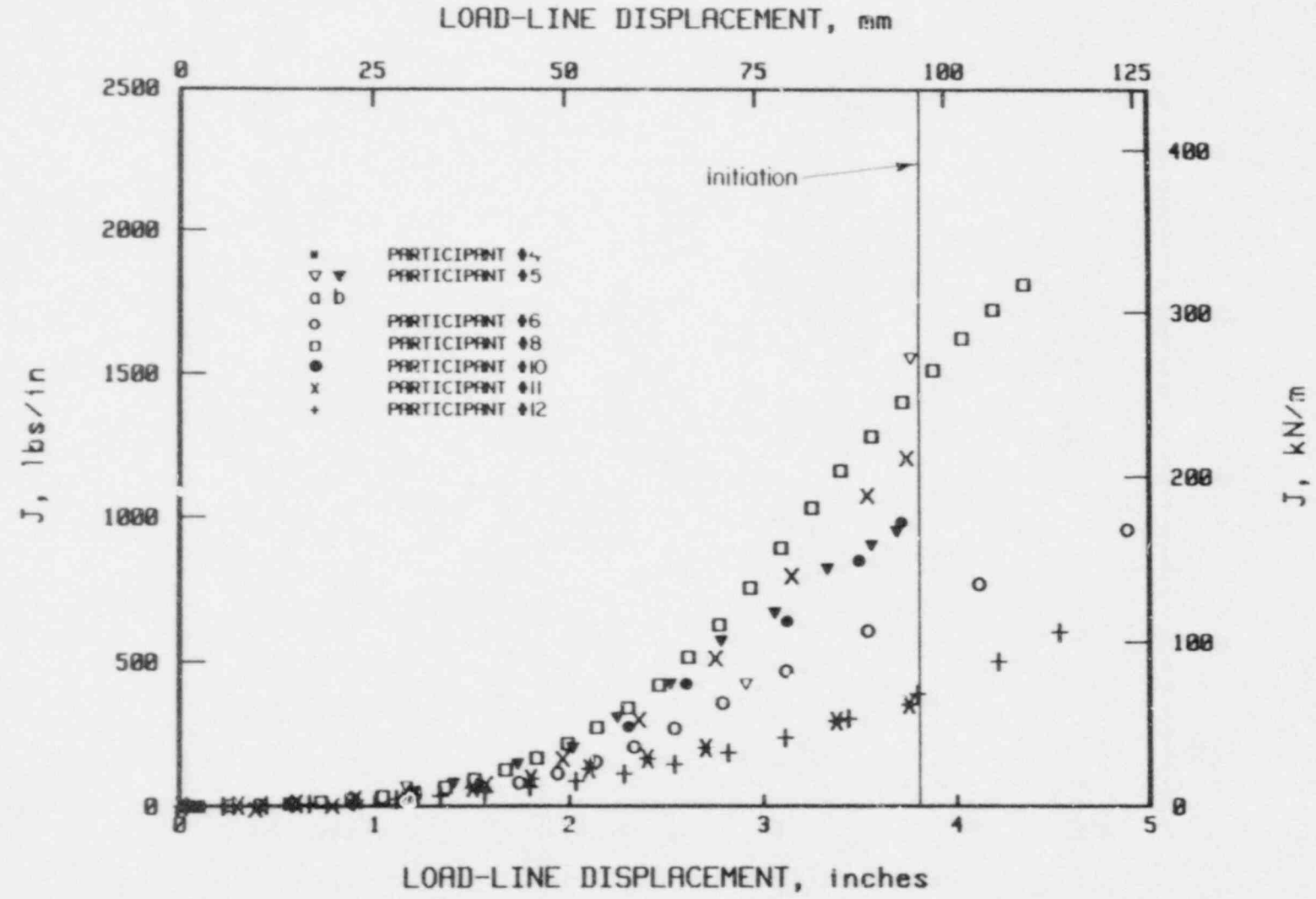

Figure 3.5.18 Comparison of J versus load-line displacement from finite element analysis of surface-cracked pipe.

SA-12/87-F3.5.18

To further investigate the possible causes of this difference, the J at initiation versus the number of nodes in the ligament was examined. Figure 3.5.19 shows this comparison. This shows that the greater the number of nodes, the lower the J value. Hence mesh refinement is a critical consideration in this surface crack analysis. For this problem it appears that 9 or more nodes in the ligament would be needed to get good results. The solutions by Participants 4 and 12 satisfy this requirement. Their value of J at initiation was approximately 390 in-lb/in^2 (68.3 kN/m).

From this exercise it was found that a given mesh refinement may produce satisfactory results in the linear-elastic regime while producing poor results in the nonlinear elastic-plastic regime. Hence, one must be careful in verifying a mesh refinement criterion for nonlinear finite element problems.

Estimation Scheme Solutions

Five participants solved the surface-cracked pipe problem using estimation schemes to calculate the J-R curve. The different approaches are listed in Table 3.5.8. Figure 3.5.20 shows a comparison of the J-R curves. In general, these values are higher than the finite element solutions. The finite element value of 390 in-lb/in^2 (68.3 kN/m) is lower than any of the estimation scheme values at crack initiation.

Discussion of Second Analytical Round-Robin

The following points summarize the important aspects of this round-robin.

- For the FWFN(T) specimen, the finite element J-R curves were in excellent agreement.
- For the FWFN(T) specimen, the J-estimation scheme results showed considerable scatter, although proper modeling of the constant-displacement loading condition gave reasonable agreement with the finite element results.
- For the surface-cracked pipe, the finite element results showed that mesh refinement in the ligament of the crack was a primary factor for scatter in the data for J at crack initiation. The scatter on J was large, even though the global load and a far-field displacement were predicted well. The finite element J values were in good agreement in the linear-elastic region, but diverged in the elastic-plastic region. Hence, evaluation of mesh refinement by linear-elastic analysis is not sufficient for an elastic-plastic problem. For the surface crack problem investigated in this round-robin it appears that nine or more nodes are needed in the ligament.

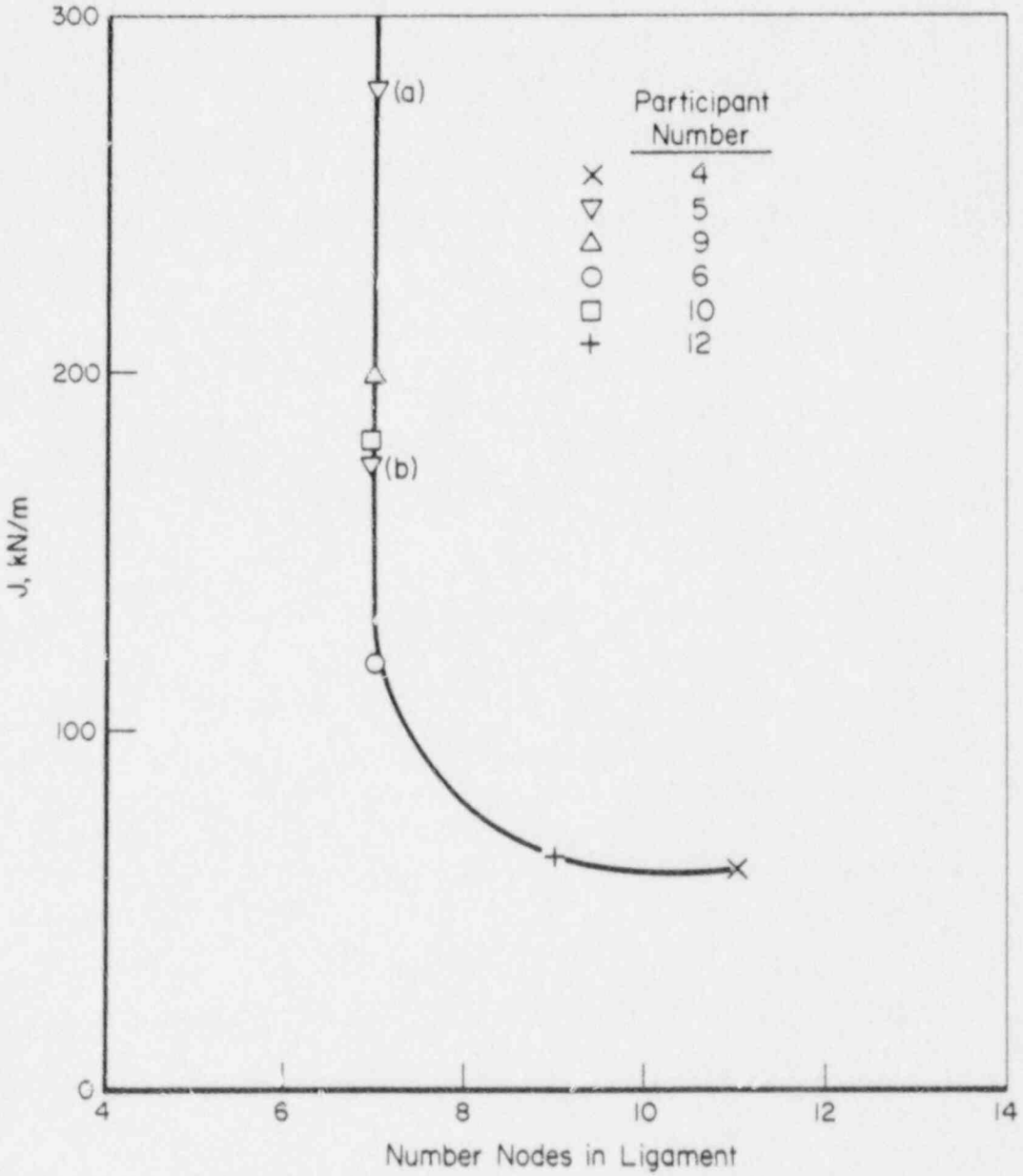

SA-12/87-F3.5.19

Figure 3.5.19 Comparison of J at initiation versus number of nodes in ligament from FEM analysis of surface-cracked pipe.

Table 3.5.8. Summary of estimation methods for surface-cracked pipe problem.

Participant	Description
1	GE/EPRI surface-cracked pipe solution where ovalization (buckling) correction used to modify solution.
2	R6 Rev. 3.
3	GE/EPRI surface-cracked pipe analysis.
4	Modification of GE/EPRI 360-degree surface-cracked pipe solution where finite length flaw accounted for.
5	R6 Rev. 3 where finite element solutions developed for use in K_r term.

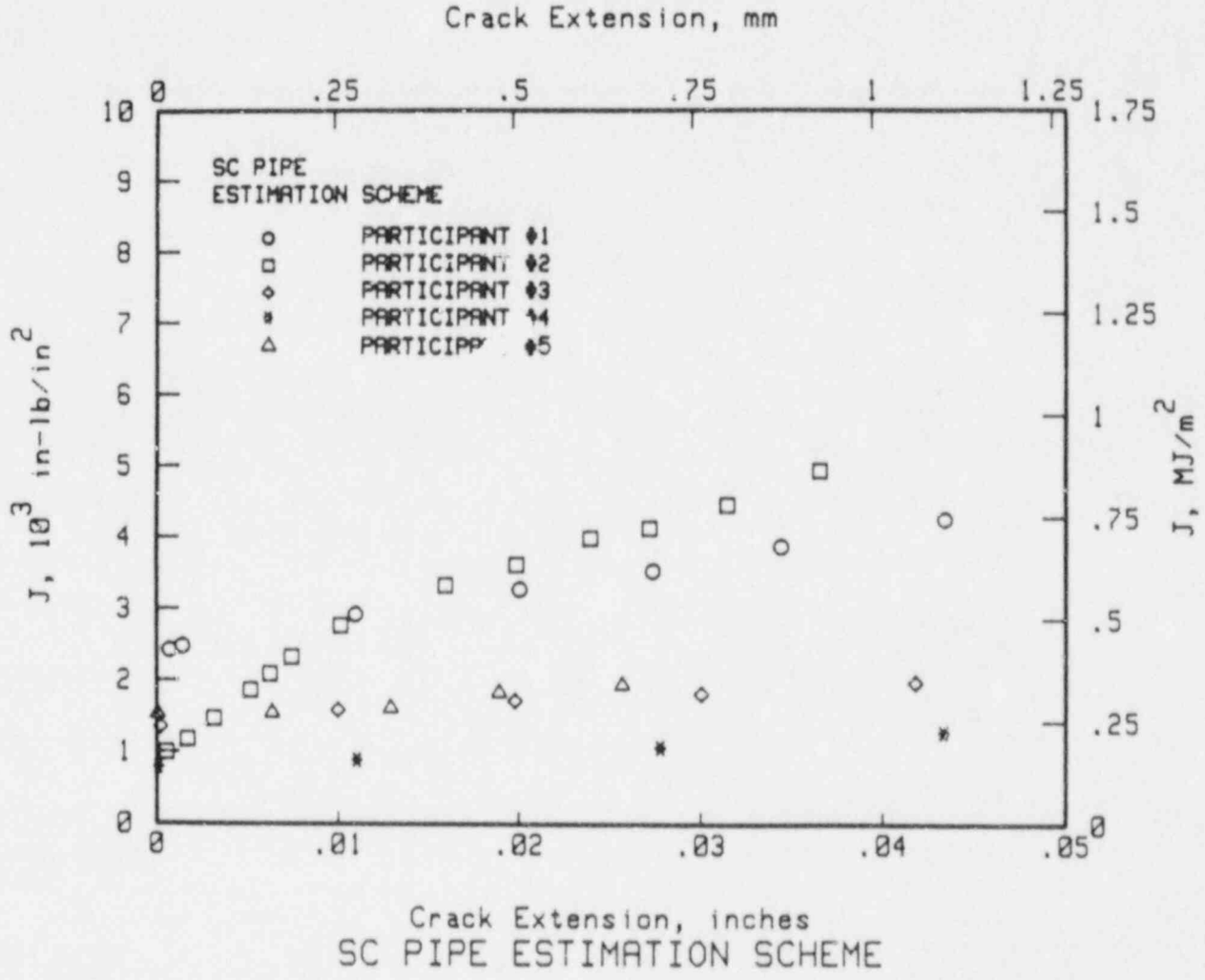

Figure 3.5.20 Comparison of J-R curves calculated from J-estimation schemes for the surface-cracked pipe problem.

SA-12/87-F3.5.20

- All the surface-crack estimation schemes gave J values that were higher than the best finite element results. For application purposes, this may be conservative since these schemes overpredict the crack driving force, hence they will underpredict the loads for a given J-R curve.

- The finite element values that appear to be the best for the FWFN(T) specimen and the surface-cracked pipe show that the J at initiation from the pipe was approximately 65 percent of the J at initiation from the FWFN(T) specimen. The finite element (using the solutions with more than 9 nodes in the ligament) calculated surface-cracked pipe J value at initiation was lower than the J_{Ic} value from the C(T) specimen. Hence using a pipe finite element analysis, with careful consideration of the mesh refinement, may overpredict the loads for the cracked pipe when conducting an application phase calculation.

These results will be further reviewed and published in a future document.

References for Section 3.5

3.5.1 Wilkowski, G. M., and others, "Degraded Piping Program - Phase II," Semiannual Report, October 1985-March 1986, NUREG/CR-4082, Vol. 4, September 1986.

3.5.2 Ernst, H. A., "Material Resistance and Instability Beyond J-Controlled Crack Growth", in C. F. Shih and J. P. Gudas (eds.), Elastic-Plastic Fracture: Second Symposium, Vol. I - Inelastic Crack Analysis, ASTM STP 803, American Society for Testing and Materials, 1983, pp. I-191 to I-213.

3.5.3 Ahmad, J., and others, "Elastic-Plastic Finite Element Analysis of Crack Growth in Large Compact (Tension) and Circumferentially Through-Wall-Cracked Pipe Specimen - Results of the First Battelle/NRC Analysis Round-Robin", NUREG/CR-4573, October 1986.

3.5.4 Kanninen, M. F., and others, "Instability Predictions for Circumferentially Cracked Type 304 Stainless Steel Pipes Under Dynamic Loading", Final report on EPRI Project T118-2, EPRI Report Number NP-2347, April 1982.

3.5.5 Takahashi, Y., and others, "Comparison of Finite Element and J-Estimation Scheme Solutions in Ductile Fracture Analysis of Stainless Steel Piping with Circumferential Through-Wall Cracks", ASME Paper PVP No. 87-PVP-31, 1986.

3.5.6 Wilkowski, G. M., and others, "Degraded Piping Program - Phase II", Semiannual Report, October 1984-March 1985, NUREG/CR-4082, Vol. 2, July 1985, see Section 3.2.

4. SIGNIFICANCE OF RESULTS TO DATE

The Degraded Piping Program will supply results that provide a basis for regulatory decisions regarding leak-before-break (LBB) and in-service flaw assessment. The significance of our results are summarized in terms of how they may affect regulatory technical needs.

Section 4.2 of the previous semiannual report (Ref. 4.1) summarized the significance of the program results to date. The following section provides such a summary, but includes results from the current reporting period. During that period, we have completed five topical reports, each of which is summarized in this report.

The experimental and analytical efforts within the scope of the Degraded Piping Program were undertaken in part to determine the need for any further efforts. As findings came to light, some efforts were slightly expanded, while other efforts were not pursued. The following summary describes the activities of the third year. These activities have contributed considerably to the understanding of the application of elastic-plastic fracture mechanics (EPFM) to nuclear piping systems. These contributions relate to piping materials at light-water reactor (LWR) temperatures, especially concerning

- Pipe fracture analyses
- In-service flaw assessment criteria
- Material characterization and unusual failure mechanisms.

The discussions below are the basis for the Executive Summary in this report. Previous semiannual reports are given in References 4.2 to 4.5.

References for Section 4

4.1 Wilkowski, G. M., and others, "Degraded Piping Program - Phase II", Semiannual Report, April 1986-September 1986, NUREG/CR-4082, Vol. 5, April 1987.

4.2 Wilkowski, G. M., and others, "Degraded Piping Program - Phase II", Semiannual Report, March 1984-September 1984, NUREG/CR-4082, Vol. 1, January 1985.

4.3 Wilkowski, G. M., and others, "Degraded Piping Program - Phase II", Semiannual Report, October 1984-March 1985, NUREG/CR-4082, Vol. 2, July 1985.

4.4 Wilkowski, G. M., and others, "Degraded Piping Program - Phase II", Semiannual Report, April 1985-September 1985, NUREG/CR-4082, Vol. 3, March 1986.

4.5 Wilkowski, G. M., and others, "Degraded Piping Program - Phase II", Semiannual Report, October 1985-March 1986, NUREG/CR 4082, Vol. 4, September 1986.

4.1 Application of Circumferentially Cracked Pipe Results to LBB Analyses

The discussions in this section refer to LBB applications. In these cases, design changes can be justified in a plant-specific manner. The significance of the results to current LBB methodology and the possible applications for future LBB design consideration are discussed in the following sections.

4.1.1 Significance to Current LBB Analyses

Current LBB analyses accepted by the U.S. NRC require the postulation of a through-wall circumferential crack (Ref. 4.1.1). This postulated through-wall crack must be shown to be detectable by leakage at normal operating conditions and the crack must be stable at faulted loads. Safety factors are applied to the detectable leak rate used in determining the size of the postulated crack, as well as to the faulted loads used in the crack stability (or pipe fracture) analyses (Ref. 4.1.2).

To validate the current LBB analyses for through-wall-cracked pipe, fracture experiments have been conducted on 4-inch (102-mm) to 42-inch (1067-mm) diameter pipe (Ref. 4.1.3). This includes recent experiments on a 28-inch (711-mm) diameter stainless steel recirculation pipe removed from service, and a 36-inch (914-mm) diameter by 2.87-inch (73-mm) thick cold-leg pipe from a cancelled pressurized-water reactor (PWR), see Sections 2.1 and 2.7 in this report. Most of the pipes were tested in pure bending, but some experiments have been conducted under pure pressure or pressure plus bending to failure. This approach was taken since nuclear piping systems experience different ratios of bending to axial membrane stresses. The through-wall cracked pressurized pipe experiments were extremely difficult to conduct at 550 F (288 C), and required the development of a high temperature rubber bladder to contain the pressure.

Evaluation of Limit-Load Analyses

These experimental results were used along with the material characterization data to assess the various pipe fracture analyses. The simplest type of analysis is the net-section-collapse (NSC) analysis (Refs. 4.1.4 and 4.1.5). The NSC analysis, a limit-load analysis, is based on the assumption that the pipe cross-section becomes fully plastic at the location of the crack. Stated another way, the material is sufficiently tough that failure will be controlled by the flaw size and the strength of the material. The results of this program showed that toughness alone is not enough to ensure that failure loads will reach the NSC predicted loads. The diameter of the pipe is an important consideration, where the larger the pipe diameter the lower the failure stress. This was demonstrated in an experiment on a very tough (wrought Type 304 stainless steel) 42-inch (1067-mm) diameter pipe. A plastic-zone screening criterion (PZSC) was developed to show when the NSC analysis is appropriate to use, and when more sophisticated EPFM analyses should be used (Ref. 4.1.3). The dimensionless plastic-zone parameter used in

the screening criterion was also used to develop an empirical relation for predicting the maximum load with 95 percent reliability (that is, two standard deviations below the average of the failure stresses) (Ref. 4.1.6, Section 4.1). This relation could be used to provide guidelines as to when simple limit-load analyses can be used in the NRC's LBB analysis procedure (Ref. 4.1.2).

Evaluation of J-Estimation Scheme Analyses

Many EPFM analyses have been evaluated by comparing the predicted to experimental loads and displacements (Refs. 4.1.3, 4.1.7, and 4.1.8). The analyses used were based on the J-integral or modifications of it. These are relatively simple engineering estimation schemes used to make approximate predictions of the pipe fracture behavior. They approximate more advanced EPFM technology without resorting to elaborate, costly, and time consuming finite element analyses. An IBM-PC user-friendly computer code called NRCPIPE has been developed to facilitate analysis efforts. It incorporates all of the currently accepted J-estimation scheme analyses for cracked pipe. An initial version of this code has been provided to the U.S. NRC staff. Currently, changes are being made to make the program more user-friendly (Section 3.4). Following that, a procedure will be incorporated to reduce the computation time greatly for some of the analysis schemes.

For through-wall cracked pipe, the analyses included in this code are the EPRI/GE analysis (Ref. 4.1.9), the NUREG/CR-3464 analysis by Paris (Ref. 4.1.10), the LBB.NRC method (Ref. 4.1.11), two methods developed in this program LBB.BCL1 and LBB.BCL2 (Ref. 4.1.7), two recent modifications to the EPRI/GE analysis (Refs. 4.1.7 and 4.1.12), and the CEGB R6 method--revision 3 (Ref. 4.1.13). One proposed modification to the EPRI/GE method (Section 2.0 of Ref. 4.1.12) has recently been shown (Ref. 4.1.7) not to provide unique predicted loads for a given material stress-strain curve. A correction is given in our topical report on this subject, NUREG/CR-4853 (Ref. 4.1.7).

Results of several comparisons showed that the most conservative prediction of the load at crack initiation was obtained using the original EPRI/GE method. The LBB.NRC and the LBB.BCL methods were the most accurate, but in a few cases they overpredicted the initiation loads. The Paris analysis was somewhat less accurate, which might be expected since it was the only analysis which did not include the strain-hardening of the material. In regard to fitting the material stress-strain curve for these analyses, more consistent results were found when the curve was fit throughout the entire strain region (Ref. 4.1.3).

Using Maximum Load Rather Than Crack Initiation Load

Past LBB analyses frequently have been based on the load at crack initiation. The experimental results in this program show that there may be a higher safety margin on load in using maximum load. For large diameter and/or low toughness pipe, the maximum load may be twice as high as the initiation load (Ref. 4.1.3). Maximum load predictions were made using both the standard

deformation theory J-R curves (Ref. 4.1.14) determined by ASTM procedures, as well as the Modified J proposed by Ernst (Ref. 4.1.15).

The original EPRI/GE method underpredicted the maximum loads by a range of 0 to 50 percent (depending on the particular pipe analyzed), while the other methods were reasonably accurate when the deformation theory J-R curves were used. When the Modified J-R curve was used, the EPRI/GE method became the most accurate. The other methods using modified J occasionally overpredicted the maximum loads.

While the comparisons with these data suggest that using the EPRI/GE method with the Modified J-R curve gives the best agreement with the experimental data, there is concern that this may be fortuitous. Part of this concern is based on the fact that even with large amounts of crack growth, the Modified J-R curve values continue to increase rather than reaching a steady-state fracture toughness which is intuitively expected (Ref. 4.1.16). Other more advanced fracture mechanics parameters, such as the crack tip opening angle (CTOA) and incremental plasticity versions of J ($\hat{J}$ and T_p^*) reach a steady-state value during crack growth (Ref. 4.1.17). The experimental data support this in that the observed CTOA reaches a constant in the pipe experiments. Unfortunately, these more advanced parameters require detailed finite element analysis, and simple estimation schemes do not exist at this time.

Assessment of Cracks in Welds

Most of the concern for flaws is at locations either adjacent to or in welds. Some welds are left in the as-welded condition while others may be stress relieved or solution annealed. An interesting result from a series of as-welded and solution-annealed, stainless steel, submerged arc welded (SAW) pipe experiments showed that the actual strength of the weld needs to be considered to make more accurate predictions (see Section 2.7 in this report). This is important, since most analysts use the base metal strength when analyzing cracks in welds. Hence, they would not predict any difference between as-welded and solution-annealed welds. In reality, the J-integral estimation schemes (for both laboratory specimens and pipes) are based upon a homogeneous material in the structure rather than the composite nature of the welded structure. The evaluation of cracks in welds involves yet another assumption in the J-estimation scheme analyses.

Finite Element Analysis Results

To gain further confidence in the estimation schemes, very detailed three-dimensional elastic-plastic finite element analyses were conducted for three through-wall cracked pipe experiments. (One of these was used as a problem in an international round-robin [Ref. 4.1.18].) These results showed that in general all the analyses tend to predict the experimental load-displacement record very well up to crack initiation, but they underpredict the experimental loads with increasing crack growth. It appears that further efforts are needed to improve the crack growth modeling procedures. As a result of this work, it is

anticipated that if prudent finite-element-analysis procedures are used as the basis of a licensing submittal, then the predicted loads will be conservative.

Apparent Toughness Reduction Due to Complex-Crack Geometry

Another possible consideration in pipe fracture analysis comes from complex-cracked-pipe fracture behavior. A complex-crack is a through-wall crack with a surface crack around the cracked cross-section. This type of crack was found in a safe end at the Duane Arnold plant in 1978 (Ref. 4.1.19). The results to date (Ref. 4.1.20) suggest that the presence of even a shallow surface crack could significantly reduce the apparent initiation toughness and tearing resistance of the pipe. This is believed to be due to a radial crack driving force contribution and/or additional constraint at the crack which is ignored in the analyses. The current bounding results show that if there was an internal surface crack or defect that was 10 percent of the pipe thickness, then the apparent fracture resistance could be reduced by 25 to 50 percent. Since the 10-percent defect depth is acceptable by ASME Article IWB-3514.3, its possible role in reducing the apparent toughness could have some impact on pipe fracture behavior.

4.1.2 Possible Future Applications of LBB

There are several potential applications for design improvements based on pipe fracture analyses. Some of this program's results are discussed in light of these possible applications.

Improved Instability Predictions for Secondary Loads

One improvement in current pipe fracture analyses would involve use of more accurate methods for evaluating the instability of a pipe where there are significant thermal expansion stresses. These stresses are secondary or displacement-controlled stresses. Such stresses, when combined with sufficient pipe lengths and cracks in low toughness materials, could have enough stored elastic energy to create an instability (Ref. 4.1.21). Thermal expansion stresses are displacement-controlled and, if these stresses are significant, then the displacement predictive capability of the analyses needs to be evaluated. The results from this program involved making improvements in the J-integral estimation schemes to predict the load-displacement (or moment-rotation) relation for through-wall cracked pipe (Ref. 4.1.7). If this relation can be predicted for a cracked pipe, then structural mechanics can be used to calculate the compliance of the pipe needed to create an instability. This approach allows stability predictions to be made in load-displacement space rather than J-integral/tearing modulus (J/T) space (Section 2.9). J/T space instability calculations have on occasions in the past led to erroneous conclusions since the physical significance of the problem was not obvious, i.e., stability was predicted for a case where the applied J corresponded to the material J-R curve where Δa was twice the ligament of the surface crack (Ref. 4.1.5). Hence, in conducting a J/T space instability analysis, one also needs to examine the physical predictions of load, displacement, and crack growth.

The energy balance instability method, discussed in Section 2.9, offers an analysis method that considers the instability for stress components that have any combination of load-controlled and displacement-controlled stresses.

From the comparison of predicted displacements to actual displacements from pipe fracture experiments, it has been found that all of the current through-wall-cracked pipe J-estimation analyses give generally conservative predictions of compliant instability when the Deformation J-R curve was used. However, only the original EPRI/GE method underpredicts the maximum load by a range of 0 to 25 percent (depending on the particular pipe analyzed) if the Modified J-R curve is used (Ref. 4.1.7). The other methods occasionally overpredict the experimental load-displacement records, and hence would not be conservative in predicting instability.

LBB of a Surface-Cracked Pipe

The pipe fracture analyses described above deal with through-wall cracks. An equally important concern is with the fracture of a surface-cracked pipe. If a surface crack could initiate at a faulted load, then LBB might not occur. Laboratory specimen test results to date from this program have shown that one type of carbon steel stress-relieved SAW failed in a brittle (but not cleavage) manner at 550 F (288 C) in the through-the-thickness direction (Section 2.10). This weld was fabricated using procedures obtained from a PWR vendor in the United States. This fracture behavior is believed to be due to dynamic strain aging (DSA).

References for Section 4.1

4.1.1 U.S. Nuclear Regulatory Commission Pipe Study Group, "Evaluation of the Potential for Pipe Breaks", NUREG-1061, Vol. 3, November 1984.

4.1.2 Office of Nuclear Reactor Regulation, "Standard Review Plan" NUREG-0800; see "3.6.3 Leak-Before-Break Evaluation Procedures", released for public comment, Federal Register, Vol. 52, No. 167, August 28, 1987, pp. 32626-32633.

4.1.3 Scott, P., and Brust, F., "An Experimental and Analytical Assessment of Circumferential Through-Wall-Cracked Pipes Under Pure Bending", NUREG/CR-4574 September 1986.

4.1.4 Kanninen, M. F., and others, "Mechanical Fracture Predictions for Sensitized Stainless Steel Piping with Circumferential Cracks", EPRI NP-192, September 1976.

4.1.5 Kanninen, M. F., and others, "Instability Predictions for Circumferentially Cracked Type 304 Stainless Steel Pipes Under Dynamic Loading", Final Report on EPRI Project T118-2, EPRI Report Number NP-2347, April 1982.

4.1.6 Wilkowski, G. M., and others, "Degraded Piping Program - Phase II", Semiannual Report, April 1986-September 1986, NUREG/CR-4082, Vol. 5, April 1987.

4.1.7 Brust, F. W., "Approximate Methods for Fracture Analyses of Through-Wall-Cracked Pipes", NUREG/CR-4853, February 1987.

4.1.8 Wilkowski, G. M., and others, "Analysis of Experiments on Stainless Steel Flux Welds", NUREG/CR-4878, April 1987.

4.1.9 Kumar, V., and others, "Advances in Elastic-Plastic Fracture Analysis", EPRI NP-3607, August 1984.

4.1.10 Paris, P. C. and Tada, H., "The Application of Fracture Proof Design Methods Using Tearing Instability Theory to Nuclear Piping Postulating Circumferential Through-Wall Cracks", NUREG/CR-3464, September 1983.

4.1.11 Klecker, R., and others, "NRC Leak-Before-Break (LBB.NRC) Analysis Method for Circumferentially Through-Wall-Cracked Pipes Under Axial Plus Bending Loads", NUREG/CR-4572, May 1986.

4.1.12 Zahoor, A., and Gamble, R. M., "Evaluation of Flawed-Pipe Experiments", EPRI NP-4883M, November 1986.

4.1.13 Milne, I., and others, "Assessment of the Integrity of Structures Containing Defects", R/H/R6-Rev. 3, Central Electric Generating Board, England, May 1986.

4.1.14 "10th Draft of Proposed ASTM Test Procedure for Determining the J-R Curve", prepared by the Working Group on J_I-R-Curve Test Procedure.

4.1.15 Ernst, H. A., "Material Resistance and Instability Beyond J-Controlled Crack Growth", in C. F. Shih and J. P. Gudas (eds.), Elastic-Plastic Fracture: Second Symposium, Vol. I - Inelastic Analysis, ASTM STP 803, American Society for Testing and Materials, 1983, pp. I-191 to I-213.

4.1.16 Papaspyropoulos, V., Marschall, C., and Landow, M., "Predictions of J-R Curves with Large Crack Growth from Small-Specimen Data", NUREG/CR-4575, September 1986.

4.1.17 Nakagaki, M., Marschall, C., and Brust, F., "Analysis of Cracks in Stainless Steel TIG Welds", NUREG/CR-4806, December 1986.

4.1.18 Ahmad, J., and others, "Elastic-Plastic Finite Element Analysis of Crack Growth in Large Compact (Tension) and Circumferentially Through-Wall-Cracked Pipe Specimen - Results of the First Battelle/NRC Analysis Round-Robin", NUREG/CR-4573, October 1986.

4.1.19 U.S. Nuclear Regulatory Commission, "Investigation and Evaluation of Stress Corrosion Cracking in Piping of Light-Water Reactor Plants", NUREG-0531, Chapter 7, February 1979.

4.1.20 Kramer, G. and Papaspyropoulos, V., "An Assessment of Circumferentially Complex-Cracked Pipe Subjected to Bending", NUREG/CR-4687, October 1986.

4.1.21 Wilkowski, G. M., Zahoor, A., and Kanninen, M. F., "A Plastic Fracture Mechanics Prediction of Fracture Instability in a Circumferentially Cracked Pipe in Bending - Part II: Experimental Verification on a Type 304 Stainless Steel Pipe", J. Pressure Vessel Tech., Vol. 103, 1981, pp. 359-365.

4.2 Significance of Results on In-Service Acceptance Criteria for Flaws

For the evaluation of flaws in austenitic piping, an ASME Section XI criterion currently exists. Since this criterion was developed prior to the results of this program, the results of this program have been used to verify the analysis procedure, rather than to provide an initial guidance to the criterion. Acceptance criteria for flaws in ferritic piping have been nearly completed by ASME Section XI. In this case, many of the results of this program have been used in the initial development efforts. These aspects are described below.

4.2.1 Significance of Results on ASME IWB-3640 Acceptance Criteria for Flaws in Austenitic Piping

Unlike current LBB analyses, in-service acceptance criteria for flaws are based on the analysis of a surface-cracked pipe. The ASME Section XI IWB-3640 criterion was developed to assess cracks in austenitic piping (Ref. 4.2.1). This was done mainly to assist boiling-water reactor (BWR) owners in justifying continued operation until the next scheduled outage so that they could schedule pipe repair or replacement due to intergranular stress corrosion cracks (IGSCC) at that time. Recently, a procedure for evaluating flaws in stainless steel pipe was also added to the IWB-3640 analysis procedure (Refs. 4.2.2 and 4.2.3). Flux welds (SAWs and SMAWs) have a significantly lower toughness than the wrought stainless steel base metal (Refs. 4.2.4 and 4.2.5). Since IGSCCs were found in the flux welds of the main recirculation line of the Nine Mile Point plant, this became a concern with the acceptance of the ASME austenitic flaw acceptance criteria. As noted below, a series of fracture experiments were conducted on pipes with cracks in the base metal, SAWs (donated by EPRI), and a pipe removed from the Nine Mile Point power plant. The fracture behavior of the weld-overlay repair (WOR) method was also evaluated by conducting a series of experiments at BWR conditions. The results are discussed in the following four subsections.

Evaluation of Flaws in Wrought Stainless Steel Piping

Experiments on stainless steel pipe with cracks in the wrought base metal have been used to assess the IWB-3640 analysis procedure. Tables 4.2.1 and 4.2.2 summarize these data, as well as the rest of the pipe fracture data in this program. These results have shown that the anticipated safety margins are not minimums. They are better than an average, but the exact level of confidence has not been determined. This is partially a wording problem, where the phrase "minimum safety factor" should not have been used in the technical basis document (Ref. 4.2.1). The problem originated in the selection of flow stress to be equal to $3S_m$, as a simplification, without comparison to experimental data. S_m is the ASME design stress which is related to the yield and ultimate strength. A statistical analysis of the pipe experiments (Ref. 4.2.6, Section 4.1) has shown that the flow stress on the average is equal to 1.15 (yield + ultimate)/2 which is roughly equal to the average $3S_m$ value for stainless steel at 550 F (288 C). For a 95 percent reliability

Table 4.2.1 Summary of circumferentially cracked pipe experiments.

EXPT ID#	PIPE ID#	MATERIAL	OUTER DIAM, in	SCHED.	t, in	TEST TEMP, F	LOADING TYPE	TEST FACILITY	INNER SPAN, in	OUTER SPAN, in	FLAW GEOMETR
											THROUGH-WALL-CRAC
EPRI-1T	DP2-A36	SA312 304SS	4.500	80	0.354	RT	4PTB	BCL-TL	16	60	TWC
EPRI-6T	DP2-A34	SA312 304SS	2.375	80	0.237	RT	4PTB	BCL-TL	16	46	TWC
EPRI-9T	DP2-A2	SA358 304SS	16.290	100	1.031	RT	4PTB	BCL-PS	64	540	TWC
OTPIPE7	NA	SA106 Gr6C3	8.625	80	0.540	125	4PTB	DTNSRDC	12	48	TWC
4111-1	DP2-F11	SA333 GR6	4.500	80	0.350	550	4PTB	BCL-TL	32	60	TWC
4111-2	DP2-F26	A155 CK70 CL1	28.000	NA	0.930	550	4PTB	BCL-LS	132	456	TWC
4111-3	DP2-A13	SA358 304 CL1	42.000	NA	0.280	20	4PTB	BCL-LS	132	456	TWC
4111-4	DP2-F32	API 5LX65	42.000	NA	0.625	40	4PTB	BCL-LS	132	456	TWC
4111-5	9MILE PT	316SS SMAW	28.330	NA	1.189	550	4PTB	BCL-LS	132	456	TWC
4131-5	DP2-A26	SA376 304SS	6.254	120	0.549	550	4PTB	BCL-PS	48	128	TWC
4131-7	DP2-F9	SA333 GR 6	10.750	100	0.719	550	4PTB	BCL-PS	64	234	TWC
4141-1	DP2-A26	SA376 304SS	6.625	120	0.553	550	4PTB	BCL-PS	48	128	TWC
	"	SAW WELD									
4141-3	DP2-A8	SA358 304SS	16.280	100	1.031	550	4PTB	BCL-LS	132	456	TWC
	"	SAW WELD									
4141-5	DP2-A26	SA376 304SS	6.605	120	0.555	550	4PTB	BCL-PS	48	128	TWC
		(annealed SAW)									
GAM100		304 TIG WELD	4.500	80	0.340	550	4PTB	DTNSRDC	12	42	TWC
GAM200		304 TIG WELD	4.500	80	0.340	550	4PTB	DTNSRDC	12	42	TWC
GAM700		304 TIG WELD	4.500	80	0.340	550	4PTB	DTNSRDC	12	42	TWC
GAM600		304 TIG WELD	4.500	80	0.320	550	4PTB	DTNSRDC	12	42	TWC
GAM900		304 TIG WELD	4.500	80	0.330	550	4PTB	DTNSRDC	12	42	TWC
GAM1000		304 TIG WELD	4.500	80	0.320	550	4PTB	DTNSRDC	12	42	TWC
GGK100		304 SS	4.500	80	0.327	550	4PTB	DTNSRDC	12	42	TWC
GGK200		304 SS	4.500	80	0.330	550	4PTB	DTNSRDC	12	42	TWC
GGK300		304 SS	4.500	80	0.327	550	4PTB	DTNSRDC	12	42	TWC
GGK400		304 SS	4.500	80	0.322	550	4PTB	DTNSRDC	12	42	TWC
GGK500		304 SS	4.500	80	0.328	550	4PTB	DTNSRDC	12	42	TWC
3		A106 BASE	8.625	80	0.551	125	4PTB	DTNSRDC	12	48	TWC
8		A106 BASE	8.625	80	0.534	125	4PTB	DTNSRDC	12	48	TWC
10		A106 BASE	8.625	80	0.538	125	4PTB	DTNSRDC	12	48	TWC
11		A106 BASE	8.625	80	0.597	125	4PTB	DTNSRDC	12	42	TWC
12		A106 BASE	8.625	80	0.548	125	4PTB	DTNSRDC	12	42	TWC
13		A106 BASE	8.625	80	0.526	125	4PTB	DTNSRDC	12	42	TWC
14		A106 BASE	8.625	80	0.573	125	4PTB	DTNSRDC	12	42	TWC
15		A106 BASE	8.625	80	0.560	125	4PTB	DTNSRDC	12	42	TWC
											PIPE E
4121-1	DP2-A23	SA376 304SS	6.620	120	0.507	550	INT PR.	BCL-WJ	NA	NA	TWC
4121-3	DP2-A24B	SA376 304SS	6.625	120	0.500	550	INT PR.	BCL-WJ	NA	NA	EXT SC
4121-6	DP2-F901	SA333 Gr6 CS	10.750	100	0.645	550	INT PR.	BCL-WJ	NA	NA	EXT SC

(1) Pi = load at crack initiation
(2) Pm = maximum load
(3) Pl = load calculated by net-section-collapse analysis
(4) Flow Stress = (yield stress + ultimate stress)/2
(5) Flow stress = (yield stress + ultimate stress)1.15/2
(6) Flow stress = 3Sm
(7) Outside diameter of pipe without overlay
(8) Combined thickness of pipe and overlay
(9) Initial outer span for test; span length was
experiment due to large deformations remote f

INT. PRES., psi	2C/(PI)D, %	d/t, %	P_i, (1) lbs*1000	P_m, (2) lbs*1000	FLOW STRESS, ksi (4)	(5)	(6)	P_i/P_l, (3) (4)	(5)	(6)	P_m/P_l (4)	(5)	(6)
KED PIPE EXPERIMENTS UNDER FOUR-POINT BENDING													
0	37.1	100.0	14.32	14.57	63.6	73.1	60.0	1.085	0.943	1.149	1.104	0.960	1.169
0	22.9	100.0	5.71	5.74	65.5	75.3	60.0	0.996	0.866	1.086	1.001	0.870	1.092
0	36.8	100.0	51.20	53.70	75.3	86.6	60.0	0.888	0.773	1.115	0.932	0.810	1.169
0	32.8	100.0	89.50	92.50	56.4	64.9	60.0	NA	NA	NA	0.947	0.823	0.890
0	37.0	100.0	16.30	19.80	50.2	57.7	54.3	1.001	0.871	0.925	1.216	1.058	1.123
0	37.0	100.0	89.30	131.60	56.2	64.6	68.3	0.499	0.434	0.411	0.738	0.642	0.609
0	37.0	100.0	67.18	99.58	65.4	75.2	60.0	0.453	0.394	0.494	0.671	0.584	0.732
0	37.0	100.0	161.30	291.50	72.7	83.6	NA	0.446	0.387	NA	0.805	0.700	NA
0	37.0	100.0	105.74	139.33	NA	NA	52.5	NA	NA	0.494	NA	NA	0.651
0	38.6	100.0	12.30	16.70	42.7	49.0	50.9	0.958	0.833	0.804	1.250	1.087	1.049
0	34.6	100.0	23.40	32.30	55.6	63.9	54.3	0.598	0.520	0.613	0.826	0.718	0.846
0	37.1	100.0	13.30	16.60	42.7	49.0	50.9	0.834	0.725	0.700	1.004	0.873	0.942
					57.4	66.0	NA	0.620	0.540	NA	0.746	0.649	NA
0	36.7	100.0	21.30	41.20	46.3	53.2	50.9	0.408	0.354	0.371	0.788	0.685	0.718
					57.4	66.0	NA	0.329	0.286	NA	0.636	0.553	NA
0	38.6	100.0	10.40	13.60	47.9	55.1	NA	0.605	0.526	NA	0.791	0.688	N.
0	27.8	100.0	NA	17.30	54.1	62.2	51.0	NA	NA	NA	0.780	0.678	0.827
0	38.6	100.0	NA	18.70	54.1	62.2	51.0	NA	NA	NA	0.914	0.795	0.969
0	26.8	100.0	NA	17.90	54.1	62.2	51.0	NA	NA	NA	0.782	0.680	0.829
0	32.8	100.0	NA	16.50	54.1	62.2	51.0	NA	NA	NA	0.928	0.807	0.983
0	29.7	100.0	NA	18.90	54.1	62.2	51.0	NA	NA	NA	0.930	0.809	0.986
0	29.8	100.0	NA	18.17	54.1	62.2	51.0	NA	NA	NA	0.921	0.801	0.976
			NA										
0	16.0	100.0	NA	28.40	45.3	52.1	51.0	NA	NA	NA	0.935	0.813	0.830
0	21.8	100.0	NA	19.55	45.3	52.1	51.0	NA	NA	NA	0.902	0.784	0.801
0	27.2	100.0	NA	16.98	45.3	52.1	51.0	NA	NA	NA	0.926	0.805	0.823
0	33.1	100.0	NA	14.18	45.3	52.1	51.0	NA	NA	NA	0.956	0.832	0.950
0	38.6	100.0	NA	12.80	45.3	52.1	51.0	NA	NA	NA	1.050	0.913	0.933
			NA								NA		
0	30.0	100.0	NA	106.29	56.4	64.9	60.0	NA	NA	NA	0.971	0.844	0.912
0	30.2	100.0	NA	88.94	56.4	64.9	60.0	NA	NA	NA	0.837	0.728	0.787
0	26.2	100.0	NA	117.57	56.4	64.9	60.0	NA	NA	NA	0.970	0.843	0.912
0	24.8	100.0	NA	145.23	56.4	64.9	60.0	NA	NA	NA	0.875	0.760	0.822
0	29.2	100.0	NA	152.50	56.4	64.9	60.0	NA	NA	NA	0.946	0.822	0.890
0	21.5	100.0	NA	158.87	56.4	64.9	60.0	NA	NA	NA	0.971	0.843	0.912
0	19.2	100.0	157.50	175.57	56.4	64.9	60.0	NA	NA	NA	0.936	0.814	0.880
0	21.0	100.0	NA	162.79	56.4	64.9	60.0	NA	NA	NA	0.929	0.807	0.873
XPERIMENTS UNDER AXIAL MEMBRANE STRESS													
NA	38.6	100.0	98.26	107.74	42.7	49.0	50.9	0.763	0.664	0.640	0.854	0.743	0.716
NA	50.0	70.0	150.35	150.97	42.7	49.0	50.9	0.867	0.754	0.728	0.871	0.757	0.731
NA	50.0	68.0	428.75	442.81	55.6	63.9	54.3	0.858	0.746	0.878	0.886	0.770	0.907

decreasing throughout
rom overlay

Table 4.2.1 (Continued)

EXPT ID=	PIPE ID=	MATERIAL	OUTER DIAM, in	SCHED.	t, in	TEST TEMP, F	LOADING TYP	TEST FACILITY	INNER SPAN, in	OUTER SPAN, in	FLAW GEOMETR
											SURFACE-CRACKED P
4112-1	DP2-A5B	SA358 316L	15.950	40S	0.396	550	4PTB	BCL-LS	132	456	SC
4112-2	DP2-A*	SA376 304SS	6.590	40	0.276	550	4PTB	BCL-TL	24	60	SC
4112-3	DP2-A23C	SA376 304SS	6.640	120	0.536	550	4PTB	BCL-TL	24	60	SC
4112-4	DP2-A35B	SA376 304SS	6.630	XXS	0.185	550	4PTB	BCL-TL	24	60	SC
4112-5	DP2-F1	A106B	6.670	40	0.293	550	4PTB	BCL-TL	24	60	SC
4112-6	DP2-F30D	A106B	6.590	120	0.582	550	4PTB	BCL-TL	24	60	SC
4112-7	DP2-F3B	A106B	6.620	XXS	0.845	550	4PTB	BCL-TL	24	60	SC
4112-8	DP2-F29	A106B	15.850	100	1.040	550	4PTB	BCL-LS	132	456	SC
4112-9	DP2-F13	A106B	15.940	40	0.500	550	4PTB	BCL-LS	132	456	SC
4115-1	DP2-F9	SA333 Gr 6	10.440	100	0.680	550	4PTB	BCL-PS	64	175	SC
4115-2	DP2-F9	SA333 Gr 6	10.710	100	0.674	550	4PTB	BCL-PS	132	454	SC
4115-4	DP2-A27	SA376 304SS	6.620	120	0.587	550	4PTB	BCL-PS	48	100	SC
4115-5	DP2-A27	SA376 304SS	6.620	120	0.588	550	4PTB	BCL-PS	48	94	SC
4115-7	DP2-A27	SA376 304SS	6.600	120	0.549	550	4PTB	BCL-PS	48	92	SC
4115-8	DP2-A23	SA376 304SS	6.612	120	0.553	550	4PTB	BCL-TL	24	60	SC
4115-9	DP2-A23	SA376 304SS	6.630	120	0.551	550	4PTB	BCL-TL	24	40	SC
4131-6	DP2-A26	SA376 304SS	6.254	120	0.563	550	4PTB	BCL-PS	64	158	SC
4131-8	DP2-F9	SA333 GR 6	10.655	100	0.593	550	4PTB	BCL-PS	64	216	SC
EPRI13S	DP2-A8	SA358 304SS	16.280	100	1.115	RT	4PTB	BCL-PS	64	540	SC
											SURFACE-CRACKED PIPE EXP
4131-2	DP2-A27	SA376 304SS	6.627	120	0.529	550	4PTBP	BCL-PS	48	108	SC
4131-4	DP2-F9	SA333 Gr6 CS	10.741	100	0.654	550	4PTBP	BCL-PS	64	216	SC
4141-2	DP2-A26	SA376 304SS	6.582	120	0.584	550	4PTBP	BCL-PS	48	160	SC
	"	SAW WELD									
4141-4	DP2-A8	SA358 304SS	16.280	100	1.031	550	4PTBP	BCL-LS	132	456	SC
	"	SAW WELD									
4141-6	DP2-A8	SA358 304SS	16.390	100	1.040	550	4PTBP	BCL-LS	132	456	SC
		(annealed SAW)									
4142-1	DP2-A25	SA376 304SS	6.625 (7)	120	0.879 (8)	550	4PTBP	BCL-PS	48	122 (9)	SC
	DP2-A25WO	308L WOP									
4142-2	DP2-A25	SA376 304SS	6.625 (7)	120	0.891 (8)	550	4PTBP	BCL-PS	48	122 (9)	SC
	DP2-A25WO	308L WOP									
4142-3	DP2-A25	SA376 304SS	6.625 (7)	120	0.889 (8)	550	4PTBP	BCL-PS	48	122 (9)	SC
	DP2-A25WO	308L WOP									
4142-4	DP2-A8	SA358 304SS	16.380 (7)	100	1.542 (8)	550	4PTBP	BCL-LS	132	456 (9)	SC
	DP2-A25WO	308L WOP									
											COMPLEX-CRACKED P
4113-1	DP2-A24C	SA376 304SS	6.625	120	0.570	550	4PTB	BCL-TL	24	60	CC
4113-2	DP2-A24D	SA376 304SS	6.625	120	0.570	550	4PTB	BCL-TL	24	60	CC
4113-3	DP2-I1C	INCONEL 600	6.625	80	0.435	550	4PTB	BCL-TL	24	60	CC
4113-4	DP2-I1B	INCONEL 600	6.625	80	0.435	550	4PTB	BCL-TL	24	60	CC
4113-5	DP2-F30C	A106 GR B	6.625	120	0.560	550	4PTB	BCL-TL	24	60	CC
4113-6	DP2-F30B	A106 GR B	6.625	120	0.560	550	4PTB	BCL-TL	24	60	CC
4114-1	DP2-F31A	A106 Gr B CS	6.625	120	0.501	550	4PTB	BCL-PS	48	42	CC
4114-2	DP2-A23	SA376 304SS	6.545	120	0.530	550	4PTB	BCL-PS	48	144	CC
GAM1400		304 SS TIG WELD	4.500	80	0.340	550	4PTB	DTNSRDC	12	42	CC
GAM600		304 SS TIG WELD	4.501	80	0.330	550	4PTB	DTNSRDC	12	42	CC
GAM1100		304 SS TIG WELD	4.500	80	0.330	550	4PTB	DTNSRDC	12	42	CC
											THROUGH-WALL CRAC
4131-1	DP2-A26	SA376 304 SS	6.553	120	0.528	550	4PTBP	BCL-PS	48	126	THR

(1) P_i = load at crack initiation
(2) P_m = maximum load
(3) P_l = load calculated by net-section-collapse analysis
(4) Flow Stress = (yield stress + ultimate stress)/2
(5) Flow stress = (yield stress + ultimate stress)1.15/2
(6) Flow stress = $3S_m$

(7) Outside diameter of pipe without overlay
(8) Combined thickness of pipe and overlay
(9) Initial outer span for test; span length was ... experiment due to large deformations remote ...

INT. PRES., psi	2C/ (PI)D, %	d/t, %	Pi, (1) lbs*1000	Pm, (2) lbs*1000	FLOW STRESS, ksi (4)	(5)	(6)	Pi/Pl, (3) (4)	(5)	(6)	Pm/Pl (4)	(5)	(6)
IPE EXPERIMENTS UNDER FOUR-POINT BENDING													
0	51.0	66.0	22.00	25.16	46.2	53.1	41.9	0.773	0.672	0.853	0.884	0.769	0.976
0	50.0	63.0	25.46	30.10	43.2	49.7	50.9	0.853	0.742	0.725	1.009	0.877	0.857
0	52.0	66.0	57.90	61.95	42.7	49.0	50.9	1.157	1.006	0.970	1.238	1.076	1.038
0	44.0	65.0	106.80	110.35	45.6	52.4	50.9	1.242	1.080	1.113	1 284	1.116	1.150
0	51.0	63.0	23.90	38.20	49.3	56.7	54.3	0.653	0.568	0.593	1.044	0.908	0.948
0	50.0	68.0	67.80	80.30	68.2	78.4	54.3	0.818	0.711	1.027	0.969	0.843	1.217
0	53.0	63.0	98.60	119.40	60.1	69.1	54.3	0.949	0.826	1.051	1.149	1.000	1.272
0	53.0	66.0	75.30	81.76	61.4	70.6	54.3	0.831	0.722	0.939	0.902	0.784	1.020
0	54.0	66.0	32.85	39.94	63.3	72.8	54.3	0.678	0.590	0.791	0.825	0.717	0.961
0	34.0	70.0	65.40	70.50	55.6	63.9	54.3	0.869	0.755	0.889	0.936	0.814	0.959
0	43.0	77.0	22.30	25.80	55.6	63.9	54.3	0.880	0.765	0.901	1.017	0.885	1.042
0	38.0	50.0	NA	47.70	42.7	49.0	50.9	NA	NA	NA	0.940	0.819	0.789
0	38.0	75.0	NA	25.50	42.7	49.0	50.9	NA	NA	NA	0.581	0.506	0.488
0	100.0	64.7	48.74	52.45	42.7	49.0	50.9	1.186	1.034	0.996	1.277	1.113	1.072
0	100.0	62.6	61.90	63.90	42.6	49.0	50.9	1.162	1.010	0.974	1.200	1.043	1.005
0	100.0	65.5	141.75	178.30	42.6	49.0	50.9	1.267	1.102	1.062	1.594	1.306	1.335
0	54.0	69.0	17.50	17.80	42.7	49.0	50.9	1.260	1.095	1.056	1.281	1.114	1.075
0	48.0	68.0	42.25	45.40	55.6	63.9	54.3	0.904	0.786	0.926	0.971	0.845	0.995
0	47.5	66.0	72.16	93.75	75.3	86.6	60.0	0.805	0.700	1.011	1.046	0.910	1.313
ERIMENTS UNDER FOUR-POINT BENDING WITH INTERNAL PRESSURE													
3550	52.1	70.9	18.95	20.13	42.7	49.1	50.9	1.245	0.970	0.914	1.322	1.031	0.971
2650	52.5	65.9	33.14	37.25	55.6	63.9	54.3	0.917	0.751	0.950	1.031	0.844	1.068
2200	50.0	64.0	12.60	13.00	42.7	49.0	50.9	0.851	0.719	0.689	0.878	0.742	0.711
					57.4	66.0	NA	0.599	0.311	NA	0.618	0.321	NA
1600	50.0	67.0	54.40	54.80	46.3	53.2	50.9	0.925	0.778	0.823	0.931	0.783	0.829
					57.4	66.0	NA	0.711	0.603	NA	0.716	0.608	NA
1600	50.0	68.6	48.36	48.67	47.9	55.1	NA	1.282	0.673	NA	1.290	0.677	NA
1150	50.0	65.2	NA	51.26	42.7	49.0	50.9	NA	NA	NA	1.049	0.910	0.876
					50.4	57.9	NA	NA	NA	NA	NA	NA	NA
4750	50.0	63.5	30.70	31.19	42.7	49.0	50.9	0.827	0.706	0.661	0.841	0.717	0.671
					50.4	57.9	NA	NA	NA	NA	NA	NA	NA
5700	50.0	64.9	NA	29.30	42.7	49.0	50.9	NA	NA	NA	0.806	0.686	0.630
					50.4	57.9	NA	NA	NA	NA	NA	NA	NA
3250	38.0	65.4	NA	115.47	46.3	53.2	50.9	NA	NA	NA	0.956	0.816	0.850
					50.4	57.9	NA	NA	NA	NA	NA	NA	NA
IPE EXPERIMENTS UNDER FOUR-POINT BENDING													
0	37.0	31.6	24.70	27.90	42.7	49.0	50.9	0.912	0.793	0.765	1.030	0.896	0.864
0	37.0	63.2	17.00	18.20	42.7	49.0	50.9	1.102	0.959	0.925	1.180	1.026	0.990
0	37.0	34.0	23.90	26.50	58.5	67.2	60.0	0.847	0.736	0.825	0.939	0.816	0.914
0	37.0	61.0	17.70	19.50	58.5	67.2	60.0	1.023	0.889	0.996	1.127	0.980	1.098
0	37.0	31.3	26.60	33.10	68.2	78.4	54.3	0.622	0.541	0.781	0.774	0.673	0.972
0	37.0	64.3	12.40	13.90	68.2	78.4	54.3	0.526	0.457	0.661	0.844	0.734	1.060
0	37.0	47.0	14.00	18.65	68.2	78.4	50.9	0.558	0.485	0.748	0.743	0.646	0.997
0	37.0	32.0	0.00	0.00	42.7	49.0	50.9	0.000	0.000	0.000	0.000	0.000	0.000
0	42.8	38.0	NA	9.40	54.1	62.2	51.0	NA	NA	NA	1.140	0.991	1.208
0	35.6	25.6	NA	11.95	54.1	62.2	51.0	NA	NA	NA	0.938	0.815	0.994
0	40.8	24.5	NA	19.70	54.1	62.2	51.0	NA	NA	NA	1.884	1.638	1.997
KED PIPE EXPERIMENTS UNDER FOUR-POINT BENDING WITH INTERNAL PRESSURE													
2500	37.0	100.0	6.90	8.97	42.7	49.0	50.9	NA	NA	NA	NA	NA	NA

decreasing throughout
ow overlay

Table 3.1.2 Material characterization data for ferritic pipe mater

Pipe I.D.	Pipe Mat.	Pipe size Dia. in.	Wall in.	Charpy V Notch Spec size	USE,ft-lb	FATT, F	Test Temp.,F	Average YS, ksi	Average UTS, k
DP2-F29	A106B	16	1.031	Full	75	68	72	40.1	75.2
							300	36.5	87.5
							300		
							550	34.4	88.5
							550		
							550		
DP2-F9	SA333-Gr6	10	0.719	Full	115	-4	72	40.8	65.7
							300	39.8	70.0
							300		
							550	34.7	76.5
							550		
							550		
							550		
							550		
DP2-F30	A106B	6	0.562	Full	110	100	77	45.6	75.4
							300	44.7	91.1
							550	46.4	90.0
							550		
							550		
DP2-F26	A155	28	0.875	Full	102	60	72	39.1	63.6
							300	38.9	76.3
							300		
							550	33.5	78.5
							550		
							550		
							550		
DP2-F32	API-5LX65	42	0.875	Full	72	-50	72	63.0	82.
DP2-F1	A106B	6	0.280	0.58	70	-140	75	42.8	68.
							300	37.2	62.
							550	30.8	67.
							550		
							550		
DP2-F40	A516,Gr.70	Plate	1.0				550	34.1	79.
							550		
DP2-F40W2	SAW;A516,Gr.70	Plate	1.0	Full	58	68	550	64.2	104.
							550		
							550		
							550		
							550		
							550		
							550		
							550		

ials.

Tensile Properties			Fracture Toughness Data								
si % Elong.	Gage Length, inches	%, Red of Area	Spec. Type	Notch Type	% Side-grooves	Orientation	W, inches	B, inches	No. of Tests	Ji, ave. in.-lb/in.^2	dJm/da, ave. in.-lb/in.^3
29.6	1.0	61.4									
18.6	1.0	44.5	C(T)	FC	0	L-C	2.00	0.85	1	660	11020
			C(T)	FC	20	L-C	2.00	0.85	1	295	10750
24.0	1.0	41.4	C(T)	FC	0	L-C	2.00	0.85	1	635	16410
			C(T)	FC	20	L-C	2.00	0.85	1	850	12910
			FWFN(T)	SMN	10	L-R	0.71	1.6	2	2025	60950
39.1	1.0	73.0									
24.8	1.0	63.6	C(T)	FC	0	L-C	2.00	0.55	1	861	23490
			C(T)	FC	20	L-C	2.00	0.55	1	966	8700
27.3	1.0	60.0	C(T)	FC	0	L-C	2.00	0.55	1	885	31950
			C(T)	FC	20	L-C	2.00	0.55	1	900	19180
			C(T)	SMN	0	L-C	2.00	0.52	1	1700	22950
			C(T)	SMN	20	L-C	2.00	0.52	1	1120	10500
			FWFN(T)	SMN	10	L-R	0.57	2.4	4	1160	74500
38.6	0.5	62.2									
23.6	0.5	37.6	C(T)	FC	0	L-C	1.0	0.36	2	732	19350
24.0	0.5	34.4	C(T)	FC	0	L-C	1.00	0.36	2	680	19650
			C(T)	FC	20	L-C	1.00	0.36	2	588	15550
			FWFN(T)	SMN	10	L-R	0.44	1.60	2	1456	33025
34.3	1.0	69.5									
22.8	1.0	51.6	C(T)	FC	0	L-C	2.00	0.76	1	610	20670
			C(T)	FC	20	L-C	2.00	0.76	1	628	13650
29.8	1.0	53.6	C)T)	FC	0	L-C	2.00	0.76	1	1030	N.D.
			C(T)	FC	20	L-C	2.00	0.76	1	1240	19500
			C(T)	SMN	0	L-C	2.00	0.83	1	1483	N.D.
			C(T)	SMN	20	L-C	2.00	0.83	1	1180	18200
25.1	1.0	66.9	3Pt Bend	SMN	0	L-C	3.50	0.53	1	2275	37000
38.7	0.5	64.6									
32.9	0.5	70.9	C(T)	FC	0	L-C	0.80	0.23	2	2095	32260
25.0	0.5	54.7	C(T)	FC	0	L-C	0.80	0.23	2	2303	40390
			C(T)	FC	20	L-C	0.80	0.23	2	1388	23350
			FWFN(T)	SMN	10	L-R	0.22	1.00	2	1960	109600
33.0	1.0	69.5	C(T)	FC	0	L-T	2.0	1.00	1	1645	35300
			C(T)	FC	20	L-T	2.0	1.00	1	1305	20800
31.0	0.5	43.4	C(T)	FC	0	WCL	2.0	1.0	1	335	8900
			C(T)	FC	20	WCL	2.0	1.0	1	356	8370
			C(T)	SMN	0	WCL	2.0	1.0	1	735	N.D.
			C(T)	SMN	20	WCL	2.0	1.0	1	690	N.D
			C(T)	FC	0	WCL	19.0	1.0	1	1010	7900
			C(T)	FC	20	WCL	19.0	1.0	1	564	2230
			C(T)	FC	0	WCL	6.0	1.1	1	534	10070
			C(T)	FC	20	WCL	6.0	1.1	1	537	6240

level, (that is, two standard deviations below the average of the failure stresses) the flow stress was found to be very close to the average of the yield and ultimate strengths.

Evaluation of the ASME IWB-3640 Stainless Steel Criterion for Flux Weld

Recently the ASME Code IWB-3640 analysis procedure was modified to include a criterion for low-toughness flux welds (Ref. 4.2.2). This was based on a through-wall crack analysis using the EPRI/GE J-estimation scheme (Ref. 4.2.2). As previously noted, the EPRI/GE method for through-wall-cracked pipes is the most conservative J-estimation analysis. Another source of conservatism is pointed out in the PZSC, developed in this program. This has shown that through-wall-cracked pipes are more sensitive to toughness than surface-cracked pipe (Figure 2.7.8). These two points make the flux weld criterion inherently conservative. In comparing the experimental data from this program to the ASME flux weld criterion, it was found that the experimental loads were from 1 percent to 47 percent above the predicted loads when no safety factors were included in the analysis. Hence, these results tended to verify the procedure for flaws in flux welds.

An interesting recent discovery during the course of conducting these experiments was that the SAW J-R curve used in the development of this flux weld criterion was found to actually be from an SMAW (Ref. 4.2.7). The SAW J_i-values from this program are approximately 550 in-lb/in^2 (96 kJ/m^2) which is lower than the "SAW" J-R curve believed to have been used in the ASME flux weld criterion. The more representative values of J_i for submerged arc and SAWs that should have been used are 550 in-lb/in^2 (96 kJ/m^2), and 650 in-lb/in^2 (114 kJ/m^2), respectively, rather than the 650 in-lb/in^2 (114 kJ/m^2) and 990 in-lb/in^2 (174 kJ/m^2) values used in the ASME IWB-3640 technical basis document.[1] The inherent safety factor in using the EPRI/GE through-wall analysis probably compensated for these errors, especially if the Code safety margins are considered as average rather than minimum values.

Stainless Steel Heat-Affected Zone and Fusion Line Toughness

Laboratory specimens tested to simulate circumferential surface crack growth in a pipe showed that the initiation and crack growth resistance was as high in the heat-affected zone (HAZ) as it was in the base metal. Hence, sensitization of the stainless steel does not affect the ductile fracture toughness. This is consistent with findings in a past EPRI program (Ref. 4.2.8).

During this program we also found that for a stainless steel SMAW, the crack propagation resistance along the fusion line was approximately half of the

---

[1] J_i is used rather than J_{Ic} since ASTM E-813 specifically excludes stainless steels from being within the standard's scope. Hence, these values are not valid J_{Ic} values.

crack growth resistance even in the lower-toughness flux weld (Section 2.7). Current flaw assessment and pipe fracture analyses consider weld metal properties, but fusion line toughness is not considered. Since IGSCCs that initiate in the HAZ more frequently grow along the fusion line than into the weld metal, this observed lower crack propagation resistance in the fusion line may be of concern. In the laboratory experiment conducted, the crack initiated away from the fusion line, so the fusion line initiation toughness is still an unknown. This is an area where no further research activities are currently planned, but the results could affect the ASME Code flaw acceptance criteria and the NRC's pipe fracture analyses and LBB acceptance in BWR piping.

Evaluation of the Fracture Behavior of Weld-Overlay Repairs

A series of experiments was conducted to evaluate the load carrying capacity of cracked pipes with weld overlay repairs (WORs). WORs have been used in BWRs as a remedial repair method, and there is interest in leaving the WORs in place as a permanent repair. There are currently no prescribed analysis methods in the ASME IWB-3640 procedures for WORs, although they are designed in the spirit of IWB-3640. However, in the absence of firm criteria, the exact design procedures apparently have been variable. For example, one could use the total thickness in the calculations, either the mean or outside radius of either the pipe or the overlay, and if the crack is considered to be completely through the pipe one might try to use the strength of the weld metal rather than the base metal in the limit-load calculations. Three 6-inch- (152-mm-) diameter and one 16-inch- (406-mm-) diameter pipe experiments have been conducted (Ref. 4.2.9). The overlays were fabricated by NUTECH according to in-plant procedures. The results show that using the IWB-3641 tables without the safety factor is a conservative analysis. If the source equations were used, per ASME Code Case N-436 (Ref. 4.2.3), then the experiments failed at loads 9 percent below the Source Equation predictions when the safety factors were not used. If the weld metal strength was used, then the specimens used in the experiments failed well below the source equation predictions. If the thickness of the overlay is ignored, that is, the pipe thickness is used with the actual crack-depth-to thickness ratio, then all procedures would be conservative.

4.2.2 Significance of Results on Acceptance Criteria for Flaws in Ferritic Piping

Evaluation procedures for flaws in ferritic piping have been nearly completed by the ASME Section XI Committee. This procedure will be referred to as Article IWB-3650 once it has been accepted. Some aspects of this program's results relative to ferritic piping criteria in general are discussed below.

Database for Acceptance Criteria for Flaws in Ferritic Piping

Data from carbon steel pipes with surface cracks in the base metal have been developed for comparison with tentative carbon steel criteria being evaluated in the ASME Section XI Committee. This database is given in Table 4.2.1 for circumferentially cracked pipe, and Table 4.2.2 for axially cracked pipe

experiments from an older AEC program conducted at Battelle (Ref. 4.2.10). A lack of data, however, exists for carbon steel welds and large diameter thermally aged pipe. Such experiments are currently being prepared in this program (Sections 2.10 and 2.11).

Development of a Unified Statistical Criterion

One of the eventual goals of the ASME Section XI Pipe Flaw Task Group is to develop a single criterion for both austenitic and carbon steel piping. From the database in this program, we have developed a load-carrying capacity analysis that could be used for predicting the behavior of stainless steel as well as carbon steel piping and their weldments at the 95 percent reliability level (two standard deviations below the average of the failure stresses). This analysis is based upon a simplified dimensionless plastic-zone parameter. The procedure is relatively simple and is described in Reference 4.2.6, Section 4.1. It incorporates the use of a dimensionless plastic-zone parameter to determine if fully plastic or net-section-collapse conditions exist, in which case the existing IWB-3640 Source Equations would be used. If fully plastic conditions do not prevail, then a stress multiplier is used to account for the lower failure stresses. Fracture toughness is incorporated using either J-integral or Charpy data. An empirical ovalization correction function defined from the surface-cracked pipe fracture database was also included. Statistical data from this program and others were used to provide conservative correlations between Charpy data and J. If neither J-integral nor Charpy data are available, then generic lower bounds need to be established. Such lower bounds could be established from the NRC's Piping Fracture Mechanics Data Base developed for the NRC at Materials Engineering Associates (MEA) (Ref. 4.2.11).

Analytical Verification of Surface-Cracked Pipe Criteria

For the evaluation of surface-cracked pipe, there are very few existing analyses. Those used in the ASME Code are either limit-load analyses (Ref. 4.2.12), or are approximate fracture mechanics approaches. One surface-cracked pipe fracture mechanics analysis is the EPRI/GE estimation scheme (Ref. 4.2.13). This is limited to 360-degree surface-cracked pipe in tension. Consequently, a finite length surface-cracked pipe estimation scheme has been developed in this program, see Reference 4.2.14 and Section 2.2 in this report. Thick shell and thin shell analyses have been developed. The thin shell analysis tends to overpredict the experimental failure stresses, while the thick shell analysis underpredicts the experimental failure stresses. This method could be used in the future as a technical basis to improve or provide confidence in surface-cracked pipe criteria. Specifically, the ASME approach does not consider the effect of the length of the surface crack in their toughness reduction parameter.

A new specimen type has been developed to provide J-R curves that are needed to evaluate surface cracks in pipe. This specimen, described as a full-width face-notched (tension) [FWFN(T)] specimen, simulates the tension loading that occurs in the ligament of a surface crack and has the crack growing in the same direction. To the extent that orientation and geometry effects are important,

this specimen should provide better material property data for use in surface-cracked pipe fracture analyses.

To help guide and evaluate the surface-cracked pipe J-estimation scheme development discussed above, one finite length surface-cracked pipe finite element analysis was performed, modeling a carbon steel pipe experiment conducted in this program. The same pipe experiment was used in an analytical round-robin where both J-estimation schemes and finite element analyses were compared, see Section 3.5.5 in this report. These results showed that the surface-cracked finite element results are sensitive to the mesh refinement in the ligament of the surface crack. The results that appear to have the proper amount of mesh refinement, however, have J values at crack initiation (where crack initiation was determined from the experimental data) that are 60 percent of the J_i from a compact (tension) [C(T)] specimen or the full-width-face-notched (tension) [FWFN(T)] specimen. This implies that there may be a geometry effect on the J at crack initiation. Furthermore, if such an analysis were used with a given J-R curve to predict the failure loads, it would overpredict the failure stresses of the surface-cracked pipe.

References for Section 4.2

4.2.1 "Evaluation of Flaws in Austenitic Steel Piping" (Technical basis document for ASME IWB-3640 analysis procedure), prepared by Section XI Task Group for Piping Flaw Evaluation, EPRI Report NP-4690-SR, April 1986.

4.2.2 ASME Boiler and Pressure Vessel Code, Section XI, "Rules for In-Service Inspection of Nuclear Power Plant Components", Article IWB-3640, Evaluation Procedures and Acceptance Criteria for Austenitic Piping, Winter 1983 Addendum.

4.2.3 ASME Boiler and Pressure Vessel Code, Section XI, Division 1, Case N-436, "Alternative Methods for Evaluation of Flaws in Austenitic Piping", May 14, 1986, pp. 763-765.

4.2.4 Wilkowski, G. M., and others, "Analysis of Experiments on Stainless Steel Flux Welds", NUREG/CR-4878, April 1987.

4.2.5 Gudas, J. P., and Anderson, D. R., "J-R Characterization of Piping Materials and Welds", U.S. NRC 9th Water Reactor Safety Research Information Meeting, Washington, DC, October 1981.

4.2.6 Wilkowski, G. M., and others, "Degraded Piping Program - Phase II", Semiannual Report, April 1986-September 1986, NUREG/CR-4082, Vol. 5, April 1987.

4.2.7 Delwiche, D. E., and Gordon, G. M. (chair), General Electric San Jose CA (compilers), "Nine Mile Point 1 Pipe Crack Task Force Report", sponsored by Niagra Mohawk Power Corporation, Syracuse, N.Y., June 20, 1983, pp. 5-4 and 5-5.

4.2.8 Kanninen, M. F., and others, "Instability Predictions for Circumferentially Cracked Type 304 Stainless Steel Pipes Under Dynamic Loading", Final Report on EPRI Project T118-2, EPRI Report Number NP-2347, April 1982.

4.2.9 Scott, P. M., "Assessment of Design Basis for Load-Carrying Capacity of Weld-Overlay Repairs", NUREG/CR-4877, April 1987.

4.2.10 Eiber, R. J., Maxey, W. A., and Duffy, A., "Investigation of the Initiation and Extent of Ductile Pipe Rupture", BMI Report 190R to the AEC, June 1971.

4.2.11 Hiser, A. L., and Callahan, G. M., "A User's Guide to the NRC's Piping Fracture Mechanics Data Base (PIFRAC)", NUREG/CR-4894, May 1987.

4.2.12 Kanninen, M. F., and others, "Mechanical Fracture Predictions for Sensitized Stainless Steel Piping with Circumferential Cracks", EPRI NP-192, September 1976.

4.2.13 Kumar, V., and others, "Advances in Elastic-Plastic Fracture Analysis", EPRI NP-3607, August 1984.

4.2.14 Scott, P. M., and Ahmad, J. A., "Experimental and Analytical Assessment of Circumferentially Surface-Cracked Pipes Under Bending", NUREG/CR-4872, April 1972.

4.3 Potential Impact of Material Characterization Evaluations and Unusual Fracture Modes Observed in Nuclear Piping Materials on Pipe Fracture Analysis and Pipe Flaw Evaluation Procedures

During the course of this program, numerous evaluations of material properties were conducted. In some of the pipe experiments and laboratory specimen tests, unexpected results were obtained. The significance of these results is discussed below.

4.3.1 Material Characterization and Database Efforts

To evaluate pipe fracture or flaw assessment analyses, it is necessary to document material property data carefully. This information is used to evaluate the pipe fracture experiments and also provides a valuable database for use in assessing Code analysis procedures. The following data were developed for every pipe specimen tested in this program: chemical analysis; tensile test engineering and true stress-true strain curves at room temperature, 300 F (149 C), and 550 F (288 C); and Deformation Theory J-R curves and Modified J-R curves for standard compact specimens at 300 F (149 C) and 550 F (288 C). The orientation of these specimens simulated circumferential through-wall crack growth. For ferritic steels, Charpy transition curves were developed. Also for pipes tested with surface cracks, full-width-face-notched tension, FWFN(T), specimens have been tested at the pipe test temperature. These data have been included in the NRC Piping Fracture Mechanics Data Base (Ref. 4.3.1). Such information will be useful in establishing generic material lower bound or statistically acceptable toughness values for use in the ASME Code or LBB applications such as noted in NRC Standard Review Plan 3.6.3 "Leak-Before-Break Procedures".

Data that currently appear to be lacking include ferritic weld toughness (especially SMAWs), thermally aged material data, and fusion line toughness data.

Some observations made during from the material characterization efforts may impact piping analyses. These observations are described below.

Reproducibility of Tensile Test Data

In many fracture mechanics analyses, the crack driving force calculations are sensitive to the fit between the stress-strain curve data and the Ramberg-Osgood relation. To assess the reproducibility of tensile stress-strain curves, a round-robin was carried out with several NRC contractors. This showed that the various labs reasonably reproduced the true stress-strain curves at 550 F (288 C) (Section 3.5.1). These data might also be useful at some time in the future to assess the sensitivity of the pipe J-estimation schemes to statistical variations of the material strength. Currently these data are being used to assess the sensitivity of pipe fracture analyses if average, rather than lower bound, stress-strain curves are used.

Detection of Crack Initiation

For many of the nuclear piping materials evaluated in this program, it was difficult to detect the start of crack initiation in the laboratory specimen testing. The direct-current (d-c) electric potential method was used to give greater sensitivity, but in many cases it was necessary to use engineering judgment and experience to pick the point of crack initiation. Currently, it appears that more of the technical community is changing from the unloading compliance technique to the d-c electric potential method for crack growth monitoring. Consequently, there is a need to standardize a d-c electric potential procedure to detect crack initiation and to monitor crack growth to provide a verifiable database that can be used in licensing decisions. Currently, the David Taylor Research Center (DTRC) is conducting a round-robin on the d-c electric potential method which should help to standardize the method.

Reproducibility of J-R Curve Calculations

In ASTM E1152-87, Standard Test Method for Determining J-R Curves, the necessary equations to compute J from the test data are given, but no sample calculations for verification of computer programs are provided. With the advent of other versions of J, Modified J for example, it becomes more important to have a quality assurance check. During the data reduction efforts in this program, it was deemed worthwhile to conduct a calculational round-robin to see if all the NRC contractors were indeed calculating Deformation Theory and Modified J-R curves in exactly the same way (Section 3.5.2). From the given load, displacement, and crack-growth data it was found that most of the participants were calculating J-R curves that differed only by round-off error. One participant had a difference of 1 percent, because of erroneous compliance equations (different from those given) used to calculate the J-R curves. This sample calculational problem is a valuable check that added confidence to the material property data being generated, and should perhaps be adopted as an appendix to ASTM E1152-87.

Fracture Toughness Correlations with Charpy Data

More often than not, J-R curve toughness data are not available to make a practical flaw assessment. Hence, if Charpy data are available from mill reports, they can become valuable in estimating the actual toughness. Charpy data could also be used as a quality control toughness requirement for new plants, or for flaw assessments if plant records could be retrieved. In Germany, for instance, Kraftwerke Union has a Charpy energy requirement for carbon steel piping (Ref. 4.3.2).

From the data developed for the pipe materials, a lower bound Charpy plateau energy versus J correlation was verified for nuclear ferritic steels at 550 F (288 C). This correlation could be valuable in pipe fracture analyses or flaw assessment criteria. In Reference 4.3.3, Section 4.1 shows how the correlation was used in the Simplified Plastic-Zone Statistical analysis.

In addition, the Charpy data were used to develop a statistical correlation where the Charpy plateau energy could be determined if transition temperature Charpy energy and shear area percent data were available (Ref. 4.3.3, pp. 4-16). The calculated plateau energy could then be used to estimate J from the above noted correlation. This could prove useful in ferritic pipe flaw assessment criteria.

One point of caution in using Charpy to J_{Ic} correlations is that they need to be sufficiently conservative to account for the effect of dynamic strain aging, which can reduce the material's toughness. Alternatively, a screening criterion could be developed to show when a material is not susceptible to dynamic strain aging, and a less conservative Charpy to J_{Ic} correlation could be developed.

4.3.2 Extrapolation of J-Resistance Curves to Larger Amounts of Crack Growth

In the prediction of through-wall pipe fracture experiments and for pipe fracture analyses, it is sometimes necessary to extrapolate J-R curves from small specimens to larger amounts of crack growth. In NUREG-1061 Volume 3 (Ref. 4.3.4), one procedure was suggested for deformation theory J-R curves. This involved a tangent extrapolation of J-R curve data when plotted in terms of J versus the tearing modulus, T, (T is proportional to dJ/da.)

To evaluate this aproach, three different specimen sizes of the same thickness were tested in this program from plate materials, (Section 3.3 and Ref. 4.3.5). The results showed that the NUREG-1061 Volume 3 method was extremely conservative and generally unusable because of the restrictions it employs. A further assessment involved the use of the Modified J-R curves. In this analysis, it was found that, contrary to the data of Ernst, who developed the parameter (Ref. 4.3.6), the Modified J-R curve approach did not eliminate all of the geometry effects. This may be due to the fact that the nuclear piping materials tested are believed to fracture under plane stress conditions, whereas plane strain is believed to prevail in the specimens and materials used by Ernst.

In order to provide some method that might appear workable, a hyperbolic fit to the Modified J-R curve was proposed in Reference 4.3.5. This required data from a standard small specimen which gave lower J values, and data from a larger specimen of the same thickness which gave a lower T value. Results from Section 3.3 of this report suggest that a C(T) specimen with a planform size larger than 4 times the specimen thickness is needed to get a lower bound tearing resistance.

4.3.3 Determining J-R Curves for Weld Metal Specimens

In most pipe fracture and flaw assessment analyses, the critical flaw locations are in or near welds. For toughness evaluations of welds, another consideration is the specimen size selection relative to the size of the weldment. The analysis procedures used in reducing these data are based on

the assumption of a homogeneous specimen. One can imagine that if most of the specimen consists of a high-strength weld metal, then the current ASTM analysis procedures will give a J that is close to that of the weld itself. However, if most of the specimen consists of a lower strength base metal, then the ASTM calculated J could be much higher because of the deformation contributions in the lower strength base metal. The J value here is not a material property, but rather reflects geometry and dissimilar material structural interactions. Limited studies to date suggest that two specimen sizes may be needed to evaluate the behavior of a larger structure, such as a pipe with a flawed girth weld (Ref. 4.3.7). Further efforts are needed to define weld specimen design considerations, and may evolve from current welded pipe fracture experimental results.

Another important finding was that for a stainless steel flux weld, the use of the high-toughness tungsten-inert-gas (TIG) weld metal in the root and initial hot passes can affect the composite toughness of the weldment. Thinner stainless steel SAWs have a greater percentage of the tougher TIG weld metal and hence exhibit a higher toughness. Data from thinner welds should not be used to assess a thick pipe.

4.3.4 Possible Role of Dynamic Strain Aging in Causing Metallurgically Induced Instabilities in Ferritic Steels at 550 F (288 C)

In pipe fracture experiments and laboratory specimen tests at 550 F (288 C) on some nuclear grade ferritic piping materials and their weldments, limited crack instabilities were frequently observed. These crack instabilities occurred in low compliance experiments. Prior to the start of this program, such instabilities were not expected to occur. In one pipe experiment, these limited crack instabilities were found to lower the crack growth resistance by 60 percent (Ref. 4.3.8). It is believed that these crack instabilities may be due to dynamic strain aging (DSA) at the crack tip (Section 3.1.2). One concern is how well small specimen data can predict the reduction in the toughness that can occur from these metallurgically induced instabilities in a pipe. A second concern is the effect of higher strain-rates, such as those that occur in a seismic event, on the fracture resistance. A basic understanding of the possible role of DSA on these crack jumps is needed.

4.3.5 Anisotropy Effects on Crack Growth Behavior in Ferritic Steel Piping Materials

It was observed in most of the pipe experiments on ferritic pipes that the crack grew out of the circumferential plane (Section 3.1.3). For one of these materials, laboratory specimens were machined out of the pipe in several different orientations. Test data showed that the toughness was lower in the helical direction in which the crack grew. This was also confirmed by metallographic sections which showed inclusions oriented in the direction of that helical angle. This helical anisotropy probably comes from the hot forming in seamless pipe manufacturing. This failure mode was most striking in a circumferential cracked cold-leg pipe test where the pipe was in four-point bending

without internal pressure, but the crack turned into the axial direction. Since that pipe was manufactured from rolled and welded plates, the rolling direction (and hence the lowest toughness) was in the axial direction in which the crack grew (Section 2.1.3 of Ref. 4.3.3). Further study is needed to better assess the significance of the out-of-plane crack growth. For example, is it desirable to have the crack grow in the helical direction, and how can this growth easily be predicted? Another concern may be that if the low toughness direction is in the helical direction, then a combined pressure plus bending stress state or torsional loading contributions may result in lower failure stresses and become more important to consider in a pipe fracture analysis.

References for Section 4.3

4.3.1 Hiser, A. L., and Callahan, G. M., "A User's Guide to the NRC's Piping Fracture Mechanics Data Base (PIFRAC)", NUREG/CR-4894, May 1987.

4.3.2 Scott, P. M., and Ahmad, J. A., "Experimental and Analytical Assessment of Circumferentially Surface-Cracked Pipes Under Bending", NUREG/CR-4872, April 1972.

4.3.3 Wilkowski, G. M., and others, "Degraded Piping Program - Phase II", Semiannual Report, April 1986-September 1986, NUREG/CR-4082, Vol. 5, April 1987.

4.3.4 U.S. Nuclear Regulatory Commission Pipe Study Group, "Evaluation of the Potential for Pipe Breaks", NUREG-1061, Vol. 3, November 1984.

4.3.5 Papaspyropoulos, V., Marschall, C., and Landow, M., "Predictions of J-R Curves with Large Crack Growth from Small-Specimen Data", NUREG/CR-4575, September 1986.

4.3.6 Ernst, H. A., "Material Resistance and Instability Beyond J-Controlled Crack Growth", in C. F. Shih and J. P. Gudas (eds.), Elastic-Plastic Fracture: Second Symposium, Vol. I - Inelastic Analysis, ASTM STP 803, American Society for Testing and Materials, 1983, pp. I-191 to I-213.

4.3.7 Nakagaki, M., Marschall, C., and Brust, F., "Analysis of Cracks in Stainless Steel TIG Welds", NUREG/CR-4806, December 1986.

4.3.8 Wilkowski, G. M., and others, "Progress and Results From the Degraded Piping Program - Phase II", in Transactions of the 14th Water Reactor Safety Research Information Meeting, (in press).

4.4 Closure

The Executive Summary contains a discussion of the technical issues that may be considered complete as of the end of this program. The summary also addresses technical concerns which still exist, or which have been brought to light by the research conducted to date.

NRC FORM 335 (2 84) NRCM 1102 3201 3202

U.S. NUCLEAR REGULATORY COMMISSION

BIBLIOGRAPHIC DATA SHEET

SEE INSTRUCTIONS ON THE REVERSE

1 REPORT NUMBER (Assigned by TIDC, add Vol. No., if any)

NUREG/CR-4082, Vol. 6
BMI-2120

2 TITLE AND SUBTITLE

Degraded Piping Program - Phase II
Sixth Program Report
October 1986 - September 1987

3 LEAVE BLANK

4 DATE REPORT COMPLETED

MONTH: December YEAR: 1987

5 AUTHOR(S)

G. M. Wilkowski, J. Ahmad, C. R. Barnes, F. Brust, N. Ghadiali, D. Guerrieri, G. Kramer, F. Landow, C. W. Marschall, M. Nakagaki, R. Olson, V. Papaspyropoulos, M. Rosenfeld, P. Scott

DATE REPORT ISSUED

MONTH: April YEAR: 1988

7 PERFORMING ORGANIZATION NAME AND MAILING ADDRESS (Include Zip Code)

Battelle Columbus Division
505 King Avenue
Columbus, Ohio 43201

8 PROJECT/TASK/WORK UNIT NUMBER

9 FIN OR GRANT NUMBER

B8134

10 SPONSORING ORGANIZATION NAME AND MAILING ADDRESS (Include Zip Code)

Division of Engineering
Office of Nuclear Regulatory Research
U.S. Nuclear Regulatory Commission
Washington, D.C. 20555

11a TYPE OF REPORT

Technical

b PERIOD COVERED (Inclusive dates)

October 1986 - September 1987

12 SUPPLEMENTARY NOTES

13 ABSTRACT (200 words or less)

Presented herein is an Annual Report of the U.S. NRC's Degraded Piping Program - Phase II. This is the sixth program report on this program. Prior reports were semiannual reports. The intent of this program is to experimentally validate and enhance available analytical methods for evaluating the mechanical behavior of nuclear power plant piping containing circumferentially oriented defects.

Fifty-seven pipe experiments have been conducted to date. These and approximately fifty additional pipe experiments from other programs have been analyzed.

In the analytical effort, a screening criterion has been developed to show when the net-section-collapse analysis is valid. This shows that even tough materials such as stainless steel can fail at less than net-section-collapse loads if the pipe diameter is sufficiently large. Numerous predictive J-estimation schemes have been evaluated and modified. A finite length surface-cracked pipe estimation scheme has also been developed and incorporated into a computer code called NRCPIPE. This code provides a convenient way of analyzing cracked pipe with a number of currently accepted analytical methods.

Supporting research efforts involve investigating geometry effects on J-R curves, as well as characterizing the material properties for each pipe tested. The significance of all of the efforts to date relative to pipe fracture analyses and flaw assessment criteria are discussed.

14 DOCUMENT ANALYSIS - a. KEYWORDS/DESCRIPTORS

Pipe, Fracture Mechanics, Cracks, J-Integral/Tearing Modulus, Elastic-Plastic Fracture Mecnanics, Nuclear Piping Steels

b IDENTIFIERS/OPEN-ENDED TERMS

15 AVAILABILITY STATEMENT

Unlimited

16 SECURITY CLASSIFICATION

This page: Unclassified

This report: Unclassified

17 NUMBER OF PAGES

18 PRICE

*U.S. GOVERNMENT PRINTING OFFICE: 1988-202-292:80039

UNITED STATES
NUCLEAR REGULATORY COMMISSION
WASHINGTON, D.C. 20555

OFFICIAL BUSINESS
PENALTY FOR PRIVATE USE, $300

SPECIAL FOURTH-CLASS RATE
POSTAGE & FEES PAID
USNRC
PERMIT No. G-67